



MEDICAL UNIVERSITY
OF VIENNA

The Versatile Role Played by Lysine Deacetylase Inhibitors in Cancer-specific Pathways and Cell Proliferation

Doctoral thesis at the Medical University of Vienna
for obtaining the academic degree

Doctor of Philosophy

Submitted by:

Dijana Vitko

Supervisor:

Keiryn L. Bennett, Ph.D.

Mass Spectrometry and Proteomics

CeMM Research Center for Molecular Medicine

of the Austrian Academy of Sciences

Lazarettgasse 14 AKH BT 25.3

1090 Vienna, Austria

Vienna, 05/2017

DECLARATION

This thesis is comprised of published results and unpublished data that will be submitted for a publication. All the data is compiled in a cumulative format, containing a first-authored publication together with an unpublished manuscript. The author of the thesis is the first author on the published article, and a co-first author of a manuscript that will be published. Additional publications of the author of this thesis are listed at the end. These are thematically and/or technically related to the field of research, but not considered as the main part of the doctoral project. The work performed by the author of this thesis was performed at the laboratory for Mass Spectrometry and Proteomics, headed by Dr. Keiryn L. Bennett, CeMM Research Center for Molecular Medicine of the Austrian Academy of Sciences in Vienna, Austria.

Manuscript #1 is attached as a draft prior to submission: “Sub-lethal inhibition of lysine deacetylases reveals acetylation-dependent cancer vulnerabilities in Jurkat T cells”. The manuscript represents research conducted by Dijana Vitko, Peter Májek, Thomas Penz, Elisabeth Salzer, Sara Sdelci, Maria W. Górna, Michael Schuster, Christoph Bock, Kaan Boztug, Petra Beli, Stefan Kubicek, André C. Müller, Keiryn L. Bennett. D.V. and K.L.B co-designed the study. D.V. performed experiments, interpreted the data, prepared the figures and wrote the manuscript. P.M. performed data analysis, prepared figures and contributed to manuscript writing. T.P. performed RNAseq experiments; whilst M.S. performed RNAseq data analysis. E.S. and S.S. assisted with FACS analysis for apoptosis and cell cycle assay, respectively. A.C.M. and P.B. provided critical input on the protocol adjustments for the MS sample preparation. C.B., K.B. and S.K. supervised the work of T.P. and M.S.; E.S. and S.S., respectively. K.L.B. co-designed and supervised the study, contributed to the manuscript writing including critical and detailed revision.

Manuscript #2 was published under the title “FASIL-MS: an integrated proteomic and bioinformatic workflow to universally quantitate in vivo-acetylated positional isomers” in the Journal of Proteome Research, co-authored by Dijana Vitko, Peter Májek, Erika Schirghuber, Stefan Kubicek and Keiryn L. Bennett. *J. Proteome Res.* 2016, **15(8)**, 2579-2594. Reprinted with permission. D.V. performed experiments, analysed and interpreted the data, prepared the figures and wrote the manuscript. P.M. developed informatic tool for data analysis, analysed the data, prepared the figures and contributed to the manuscript writing. E.S. assisted with experiments, *i.e.*, histone extraction and immunoblot-based validation, and participated in writing and reviewing the manuscript. S.K. supervised the work of E.S., K.L.B. co-designed the experimental section, supervised the study, contributed to the manuscript writing and provided a critical and detailed revision thereof.

TABLE OF CONTENT

DECLARATION	I
TABLE OF CONTENT	II
LIST OF FIGURES	IV
LIST OF TABLES	IV
ACKNOWLEDGEMENTS.....	V
LIST OF ABBREVIATIONS	VII
ABSTRACT	X
ZUSAMMENFASSUNG	XII
1. INTRODUCTION	1
1.1. PROTEIN POST-TRANSLATIONAL MODIFICATION: ACETYLATION	1
1.1.1. Histone Acetylation	2
1.1.2. Non-histone Protein Acetylation.....	5
1.2. LYSINE ACETYLTRANSFERASES AND LYSINE DEACETYLASES.....	7
1.3. KDAC DEREGLATION IN CANCER	13
1.4. KDAC INHIBITORS (KDACis)	14
1.5. CLASSIFICATION OF KDACis.....	15
1.6. KDACis IN THE CLINICS.....	19
1.6.1. Diseases Currently Treated with KDACis	19
1.6.2. FDA-approved KDACis	20
1.6.3. KDACis in Clinical Trials	22
2. AIM	23
3. RESULTS	25
3.1. MANUSCRIPT #1: SUB-LETHAL INHIBITION OF LYSINE DEACETYLASES REVEALS ACETYLATION-DEPENDENT CANCER VULNERABILITIES IN JURKAT T CELLS	25
3.1.1. Experimental Conditions	26
3.2. FUNCTIONAL CHARACTERISATION OF KDACi-MEDIATED ALTERATION IN PROTEIN ACETYLATION	86
3.2.1. Structural Role of Lysine Acetylation in SHMT2 Oligomerisation	87
3.2.2. The Role of Lysine Acetylation in MTHFD1 Function	89
3.3. MANUSCRIPT #2: FASIL-MS: AN INTEGRATED PROTEOMIC AND BIOINFORMATIC WORKFLOW TO UNIVERSALLY QUANTITATE IN VIVO-ACETYLATED POSITIONAL ISOMERS.....	91

4. DISCUSSION.....	121
4.1. GENERAL DISCUSSION	121
4.1.1. KDACi-mediated Isoform-specific Alteration in Histone Acetylation	121
4.1.2. KDACi-driven Changes at the Systems Biology Level	122
4.1.3. Energy Metabolism of Normal and Cancer Cells	123
4.1.4. Acetylation-mediated Impact on Tumour Metabolism.....	127
4.1.5. Cancer Cell Metabolism is Characterised by the Warburg Effect	127
4.1.6. Active Serine Synthesis, One-carbon (Folate) Metabolism and Glycine Cleavage System (SOG Pathway) is Required for Biosynthesis of Macromolecular Precursors in Proliferating Cells	130
4.1.7. Functional Assessment of the KDACi-mediated Acetylation of Enzymes Within the SOG Pathway...	132
4.2. CONCLUSION AND FUTURE PROSPECTS	134
5. MATERIALS AND METHODS.....	135
5.1. CELL PROLIFERATION ASSAY.....	135
5.2. ASSESSMENT OF KDACI-MEDIATED CHANGES IN CELL MORPHOLOGY.....	135
5.3. <i>IN SILICO</i> STRUCTURAL ANALYSIS OF ACETYLATION SITES OF MTHFD1 AND SHMT2	136
6. REFERENCES	137
7. CURRICULUM VITAE	149
8. PUBLICATION LIST	152

LIST OF FIGURES

FIGURE 1. ENZYMATIC AND NON ENZYMATIC REACTION OF LYSINE ACETYLATION.	2
FIGURE 2. THE ROLE OF HISTONE PTMS IN EPIGENETIC REGULATION.....	4
FIGURE 3. FUNCTIONAL NETWORK OF PROTEIN ACETYLATION.	7
FIGURE 4. PHYLOGENETIC TREES FOR ACETYLATION WRITERS, READERS AND ERASERS.	9
FIGURE 5. PHARMACOPHORE MODEL OF KDACI INHIBITORS.	17
FIGURE 6. CHEMICAL STRUCTURES OF FDA-APPROVED KDACIS.	21
FIGURE 7. OVERVIEW OF THE COMPLEMENTARY AND UNIQUE INFORMATION OBTAINED BY THE MULTI-OMIC APPROACH TO INVESTIGATE KDACIS.	24
FIGURE 8. EFFECT OF THE KDACI TREATMENTS ON THE PROLIFERATION OF JURKAT T CELLS.	27
FIGURE 9. EFFECT OF KDACI TREATMENT ON THE MORPHOLOGY OF JURKAT T CELLS.	28
FIGURE 10. INFLUENCE OF KDACI-MEDIATED ACETYLATION CHANGES ON THE STRUCTURE OF SHMT2.	88
FIGURE 11. INFLUENCE OF KDACI-MEDIATED ACETYLATION CHANGES ON THE STRUCTURE OF MTHFD1.	90
FIGURE 12. GLUCOSE METABOLISM.	126
FIGURE 13. DIFFERENCES IN THE GLUCOSE METABOLISM OF DIFFERENTIATED AND PROLIFERATIVE CELLS.	129
FIGURE 14. SOG PATHWAY.....	131

LIST OF TABLES

TABLE 1. CLASSIFICATION OF LYSINE ACETYLTRANSFERASES.....	10
TABLE 2. CLASSIFICATION OF LYSINE DEACETYLASES.....	12
TABLE 3. REPRESENTATIVE KDACIS AND THEIR TARGETED KDACS.....	18
TABLE 4. CLINICAL INDICATIONS OF FDA-APPROVED KDACIS.....	20

ACKNOWLEDGEMENTS

I would like to thank my supervisor, Dr. Keiryn L. Bennett for the opportunity to conduct research to support my doctoral thesis in her laboratory at CeMM. Her endless support and patience was beyond my initial expectations. She gave me freedom to express my interest and develop my project(s) during the past years. Moreover, her technical expertise and hands-on knowledge in mass spectrometry-based proteomics helped me to learn and improve in the field. She was, and still is, my boss and a great friend of mine. I am grateful for her trust from the very beginning. She was investing extra time to prepare me for my next career step and continues to guide me to date. She, personally and professionally, set the values I seek for within a professional environment and appreciate as a measure of exceptional working ethics. Moreover, I would like to thank Giulio Superti Furga, Anita Ender and entire HR department at CeMM who were supportive and helpful during my Ph.D. adventure.

I am really thankful to the CeMM alumni Elena Rudashevskaya, Melanie Planyavsky, André Müller and Maria (Maja) Górna for their support and help in the laboratory. Elena supervised my first sample preparations; whilst Melanie assisted my first mass spectrometry-based analyses. André, as a senior scientist at the time, was a source of endless knowledge that reached beyond mass spectrometry-based sample preparation and maintenance of the instrumentation within the laboratory. Maja was a great friend and provided critical input about PTM influence on the protein function. Lastly, I extend my thanks to those that needed to handle me the longest – Katja Parapatits, Marie Huber and Juliane Weisser. Sharing the laboratory and the office space with these girls was a positive energy boost, regardless of occasional ‘Brigitte’ visits... daily-based laughter, bouncing throughout our office doors throughout the entire floor, was a clear indication of how we balanced our stress. I am grateful to Peter Májek for useful advice and the time invested to assist me with data analysis that was beyond my informatic knowledge. He is a friendly co-worker and highly resourceful scientist with interesting ideas to share. Alexandra Zisser, Shane Austin, Fernando J. Sialana, Robert Pazdzior and Claudia Corteczka were amazing addition to the team. They impacted our dynamic scientific discussions and definitely made our social gatherings even more cheerful.

I would also like to thank my Ph.D. committee members and scientific collaborators Dr. Stefan Kubicek and Prof. Dr. Wilfried Ellmeier for their contribution to the development of my doctoral thesis during the past years. Besides, great thanks to Nicole Boucheron, Lisa Göschl (Ellmeier laboratory), Elizabeth Salzer (Boztug laboratory), Erika Schrihuber and Sara Sdelci (Kubicek laboratory) for their collaborative spirit and *filling the gaps* where my own knowledge was not

sufficient. In addition, I want to acknowledge Branka Sarikas Radić and Melanie Six who always found time to assist me in the laboratory and help with experimental work.

On the social (aka, surviving the Ph.D.) side, I was lucky to have my *Vienna crew* that assured the best stress-out therapies I could imagine! To this end, I must acknowledge Nikolina Mladic, Ivan Bresković, Hrvoje Ribičić, Ania Skucha, Anna Siegert and my, one and only, *sister-in-crime* - Ciara Cleary, to be the best fun and remedy one can ever think off. Besides, I am grateful to my awesome flatmates, friends and shoulders I relied on - Peter Lampert and Giovanni Roma. They managed to understand me sometimes better than I did myself. They were there to laugh with me (or at me) at good times, and remained close to cheer me up when I needed it the most.

The greatest reward for the patience and understanding definitely goes to my family. My mother, Mirjana, who never understood my dissatisfaction with an easy-going, comfortable lifestyle in Croatia, but still supported me in pursuing higher goals. My *big* sister, Ivana, who never stopped *holding my back*, regardless of our age and the distance between us. Lastly, this thesis I dedicate to my father, Ivan, whose inherited stubbornness brought me where I am now. Memory of him reminds me each day of what is really important in life. He has always been my motivation to explore unknown, dream big and fear absolutely nothing. Thanks, dad!

LIST OF ABBREVIATIONS

AGC	Automatic gain control
AML	Acute myeloid leukaemia
ATP	Adenosine triphosphate
BCA	Bicinchoninic acid
BRD	Bromodomain-containing protein
CBP	CREB-binding protein
ChIP	Chromatin immunoprecipitation
CI-994	Tacedinaline, lysine deacetylase inhibitor
CID	Collision-induced dissociation
CLOCK	Clock circadian regulator
CREBBP	CREB binding protein
CTCL	Cutaneous T cell lymphoma
D ₃ -NAS	<i>N</i> -acetoxy-D ₃ -succinimide
DMSO	Dimethyl sulphoxide
DNA	Deoxyribonucleic acid
DTT	Dithiothreitol
EDTA	Ethylenediaminetetraacetic acid
ELP3	Elongator acetyltransferase complex subunit
EP300	E1A binding protein p300
ESI	Electrospray ionisation
FA	Formic acid
FACS	Fluorescence-activated cell sorting
FAD	Flavin adenine dinucleotide
FASIL-MS	Filter-aided stable isotopic labelling coupled to mass spectrometry
FASP	Filter-aided sample preparation
FC	Fold change
FDA	Food and Drug Administration
FDR	False discovery rate
FK228	Romidepsin, Istodax, lysine deacetylase inhibitor
FPKM	Fragments per kilobase of exon per million fragments mapped
FTMS	Fourier transform mass spectrometry
GCN5	General control of amino acid synthesis protein 5-like 2

GO	Gene ontology
GTF3C4	General transcription factor IIIC subunit 4
HCD	Higher-energy collision-induced dissociation
HPLC	High-performance liquid chromatography
HSC	Haematopoietic stem cell
IC ₅₀	Half-maximal inhibitory concentration
IP	Immunoaffinity purification
KAT	Lysine acetyl transferase (synonym HAT, histone acetyltransferase)
KATi	Lysine acetyl transferase inhibitor
KDAC	Lysine deacetylase
KDACi	Lysine deacetylase inhibitor
KDM	Lysine demethylase
KMT	Lysine methyltransferase
KO	Knock-out
LC	Liquid chromatography
MCP	Myeloid progenitor cell
MM	Multiple myeloma
MS-275	Entinostat, lysine deacetylase inhibitor
MS	Mass spectrometry
MSMS	Tandem mass spectrometry
MTHFD1	Methylenetetrahydrofolate dehydrogenase, cyclohydrolase and formyltetrahydrofolate synthetase 1, C-1-tetrahydrofolate synthase, cytoplasmic
MTHFD1L	Formyltetrahydrofolate synthetase, mitochondrial
MTHFD2	Methylenetetrahydrofolate dehydrogenase/cyclohydrolase, mitochondrial
MTHFD2L	Putative methylenetetrahydrofolate dehydrogenase/cyclohydrolase 2, mitochondrial
NAD ⁺	Nicotinamide adenine dinucleotide
NCE	Normalised collision energy
NCOA	Nuclear receptor coactivator
NK cell	Natural-killer cell
ORR	Overall response rate
PBS	Phosphate buffered saline
PRMT	Protein arginine methyltransferase
PTCL	Peripheral T cell lymphoma

PTM	Post-translational modification
RNA	Ribonucleic acid
SAHA	Suberoylanilide hydroxamic acid
SDS	Sodium dodecyl sulphate
SHMT1	Serine hydroxymethyltransferase, cytoplasmic
SHMT2	Serine hydroxymethyltransferase, mitochondrial
SOG	Serine synthesis, one-carbon (folate) metabolism and glycine cleavage system
SPE	Solid phase extraction
TAF1	TATA-box binding protein associated factor 1
TCA	Tricarboxylic acid (cycle)
TEAB	Triethylammonium bicarbonate
TFA	Trifluoroacetic acid
THF	Tetrahydrofolate
TIP60	60 kDa Tat-interactive protein
TMT	Tandem mass tag
t_R	Retention time
TSA	Trichostatin A, lysine deacetylase inhibitor

ABSTRACT

Lysine acetyl transferases (KATs) and lysine deacetylases (KDACs) are versatile enzymes that regulate the acetylation state of histone and non-histone proteins. KDACs are overexpressed in various types of cancer, and the inhibition thereof results in differentiation and apoptosis of tumour cells. This effect has been investigated in numerous diseases ranging from blood malignancies and solid tumours to viral infections. To date, however, the greatest medical benefits were observed in the treatment of blood cancer. KDAC inhibitor (KDACi) treatment is FDA-approved only for T cell lymphoma and multiple myeloma as a single agent or as a combinatorial therapy, respectively. Nevertheless, recent research shows promising results in extending the application of KDACis beyond blood malignancies to cardiovascular diseases, various inflammatory and neurodegenerative disorders.

This thesis focuses on several aspects to investigate how KDACis influence cancer-specific pathways, particularly proteins associated with cell proliferation. The systems-biology approach was utilised to investigate an early response to KDACis in order to focus on the initial pathways that are altered after KDACi treatment, without triggering a plethora of secondary apoptotic events. This enabled identification of the proteins that are altered in expression and acetylation after KDACi treatment. Moreover, correlation of altered gene and protein expression denoted KDACi-specific modes-of-action. Our results revealed that the energy metabolism and nucleotide synthesis-related pathways are affected even under mild, non-apoptotic drug treatment. These also included proteins that are *essential* for cell survival. In manuscript #1, the global data is debated. Additional discussion and the future perspectives of this thesis focus on cancer-specific metabolic pathways, and the potential of exploiting KDACi-mediated acetylation changes to examine novel therapeutic strategies. To this end, the influence of altered acetylation of MTHFD1 and SHMT2 was investigated in the context of protein structure, oligomerisation potential, and enzyme function.

Modification of lysine residues by acetylation has been identified on both histone and non-histone proteins. The analysis of altered histone acetylation, however, requires adaptation of the mass spectrometry-based (MS) approaches compared to analysis of non-histone protein acetylation. This is mostly due to differences in protein chemistry, *i.e.*, length and sequence of the modified peptides. To this end, our FASIL-MS approach was developed to quantitate histone site-specific lysine acetylation mediated by KDACi treatment. FASIL-MS combines a streamlined sample preparation protocol, adjustment of the MS method and an improvement in the bioinformatic tool used for MS²-based quantitation of histone acetylation. This can be further employed in various

experimental settings, such as monitoring drug- or time-dependent alterations in histone acetylation. Moreover, a combination of FASIL-MS with chromatin immunoprecipitation sequencing (ChIP-seq) can be utilised to localise certain acetylation changes at specific gene promoters.

Multiple experimental approaches are needed to systematically assess the role of KDACis. To our knowledge, this thesis comprises the most comprehensive strategy to investigate the quantitative changes after KDACi treatment in gene and protein expression, together with altered histone and non-histone acetylation. A combination of these methods with additional tools to explore the function of acetylation changes will undoubtedly shed new light on alternative strategies for targeted cancer treatment.

ZUSAMMENFASSUNG

Lysin-Acetyltransferasen (KATs) und Lysin-Deacetylasen (KDACs) sind vielseitige Enzyme, welche den Acetylierungsstatus von Histonen und anderen Proteinen regulieren. KDACs werden in verschiedenen Krebsarten überexprimiert, und ihre Hemmung kann zu Differenzierung und Apoptose der Krebszellen führen. Diese Wirkungsweise wurde für zahlreiche Krankheitsbilder wie Blutkrebs, soliden Tumoren oder viralen Infektionen nachgewiesen, wobei die bisher größte medizinische Verbesserung in der Behandlung von Blutkrebs erzielt wurde. Der therapeutische Einsatz von KDAC Inhibitoren (KDACi) ist von der FDA nur bei T-Zell Lymphomen und Multiplem Myelom als Einzel- beziehungsweise Kombinationstherapie zugelassen. Trotzdem zeigen neue Forschungsergebnisse vielversprechende Resultate für den Einsatz von KDACi bei weiteren Erkrankungen (zum Beispiel bei kardiovaskulären, neurodegenerativen Erkrankungen und Infektionskrankheiten).

Der Schwerpunkt dieser Arbeit liegt darauf, unter verschiedenen Gesichtspunkten zu erforschen wie KDACi krebsspezifische Signaltransduktionswege beeinflussen können; mit besonderem Fokus auf Proteine, die in der Zellproliferation eine wichtige Rolle spielen. Um die frühe Reaktion auf eine KDACi Behandlung zu untersuchen, wurde ein systembiologischer Ansatz gewählt. Diese Herangehensweise stellt den Fokus auf unmittelbar betroffene Signaltransduktionswege sicher, und vermeidet die Auslösung zahlreicher sekundärer effekte durch Apoptose. Dadurch konnten Proteine identifiziert werden, die als Folge einer KDACi Behandlung ihre Expression und ihren Acetylierungsstatus verändern. Des Weiteren kann durch die Korrelation der Differenzen in Gen- und Proteinexpression auf eine spezifische Wechselwirkung geschlossen werden. Unsere Ergebnisse zeigen den Einfluss von KDACi auf Energiemetabolismus und mit Nukleotidsynthese in Zusammenhang stehende Signaltransduktionswege bereits bei geringer, nicht-apoptotischer Dosis. Diese Resultate umfassen unter anderem auch Proteine, die *essentiell* für das Überleben von Zellen sind. Die Gesamtheit der Daten wird im Überblick in Manuskript #1 erörtert. Die weiterführende Diskussion und der Ausblick dieser Arbeit beschäftigen sich vor allem mit krebsspezifischen Stoffwechselwegen und dem Potential, das die Erforschung eines durch KDACi beeinflussten Acetylierungsprofils in der Krebstherapie besitzt.

Wir untersuchten den Einfluss der veränderten Acetylierung von MTHFD1 und SHMT2 auf Proteinstruktur, Oligomerisationsfähigkeit und Enzymfunktion. Eine Modifikation von Lysinresten durch Acetylierung wurde sowohl bei Histonen, als auch bei anderen Proteinen festgestellt. Zur Analyse der Histonacetylierung musste der übliche auf Massenspektrometrie (MS) basierende experimentelle Ansatz jedoch angepasst werden. Dem liegen insbesondere proteinchemische

Unterschiede zugrunde, wie zum Beispiel Länge und Sequenz der betroffenen Peptide. Zu diesem Zweck entwickelten wir die FASIL-MS Strategie, die es uns ermöglichte, durch KDACi Behandlung hervorgerufene Lysinacetylierung positionsspezifisch auf Histonen zu quantifizieren. FASIL-MS kombiniert ein effizientes Probenvorbereitungsprotokoll und eine adaptierte MS Methode mit einer verbesserten bioinformatischen Auswertung der MS²-basierten Quantifizierung der Histonacetylierung. Dies kann zur Untersuchung weiterer experimenteller Fragestellungen herangezogen werden, beispielsweise zur Beobachtung von Veränderungen der Histonacetylierung in Abhängigkeit von Behandlungszeitpunkt, -dauer, oder Art des Inhibitors. Außerdem können durch die Kombination von FASIL-MS mit Chromatinimmunopräzipitation-Sequenzierung (ChIP-Seq) bestimmte Abweichungen der Acetylierung an spezifischen Genpromotorregionen lokalisiert werden.

Es benötigt zahlreiche Versuchsanordnungen, um die Rolle von KDACi systematisch zu analysieren. Nach unserem Wissen stellt diese Arbeit die bisher umfassendste Strategie zur Erforschung der durch KDACi Behandlung ausgelösten quantitativen Änderungen in Gen- und Proteinexpression, Histon- und sonstiger Proteinacetylierung dar. Eine Kombination mit weiteren Methoden zur Untersuchung von Differenzen im Acetylierungsprofil wird zweifelsohne neue Einblicke in Alternativen für die zielgerichtete Krebstherapie gewähren.

1. INTRODUCTION

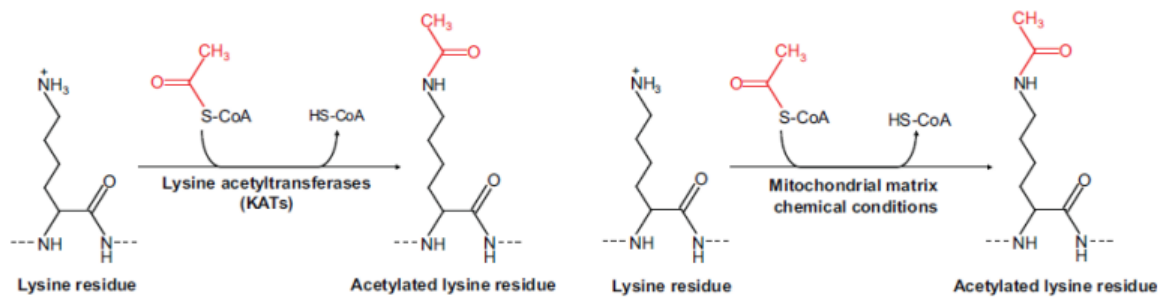
1.1. Protein Post-translational Modification: Acetylation

Protein acetylation is a modification of the primary amino groups that can occur co-translationally or post-translationally. In the former case, the α -amino group of the first amino acid in the protein sequence is irreversibly acetylated by the N-terminal acetyltransferases. The function of this protein modification is still controversial. Nevertheless, to date α -amino acetylation has been linked to regulation of protein synthesis, stability and localisation (Yang & Gregoire, 2007). On the contrary, acetylation of ϵ -amino group on lysine residues within the protein amino-acid sequence is post-translationally regulated. This *N*- ϵ -acetylation is reversibly controlled by lysine acetyltransferase (KAT) and lysine deacetylase (KDAC) (de Ruijter et al, 2003; Marmorstein & Roth, 2001; Roth et al, 2001). In this study we were focused on post translationally-modified proteins and thus throughout the text acetylation refers to lysine side chain (ϵ -amino) modification.

Figure 1.A shows the enzymatic reaction of lysine acetylation by KATs, that utilise acetyl CoA as a donor for an acetyl group. Nevertheless, Weinert *et al.* (Weinert et al, 2014) recently showed that acetylation of lysine residues in mitochondria can be non-enzymatically modified. In this case, the acetyl group is chemically added onto the lysine residues from the acetyl CoA and the level of protein acetylation correlated with the free acetyl CoA present in the mitochondrial matrix. The reverse reaction whereby an acetyl group is removed from the lysine residues is catalysed either by classical KDACs that utilise zinc as a cofactor, or sirtuins that require NAD^+ as a co-substrate for the enzymatic reaction (Figure 1.B).

Acetylation of histone proteins was discovered in the 1960s by Phillips *et al.* (Phillips, 1963) and Allfrey *et al.* (Allfrey et al, 1964) who observed that acetylated histones were more accessible to RNA polymerase and promoting transcription. Thus, these researchers were the first to correlate acetylation of histones with regulation of RNA synthesis. Later, the chemical structure of *N*-acetylated lysine residues was resolved by Gershey *et al.* (Gershey et al, 1968), but it was not until the mid-1990s that the first KATs and KDACs were linked to histone acetylation and subsequent modulation of gene expression.

A



B

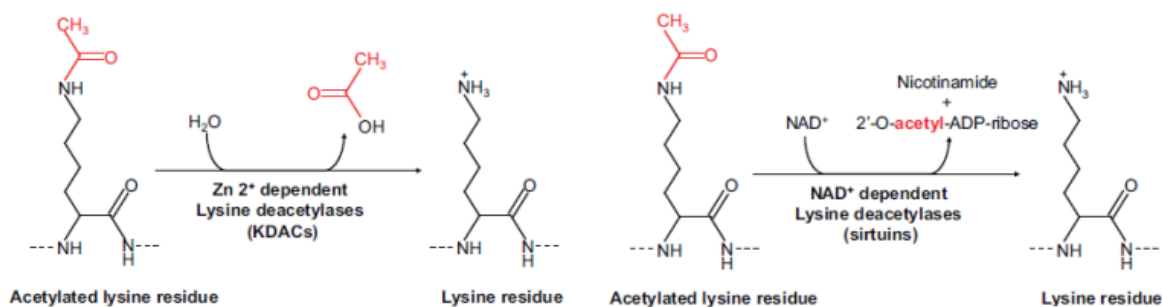


Figure 1. Enzymatic and Non Enzymatic Reaction of Lysine Acetylation.

(A) Lysines can be acetylated via enzymatic reaction by KATs or non-enzymatically in the mitochondrial matrix. The acetyl group in each case is transferred from the Acetyl CoA to the side chain of lysine residue of histone and non-histone proteins. (B) Classical KDAC are zinc dependent and hydrolyse acetyl group from the lysine side chain resulting in non-acetylated lysine residue and acetic acid. On the contrary, sirtuin family of KDACs are NAD⁺ dependent and remove the acetyl moiety from the lysine side chain by generating nicotinamide and 2'-O-acetyl-ADP-ribose. KAT, lysine acetyltransferase; KDAC, lysine deacetylase. The figure was adapted from Gil *et al.* (Gil *et al.*, 2017).

1.1.1. Histone Acetylation

Chromatin has a flexible structure that, in essence, is comprised of a DNA molecule that is wrapped around the histone proteins. This is referred to as the nucleosome. During the cell cycle, the compact nucleosome structure is released to allow the replication of the DNA or transcription

of certain gene loci. These processes are well-timed and strictly-regulated in order to assure error-free replication or RNA transcription.

Histones are highly-modified on the N-termini. The specific localisation and type of modification, or the combination thereof, are crucial for epigenetic regulation of gene activation/inactivation, DNA replication and DNA damage repair. Acetylation and methylation were the first PTMs discovered on histone proteins. The function of these modifications was initially related to RNA synthesis (Allfrey et al, 1964). Today, however, more complex histone modifications have been described. These, for instance, include mono-, di-, trimethylation, propionylation, butyrylation, succinylation, phosphorylation, ubiquitination and ADP ribosylation. A detailed overview of the current status of identified histone PTMs is provided by Huang *et al.* (Huang et al, 2014). Here, hundreds of PTMs and the specific localisation along the histone primary sequence is indicated.

Moreover, some amino acids can be modified by more than one PTM. For instance, lysine residues can be acetylated, but also methylated or succinylated. To this end, coordinated removal of one; and subsequent addition of another functional group is required. These processes are well-orchestrated and require enzymes that catalyse the addition of a certain PTM by so-called epigenetic writers, or removal thereof by epigenetic erasers. In the case of acetylation, KATs are considered acetylation writers, whilst KDACs erase the acetyl group from the lysine residues. Similarly, the writers and erasers of a methyl group are called lysine methyltransferases and lysine demethylases. In addition, proteins that recognise a certain modification are called epigenetic readers. For instance, bromodomain-containing proteins (BRDs) and chromodomain-containing proteins recognise and bind acetylated and methylated histones, respectively. Shown schematically in Figure 2. is the dynamic cycle of addition and removal of a histone modification, exemplified by acetylation, methylation and phosphorylation.

The variety of histone PTMs, co-existence and potential crosstalk between some of the neighbouring modifications add complexity to understanding the function of a specific histone PTM. Recently, a systems level analysis of histone H3 PTMs revealed a significant crosstalk between the PTMs on histone H3 N-terminus in mouse embryonic stem cells (Schwammle et al, 2016). Positive crosstalk (co-dependent marks) were observed between neighbouring acetylated and mono-methylated residues, whilst negative crosstalk (mutually exclusive PTMs) were most common amongst di- and tri-methylated lysine residues. Interestingly, histone-modifying enzymes are usually part of multiprotein complexes. To this end, modification of one amino acid residue can create a docking site and anchor an entire multi-subunit protein complex

with an additional chromatin remodelling function (Lee et al, 2010; Falkenberg & Johnstone, 2014).

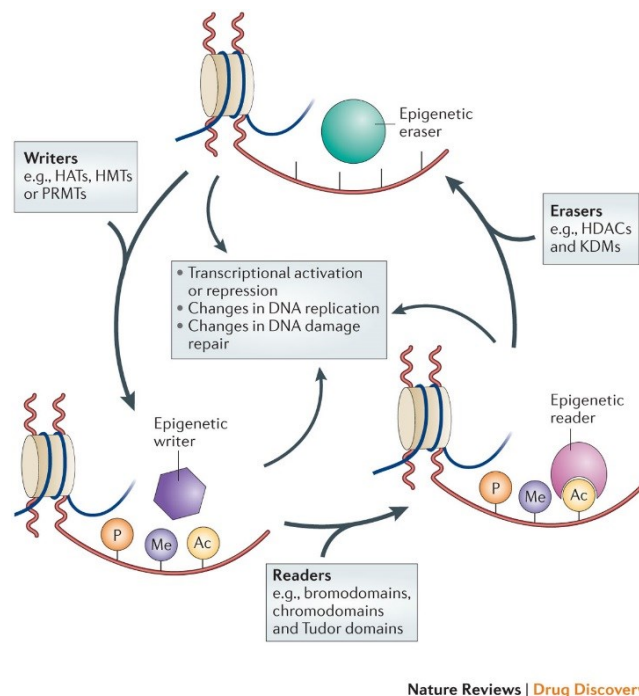


Figure 2. The role of Histone PTMs in Epigenetic Regulation

Histone N-termini (histone tails) are prone to a variety of post-translational modifications. Some of the most common PTMs are lysine acetylation, methylation or serine/threonine phosphorylation. Epigenetic writers are enzymes that catalyse the addition of a certain PTM to an amino acid residue on the histone proteins. For example, KATs, HMTs and PRMTs acetylate or methylate histone tails. These PTMs are readily recognised by epigenetic readers, for instance, bromodomain and chromodomain-containing proteins that bind acetylated and methylated residues, respectively. Lastly, the removal of histone PTMs is achieved by epigenetic erasers. In this case, for example, KDACs remove an acetyl group from the lysine residues, whilst KDM hydrolyse the methylated lysine/arginine residues. Thus, the respective amino acid is now available for another PTM modification. KAT, lysine acetyltransferase; KDAC, lysine deacetylase; KDM, lysine demethylase; KMT (HMT), lysine (histone) methyltransferase, PRMT, protein arginine methyltransferase. Figure was taken from Falkenberg & Johnstone, 2014.

1.1.2. Non-histone Protein Acetylation

Histone proteins are abundant within a cell and acetylation thereof does not require an immunoaffinity purification (IP) step prior to MS analysis. On the contrary, acetylated non-histone proteins vary in abundance. Moreover, the stoichiometry of non-histone protein acetylation is low (Wienert et al, 2014). In particular, an average acetylation level for most lysine acetylated sites is in the 0-5% range, with the majority of the acetylated peptides not exceeding 1% compared to the non-acetylated counterpart. To this end, an immunoaffinity purification (IP) of acetylated non-histone proteins (peptides) is required. An enrichment step enables the detection of low-abundance acetylated sites by decreasing the background of non-acetylated proteins. Subsequently, the probability of detecting acetylated peptides and quantitating the acetylated sites by mass spectrometry (MS) is increased.

Improvement in sensitivity of the mass spectrometers and optimisation of the enrichment strategies enabled identification of thousands acetylation sites on histone and non-histone proteins. The first large-scale proteomic study was done by Choudhary *et al.* (Choudhary et al, 2009). High-resolution MS analysis of three different cell lines (A549, MV4-11 and Jurkat T cells) treated with two KDACis, SAHA and MS-275, resulted in identification of 3,600 acetylation sites on 1,750 proteins. The proteins that were acetylated were mostly involved in RNA splicing, DNA damage repair, regulation of the cell cycle and nuclear transport, but also involved in actin cytoskeleton remodelling, chaperon function and ribosome assembly (Figure 3). Besides, they reported that enrichment strategy increased the number of detected acetylation sites 60-fold. An increase in number of acetylated peptides was observed after IP enrichment compared to the samples that were not enriched via anti-acetyl lysine antibody (3.44% compared to only 0.058%, respectively). Each cell type, however, showed overlapping and unique acetylation pattern. Therefore, in practice it is difficult to determine a universal value of the number of acetylated sites which can be identified in eukaryotic cells.

To date, the specificity of the anti-acetyl antibodies improved and the overall sample preparation was optimised. To this end, large scale acetylation studies were performed in the functional context, for instance to determine specific protein acetylation affected by different classes of KDACis (Scholz et al, 2015). The initial study was done in HeLa cells where on average >3,200 acetylation sites were quantitated after each of 19 KDACis treatment compared to DMSO control. Of note, only 6.2% of identified acetylated sites were regulated by KDACis. This result suggested that majority of acetylated proteins are constitutively modified, and that KDACi effects only small, but specific proteins targets. Moreover, while the low level of acetylation may not affect global

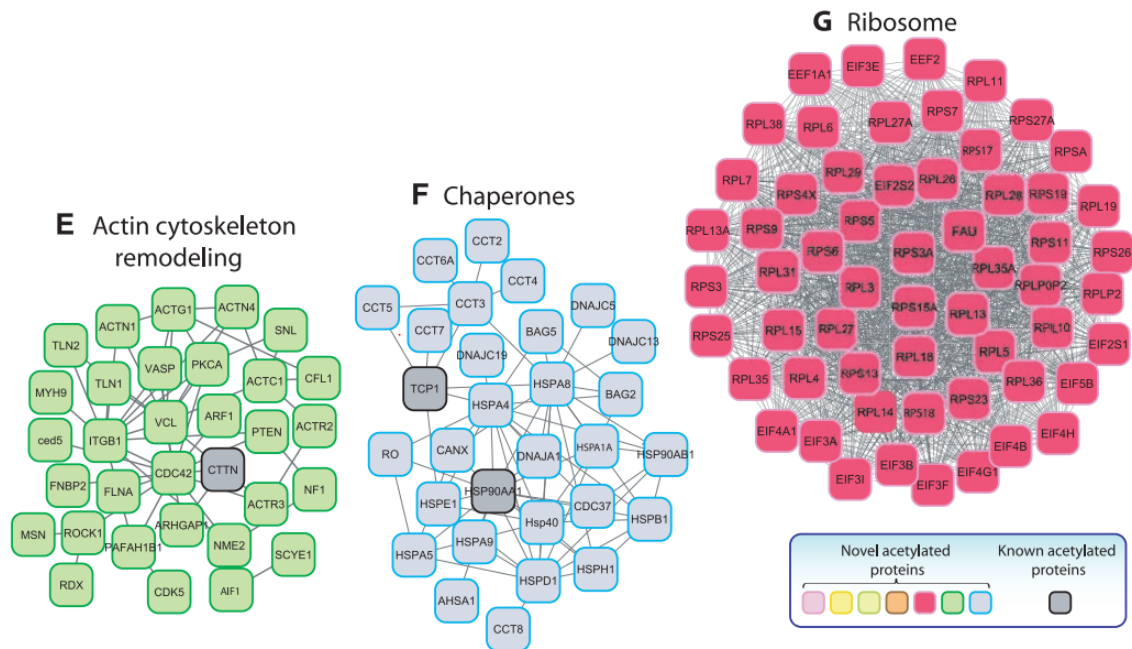


Figure 3. Functional Network of Protein Acetylation.

Large-scale proteomic analysis by Choudhary *et al.* revealed that acetylated proteins are involved in (A to G) RNA splicing, DNA damage repair, cell cycle, nuclear transport, actin cytoskeleton remodelling, chaperon function and ribosome assembly. The protein acetylation was newly reported is marked in colours, whilst the known protein acetylation is left gray. Figure was taken from Choudhary *et al.* (Choudhary et al, 2009).

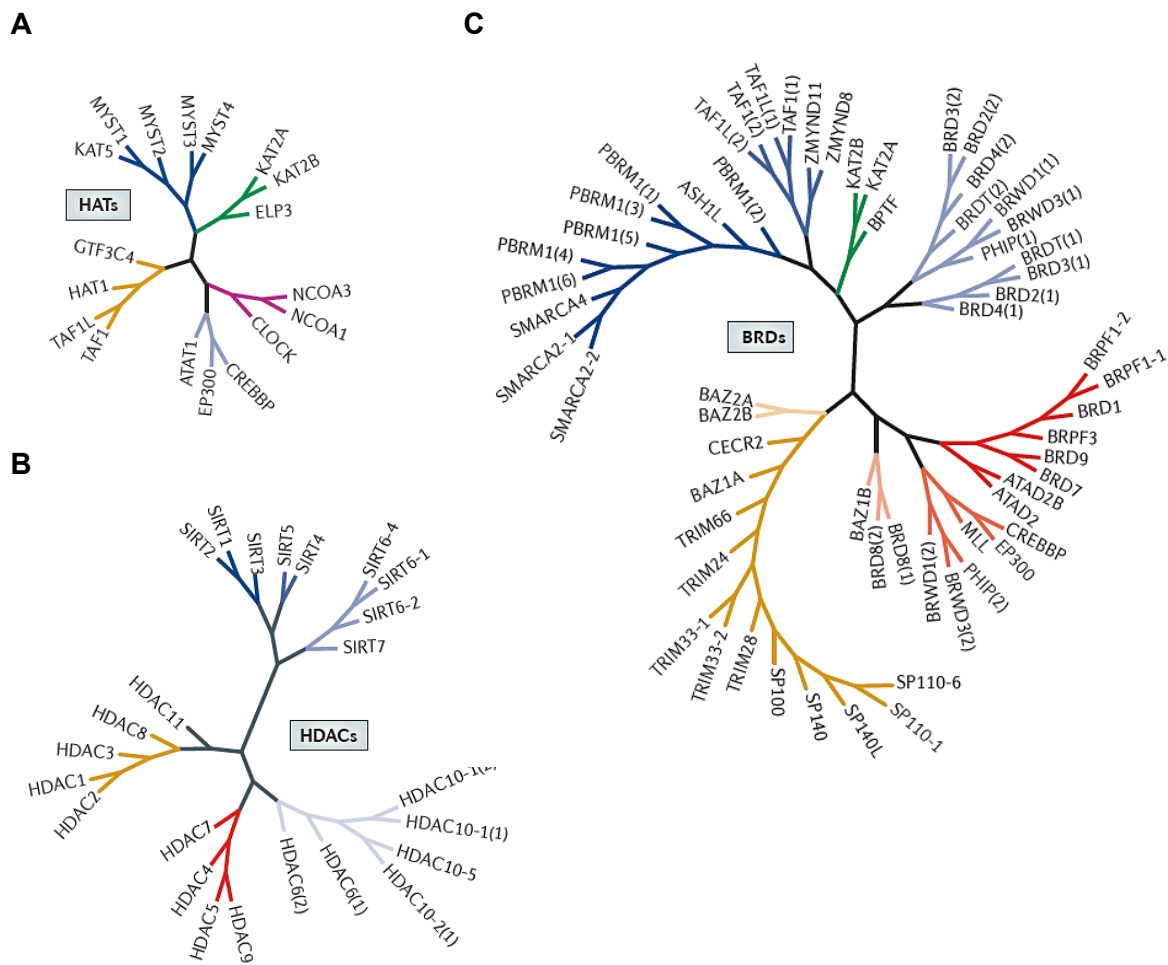
1.2. Lysine Acetyltransferases and Lysine Deacetylases

KATs and KDACs are evolutionary-conserved enzymes responsible for maintaining homeostasis of cellular acetylation on histone and non-histone protein substrates (de Ruijter et al, 2003; Marmorstein & Roth, 2001; Roth et al, 2001). Moreover, the expression and activity of these enzymes is tightly coordinated to drive processes crucial for cell survival, such as regulation of cell cycle progression and cell differentiation. Figure 4.A and B represent phylogenetic trees for KATs and KDACs (previously referred to as HATs and HDACs or histone acetyltransferases and histone deacetylases, respectively). The classification of KATs was based on subcellular localisation, *i.e.*, nuclear and cytoplasmic (Valor et al, 2013). Recent studies, however, suggest

that some of the KATs shuttle between the cytoplasm and the nucleus and that this is dependent on the stimulus and/or PTMs (Blanco-Garcia et al, 2009; Hass et al, 2005; Wong et al, 2004). To this end, current classification is based on the structure and/or function of the KATs. The official symbols for KATs and synonyms that are commonly-used are listed in Table 1. Classification of the KDACs, however, depends on the cofactor that is required for enzymatic activity. Classical KDACs utilise zinc as a cofactor within the active site that aids the removal of the acetyl group; whilst sirtuins require NAD⁺ for catalytic function. The classification of KDACs is summarised in Table 2. Additionally, protein length, sub-cellular localisation and the main function of the KATs and KDACs is also provided.

Changes in histone acetylation by KATs and KDACs epigenetically regulate the activation state of gene promotor regions. An increase in histone acetylation mediated by KATs is a commonly observed activation mark; whilst an opposing event, removal of the acetyl group by KDACs, silences affected genes. This is mostly due to a combination of the chemically-driven changes in histone proteins and, consequently, the interaction with the DNA. In brief, non-acetylated histones contain a high density of free, positively-charged lysine residues that electrostatically interact with negatively-charged DNA molecules and favour compact, transcriptionally less accessible gene loci (heterochromatin). On the contrary, when the lysines on the N-termini are acetylated, the neutralisation of the positively-charged amino group by acetylation relaxes the chromatin structure (euchromatin). This enhances the accessibility of the gene promoters for DNA-binding proteins that mediate DNA replication and transcription (Ge et al, 2013; Rajagopal et al, 2014; Tong et al, 1998; Vempati et al, 2010). Well-orchestrated recruitment of various multiprotein complexes to specific DNA motif sites is required for DNA and RNA synthesis (Becher et al, 2014; Joshi et al, 2013; Khochbin & Kao, 2001; Kuzmichev & Reinberg, 2001). The recruitment of these macromolecular entities and the composition thereof is timed precisely to ensure error-free DNA replication and transcription processes, respectively. In addition, acetylation of lysine residues forms a docking site for the recruitment of bromodomain-containing proteins (BRDs). BRDs are more diverse in structure than KATs and KDACs and can be catalytically active or inactive. Shown in Figure 4.C is the phylogenetic tree for BRDs. These proteins have a crucial role in cell-cycle progression, DNA replication and damage repair (Filippakopoulos et al, 2012; Sanchez & Zhou, 2009). Moreover, many BRDs are often mutated in cancer. For instance, bromodomain-containing protein 1 (BRD1) is mutated in acute lymphoblastic leukaemia, whilst protein polybromo-1 (PBRM1) is altered in renal and breast cancer. Interestingly, some bromodomain-containing KATs, e.g., KAT3A (CBP) and KAT3B (EP300) are mutated in various cancers. These include acute lymphoblastic/myeloid leukaemia, B-cell lymphoma, non-Hodgkin's lymphoma and

bladder cancer. These, and other epigenetic regulators with recurrently-mutated reader domains in cancer are reviewed by Dawson *et al.* (Dawson et al, 2012).



The phylogenetic representation of clustering lysine/histone acetyltransferases (K/HATs, acetylation writers), lysine/histone deacetylases (K/HDACs, acetylation erasers) and bromodomain-containing proteins (BRDs, acetylation readers). The clustering is based on structural and, sometimes, functional similarities between the proteins within the same family. Different colours represent different phylogenetic branches. Multiple alignment of the protein domains represented in the figure was performed by Arrowsmith *et al.* (Arrowsmith et al, 2012). When the domain is present many times in the protein, the protein is shown several times in the tree. The sequential number is given in brackets. In addition and according to the Swiss-Prot nomenclature, protein variants are marked with a hyphen.

Table 1. Classification of Lysine Acetyltransferases.

The main KAT families are: (i) GNAT, (ii) p300/CBP, (iii) MYST, (iv) transcription factor-related, and (v) nuclear receptor-associated KATs. KAT1 (HAT1) is the only member that does not fall under other families, and the only one that is localised solely to the cytoplasm. CBP, CREB-binding protein; CLOCK, clock circadian regulator; ELP3, elongator acetyltransferase complex subunit; EP300, E1A binding protein p300; GCN5, general control of amino acid synthesis protein 5-like 2; GTF3C4, general transcription factor IIIC subunit 4; HSC, haematopoietic stem cell. MPC, myeloid progenitor cell; NCOA, nuclear receptor coactivator; TAF1, TATA-box binding protein associated factor 1; TIP60, 60 kDa Tat-interactive protein. Data taken from various sources (Agudelo Garcia et al, 2017; Sun et al, 2015; Valor et al, 2013; www.genenames.org; www.uniprot.org).

LYSINE ACETYLTRANSFERASES					
Family	Approved symbol (synonyms)	Approved Name	Size (aa)	Cellular localisation	Physiological Function
-	HAT1 (KAT1)	histone acetyltransferase 1	419	cytoplasm	DNA-damage repair in response to free radical damage, replication-coupled chromatin assembly
GNAT	KAT2A (GCN5)	lysine acetyltransferase 2A	837	nucleus/cytoplasm	regulates B cell apoptosis, promotes cell differentiation
	KAT2B (PCAF)	lysine acetyltransferase 2B	832	nucleus/cytoplasm	promotes AML-dependent transcription, regulates E2F1-dependent cell proliferation
	ELP3 (KAT9)	elongator acetyltransferase complex subunit	547	Nucleus/cytoplasm	regulation of transcriptional elongation and cell migration
p300/CBP	CREBBP (KAT3A, CBP)	CREB binding protein	2,442	nucleus	promote self-renewal and block differentiation in HSCs, nucleotide excision repair
	EP300 (KAT3B, p300)	E1A binding protein p300	2,414	nucleus	block proliferation and promote differentiation in HSCs and MPCs, regulates Foxp3(+) Treg cell function and homeostasis, promotes Notch3-induced T cell proliferation

MYST	KAT5 (TIP60, PLIP)	lysine acetyltransferase 5	513	nucleus	tumour suppressor role, modulation in DDR signalling
	KAT6A (MOZ, MYST3)	lysine acetyltransferase 6A	2,004	nucleus	generate and maintain HSCs, promotes HSCs proliferation
	KAT6B (MORF, MYST4)	lysine acetyltransferase 6B	2,073	nucleus	positive and negative regulation of transcription , required for RINX2-dependent transcriptional activation
	KAT7 (HBO1, MYST2)	lysine acetyltransferase 7	611	nucleus	promotes foetal liver erythropoiesis
	KAT8 (HMOF, MYST1)	lysine acetyltransferase 8	458	nucleus	regulates cell differentiation and early foetal haematopoiesis
Transcription-factor related	GTF3C4 (KAT12, TCIIIC90)	general transcription factor IIIC subunit 4	822	nucleus	interaction with the RNA polymerase III machinery, essential for generation of small nuclear and cytoplasmic RNAs
	TAF1 (KAT4, DYT3)	TATA-box binding protein associated factor 1	1,872	nucleus	essential for progression of the G1 phase of the cell cycle
Nuclear-receptor associated	NCOA1 (KAT13A, SCR1)	nuclear receptor coactivator 1	1,441	nucleus	hormone-dependent transcriptional activation
	NCOA3 (KAT13B, ACTR)	nuclear receptor coactivator 3	1,424	nucleus	hormone-dependent transcriptional activation, coactivation of the NF-kB pathway
	NCOA2 (KAT13C, TIF2)	nuclear receptor coactivator 2	1,464	nucleus, cytoplasm	hormone-dependent transcriptional activation, coactivation of the NF-kB pathway
	CLOCK (KAT13D, KIAA033)	clock circadian regulator	846	nucleus, cytoplasm	regulation of various physiological processes through generation of 24-h circadian rhythms in gene expression, affecting glucose and lipid metabolism

Table 2. Classification of Lysine Deacetylases.

KDAC are essentially classified into four classes: classical KDACs comprising of Class I, II and IV, and the sirtuin family of KDACs, *i.e.*, Class III. Classical KDACs are characterised by dependency on binding a zinc ion into the active site that is a critical for catalytic activity. On the contrary, sirtuins require NAD⁺ for enzymatic function. Additionally, subcellular localisation varies between and within, certain classes. KDAC Class I and IV are exclusively localised in the nucleus, whilst Class II is either cytoplasmic or shuttles between the nucleus and the cytoplasm. Sirtuins are the only family that is found in mitochondria. Certain sirtuins are also localised within the nucleus and/or cytoplasm. The information provided was from various sources (Dunn and Rao, 2017; Manal et al, 2016; Yoshida et al, 2017), with the majority based on the review by Mottamal *et al.* (Mottamal et al, 2015). ATP, adenosine triphosphate; KDAC, lysine deacetylase; SIRT, sirtuin.

METAL (Zn ²⁺) DEPENDENT				
Class	Members	Size (aa)	Cellular localisation	Physiological Function
I	KDAC1	483	nucleus	cell survival and proliferation
	KDAC2	488	nucleus	cell survival, insulin resistance,
	KDAC3	428	nucleus	cell survival and proliferation
	KDAC8	377	nucleus	cell proliferation
IIa	KDAC4	1084	nucleus/cytoplasm	regulation of skeletogenesis and gluconeogenesis
	KDAC5	1122	nucleus/cytoplasm	cardiovascular growth and function, gluconeogenesis, cardiac myocytes and endothelial function
	KDAC7	912	nucleus/cytoplasm	thymocyte differentiation, endothelial function, gluconeogenesis
	KDAC9	1069	nucleus/cytoplasm	homologous recombination, thymocyte differentiation, cardiovascular growth and function
IIb	KDAC6	1215	cytoplasm	cell motility, control of cytoskeletal dynamics
	KDAC10	669	cytoplasm	homologous recombination, autophagy mediated cell-survival
IV	KDAC11	347	nucleus	immunomodulators, DNA replication

NAD ⁺ DEPENDENT (SIRTUINS)				
Class	Members	Size (aa)	Cellular localisation	Physiological Function
III	SIRT1	747	nucleus/cytoplasm	aging, redox regulation, cell survival, autoimmune system regulation
	SIRT2	389	nucleus	cell survival, cell migration and invasion
	SIRT3	399	mitochondria	urea cycle, redox balance, ATP regulation, metabolism, apoptosis and cell signalling
	SIRT4	314	mitochondria	energy metabolism, ATP regulation, metabolism, apoptosis and cell signalling
	SIRT5	310	mitochondria	urea cycle, energy metabolism, ATP regulation, metabolism, apoptosis and cell signalling
	SIRT6	355	nucleus	metabolic regulation
	SIRT7	400	nucleus	apoptosis

1.3. KDAC Deregulation in Cancer

Altered expression of KDACs has been observed in various types of diseases, including HIV, solid tumours and blood malignancies (Choi et al, 2001; Daigle et al, 2010; Halkidou et al, 2004; Jakopovic et al, 2013; Muller et al, 2013; Regna et al, 2015; Saji et al, 2005; Tang et al, 2013; Van Damme et al, 2012; Zhang et al, 2005; Zhang et al, 2004; Zhu et al, 2004). By modulating p53 tumour suppressor and Rb-E2F1 pathways (Luo et al, 2000; Xu, 2003; Zhao et al, 2005) that mediate control of cell death, *i.e.*, apoptosis, KDACs were found to facilitate cell cycle progression of transformed cells. KDACs are the key proteins that regulate cellular function such as proliferation, cell cycle regulation and apoptosis, and aberrant expression/function thereof has been correlated with tumour development (Joshi et al, 2013). Moreover, the inhibition of KDACs with small molecules reverses the effect and inducing apoptosis in proliferating cancer cells (Rosato et al, 2003; Zhang et al, 2004). Thus, KDAC inhibitors (KDACi) have gained interest in cancer treatment and inspired research on developing KDACis that are KDAC class specific, or even target single KDAC members (Bieliauskas & Pflum, 2008; Bradner et al, 2010; Itoh et al, 2008; Ma et al, 2016; Schafer et al, 2009; Smil et al, 2009).

1.4. KDAC Inhibitors (KDACis)

The interest in KDACis as drugs for the treatment of transformed cells was initiated when dimethyl sulphoxide (DMSO, a commonly-utilised solvent for dissolving solid chemical compounds) was shown to induce differentiation of cancerous cells. In particular, Friend *et al.* observed differentiation of murine erythroleukemia cells when DMSO was added to the cell culture (Friend *et al.*, 1971; Friend & Scher, 1975; Marks & Breslow, 2007). Further investigations revealed that DMSO binds the active site of KDACs, *i.e.*, a catalytic domain with deacetylase activity that removes acetyl moieties from the targeted proteins. When this activity is inhibited by KDACis, an increase in acetylation was observed on the proteins that are substrates of inhibited KDACs. This increase in acetylation can be utilised as a means to identify KDAC substrates.

Structural analogues of DMSO were further developed and assessed as KDACis. These showed various beneficial effects in the differentiation of tumour cells, induction of cell cycle arrest, triggering apoptosis, blocking angiogenesis and mediating cellular immunogenicity (West & Johnstone, 2014). The specific outcome was, however, highly dependent on the specificity and the concentration of the KDACi utilised and importantly, variable according to the tissue and particular cell-type under investigation.

Today, substantial efforts are directed towards developing isoform-specific KDACis that will selectively inhibit single KDACs. This, however, represents an immense challenge due to the high homology of KDACs within a specific class. So far, progress in the field has been made towards developing class-specific KDACi (Bieliauskas & Pflum, 2008; Itoh *et al.*, 2008; Su *et al.*, 2008; Varghese *et al.*, 2008); and isoform-specific inhibitors have been successfully synthesised against HDAC6 (Smil *et al.*, 2009) (class II) and KDAC8 (class I). The crystal structures of KDAC1 and 2 have aided the design of more selective inhibitors of KDAC1 and 2 (Bressi *et al.*, 2010; Zhang *et al.*, 2013). Nevertheless, these two enzymes usually exist in multiprotein complexes (as a monomer, homo or heterodimer) (Ahringer, 2000; Becher *et al.*, 2014; Brunmeir *et al.*, 2009), thus it is yet to be determined to what extent these molecules can be utilised to only investigate the function of a single KDAC.

KDACis are known to induce cell cycle arrest due to the DNA damage and cell cycle checkpoint activation (Robert *et al.*, 2011; Zhang & Zhong, 2014). Persistent DNA damage eventually leads to cell death (apoptosis). In this case, subsequent DNA damage repair (cell survival) or apoptosis (cell death) mechanisms are activated as secondary events to KDACi treatment. Efficient KDACi

treatment generally results in a decrease and increase in anti- and pro-apoptotic proteins, respectively. Therefore, inhibition of KDACs became an attractive anti-cancer strategy to improve existing patient treatments. These events are usually drug-dependent, and trigger apoptosis via multiple apoptosis signalling pathways (*i.e.*, extrinsic and intrinsic) (Inoue et al, 2004; Morales et al, 2010; Rosato et al, 2003; Shao et al, 2004; Stahnke et al, 2001). With a moderate KDACi treatment, however, the focus is on the early response to KDACi treatment; whilst the secondary events are minimised.

1.5. Classification of KDACis

Classical KDACs structurally differ from the sirtuins with respect to the substrate-binding pocket and the cofactor required for enzymatic activity, *i.e.*, Zn^+ and NAD^+ , respectively. These differences directly influence the molecular mechanism of the KDAC enzymatic activity and, consequently, KDACi selectivity. Here the focus is on the classical KDACs and the inhibition thereof, which does not directly influence the activity of the sirtuin family of KDACs.

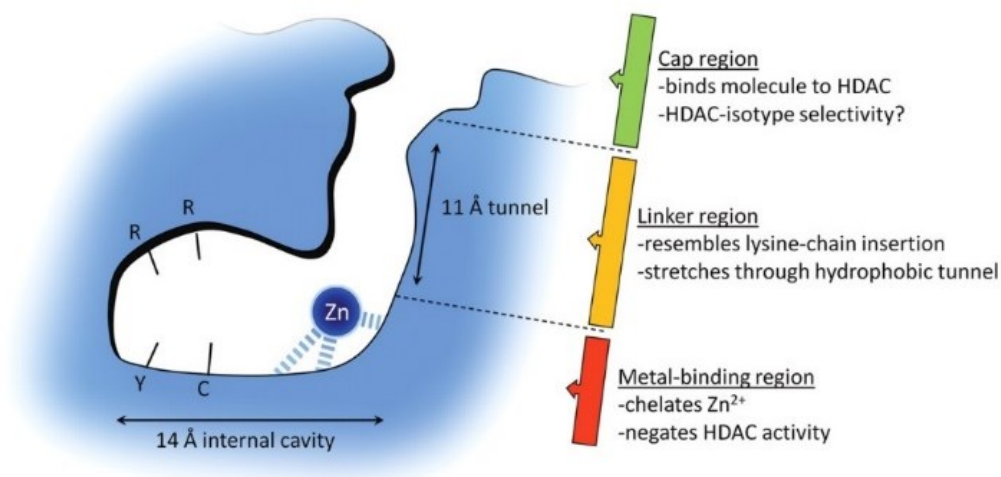
KDACis are found in nature or can be chemically synthesised. Many of the small molecules that inhibit KDACs were initially identified by probes against KDAC activity. Nevertheless, emerging resolution of crystal structures, design and *in silico* prediction of the three-dimensional chemical structure aids in predicting the structure of the small molecule to specifically accommodate the binding pocket of the catalytic domain of the KDAC. To date, the most promising approach is to investigate the basic chemical structures that are already shown to be effective KDACis. With this, the modification of the molecule is made in order to increase: (i) selectivity of the KDACi; and/or (ii) potency thereof.

In general, KDACis need to satisfy certain physicochemical properties that are required for binding to the active site of KDACs (Figure 5.). To this end, the structure of the inhibitor can be segregated into functional groups. Namely, *cap region* is a hydrophobic, usually aromatic, moiety that interacts with the KDAC via the external surface; whilst the *metal-binding domain* (*zinc-binding domain*) interacts with a metal ion within the active site. The *linker region* is the part that connects the *cap* with the *metal-binding region*. In particular, the *linker* can be varied in order to improve the interaction of the other groups with the targeted parts on the enzyme. In fact, the *metal binding region* is crucial in determining the affinity with which the inhibitor binds to the active site of the KDAC and thus mediating potency. The *metal-binding region* of hydroxamic acids show the

strongest interaction. Benzamides, carboxylic acids and thiols sequentially have lower inhibition potencies. The binding pocket of KDACis is represented in Figure 5.A.

Current KDACis are classified into four groups based on the chemical structure of the *metal-binding domain*: (i) hydroxamates; (ii) cyclic peptides; (iii) benzamides; and (iv) short-chain fatty acids. Representatives of hydroxamate-based KDACis are suberoylanilide hydroxamic acid (SAHA, Vorinostat) and trichostatin A (TSA). Cyclic peptides include romidepsin (FK228, Istodax); whilst MS-275 and CI-994 belong to the group of synthetic benzamide derivatives. The fourth group is comprised of short-chain fatty acids such as valporic acid, phenylacetyte and butyrate. Of note, the range of concentration that is required to inhibit a particular KDAC is variable. Moreover, the reported values of certain KDACis that is required to induce cell cycle arrest and apoptosis is cell-type dependent. KDACis within class I are ubiquitously expressed. Thus, the effect of inhibitors that target this particular class was expected to be comparable across different cells, regardless of origin. The chemoproteomic profiling of KDACis, however, revealed that even Class I KDACis have a selectivity towards different complexes that vary between the cell types (Bantscheff et al, 2011). In addition, the effect of KDACis that target Class II and/or Class IV depends on the cell type-specific expression of the targeted KDACs. The clinical benefits of KDACis is focused on identifying potentially novel KDACis present in nature or biosynthesised by microbes (Kim & Hong, 2015). The structural properties of KDACis have a direct influence on the ability to bind certain KDACs. Therefore, the classification of inhibitors can be also made on a specificity basis. To this end, KDACis can be classified as: (i) non selective (pan) inhibitors that reduce deacetylase activity of a wide range of classical KDACs (*i.e.*, hydroxamates); or (ii) class-specific (*i.e.*, Class I KDACis romidepsin and MS-275). In the case of class-specific KDACis, preferential inhibition of a specific KDAC class is observed; whilst the remaining members of a KDAC family are unaffected. This kind of classification is less preferred due to a selective dependency on the inhibitory concentration. This means that at a low concentration range, KDACis can be class-specific. Nevertheless, in the higher concentration range this inhibitor can non-selectively act against a broader range of KDACs. To avoid this confusion and misinterpretation, the classification based on the chemical structure of KDACis is usually preferred.

A



B

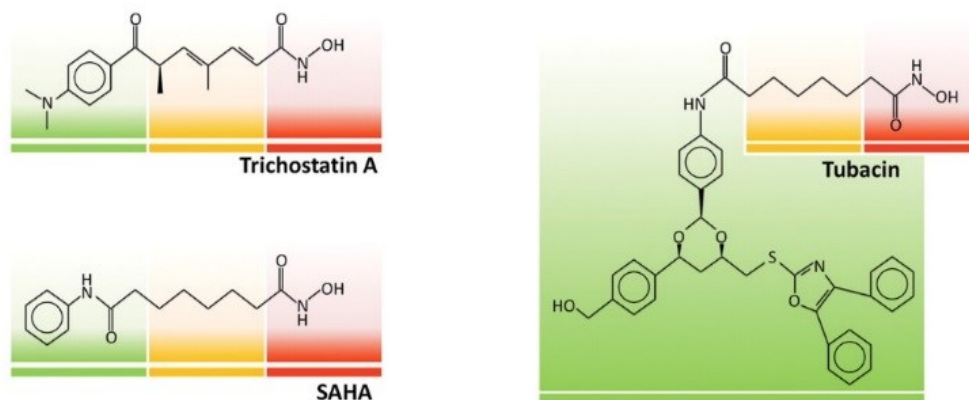


Figure 5. Pharmacophore Model of KDAC Inhibitors.

(A) Crystal structure of the active site of KDACs resulted in the design of a common pharmacophore model of KDACis. The model is comprised of three functional groups that are part of each KDACi: a hydrophobic *cap region* (green), a *linker* (yellow), and a *metal-binding region* (red). (B) Functional groups of the well-known KDACis TSA, SAHA and tubacin are coloured to visualise the regions of the molecule with a specific function. The figure was adapted from Hancock *et al.* (Hancock et al, 2012).

Table 3. Representative KDACis and Their Targeted KDACs.

Representative inhibitors of the KDACis are assembled into four groups, according to chemical structure: hydroxamic acids, benzamides, cyclic peptides and aliphatic (carboxylic) acids. Commonly-reported KDAC classes, or particular KDACs, that are inhibited by a specific KDACi are listed. Additionally, a molar concentration range that was shown to arrest cell growth and/or induce apoptosis of transformed cells is given. KDAC, lysine deacetylase; KDACi, lysine deacetylase inhibitor; SAHA, suberanilohydroxamic acid; TSA, Trichostatin A. Taken from various sources (Butler et al, 2006; Liu and Zhuang, 20015; www.medicographia.com; www.medkoo.com; www.seleckchem.com).

COMPOUND	TARGETED KDAC	POTENCY
Hydroxamic acid		
TSA	Class I, II, IV	μM
SAHA (Vorinostat, Zolinza®)	Class I, II, IV	μM
Belinostat (PDX-101, Beleodaq™)	Class I, II, IV	μM
Panobinostat (LBH-589, Faridak)	Class I, II, IV	μM
Quisinostat (JNJ-28481585)	Class I, II, IV	μM
Resminostat (4SC-201, BYK-406740)	Class I, II, IV	μM
SPH-141	Class I, II, IV	μM
Pracinostat (SB-939)	Class I, II, IV	nM
Abexinostat (PCI-24781, CG-781)	Class I, II, IV	nM
Givinostat (ITF-2357)	Class I, II	nM
Tubacin	KDAC6	mM
Benzamides		
Entinostat (MS-275, SNDX-257)	Class I, II, IV	μM
Chidamide (Tucidinostat, CS-055)	Class I, KDAC10	μM
Macetinostat (MGCD-0103)	Class I, IV	μM
Cyclic Peptides		
Romidepsin (FK-228, Istodax®)	Class I	nM
Aliphatic acids, Carboxylate		
Sodium butyrate	Class I, IIa	mM
Valporic Acid (VPA)	Class I, IIa	mM

1.6. KDACis in the Clinics

The discovery of the KDACi-induced effect on differentiation and apoptosis of transformed cells opened a new avenue into the development of anti-cancer drugs that soon entered pre-clinical and clinical trials. KDACis from the hydroxamate class were shown to be the most promising drug candidates as these evoked the wanted cytotoxic effect in well-tolerated concentrations. The effect of these compounds were versatile and dependent on: (i) cell type; (ii) particular molecular defects present within the cancer cells/disease; (iii) the dose administered and, finally; (iv) the KDACi specificity. Clinical studies were initiated for solid tumours and blood malignancies; with the latter resulting in the greatest overall response rate (ORR).

1.6.1. Diseases Currently Treated with KDACis

Lymphoma is a prevalent blood cancer characterised by uncontrolled proliferation of lymphocytes (white blood cells). Classification is usually based on the type of lymphocytes involved (B or T lymphocytes, natural killer (NK) cells), morphology, size and growth rate of the neoplastic cells or areas of presentation (central nervous system, skin *etc.*). Hodgkin's lymphoma (Hodgkin's disease) is diagnosed by the presence of abnormal B lymphocytes, so-called Reed-Sternberg cells. All other lymphomas are non-Hodgkin's lymphomas that can involve neoplastic transformation of NK cells, B or T lymphocytes. The outcome of the treatments that are currently available depends on the type of lymphoma that is treated. Therefore, correct diagnosis within a certain class is essential for appropriate patient treatment.

Multiple myeloma (MM) is characterised by abnormal proliferation of clonal plasma cells and is usually accompanied by the production of a monoclonal antibody. In patients, myeloma cells overcrowd the normal plasma cells and other blood-forming cells in the bone marrow. Patients suffer from low blood counts and secondary damage due to the deposition of produced antibodies within organs throughout the body. If there is only one tumour within the body that originated from the abnormal plasma cell growth, it is termed solitary plasmacytoma. On the other hand, many of these tumours reside in different locations within the body and is therefore referred to as MM. MM is the second most common blood cancer, after non-Hodgkin's lymphoma (Atadja, 2009; Siegel et al, 2015; Sivaraj et al, 2017).

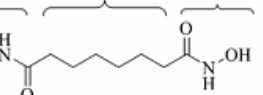
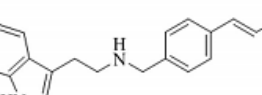
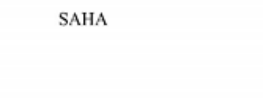
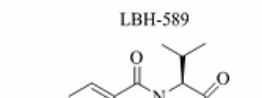
1.6.2. FDA-approved KDACis

In 2006, the first KDACi Zolinza® (Vorinostat, SAHA) was approved by the Food and Drug Administration (FDA) for treatment of cutaneous T-cell lymphoma (CTCL). Later, a cyclic peptide Istodax® (romidepsin, depsipeptide, FK-228) was approved for CTCL and peripheral T-cell lymphoma (PTCL). Belodaq® (Belinostat, PXD-101) is the third KDACi which was granted FDA approval in 2014, and became a treatment option for relapsed or refractory PTCL. The most recent KDACi on the market is Farydak® (panobinostat, LBH-589), a non-selective KDACi which was approved by the FDA in 2015. Contrary to the previous KDACis, Farydak® is used as a combinatorial treatment against multiple myeloma (Table 4.) (Bodiford et al, 2014; Klimek et al, 2008; Lee et al, 2015; Yoon & Eom, 2016; Sivaraj et al, 2017).

Table 4. Clinical Indications of FDA-approved KDACis.

Four KDACis are currently in clinical use for blood malignancies. The table summarises the route of administration, targeted classes of KDACs and the FDA-approved indications. Moreover, observed side effects (rated as 3-4 grade) are provided. CTCL, cutaneous T-cell lymphoma; FDA, food and drug administration; PTCL, peripheral T-cell lymphoma; SAHA, suberoylanilide hydroxamic acid; KDAC, lysine deacetylase; KDACi, lysine deacetylase inhibitor. Data taken from Bodiford *et al.*, Yoon & Eom (Bodiford et al, 2014; Yoon & Eom, 2016).

KDACi TRADENAME (CHEMICAL NAMES)	STRUCTURE- BASED CLASSIFICATION	ROUTE OF ADMINISTRATION	KDAC TARGETS	FDA-APPROVED INDICATION	SIDE EFFECTS
Zolinza® (Vorinostat, SAHA)	Hydroxamate	Oral	Class I Class II	CTCL	nausea, increased risk for infections, fatigue, thrombocytopenia
Istodax® (Romidepsin, FK-228)	Cyclic peptide	Intravenous	Class I	CTCL, PTCL	diarrhoea, fatigue, nausea, anorexia, thrombocytopenia, anaemia
Belodaq® (Belinostat, PXD-101)	Hydroxamate	Intravenous	Class I, Class II, Class IV	PTCL	nausea, vomiting, lethargy, fatigue, constipation, flushing, diarrhoea
Farydak® (Panobinostat, LBH-589)	Hydroxamate	Oral	Class I, Class II, Class IV	Multiple myeloma	nausea, fatigue, diarrhoea, thrombocytopenia, anaemia, anorexia,

Surface recognition	Linker	Zinc binding	
			
SAHA			
			
LBH-589			
			
PXD-101			
			
FK-228			

The figure shows two chemical structures. On the left is a hydroxamic acid ligand, $\text{Ph-NH-C(=O)-CH}_2\text{(CH}_2\text{)}_5\text{-C(=O)-NHOH}$, coordinated to a Zn^{2+} ion. The Zn^{2+} ion is shown with two other generic ligands (represented by lines) and is coordinated to the oxygen of the hydroxamic acid group and the nitrogen of the amide group. On the right is a benzamide ligand, Ph-NH-C(=O)-NH-Ph , coordinated to a Zn^{2+} ion. The Zn^{2+} ion is shown with two other generic ligands and is coordinated to the oxygen of the amide group and the nitrogen of the amine group.

hydroxamic acid

benzamide

romidepsin

reduction

Zn^{2+}

(A) Chemical structure of four KDACis that have been approved by the FDA to date. (B) Direct interaction of the hydroxamic acid- and benzamide-based KDACis with the zinc ion in the active site of KDACs or (C) after the reduction of thiol group within the romidepsin chemical structure. SAHA, suberanilohydroxamic acid; LBH-589, panobinostat; PDX-101, belinostat. Figure was taken from Hsu *et al.* and Lombadry *et al.* (Hsu et al, 2017; Lombardi et al, 2011).

All KDACis currently utilised in the clinic are the second-layer treatment option. This means that the patients need to undergo one previous unsuccessful treatment. Commonly, KDACis show a toxicity level grade 3/4 and the most frequent side effects are fatigue, thrombocytopenia, anaemia, nausea and vomiting. Table 4. contains an overview of current FDA-approved KDACis, with a clinical indications and the side-effects reported after long-term drug administration. The chemical structure of each KDACi approved by the FDA is shown in Figure 6.A. Of note, hydroxamic acid- and benzamide-based KDACis bind the zinc ion directly (Figure 6.B); whilst romidepsin (cyclic peptide) is a pro-drug that is converted into an effective KDACi only after reduction within the cell (Figure 6.C) (VanderMolen et al, 2011).

1.6.3. KDACis in Clinical Trials

The combination of more FDA-approved KDACis is under assessment in attempts to increase and improve the patient response rate, with unaltered or decreased toxicity rate. In addition, KDACis are evaluated in combination with immunomodulatory drugs (lenalidomide, dexamethasone), DNA-intercalating agents of nucleotide analogues (daunorubicin, 5-azacytidine, cytosine arabinoside) or proteasome inhibitors (bortezomib). There are 88 studies that are currently evaluating KDACis in different stages and different settings. SAHA dominates with 44 active studies, followed by panobinostat and romidepsin that are the focus of 21 and 11 active trials, respectively. Belinostat, however, is only being actively assessed in two studies: treatment of solid tumours and relapsed, aggressive B-cell non-Hodgkin's lymphoma.

Many of the KDACis that are currently investigated in different stages of clinical trials. Moreover, already approved KDACis are also under evaluation for different diseases and/or as a combinatorial treatment. For instance, the immunomodulatory drug lenalidomide in combination with romidepsin is being assessed for the treatment of relapsed or refractory peripheral T-cell lymphoma or myeloma. In addition, the beneficial combination of lenalidomide with SAHA treatment after autologous stem cell transplant is being assessed in the treatment of MM (*ClinicalTrials.gov*).

2. AIM

Integration of quantitative transcriptomics, global expression- and acetyl-proteomics is crucial to investigate the role of KDACis on the transcriptional and (post)translational level. Moreover, proteins that change in acetylation, but remain unaltered in overall expression are interesting for further functional investigation. Figure 7. summarises the overlapping and unique information that can be obtained by integrating multi-omic data. To our knowledge, this thesis represents the most comprehensive study and multi-omic data integration to investigate the role of KDACis to date.

The first manuscript enclosed focuses on the versatility of KDACis in the context of gene and protein expression, combined with non-histone protein acetylation. These data are further utilised to depict KDACi-mediated cancer-specific changes in protein abundance and acetylation. Moreover, observed changes in proteins that are essential for cell survival are investigated as a potential biomarkers and/or novel drug targets. The second, published article is directed towards methodological improvements to analyse histone protein acetylation. Analysis of histone PTMs requires additional steps in the sample preparation, *i.e.*, isolation of the nuclei and *in vitro* labelling of the free lysine residues. Here we show that this can be streamlined by utilising our developed FASIL-MS approach.

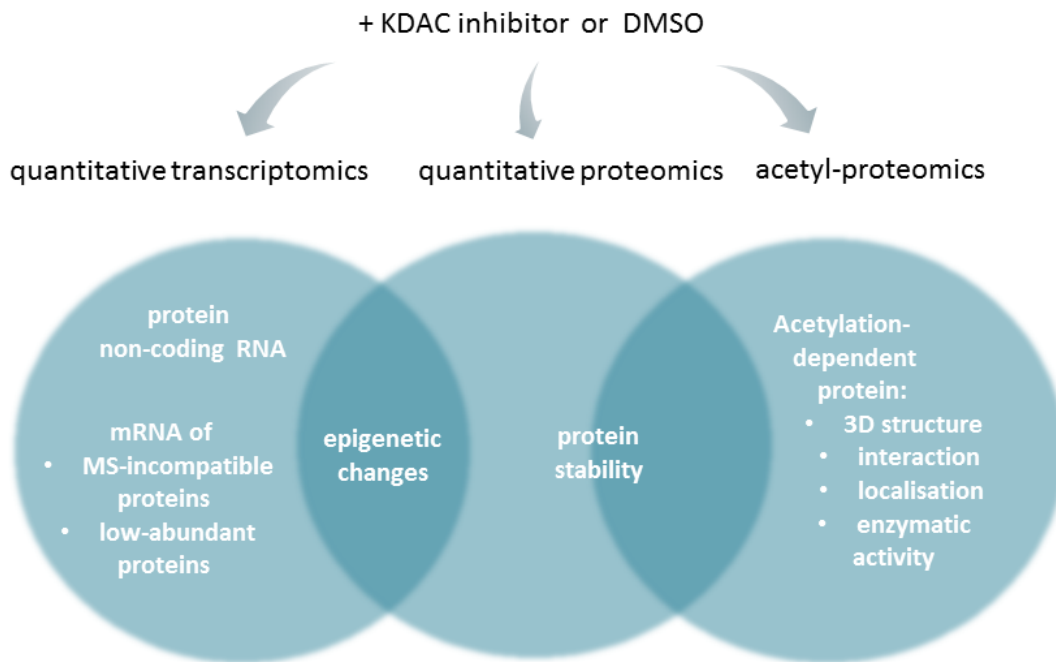


Figure 7. Overview of the Complementary and Unique Information Obtained by the Multi-omic Approach to Investigate KDACis.

Changes that correlate on the quantitative transcriptomic and proteomic levels are most probably due to epigenetically altered gene expression. Each data set, however, contains unique information that is unattainable with another approach. Namely, transcriptomic data contains: (i) transcripts that do not code for a protein amino-acid sequence; (ii) changes in expression at the epigenetic level of these proteins that are difficult to isolate and/or observe by mass spectrometry-based analyses; and (iii) low-abundance (protein-coding) mRNA due to higher sensitivity of the RNA sequencing compared to the proteomic approach. On the other hand, integration of the quantitative proteomic and acetyl-proteomic changes can aid in understanding whether acetylation can mediate protein stability. Moreover, the changes that occur only at the acetylation level, without observed altered protein thereof, direct further functional inspection of the altered protein acetylation. This includes, but is not limited to, changes in the protein 3D structure, protein-protein or protein-DNA/RNA interaction, mediating protein (re)localisation or enzymatic function.

3. RESULTS

3.1. Manuscript #1: Sub-lethal Inhibition of Lysine Deacetylases Reveals Acetylation-dependent Cancer Vulnerabilities in Jurkat T cells

Dijana Vitko, Peter Májek, Thomas Penz, Elisabeth Salzer, Sara Sdelci, Maria W. Górna, Michael Schuster, Christoph Bock, Kaan Boztug, Stefan Kubicek, André C. Müller, Keiryn L. Bennett

KDACis have been utilised to investigate the function of KDACs in diverse diseases related to the T cell biology (Abraham & Weiss, 2004; Desai et al, 2000; Katika et al, 2012; Kim & White, 2006; Mayya et al, 2009). To date, the Food and Drug Administration (FDA) have approved four KDACis for the treatment of blood malignancies. These are: cutaneous and peripheral T cell lymphoma, and multiple myeloma. In this study, the Jurkat T cell line was used as a well-established model system to investigate the effect of KDACis on transformed, highly proliferating T cells (Choudhary et al, 2009; Mayya et al, 2009; Rosato et al, 2003). Previous research has primarily focused on the apoptotic pathways triggered by KDACis. In our study, however, a different approach was undertaken. Firstly, the effect of the chosen KDACis was monitored under mild, non-apoptotic conditions. This condition assured minimal occurrence of secondary effects triggered by cell death. Thereby enabling investigation of the initial, early response to KDACis. Secondly, the integration of the tri-omic approach was beneficial to determine both the common and unique contribution of each data set investigated. Finally, this integrative approach will aid our understanding on the versatile role that KDACis play in the initial mechanisms that are activated during treatment and ultimately leads to malignant cell death.

3.1.1. Experimental Conditions

The experimental conditions that were chosen to investigate the early response of the KDACis were based on the half-maximal inhibitory (IC_{50}) concentration determined from conducted viability assays (Manuscript #1, Supplementary Figure S1.A and B). The IC_{50} concentration after 72 h of incubation for TSA and RD was determined to be 460 nM and 2.8 nM, respectively. The intention was to analyse the cells that are affected by the drug, but have not undergone apoptosis. Therefore, the Jurkat T cells were treated with at the IC_{50} concentration for only 24 h; whereby an increase in apoptotic cell population was not observed (Manuscript #1, Supplementary Figure S2). Nevertheless, these treatment conditions increased acetylation of the histone proteins (Manuscript #1, Supplementary Figure S1.C) which is an indication of KDAC inhibition and confirmation of the drug effect on the cells. Moreover, after only 24 h KDACi treatment there was an observable change in proliferation and morphology of the Jurkat T cells (Figure 8 and 9, respectively). Taken together, the IC_{50} concentration treatment for 24 h was deemed as suitable to investigate the early, non-apoptotic response to KDAC inhibitors, TSA and RD.

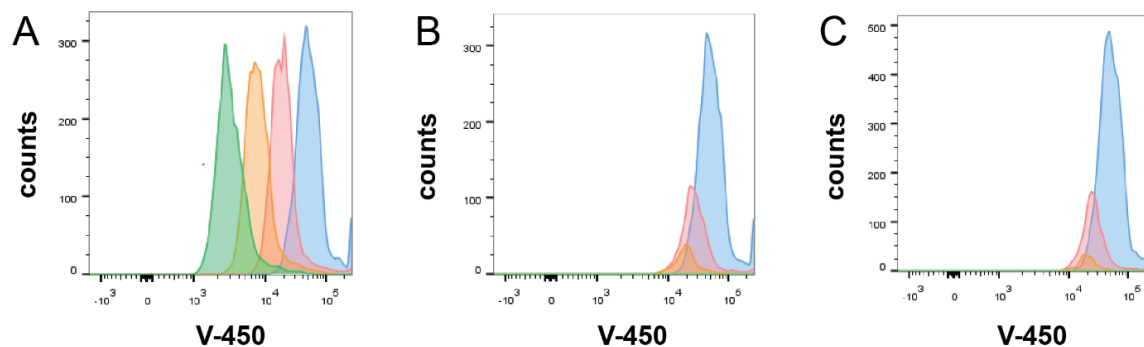


Figure 8. Effect of the KDACi Treatments on the Proliferation of Jurkat T Cells.

The proliferation assay was performed on Jurkat T cells treated with: (A) DMSO 0.1%, (B) TSA and (C) RD at IC_{50} concentrations. Jurkat T cells were stained with the V-450 dye that permeabilises the cell, and decreases in intensity as the cells proliferate, *i.e.*, is equally distributed in the daughter cells during proliferation. Samples were taken immediately after seeding the cells (blue), 24 h (pink), 48 h (orange) and 72 h (green) after incubation. All samples were analysed by FACS. Reduction of the dye intensity represented on the x-axes indicates proliferation of the cells. After DMSO treatment, cells continued to proliferate throughout 3 days of culture; whilst the defect in proliferation was observed after 24 h in the cells treated with the KDACis. DMSO, dimethyl sulphoxide; FACS; fluorescence-activated cell sorting; KDACi; lysine deacetylase inhibitor; RD, romidepsin; TSA, trichostatin A.

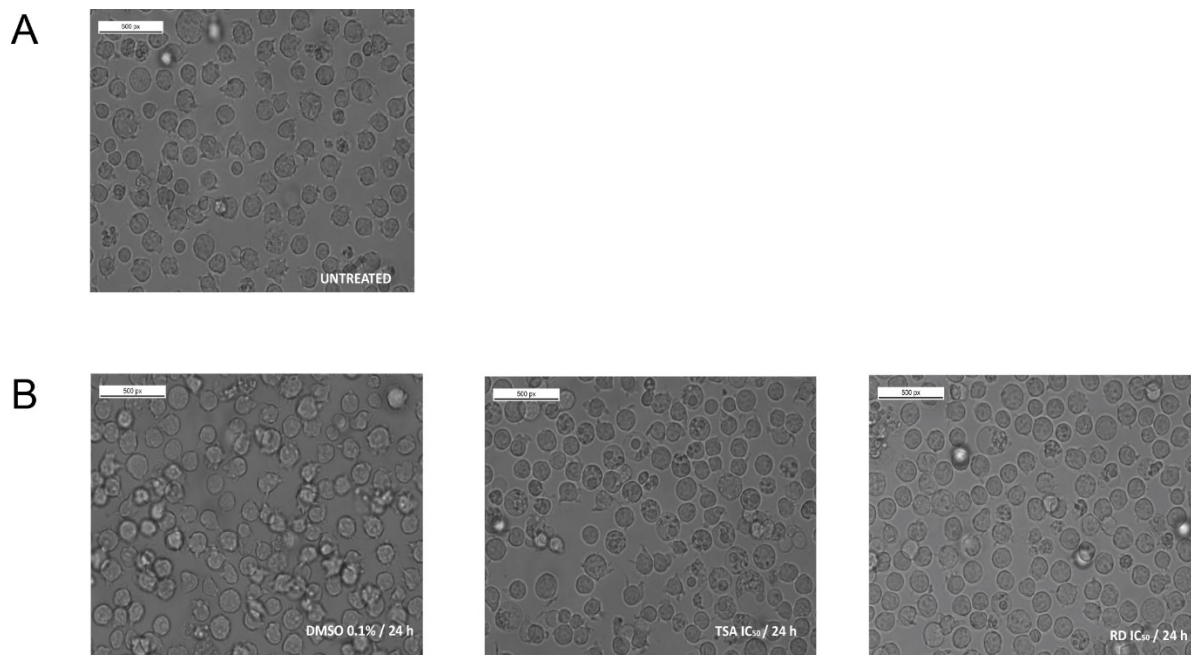


Figure 9. Effect of KDACi Treatment on the Morphology of Jurkat T Cells.

Jurkat T cells were seeded at concentration 1×10^6 cells/mL. The microscopic image was taken after (A) seeding, and (B) 24 h treatment with 0.1% DMSO, or the KDACi at IC₅₀ concentration. Visually, the DMSO-treated cells continued to proliferate without observable change in morphology. KDACi-treated cells, however, did not proliferate at the same rate as DMSO-treated cells. Certain cells acquired a granulated, swollen shape that is indicative of the drug influence on cell physiology. DMSO, dimethyl sulphoxide; KDACi, lysine deacetylase inhibitor; RD, romidepsin; TSA, trichostatin A.

Sub-lethal Inhibition of Lysine Deacetylases Reveals Acetylation-dependent Cancer Vulnerabilities in Jurkat T cells

Dijana Vitko,¹ Peter Májek,¹ Thomas Penz,¹ Elisabeth Salzer,¹ Sara Sdelci,^{1,2} Maria W. Górna,³ Michael Schuster,¹ Christoph Bock,^{1,4} Kaan Boztug,^{1,5} Stefan Kubicek,^{1,2} André C. Müller,^{1#} Keiryn L. Bennett^{1*}

¹ CeMM Research Center for Molecular Medicine of the Austrian Academy of Sciences, Vienna, Austria

² Christian Doppler Laboratory for Chemical Epigenetics and Antiinfectives, CeMM, Vienna, Austria

³ Biological and Chemical Research Centre, University of Warsaw, Warsaw, Poland

⁴ Department of Laboratory Medicine, Medical University of Vienna, Vienna, Austria

⁵ Ludwig Boltzmann Institute for Rare and Undiagnosed Diseases, CeMM, Vienna, Austria

Current address: Thermo Fisher Scientific GmbH, Vienna, Austria

* To whom correspondence should be addressed: Keiryn L. Bennett, CeMM Research Center for Molecular Medicine of the Austrian Academy of Sciences, Lazarettgasse 14, AKH Building BT 25.3, A-1090 Vienna, Austria, E-mail: kbennett@cemm.oeaw.ac.at, Tel: +43-1-40160-70010, Fax: +43-1-40160-970000

Running title: Dissecting KDACi-dependent cancer vulnerabilities

Keywords: acetylation, essentiality, lysine deacetylase inhibitors, mass spectrometry, cancer metabolism

Abbreviations: AML, acute myeloid leukaemia; BCA, bicinehoninic acid; CTCL, cutaneous T cell lymphoma; FA, formic acid; FACS, fluorescence-activated cell sorting; FASP, filter-aided sample preparation; FC, fold change; FDA, Food and Drug Administration; FPKM, fragments per kilobase of exon per million fragments mapped; KO, knock-out; IC₅₀, half-maximal inhibitory concentration; LC-MSMS, liquid chromatography tandem mass spectrometry; KAT, lysine acetyltransferases; KDAC, lysine deacetylase; KDACi, lysine deacetylase inhibitor; KDM, lysine demethylase; KMT, lysine methyltransferase; PTCL, peripheral T cell lymphoma; PTM, post-translational modification; RD, romidepsin; SDS, sodium dodecyl sulphate; TEAB, triethylammonium bicarbonate; *t_R*, retention time; TSA, trichostatin A

1. ABSTRACT

Inhibition of lysine deacetylases (KDACs) has shown promise in the treatment of haematological malignancies, *i.e.*, lymphoma and multiple myeloma. To which extent this is a consequence of chromatin-mediated changes in gene expression, mRNA-to-protein translation, or altered acetylation is key to understanding the mode-of-action of KDAC inhibitors (KDACis). In this study, the differences in acetylation, protein and gene expression were concurrently monitored in Jurkat T cells after KDAC inhibition with trichostatin A (TSA) and romidepsin (RD). The focus was on the early cellular response to KDACi treatment that is relevant for cancer growth. Thus, TSA and RD were administrated at sub-lethal doses for 24 h to eliminate secondary events triggered by apoptosis. The two KDACis had distinct profiles for the differentially-expressed genes and proteins. Interestingly, the majority of the proteins that changed in acetylation remained unaltered at the protein expression level. The mild drug-treatment revealed alterations in protein abundance and acetylation for proteins that are essential for cell survival. Many of which are cancer-specific metabolic enzymes and thus could be investigated further as potential drug targets.

2. INTRODUCTION

Protein acetylation was initially observed on histones and functionally linked to the activation of gene transcription (Brownell et al, 1996; Taunton et al, 1996). Today, however, it is evident that histones are not the only proteins that are acetylated. With the discovery of acetyl groups on non-histone proteins, *e.g.*, α -tubulin (Piperno et al, 1987) and p-53 (Gu & Roeder, 1997), interest in exploring the role of this modification beyond regulation of gene expression has gained momentum. The first discoveries were made by utilising specific antibodies generated against a certain acetylated protein. Nevertheless, these methods were dependent on the availability of monoclonal antibodies, and could not be universally utilised to discover novel acetylated proteins. Improvements in immunoaffinity enrichment strategies, mass spectrometry instrumentation, and data analysis approaches have resulted in a steady increase in the number of acetylated proteins/peptides identified. A comprehensive overview on the progression in acetylation studies during the last decade is reviewed by Baeza *et al.* (Baeza et al, 2016). In contrast to phosphorylation, which is an evolutionary more recent PTM that generally occurs in protein loops; acetylation is usually evident in protein domains and is seemingly more evolutionary conserved (Weinert et al, 2011a; Woo & Li, 2012). This explains initial findings that protein acetylation is primarily involved in essential cellular processes such as cell proliferation, metabolic processes, DNA replication and damage response.

The acetylation status of the proteins within the cell is controlled by two classes of enzymes: lysine acetyl transferases (KATs) that catalyse the addition of an acetyl group onto specific lysine residues, and lysine deacetylases (KDACs) that remove the moiety. The former are referred as acetylation *writers* whilst the latter are known as *erasers*. In addition, proteins involved in recognition and binding to acetylated lysine residues, *i.e.*, bromodomain-containing (BRD) proteins, are known as acetylation *readers*. To date, however, clinical focus is mainly on KDACs as inhibition thereof induces differentiation, cell cycle arrest and/or apoptosis of rapidly proliferating malignant cells (Baradari et al, 2006; Marks et al, 2000; Telles & Seto, 2012; Zhang & Zhong, 2014).

Based on sequence homology with the conserved yeast enzymes, KDACs are divided into four classes: KDAC class I, II, III and IV. KDAC class I, II and IV require zinc ion for catalytic activity and are known as *classical* KDACs. On the contrary, KDAC class III bind NAD^+ and are referred as sirtuins. Therefore, non-selective *classical* KDACi that compete for the zinc-binding pocket at the catalytic site of KDAC are efficient in inhibiting classical KDACs; whilst sirtuins remain

unaffected. In this study, the focus is on the classical KDACs. KDAC class I comprises ubiquitously-expressed nuclear enzymes that share homology with yeast protein Rpd3: KDAC 1, 2, 3 and 8. KDAC class II is divided into two subclasses, IIa and IIb; both related to the yeast deacetylase Had1. The former consist of KDAC 4, 5 and 7; whilst the latter has two members: KDAC 6 and 10. KDACs within class II have tissue-specific expression and can shuttle between the nucleus and cytoplasm. Of note, KDAC 6 and 10 are the only KDAC members with two catalytic domains. Lastly, KDAC class IV consists of a unique member, KDAC 11, that localises to the nucleus and is the most under-investigated of the KDACs (Minucci & Pelicci, 2006).

To date, the Food and Drug Administration (FDA) has approved four KDACis for clinical treatment. Suberoylanilide hydroxamic acid (Vorinostat, Zolinza) and Romidepsin (Istodax) were the first KDACis approved in 2006 and 2009, respectively, for the treatment of cutaneous and peripheral T cell lymphoma (PTCL and CTCL). Recently, another two KDACis were added to the FDA-approved drug portfolio; belinostat (Belodaq) and panobinostat (Fraydak). Similar to Vorinostat and Istodax, Belodaq is utilised as a single agent for the treatment of PTCL and CTCL; whilst Fraydak gained approval as a combinatorial drug to treat multiple myeloma. Fraydak is the first KDACi approved for the treatment of this disease (www.fda.gov). Although efficient in eliminating cancer cells, KDACis are still considered a second-layer treatment due to the multiple side effects that are evoked. Administration of certain KDACis thus occurs only after patients have previously undergone one or more unsuccessful clinical treatments. In addition to the approved drugs, there are more than 20 ongoing clinical trials that investigate different classes of KDACi as single agents or in combinatorial treatment. These trials are mainly focused on haematological malignancies, but also investigate the KDACi effect on solid tumours and as antiviral agents (www.clinicaltrials.gov). On the contrary, KAT inhibitors (KATi) have not yet resulted in any FDA approval. Nevertheless, clinical conditions that are correlated with dysfunction of different KAT families are currently being investigated and small molecules that inhibit acetyl-transferase activity are beginning to undergo clinical trials. The current state of KATis and potential as a drug treatment in the clinic was recently reviewed by Simon *et al.* (Simon *et al.*, 2016).

To reduce side effects in patients currently treated with KDACis, great efforts are being made towards the synthesis of KDAC isoform-specific inhibitors (Everitts *et al.*, 2013; Ononye *et al.*, 2012). Nonetheless, targeting a single KDAC may still not be the best therapeutic approach as class I KDACs are ubiquitously-expressed and play a pivotal role in proliferation and regulation of the normal cell cycle progression. Moreover, many KDACs have tissue-specific expression, each with a distinct role depending on the cell/tissue of origin. Thus, targeting any of the KDACs will

have a more widespread effect than just eliminating cancer cells. A systematic investigation of the effect of KDACis on malignant cells is therefore a promising alternative to identify cancer-specific pathways affected by these drugs. Such an approach will progress and aid our understanding of the complex nature of the cellular response to KDACis. Ultimately, identifying cancer-specific changes in protein acetylation that lead to proliferative dysfunction will open numerous opportunities to investigate the functional aspect of certain acetylation site. This will lead to alternative approaches to specifically inhibit certain protein function/interaction and, finally, minimise or eliminate deleterious effects of KDACis on healthy cells.

Multiple studies have focused on apoptotic pathways triggered by various KDACis. In our approach, however, the early response to KDAC inhibition was investigated. The treatment conditions were chosen to allow Jurkat T cells to undergo a full replication cycle (24 h); whilst still assuring that no major apoptotic events occur prior to cell harvest. This was to eliminate secondary events that usually occur after prolonged drug treatment that eventually leads to cell death. This initial response to KDACi was assessed using a systems biology approach by quantitating the changes that occur at the transcriptional, global protein and acetylation abundance levels (Figure 1).

3. RESULTS

3.1 Moderate KDACi-treatment Elicits Histone Acetylation in Jurkat T cells without Markedly Increasing Apoptosis

Different classes of KDACi manifest distinct, inhibitory effects on cell proliferation. In order to compare the KDACi effect of TSA and RD; the potency of the two drug was assessed firstly via a cell viability assay. The half maximal inhibitory concentration (IC_{50}) of TSA and RD in Jurkat T cells was determined as 460 nM and 2.8 nM, respectively (Supplementary Figure S1.A and B). This data confirmed previous reports on the higher potency of class I-specific drugs compared to non-selective KDAC inhibitors (Bolden et al, 2006).

In our study, a 24 hour KDACi-treatment was chosen whereby the Jurkat T cells undergo a full replication cycle. This is to allow proteins to be synthesised, degraded or modified, throughout the entire replication stage. Therefore, the drug-treatment efficiency after 24 hour treatment at the IC_{50} concentration of the KDACi or vehicle (DMSO control) was assessed. Increases in histone acetylation were monitored after a 24 hour treatment to confirm the drug efficiency. Immunoblot analysis revealed the increased in histone protein acetylation after 24 hours TSA and RD treatment (Supplementary Figure S1.C). KDACi-induced apoptosis was additionally verified by flow cytometry analysis for the expression of specific apoptotic markers. After a 24 hour period under the specified drug-treatment conditions, there was no increase in number of an early nor late apoptotic cell population (Supplementary Figure S2). As a consequence of KDACi-treatment, no prominent apoptosis of Jurkat T cells was observed. Thus, treatment for 24 hours at the determined IC_{50} concentrations was chosen to investigate the early response to KDACi treatment. Moreover, an effect on cell cycle progression was assessed by a cell cycle assay. The percentage of cells in each cell-cycle phase were compared between the drug-treated and control conditions. Overall, KDACis did not alter the cell cycle stage distribution of the treated Jurkat T cells. The one exception was the TSA-induced arrest of the cells in the G1 phase (<20% increase, Supplementary Figure S3).

3.2 Class I-specific KDAC Inhibition Triggers Differential Expression of Distinct Gene Sub-sets Compared to Non-selective KDAC Inhibition

The modulation of gene expression in Jurkat T cells influenced by KDACis was assessed by RNA sequencing. Relative quantitative differences in the gene expression of TSA- and RD-treated cells were determined by comparison with DMSO-treated control cells. As both TSA and RD target nuclear KDACs, it was expected that these two drugs would elicit a similar response at the gene expression level. Surprisingly, <20% of the significantly-altered genes were shared between the drug treatments (Figure 2.A). Even by targeting the same nuclear sub-set of KDACs, our data revealed that these drugs have a distinct, drug-specific effect on gene expression.

To directly compare transcriptional and (post-)translational changes, identified transcripts were firstly intersected with the proteomic data and mapped to the respective proteins. Only transcripts that were increased or decreased by 1.25-fold compared to the DMSO control were considered as altered. The 1.25 threshold was determined by requiring that 95% of gene expression changes between the DMSO-treated biological replicates are less extreme than the threshold (Supplementary Figure S4). Thus, for subsequent gene ontology analysis and comparison of transcriptomic and proteomic data, only the transcripts with a q-value <0.05 and a fold change (FC) of 1.25 relative to the DMSO-treated control were considered.

Filtering the data as described, resulted in 1,258 and 1,027 differentially-expressed genes in the TSA- and RD-treated cells, respectively, compared to the control condition. For the TSA treatment, 405 and 853 transcripts were up- and downregulated, respectively; whilst RD treatment mediated an increase and a decrease of 217 and 810 transcripts, respectively (Figure 2.A). The observed tendency towards a higher gene silencing effect after KDAC inhibition was unexpected as inhibition of deacetylase function enhances transcription of targeted gene loci. The greater number of downregulated transcripts is thus indicative of gene expression regulatory mechanisms that extends beyond histone acetylation and subsequent opening of the chromatin structure.

3.3 KDACi-induced Alterations in Gene Expression Does Not Fully Predict Alterations in Protein Abundance

TSA and RD treatment resulted in both common and distinct alterations in gene transcription. Therefore, a further aim was to quantitate the changes in protein abundance in order to

investigate: (i) if alteration in protein abundance is drug-specific; and (ii) whether the changes in gene transcription correlate with alterations at the protein expression level. The FC threshold for the proteomic data was obtained in the same way as for the transcriptomic data. Namely, the requirement that 95% expression changes between biological replicates of DMSO-treated samples had to be under the FC cut-off. Interestingly, the protein expression data showed higher reproducibility compared to the transcriptomic expression values. Therefore, the resultant FC cut-off was determined as 1.1. Thus, further data analysis was based on filtering significantly-regulated proteins with a q-value <0.05 and a FC of 1.1 relative to the DMSO-treated control.

As indicated in the previous section, the number of downregulated transcripts was comparable between the two drug treatments. Compared to RD treatment, however, the number of upregulated genes was twice as high following exposure to TSA. This was not the case for the proteins affected by these drugs. KDAC inhibition with TSA resulted in 1,892 significantly-altered proteins; whilst only 481 proteins were regulated in the RD-treated sample (Figure 2.B). Contrary to the transcriptomic data, the proteomic approach revealed that TSA induced more uniquely-altered proteins compared to RD. This confirmed that not all KDACi-induced alterations at the gene expression level are converted to the same observation at the protein level. Proteins significantly-regulated by two KDACi treatments were almost exclusively positively-correlated, *i.e.*, up- or downregulated by both treatments. Only 11 proteins had an opposing correlation in abundance between the two drug treatments.

Alteration of the protein abundance mediated by the two drugs affected proteins located in the cytoplasm and nucleus to the same extent (Figure 2.C). On the contrary, proteins compartmentalised in the nucleolus were preferentially downregulated by both treatments; whilst plasma membrane-, lysosome-, and to a lesser extent mitochondrion-located proteins were preferentially upregulated. KDACi-regulated proteins were involved in signal transduction and cell communication, energy pathways, regulation of cellular metabolism and, in particular, nucleic acid-related metabolic processes (Figure 2.D).

Figure 3 represents an alignment of regulated genes and proteins after TSA and RD treatment relative to the DMSO control. TSA treatment showed no correlation of the altered gene and protein expression (Figure 3.A, $R=0.01$); whilst RD-induced changes on transcriptional and protein expression level partially overlapped (Figure 3.B, $R=0.43$). This result confirms that changes in protein abundance after RD treatment are to some extent a consequence of altered gene transcription. TSA, however, revealed a more complex mechanism of mediating protein abundance extending beyond differential gene expression.

3.4 KDACi-associated Acetylation Changes Predominantly Occur on Proteins with an Unaltered Abundance

Altered acetylation can have different consequences on protein function. A modified protein can either have a defined stability compared to the unmodified version; or the modification can alter protein function, *i.e.*, enzymatic activity, protein-protein and/or protein-DNA interaction (Choudhary et al, 2009). The former reason can influence protein abundance (protein stabilisation or degradation); whilst the latter may not result in any obvious changes at the protein quantitative level. To identify relevant changes in protein acetylation that are not a consequence of altered protein expression; the proteomic and acetylation data were intersected. With this, focus was directed to the proteins that solely change in acetylation; whilst respective protein abundance remains unaffected. Nevertheless, the proteins that were reversely affected in abundance and acetylation, *i.e.*, increased or decreased in acetylation and abundance (or *vice versa*) were still considered. As this study focuses on KDACi-driven acetylation of non-histone proteins; acetylated histones were excluded from further functional analyses.

The majority of the acetylated proteins identified in our study did not show changes in protein abundance (Figure 4.A and B). Only 19 and 3 differentially-acetylated proteins showed alignment with the protein expression data for TSA and RD treatment, respectively. For these proteins it was not straightforward to determine whether acetylation is a cause of altered protein abundance, or an unaltered steady-state modification that appears to change with altered protein abundance. Therefore, these were not considered for the functional assessment of KDACi-driven changes in protein acetylation. On the contrary, 25 and 7 proteins showed a reversed correlation between changes in protein abundance and acetylation after TSA and RD treatment, respectively. Indeed, it is possible that localisation of the acetyl group evokes adverse effects on protein folding and subsequent stability. Thus, such acetylation events were still considered as relevant.

RD treatment altered the acetylation pattern of 203 proteins, of which 167 increased and 36 decreased in acetylation relative to the vehicle control. TSA, however, altered the acetylation of 128 proteins, 83 that were increased and 45 decreased in acetylation (Supplementary Table T1). Although TSA has a broader inhibition profile against the classical KDACs compared to RD; a lower number of proteins with altered acetylation levels was observed. Many of differentially-acetylated proteins were altered by both treatments; with a smaller fraction that was reversely altered in acetylation depending on the KDACi treatment. Even though the two KDACis have different profiles, the proteins that were commonly affected by acetylation after the treatments

were involved in regulation of energy pathways and metabolism, nucleic acid and protein metabolic pathways (Figure 4.C and D).

3.5 KDACis Affect Abundance and Acetylation of the Proteins Essential for Cell Proliferation

Based on reduction in proliferation after single-gene knockout (KO), a recent study identified 2,501 essential genes that were required for cell survival either in the HAP1 or KBM7 cell line (Blomen et al, 2015). This list of *essential* genes was intersected with the proteins that were downregulated at the protein level in our study. To investigate whether the changes in acetylation could influence cell survival, the same procedure was performed for the proteins that were altered in acetylation. Contrary to protein expression data, up- and downregulation of the protein acetylation can be detrimental to protein function, and thus both changes are considered as relevant. RD and TSA downregulated 115 and 489 proteins that were *essential* for cell survival, respectively (Figure 5.A and Supplementary Table T2). On the other hand, change in acetylation of 100 and 56 *essential* proteins in the relevant RD- and TSA-treated samples was observed (Figure 5.B and Supplementary Table T3). Forty *essential* proteins were differentially-acetylated after both drug treatments; whilst 60 proteins were specifically altered in acetylation by RD only and 16 after TSA only treatment. Interestingly, from 40 essential proteins differentially acetylated by the two KDACi treatments, 15 reversely changed in acetylation abundance. Five proteins (RRP15, RLP10A, RLP31, RBBP4 and COX17) were increased and decreased after TSA and RD treatment, respectively; whilst twice as many showed an opposite trend (NUDT21, PGAM1, SARNP, HSPA8, EXOSC8, HNRPA1, NPM1, RBM10, VCP, SUB1). An increase in acetylation was observed on more *essential* proteins than a decrease in acetylation. In total, 89 and 36 *essential* proteins were increased after the corresponding RD or TSA treatment; whereas only 11 and 20 proteins were decreased in acetylation.

3.6 Differential Acetylation of *Essential* Proteins is Only Partially Shared Between TSA and RD Treatments

A comparison of the TSA- and RD-driven changes in acetylation of *essential* proteins was also assessed. TSA and RD shared affinity towards inhibition of the common, class I KDACs. Thus, the observed overlap of the proteins affected by the two treatments was not entirely unexpected.

Nevertheless, a large number of drug-specific acetylation changes on *essential* proteins was also apparent (Figure 6.A and B, Supplementary Table T3). The next step was to illustrate to which extent *essential* changes in acetylation are redundant between the two drug treatments. To answer this, *essential* proteins that were differentially-acetylated with both, or uniquely after a single drug administration were enriched for biological processes (Figure 6.C). Differentially-acetylated *essential* proteins that were common to both drug treatments were represented by all enriched biological processes. One exception was DNA repair, where only a TSA-specific influence was observed. Surprisingly, certain biological processes were largely influenced by a specific KDACi treatment. In particular, regulation of TSA-specific *essentiality* in the context of acetylation was more evident in the control of nucleotide metabolism, signal transduction, cell communication and cell growth. On the contrary, RD-specific *essentiality* showed a greater influence on (protein) metabolism and energy pathways.

Despite the knowledge that the abundance of these proteins does not change, it was not straightforward to predict how acetylation influences the function of the affected cellular process. Therefore, the same data were utilised to investigate the potential influence of acetylation on the molecular function of *essential* proteins (Figure 6.D). This was to correlate the differential acetylation to certain protein molecular function that would aid in understanding whether this PTM mediates protein structure; protein/DNA binding or, in particular, certain enzymatic activity. To a certain degree, chaperone function, regulation of transcription (factor) activity and DNA binding was influenced by both drugs. Interestingly, *essential* proteins that were structurally-related to ribosomes were predominantly influenced by RD treatment (with no additional TSA-specificity); whilst proteins structurally-related to the cytoskeleton were primarily affected by TSA (with no additional RD-specificity). Of note, proteins with ligase activity were not affected by acetylation changes after treatment with both KDACis. Overall, these data will aid in focusing further functional studies to investigate the relevance and consequence of acetylation changes that are necessary for cell survival.

4. DISCUSSION

To date, multiple studies have been performed in attempts to elucidate the mechanism(s) by which KDACs induce cell cycle arrest and, consequently, promote apoptosis of malignant cells. The outcome of these studies, however, was largely dependent on the KDACi utilised, *i.e.*, the specificity of the targeted KDAC(s) and the chosen treatment condition. In the majority of reported large-scale studies, cell lines were treated with a concentration of the drug such that a large population (up to 50%) of the cells underwent apoptosis. This effect is also taken as one of the read-outs to confirm the efficiency of the drug treatment (Mackmull et al, 2015). Taking into account the diverse role that KDACs play in cell cycle control and apoptosis, these studies could not deconvolute the events that are due to a direct response to KDAC inhibition from those that are triggered as a secondary response to cell death. Studies of time-course drug treatments have been undertaken to dissect early from later events and, additionally, apoptosis-inducing drugs were included in the comparison to normalise for common apoptotic effect (Mackmull et al, 2015). Nevertheless, drug treatments under the time required for a full replication cycle of the cell line (<24 h for Jurkat T cells) may not be optimal to observe all the changes across the cell cycle. Moreover, it is known that KDACs show different pathways for triggering apoptosis, *e.g.*, intrinsic and extrinsic (Inoue et al, 2004; Li et al, 2016; Morales et al, 2010; Rosato et al, 2003; Shankar et al, 2005; Shao et al, 2004; Sung et al, 2010; Zhang & Zhong, 2014). Thus, using one apoptosis-inducing drug might not be ideal to normalise for the diversity of the apoptotic events observed after KDAC inhibition.

To our knowledge, previously-reported studies concerning KDAC function either integrated transcriptomic and proteomic changes (Subbannayya et al, 2016), or focused on global proteome changes that were intersected with alterations in acetylation (Choudhary et al, 2014). Most of the large-scale proteomic studies also focused only on immunoaffinity purification of acetylated peptides and mapping the changes that occurred in protein acetylation (Choudhary et al, 2009; Scholz et al, 2015; Weinert et al, 2011a; Weinert et al, 2011b). Here, however, the influence of KDACs on KDAC function was investigated at three levels: changes in both gene and protein expression, and the alterations that occur in protein acetylation. Moreover, our findings revealed that each of these three experimental aspects returned unique information that aided in characterising the action of the chosen KDACs. This data could not be exclusively observed with any one method and thus required the integration of the three-omic approaches.

Integration of the transcriptomic and proteomic data revealed that changes in protein abundance after RD treatment is a major consequence of the epigenetically-driven changes in gene expression; whilst a large proportion of the quantitative changes in protein expression did not correlate with alterations at the transcriptomic level. Moreover, for such an analysis the focus was on the transcripts with a protein product that was also detected in the proteomic data. The number of protein-coding transcripts, however, was greater than the number of proteins identified from the proteomic data. This is commonly observed in large-scale experiments where proteomic and transcriptomic data are compared. Reasons for this may be: (i) the higher sensitivity and dynamic range of RNAseq compared to LC-MSMS analysis; and/or (ii) the fact that following enzymatic digestion, some peptides are neither retained on the HPLC column nor observed by MS. Thus, observed changes in protein-coding transcripts of protein products that were not identified by MS are potentially still relevant for determining the mode-of-action of a specific KDACi.

CD8A receptor subunit, granzymes (*GRZM*) and *EOMES*, for instance, have been previously correlated with T cell plasticity and the acquisition of the cytotoxic CD8 effector program of differentiated CD4⁺ helper T cells upon conditional KDAC1/2 deletion (Boucheron et al, 2014). These transcripts were upregulated by KDACi treatment. No corresponding protein product, nor the alteration thereof, was observed at the proteomic level. Small effector molecules that are often secreted and act as immune modulators can still have a crucial impact on the surrounding cells. Thus, in this case the transcriptomic data clearly complemented the proteomic analyses. Moreover, transcriptional changes in *FIBCD1*, a protein functionally linked to acetylation (Schlosser et al, 2009), and *NELL2* (EGF-like protein) were only observed upon RD treatment. Both were completely absent in the TSA- and DMSO-treated samples. Likewise, transcriptional downregulation of *CD86*, a surface molecule involved in the early T cell receptor stimulation and IL2-dependent signal transduction, has been observed upon TSA treatment (Tao et al, 2007). Cell surface proteins are often highly hydrophobic and not easily purified nor detected by standard LC-MS techniques. These examples indicate that a drug-specific change in a protein might be relevant for the cytotoxic effect of KDACis, but cannot be easily identified solely by utilising a proteomic experimental approach.

KDACi-mediated alteration in protein abundance mostly affected proteins involved in regulation of metabolic pathways, cell communication and signal transduction (Figure 2.D). Interestingly, enriched pathways showed a preferential increase in protein abundance after administration of both KDACis. The nucleotide-related metabolism, however, was predominantly enriched in

proteins that were decreased in abundance. This indicates a potentially lower activity or a defect in generation of precursors for DNA synthesis and rapid proliferation of cancerous cells.

TSA downregulated proteins that are important for T cell proliferation (TCF), synthesis of DNA (MCM, POL) and gene expression (E2F, EIF) (Alinari et al, 2012; Finzer et al, 2004; Takahata et al, 2009; Zhang et al, 2014). This proved that even a mild TSA treatment can display a common effect already observed with the other KDACi and/or prolonged or more vigorous treatment. Importantly, proteins that were mostly affected with both KDACi treatments were involved in (malignant) cell proliferation, *i.e.*, TAL1, TCF3, GNL3L, CBFA2T3, MYC. To this end, KDACi-downregulated proteins involved in growth arrest and decreased T cell proliferation indicated that KDACis, directly or indirectly, decrease abundance of the proteins that drive disease progression. This is of clinical relevance for cancers driven by either overexpression or mutation in these proteins. Targeting these would more specifically affect cancer cells, with a reduced or no effect on the surrounding healthy cells. Moreover, the E3-ubiquitin ligase RNF168 that was recently identified as an important factor in DNA damage signalling, was downregulated after TSA, but upregulated after RD treatment. Regardless of the KDACi treatment, RNF168 transcripts remain unchanged indicating that alteration occur either at the transcriptional or post-transcriptional level. In addition, understudied SLC transporters involved in nucleotide transport (SLC43A3 and SLC29A) were commonly downregulated by both KDACis investigated in this study. These transporters have not been yet correlated with the KDAC function, thus it will be important to further functionally characterise their role in cell proliferation.

The majority of the proteins that were changed in acetylation remained unaltered in abundance (Figure 4). Nevertheless, the processes affected with acetylation changes corresponded to those influenced by changes in protein abundance. To this end, both the quantitative proteomic and acetyl-proteomic data showed altered cell metabolic pathways as an initial response to KDACi treatment. It is important to note that these two data sets are not redundant and contain distinct protein sub-sets. That is, quantitative proteomics focused on the proteins that were altered in expression; whereas the acetyl-proteomic data concerned proteins not altered in expression but changed at the acetylation level (or reversely correlated with acetylation changes). In our data set, the majority of differentially-acetylated proteins did not show a change in protein abundance (Figure 4.A and B). This led to conclusion that the role of KDACi-altered acetylation under the examined treatment conditions potentially influences protein conformation, protein/DNA interactions or enzymatic function, rather than mediating protein stability/degradation.

Interestingly, one of the most represented process affected by the acetylation changes was again regulation of the nucleic acid metabolism (Figure 4.C and D).

To further investigate the extent to which moderate KDACi-treatment can be detrimental for cell survival, the quantitative and acetyl-proteomic data was intersected with the proteins that are considered essential for cell proliferation and survival. A recent study focused on determining the genes that are vital for fitness of haploid cells utilising genetic knock-outs of a single gene copy and monitoring the subsequent effect on cell proliferation (Blomen et al, 2015). When a gene was knocked-out and the result thereof was a reduction in cell proliferation, or cell death, this gene was considered *essential*.

Due to the nature of experimental approach, *gene essentiality* determined via single gene knock-outs was only suitable for comparison with the proteins that were downregulated by KDACi treatment. The gene KO and decrease in protein abundance thereof can elicit a similar effect on cell proliferation as drug-induced protein downregulation in this study. In our experimental setting, 103 *essential* proteins were downregulated regardless of the KDACi treatment; whilst 386 and 12 proteins were uniquely decreased in expression after TSA and RD treatment, respectively (Figure 5). Five *essential* proteins that were downregulated by both KDACi treatments are related to acute myeloid leukaemia (MYC, CBFA2T3, GNL3, DDX3 and U2AF1). Proteins such as MYC and CBFA2T3 drive malignant cell proliferation and are not usually present or constitutively active in normal cells. Thus, targeting these would preferentially influence proliferation of the malignant over non-transformed cells.

Acetylation can affect *essential* proteins by changing activity levels or abundance. Protein abundance can remain unaltered and an increase or decrease in the acetylation of particular protein and/or lysine residue can modify protein-protein and protein-DNA interaction. Conversely, changes in acetylation can directly influence the stability of the protein and thus protein function is regulated via changes in abundance. Contrary to the reasoning applied to the quantitative proteomic data, here the focus was on all *essential* proteins that were altered in acetylation after data normalisation to the protein expression level. Therefore, all differentially-acetylated proteins that: (i) remain unaltered in abundance or; (ii) showed a reverse alteration in abundance and acetylation were considered. This was to identify the proteins that are essential for cell survival, but acetylation changes can influence the function thereof. In total, 56 and 100 proteins with altered acetylation were found to be essential for cell survival after TSA- and RD-treatment, respectively. Interestingly, two of the *essential* proteins altered in acetylation were, again, related to the nucleotide biosynthesis. Namely, methylenetetrahydrofolate dehydrogenase (MTHFD1) and

serine hydroxymethyltransferase 2 (SHTM2). These proteins are involved in metabolic pathways and *de novo* synthesis of precursors for DNA replication in rapidly-proliferating cells. Of note, acetylation of these proteins occurred on multiple lysine residues. Investigation of the the specific modification sites on MTHFD1 revealed that acetylation changes upon KDACi treatment occurred on protein loop regions. Here, the PTM can modify the protein 3D structure. In addition, modification within the formyltetrahydrofolate synthetase (catalytic) domain can influence protein-ligand binding and enzymatic function thereof. On the other hand, acetylation changes on the mitochondrion-localised SHTM2 occurred at the protein interface. This might be essential for SHMT2 oligomerisation; a requirement for protein function.

Many *essential* proteins were altered in acetylation by one drug-treatment only. This suggested that TSA and RD affect the acetylation status of proteins essential for cell survival in a specific manner, and thus can lead to cell death via distinct cellular pathways. Figure 6.C and D depict RD- and TSA-specific and common protein acetylation changes correlated to enriched protein biological processes and molecular function, respectively.

KDACi-mediated alterations in protein acetylation concurrent with changes in protein abundance can either be a result of: (i) KDACi-driven alterations in protein expression that is ubiquitously acetylated (and this change in acetylation is also observed); or (ii) KDACi-driven alterations in protein stability that causes stabilisation or degradation of the PTM-modified protein (and subsequent change in protein abundance is also observed). These two scenarios cannot be solely explained by intersecting quantitative proteomic and acetyl-proteomic data. To this end, KDACi-driven changes at the transcriptomic level can assist in distinguishing whether after a drug treatment the corresponding gene of an acetylated protein is differentially expressed; or the KDACi alters a pre-existing protein and subsequently influences the stability/degradation thereof.

One example of these two distinct effects in our study is c-MYC. c-MYC was previously investigated in the context of KDACi effect on cancer cells. It was recently reported that two KDACis, SAHA (non-selective KDACi) and MS-275 (class I-specific KDACi), induce acetylation of c-MYC at K323. This PTM was then related to downregulation of *MYC* mRNA and protein expression in acute myeloid leukaemia (AML) cell lines and primary breast cancer cells (Angela et al, 2016). Regardless of the drug treatment, in our study MYC was downregulated at both the protein and acetylation level. The transcriptomic results, however, showed KDACi-dependent differences on *MYC* expression. RD and TSA treatment resulted in down- and upregulation of *MYC* transcription, respectively. Together it is tempting to hypothesise that the observed downregulation and acetylation of MYC after RD treatment is due to epigenetically-driven

changes on the *MYC* promotor that silences gene expression. On the contrary, TSA-treatment showed significant transcriptional upregulation of *MYC*, but a decrease in protein abundance and acetylation. This is perhaps explained by TSA-mediated *MYC* acetylation and subsequent protein degradation (observed as a decrease in *MYC* abundance and acetylation).

A systematic approach that combines transcriptomic, quantitative proteomic and acetyl-proteomic characterisation of KDACis is imperative to dissect the vast effects that inhibition of KDACs have on cell proliferation. Each of the approaches undertaken in this study returned unique data that complemented the other approaches. Nevertheless, it still represents a starting point for follow-up –omic approaches and targeted functional investigation at the level of the individual proteins. For example, acetylation changes in metabolic proteins can be functionally addressed by mass spectrometry-based metabolomic analyses. In this case, functional consequence, *i.e.*, gain or loss of enzymatic function related to acetylation, can be assessed by monitoring the changes in metabolites upstream and downstream of investigated enzyme. Moreover, the effects of KDACi treatment can be supplemented by the directed-mutation of the lysine residue affected by acetylation and monitoring the metabolic changes to confirm the KDACi effect.

5. CONCLUSION

KDACis evoke differentiation of transformed cells and induce cell death via various drug-specific apoptotic pathways. Initial pathways that could be crucial for determining the cell fate might, however, remain masked by a plethora of secondary effects that occur as a result of an extreme drug treatment. Therefore, here the focus was on the early response to KDACi treatment. To investigate the multivalent role of acetylation in this context, KDAC function was inhibited in Jurkat T cells by two KDAC inhibitors: TSA and RD under mild, non-apoptotic treatment. The global cellular response to RD and TSA treatment was monitored to depict relative changes in mRNA, protein abundance, and protein acetylation. RD treatment resulted in well-correlated changes in gene and protein expression, whereas TSA treatment showed poor correlation thereof. This result confirmed a mechanistically-distinct cellular response to RD and TSA. Moreover, the majority of the proteins with altered acetylation, were not significantly changed in abundance; indicating that the major role of non-histone protein acetylation is in regulating protein activity, interaction and localisation, rather than stability/degradation. Importantly, protein-acetylation changes occurred on proteins crucial for energy metabolism, nucleic acid synthesis and cell signal transduction with a common and distinct set mediated by the each drug. A systems biology approach is necessary to investigate the role of RD and TSA at the transcriptomic (epigenetic) and (post)-translational level. Moreover, acetylation changes on proteins that are unaltered in abundance provide an additional layer of information to characterise the mechanism-of-action of such drugs and will undoubtedly contribute to deciphering the role of this PTM in cancer. The information obtained with this approach will aid diagnostics through the discovery of novel PTM-specific 'biomarkers' and certainly, uncover new approaches to target cancer-specific cellular pathways.

6. MATERIALS AND METHODS

6.1 Determination of TSA and Romidepsin Half Maximal Inhibitory Concentration (IC₅₀)

Half maximal inhibitory concentration (IC₅₀) for TSA and RD was determined utilising CellTiter-Luminescent Cell Viability Assay Glo® (Promega GmbH, Mannheim, DE) according to the instructions provided by the manufacturer. In brief, Jurkat T cells were seeded into a 96-well plate at 20,000 cells per well and treated with decreasing drug concentrations, ranging from 10 to 0 µM, or DMSO as a control. After incubation for 72 h at 37°C and 5% CO₂, the plate was equilibrated at room temperature (RT) and CellTiter-Glo® reagent was added to lyse the cells and release adenosine triphosphate (ATP). ATP levels were measured and correlated with active metabolism and cell viability. The luminiscense signal was recorded after 10 min on a multi-well plate reader SoftMax® Pro 5 (Molecular Devices, CA) and the IC₅₀ concentration was determined utilising GraphPad Prism® 4 software (GraphPad Software, La Jolla California USA; www.graphpad.com).

6.2 Cell Culture and KDAC Inhibition

Suspension Jurkat T cells (Clone E6-1, ATCC® TIB-152™) were cultured in RPMI-1640 cell culture medium developed by Moore *et. al.* (Hanss & Moore, 1964) at Roswell Park Memorial Institute. Medium was supplemented with 10% foetal bovine serum (FBS, Life Technologies, Paisley, UK) and 1× penicillin/streptomycin (Sigma-Aldrich, Steinheim, GE). One and a half million cells per mL were seeded in cell culture flasks (Sigma-Aldrich, Steinheim, GE) and treated for 24 h at 37°C and 5% CO₂ with 0.1% dimethylsulfoxide (DMSO; Merck, Darmstadt, GE), or the KDACi drug at the IC₅₀ concentration, *i.e.* 460 nM or 2.8 nM for TSA and romidepsin, respectively.

6.3 Cell Viability Assay

One million cells were centrifuged at 350 r.p.m. to remove the cell culture media and washed with 1× binding buffer pre-diluted from the 10× stock solution provided by the manufacturer (0.1 M HEPES, pH 7.4; 1.4 M NaCl; 25 mM CaCl₂; BD Biosciences, San Jose, CA). After a second centrifugation step, cells were resuspended in 1× PBS at 1×10⁶ cells per mL and 2 µL of Annexin V and 7-amino-actinomycin D (7-AAD) staining solution (BD Biosciences, San Jose, CA) were

added to 100 μ L of the cell suspension and incubated for 10 min on ice. Cells were washed with 1 \times PBS, centrifuged, and finally resuspended in 200 μ L 1 \times binding buffer prior to analysis with the flow cytometry analyser BD LSR Fortessa™ (BD Bioscience, San Jose, CA). Unstained cells were utilised as a negative control whilst the positive control comprised of 1:1 ratio of heat-treated (60°C for 5 min) and non-heated cells, stained as described above. The purpose of the positive control was to assess the efficiency of Annexin V and 7-AAD staining of the cells that contain both early and late apoptotic cell populations.

6.4 Cell Cycle Assay

Jurkat T cells were seeded in a 12-well plate at a concentration of 1 million cell per mL and treated with 0.1% DMSO (control) or IC₅₀ concentration of TSA and romidepsin. Treatment was performed in triplicates and the treated cells were incubated at 37°C for 24 h. Cells were washed twice with PBS, fixed in 70% ethanol and stored at -20°C until further examination. Prior to FACS analysis, each sample was washed twice with PBS to remove the 70% ethanol. Finally, cells were centrifuged at 850 \times g for 5 min and resuspended in 500 μ L PBS solution containing 100 μ g/mL ribonuclease I (RNase, Sigma-Aldrich, Steinheim, GE) and 50 μ g/mL propidium iodide (PI, Sigma-Aldrich, Steinheim, GE). Cells were incubated for 10 min at 37°C and analysed by BD FACSCalibur Flow Cytometer (BD Biosciences, San Jose, CA). Data was processed and visualised utilising FlowJo software v10, and the percentage of cells in a particular phase of the cell cycle were assessed via Cell Cycle Platform embedded as an optional software tool.

6.5 Anti-acetyl Lysine Antibody Staining

Jurkat T cells treated with DMSO (0.1%), TSA or RD at IC₅₀ concentration for 24 h were harvested and lysed in 50 mM HEPES buffer (Merck, KgaA, Darmstadt, DE), pH 8.5 supplemented with 2% sodium dodecyl sulphate (SDS; SERVA Electrophoresis GmbH, DE). Protein amount was determined utilising bicinchoninic acid (BCA) assay (ThermoScientific, Rockford, IL). Twenty micrograms of total protein lysate was reduced with β -mercaptoethanol (\geq 99.0%, SIGMA-Aldrich Chemie, GmbH, DE) and loaded on a 4-12% gradient SDS-PAGE gel. Separated proteins were first transferred onto a 0.45 μ m pore-size nitrocellulose membrane (GE Healthcare Life Sciences, Vienna, AT) and the membrane was blocked with 5% milk for 1 h at room temperature (RT, 20-

25°C) and further incubated overnight at 4°C with primary anti-acetyl lysine antibody (ICP0380, Imunechem Pharmaceuticals Inc., CA) at 1:1,000 dilution in 5% milk containing 0.1% Tween 20 (v/v) (Sigma-Aldrich, Steinheim, GE). Excess of the antibody was removed with 3 × 5 washes in 1× PBS containing 0.1% Tween 20 (PBST). The membrane was then incubated with a goat-derived anti-rabbit secondary antibody coupled to horseradish peroxidase (HRP) at 1:5,000 dilution in PBST. After 1 h of incubation at RT, proteins were visualised by adding a peroxide buffer and measuring the light emission excited from the HRP bound to the proteins on the membrane (chemiluminescence).

6.6 RNA Purification

Half a million Jurkat T cells treated for 24 h with 0.1% DMSO, IC₅₀ concentration of TSA or RD were disrupted in 350 µL RTL buffer (RNeasy Lysis Buffer; QIAgen GmbH, Hilden, DE) supplemented with 0.01% β-mercaptoethanol (≥99.0%, SIGMA-Aldrich Chemie, GmbH, DE) to release the RNA from the cells. Complete lysate content was loaded onto a QIAshredder spin column (QIAgen GmbH, Hilden, DE) placed into a 2 mL collection tube and centrifuged for 2 min at full speed. Compared to the sample volume, one volume of 70% RNase-free ethanol (Molecular Biology Grade Ethanol 500 mL, Thermo Fisher Scientific, Geel, BE) was added prior to loading onto the RNeasy spin column (QIAgen GmbH, Hilden, DE). After 3 washing steps with 70% RNase-free ethanol, RNA bound to the column was eluted with 2 × 40 µL RNase-free water (nuclease-free water (not DEPC-Treated) Ambion™, Thermo Fisher Scientific, Geel, BE) and centrifuged into a collection tube.

6.7 Quantitative Transcriptomics

The amount of total RNA was quantitated using the Qubit 2.0 fluorometric quantitation system (Thermo Fisher Scientific, Geel, BE) and the RNA integrity number (RIN) was determined using the Experion automated electrophoresis system (Bio-Rad Laborated Ltd., Vienna, AT). RNA-seq libraries were prepared with TruSeq Stranded mRNA LT sample preparation kit (Illumina Inc., San Diego, CA) using Sciclone and Zephyr liquid handling robotics (PerkinElmer Inc., Waltham, MA). Library amount was quantitated using the Qubit 2.0 fluorometric quantitation system and the size distribution was assessed using the Experion automated electrophoresis system. For

sequencing, libraries were pooled, diluted and sequenced on an Illumina HiSeq 3000 using 50 bp single-read chemistry. Base calls provided by the Illumina Realtime Analysis software were converted into BAM format using Illumina2bam and demultiplexed using BamIndexDecoder (<https://github.com/wtsi-npg/illumina2bam>). Transcriptomic analyses were performed using the Tuxedo suite. TopHat2 v2.0.10 (Kim et al, 2013) was supplied with reads passing vendor quality filtering (PF reads) and the Ensembl transcript set (*Homo sapiens*, e75, February 2014) as reference. TopHat2 analyses were run independently for each replicate. Using the Ensembl e73 transcriptome as the reference and *de novo* assembly of transcript models, Cufflinks v2.2.1 (Trapnell et al, 2013) was used to assemble transcripts from spliced read alignments. Differential expression of the transcripts was assessed with Cuffdiff v2.2.1 (<http://www.nature.com/nbt/journal/v28/n5/full/nbt.1621.html>). Transcriptome sets of all replicates for each sample group were combined with Cuffmerge. Finally, cummeRbund (<http://www.bioconductor.org/packages/release/bioc/html/cummeRbund.html>) and biomaRt (<http://www.bioconductor.org/packages/release/bioc/html/biomaRt.html>) were used in combination with customised R scripts to perform quality assessment and further refine the analysis results.

6.8 Quantitative Proteomics

Quantitative proteomic analysis was performed to compare the changes in protein abundance in the Jurkat T cells treated in replicates with 0.1% DMSO, 460 nM TSA and 2.8 nM romidepsin. Cells were harvested after 24 h treatment, washed 3× with 1× ice-cold PBS and lysed in 50 mM HEPES buffer (Merck, KGaA, Darmstadt, DE), pH 8.5 supplemented with 2% sodium dodecyl sulphate (SDS; SERVA Electrophoresis GmbH, DE). The protein amount in each sample was determined with the bicinchoninic acid assay (BCA, Pierce Biotechnology, ThermoScientific, IL) and the following downstream sample processing was adapted from the filter-aided sample preparation method (FASP) (Manza et al, 2005; Wisniewski et al, 2009). Briefly, two biological replicates, each containing 100 µg protein of DMSO-, TSA- and romidepsin-treated Jurkat T cells were reduced with 100 mM dithiothreitol (DTT) and transferred into VIVACON 500 filter units (Vivaproucts Inc., Littleton, MA). SDS-containing buffer was removed from the sample by centrifugation and exchanged with 8 M urea in 100 mM Tris-HCl buffer. Proteins were alkylated with 50 mM iodoacetamide (IA) and washed with 50 mM triethyl ammonium bicarbonate (TEAB). DTT, IA and TEAB were all purchased from SIGMA-Aldrich (SIGMA-Aldrich Chemie, GmbH, DE).

Finally, porcine trypsin (Promega Corp., Madison, WI) was used for protein digestion in an enzyme-to-protein ratio of 1:100 w/w.

For relative protein quantitation, the set of six samples were separately derivatised with TMT 6-plex reagents (ABI, Framingham, MA) according to the instructions provided by the manufacturer. Biological replicates of the DMSO treated cells were labelled with TMT 126 and 127, replicates of the TSA treated cells with TMT labels 128 and 129, whilst TMT channels 130 and 131 were used to label replicates of the romidepsin treated cells. The TMT-labelled tryptic digests were pooled and concentrated by solid phase extraction (SPE) (MacroSpin columns 30-300 µg capacity, The Nest Group Inc., Southborough, MA) prior to offline fractionation as described below.

6.9 Acetyl-lysine Immunoaffinity Purification

Jurkat T cells were treated with DMSO, TSA or RD as described above, washed 3× with 1× PBS, and centrifuged to obtain cell pellets. Cells were lysed in 8M urea buffer supplemented with 2 mM EDTA, 1× phosphatase inhibitor (PhosSTOP, Roche Diagnostics, DE) and 1× protease inhibitor cocktail (PIC, Sigma-Aldrich Chemie, GmbH, DE) and DNA was sheared by sonication (Covaris S220, Covaris, Inc., Woburn, MA) to reduce sample viscosity. After the centrifugation step at 4,000 × g for 15 min, clarified supernatants were transferred to fresh 50 mL Falcon tubes and the protein amount determined via Pierce™ 660nm Protein Assay (Fisher Scientific, AT). Protein equivalent to 3 × 30 mg of each treatment condition, *i.e.* biological triplicates, were used for further acetyl-lysine immunoaffinity purification (IP). The volume of the lysis buffer was normalised across the samples to contain 8 M urea and 100 mM TEAB at the final concentration. Proteins were reduced with 10 mM DTT at 56°C for 1 h and alkylated by adding 60 mM IA for 45 min at room temperature in the dark. Alkylation step was quenched by adding 30 mM DTT to each sample. Prior to protein digestion, the urea buffer was diluted to 1.6 M, but the TEAB concentration was maintained at 100 mM and pH 7.5-8 and, finally, sequencing grade trypsin was added in an enzyme-to-protein ratio of 1:100 w/w. Due to the high protein content, the digestion was performed twice with each incubation for 24 h at 37°C. Digests were acidified with 30% TFA, to a final concentration of 2% and purified on two Sep-Pak C18 cartridges per sample (30 mg). Each C18 cartridge was activated with 0.7 mL 100% acetonitrile and conditioned with 7.0 mL 0.1% TFA. Acidified and clarified digests were loaded onto the Sep-Pack columns in successive steps, and washed with an additional 12 mL 0.1% TFA. Peptides bound to the column were eluted with 1.5 mL 50% ACN, and the two eluates from the same sample that were split before the purification

were recombined. Eluted peptides were lyophilised to remove organic solvent and residual TFA prior to performing the acetyl-lysine IP.

Digested and lyophilised peptides were immunoprecipitated with 150 μ L anti-acetyl lysine antibody conjugated to agarose beads (ImmuneChem Pharmaceuticals Inc., Burnaby British Columbia, CA). The peptides were re-solubilised in the IP buffer (50 mM MOPS, 50 mM NaCl, pH 7.2; MOPS \geq 99.5%, SIGMA-Aldrich Chemie, GmbH, DE) and incubated with the antibody overnight at 4°C on a rotational wheel. After the incubation, the beads were washed with 3 \times 1 mL IP buffer and 3 \times 1 mL water, with inverting the tubes manually to homogenise sedimented agarose beads and centrifugation step at 1,000 \times g between each washing step. Peptides were eluted from the beads by adding 4 \times 100 μ L 0.15% TFA and agitation at 1,000 rpm for 5 min at RT. Eluted peptides were additionally purified on C18 MidiSpin columns (60 μ g capacity; The Nest Group Inc., Southborough, MA) according to the instructions provided by the manufacturer. After elution from the column, samples were concentrated in a vacuum centrifuge and neutralised with 1 M TEAB as required prior to offline fractionation. To reduce sample complexity, each sample was fractionated by reverse-phase (RP) LC system at pH 10 into 20 fractions. Each fraction was then further analysed by online LC-MSMS at pH 2.4. Solvent composition, method details and LC configuration for the offline fractionation system are described in detail below.

6.10 Offline Fractionation

Pooled TMT-labelled samples for global quantitative analysis and acetyl-lysine immunopurified samples for quantitation of acetylated peptides were basified with 20 mM ammonium formate after the purification step and prior to offline fractionation. Twenty μ L pooled TMT-labelled samples for quantitative proteomic analysis were injected onto a Phenomenex column (150 \times 2.0 mm Gemini®NX-C18 3 μ m 110Å; Phenomenex, Torrance, CA, USA) on an Agilent 1200 series HPLC (Agilent Biotechnologies, Palo Alto, CA) with UV detection at 214 nm. Immunoaffinity-purified samples, *i.e.* 3 \times DMSO-, TSA, and romidepsin-treated samples, were separately fractionated. Twenty μ L of each sample was injected onto a monolithic capillary column (Dionex PepSwift®, 0.5 \times 50 mm Pep Swift RP, Dionex Corporation, Sunnyvale, CA). HPLC solvent A consisted of 20 mM ammonium formate, pH 10 in 5% acetonitrile and solvent B contained 20 mM ammonium formate, pH 10 in 90% acetonitrile. TMT-labelled and immunoaffinity-purified peptides were separated at flow rate of 100 and 4 μ L/min, respectively, and eluted from the column with a stepped gradient ranging from 0 to 100% solvent B. Seventy two time-based fractions were

collected over the 60 min elution profile and pooled into 50 HPLC vials based on the UV trace in the case of TMT-labelled fractionation, whereas immunoaffinity-purified samples were directly fractionated into 20 fractions over the 80 min elution profile. Organic solvent was removed in a vacuum centrifuge, and samples were reconstituted with 5% formic acid prior to LC-MSMS analysis (Bennett et al, 2011).

6.11 Liquid Chromatography Mass Spectrometry

Individual fractions collected after offline fractionation were further analysed at pH 2.4 using an Agilent 1200 nano-HPLC system (Agilent Biotechnologies, Palo Alto, CA) coupled to a hybrid linear trap quadrupole (LTQ) Orbitrap Velos mass spectrometer (ThermoFisher Scientific, Waltham, MA) utilising the Xcalibur software version 2.1. for data acquisition. The HPLC system with one precolumn and one analytical column (Agilent Biotechnologies, Palo Alto, CA) was coupled to the mass spectrometer via a nanoelectrospray ion source with a liquid junction (Proxeon, Odense, Denmark). Single fractions were loaded onto a trap column (Zorbax 300SB-C18 5 μ m, 5 \times 0.3 mm, Agilent Biotechnologies, Palo Alto, CA) with a binary pump at a flow rate of 45 μ L/min. Solvents for LCMS separation were composed of 0.1% trifluoroacetic acid (TFA) in water (solvent A) and 0.1% TFA in 70% methanol and 20% isopropanol (solvent B). The peptides were eluted by back-flushing from the trap column onto a 16 cm fused silica analytical column with an inner diameter of 50 μ m packed with C18 reversed-phase material (ReproSil-Pur 120 C18-AQ, 3 μ m, Dr. Maisch GmbH, Ammerbuch-Entringen, DE). Elution was achieved with a 27 min gradient ranging from 3 to 30% solvent B, followed by a 25 min gradient from 30 to 70% solvent B and, finally, a 7 min gradient from 70 to 100% solvent B at a constant flow rate of 100 nL/min.

The analyses were performed in a data-dependent acquisition mode. The top 10 or 15 most intense ions were selected for higher-energy collision-induced dissociation (HCD) and collision-induced dissociation (CID), respectively. TMT-labelled samples were analysed by HCD method with a normalised collision energy (NCE) of 40%, whereas immunoaffinity-purified samples were analysed with both CID and HCD with an NCE of 30%. Dynamic exclusion of selected ions for MS² fragmentation was 60 s and a single lock mass at m/z 445.120024 Si(CH₃)₂O)₆ (Olsen et al, 2005) was used for internal mass calibration with a target loss mass abundance of 0%. Maximal ion accumulation time allowed for MS¹ was 500 ms in the C-trap; and for MS², ion accumulation times were 50 ms in the LTQ (CID) and 200 ms in the C-trap (HCD). Overfilling of the C-trap was

prevented by automatic gain control (AGC) and set to 10^6 ions for a full FTMS scan and 5×10^5 ions for MSⁿ mode. Intact peptides were detected in the Orbitrap mass analyser at a resolution of 60,000 (CID) and 30,000 (HCD). Fragment ion resolution for HCD was 7,500. Signal threshold for triggering MS² fragmentation was 5,000 and 2,000 ion counts for HCD and CID, respectively.

6.12 Mass Spectrometry Data File Processing

Raw MS files were analysed with Proteome Discoverer version 1.4 (ThermoFisher Scientific, Waltham, MA, USA). For TMT-labelled quantitative proteomic experiment precursor and fragment ion mass tolerance were set to ± 10 ppm and ± 0.1 Da, respectively. Carbamidomethylation of cysteine residues, TMT labelling on peptide N-termini and side chain of lysines were set as a static modification, whereas methionine oxidation was set as dynamic modifications. For the immunoaffinity-purified samples, the precursor ion mass tolerance was ± 10 ppm whereas the fragment ion mass tolerance was adjusted for the appropriate MS method: ± 6 Da for CID and ± 0.02 Da for HCD. Carbamidomethylation of cysteine residues was the only fixed modification; whilst methionine oxidation, acetylation of protein N-termini and lysine side chains were set as variable modifications. Trypsin was defined as the protease with 2 and up to 4 miscleavage sites allowed for the TMT-labelled samples and immunoaffinity-purified samples, respectively. For the acetyl-enriched data, carbamidomethylation of cysteine residues was defined as a fixed modification and methionine oxidation, protein N-terminal and peptide lysine acetylation were set as variable modification. Label free peptide quantitation was performed on the MS¹ trace via area-under-the-curve integration for the acetylated peptide.

Peak lists was searched against the human SwissProt database version v2014.07_20141023 (40,984 sequences including isoforms obtained from varsplic.pl and appended known contaminants), with Mascot and MS Amanda. The percolator node of Proteome Discoverer 1.4 was utilised to remove peptides with a false discovery rate (FDR) of $>1\%$, based on the q-value after the decoy database search (Tu et al, 2015). Finally, MS spectra were manually assessed for quality to determine the threshold for excluding spectra with a poor fragmentation pattern. Based on this criterion, peptides with a Mascot and Amanda score <18 and <100 , respectively, were excluded from further data analysis. Only peptides with a high confidence, rank 1 and >6 amino acids in length were considered.

For both the proteomic and acetyl-proteomic quantitative data, additional software packages were utilised to ensure the reproducibility and quality of the peptide/protein quantitation. All PSMs corresponding to TMT-labelled peptides that passed the Proteome Discoverer filtering were extracted and re-processed via Isobar (Breitwieser et al, 2011). Isobar was primarily utilised to calculate the statistical significance of the quantitative proteomic data. Isobar software provides two P-values for each calculated ratio, *i.e.*, P-value ratio, further adjusted for FDR (q-value), and a P-value sample. Final filtering was achieved by considering the less significant of the two P-values for each protein ratio. Details of the Isobar algorithm developed for quantitative proteomic data analysis is described by Breitwieser *et al.* (Breitwieser et al, 2011).

To increase confidence in the acetyl-proteomic quantitation, Skyline 3.5 (MacLean et al, 2010) was utilised to re-assign MS¹-based peptide area-under-the-curves. Only peptides quantitated by both the Proteome Discoverer and Skyline algorithms and that were within <2-fold change of each other in quantitation were considered. Acetylated peptides identified/quantitated at least twice from the triplicate measurements were included. Due to the acetyl-enrichment step, it is possible that some of the identified acetylated peptides in the drug-treated samples are completely absent in the control samples (or *vice versa*). Therefore, acetylated peptides that were quantitated in at least two triplicates for one experimental condition but were absent in the other condition were also considered.

6.13 Data Analysis

RNA sequencing was performed in triplicates for the DMSO, TSA and RD-treated samples. After utilising a standardised pipeline for alignment via the Cufflinks package (Pertea et al, 2016), transcriptome assembly and differential expression were performed. Data was firstly filtered for significantly-altered expression between KDACi treatment compared to the DMSO control ($q < 0.05$). In addition, 1.25 fold change cut-off was applied on the data. The FC cut-off was determined by requiring that 95% of gene expression changes between the DMSO-treated biological replicates are less extreme than the cut-off (Supplementary Figure S4).

Quantitative proteomic data was analysed via Proteome Discoverer 1.4. and Isobar (Breitwieser et al, 2011) as described before. Proteins significantly altered in expression ($p < 0.05$) after KDACi treatment compared to the control were additionally filtered for the fold change difference. Similarly to the transcriptomic data, a FC cut-off of 1.1 was determined by requiring that 95% of

protein expression changes between the DMSO-treated biological replicates are less extreme than the cut-off.

Acetylated peptides were firstly identified and quantitated in each single replicate measurement. Each tandem mass spectrum was assigned to a peptide, plus the number of acetylated lysines and the area quantitated by Proteome Discoverer 1.4 and Skyline 3.5. Area-under-the-curve of 2 or 3 replicate measurements per treatment condition were averaged and a single FC value was assigned to each acetylated peptide. For the cases where the peptides were entirely absent, across all three replicates in the drug-treated or vehicle control conditions and present in at least 2 replicates of other condition, FC could not be calculated and an arbitrary FC = 2 was assigned.

Gene ontology enrichment and the overlap of the multiple data sets and comparisons thereof was assessed by the functional enrichment analysis tool FunRich v3.0 (Benito-Martin & Peinado, 2015; Pathan et al, 2015). Respective GO data was exported as an excel file and the representative graphs were readjusted in colour to match the drug-treated colour code utilised throughout the manuscript.

7. ACKNOWLEDGEMENTS

The authors would like to thank all members past and present of the Bennett, Colinge and Ellmeier laboratories. Thanks are also extended to the Superti-Furga and Kubicek laboratories for providing the Jurkat T cell line and KDAC inhibitors, respectively. We thank Branka Radić Sarikas for assistance with the IC₅₀ determinations and Jacques Colinge for advice on the experimental design and optimisation of the quantitative proteomic data analysis. Great appreciation for providing a critical input on sample preparation for the anti-acetyl-lysine immunoprecipitation experiments is directed to Petra Beli from the Institute of Molecular Biology in Mainz (Germany) and Christian Schölz from the NNF Center for Protein Research in Copenhagen (Denmark). Research in the Bennett and Kubicek laboratories is supported by the Austrian Academy of Sciences and the Austrian Federal Ministry of Science, Research and Economy, the National Foundation for Research, Technology, and Development, and the Marie Curie Career Integration Grant EPICAL.

8. AUTHOR CONTRIBUTIONS

K.L.B., A.C.M. and D.V. design the proteomic experimental part; whilst T.P., M.S. and C.B. were in charge of the transcriptomic analysis. K.B. and S.K. participated in discussion and provide a critical input to aid project development. D.V. performed sample preparation, quantitative proteomic and acetyl-proteomic LC-MSMS analyses, and RNA isolation prior to the quantitative transcriptomic analyses. A.C.M. assisted in acetyl-proteomic sample preparation. T.P. prepared the RNA libraries and performed RNA sequencing; whilst M.S. analysed the transcriptomic data. P.B. gave critical advice on sample preparation for immunoaffinity purification of acetylated peptides. E.S. assisted with FACS analysis to assess drug-induced cell apoptosis; whilst S.S. assisted in determining the cell cycle profile of the drug-treated and control Jurkat T cells. P.M. and D.V. performed the proteomic data analysis. P.M. assessed data reproducibility, and integration of the -omic data. Functional interpretation of the data was performed by D.V., P.M. and M.W.G. D.V., P.M. and K.L.B. contributed to manuscript writhing, with a final, critical, revision of the entire content by K.L.B.

9. CONFLICT OF INTEREST

The authors declare that there is no conflict of interest.

10. REFERENCES

- Alinari L, Prince CJ, Edwards RB, Towns WH, Mani R, Lehman A, Zhang X, Jarjoura D, Pan L, Kinghorn AD, Grever MR, Baiocchi RA, Lucas DM (2012) Dual targeting of the cyclin/Rb/E2F and mitochondrial pathways in mantle cell lymphoma with the translation inhibitor silvestrol. *Clinical cancer research : an official journal of the American Association for Cancer Research* **18**: 4600-4611
- Angela N, Carafa V, Conte M, Tambaro FP, Abbondanza C, Martens JH, Nees M, Benedetti R, Pallavicini I, Minucci S, Garcia-Manero G, Iovino F, Lania G, Ingenito C, Belsito Petrizzi V, Stunnenberg HG, Altucci L (2016) c-Myc modulation & acetylation is a key HDAC inhibitor target in cancer. *Clinical cancer research : an official journal of the American Association for Cancer Research*
- Baeza J, Smallegan MJ, Denu JM (2016) Mechanisms and Dynamics of Protein Acetylation in Mitochondria. *Trends Biochem Sci* **41**: 231-244
- Baradari V, Huether A, Hopfner M, Schuppan D, Scherubl H (2006) Antiproliferative and proapoptotic effects of histone deacetylase inhibitors on gastrointestinal neuroendocrine tumor cells. *Endocr Relat Cancer* **13**: 1237-1250
- Benito-Martin A, Peinado H (2015) FunRich proteomics software analysis, let the fun begin! *Proteomics* **15**: 2555-2556
- Bennett KL, Funk M, Tschernutter M, Breitwieser FP, Planyavsky M, Ubaida Mohien C, Muller A, Trajanoski Z, Colinge J, Superti-Furga G, Schmidt-Erfurth U (2011) Proteomic analysis of human cataract aqueous humour: Comparison of one-dimensional gel LCMS with two-dimensional LCMS of unlabelled and iTRAQ(R)-labelled specimens. *J Proteomics* **74**: 151-166
- Blomen VA, Majek P, Jae LT, Bigenzahn JW, Nieuwenhuis J, Staring J, Sacco R, van Diemen FR, Olk N, Stukalov A, Marceau C, Janssen H, Carette JE, Bennett KL, Colinge J, Superti-Furga G, Brummelkamp TR (2015) Gene essentiality and synthetic lethality in haploid human cells. *Science*
- Bolden JE, Peart MJ, Johnstone RW (2006) Anticancer activities of histone deacetylase inhibitors. *Nat Rev Drug Discov* **5**: 769-784

- Boucheron N, Tschismarov R, Goeschl L, Moser MA, Lagger S, Sakaguchi S, Winter M, Lenz F, Vitko D, Breitwieser FP, Muller L, Hassan H, Bennett KL, Colinge J, Schreiner W, Egawa T, Taniuchi I, Matthias P, Seiser C, Ellmeier W (2014) CD4(+) T cell lineage integrity is controlled by the histone deacetylases HDAC1 and HDAC2. *Nat Immunol* **15**: 439-448
- Breitwieser FP, Muller A, Dayon L, Kocher T, Hainard A, Pichler P, Schmidt-Erfurth U, Superti-Furga G, Sanchez JC, Mechtler K, Bennett KL, Colinge J (2011) General statistical modeling of data from protein relative expression isobaric tags. *J Proteome Res* **10**: 2758-2766
- Brownell JE, Zhou J, Ranalli T, Kobayashi R, Edmondson DG, Roth SY, Allis CD (1996) Tetrahymena histone acetyltransferase A: a homolog to yeast Gcn5p linking histone acetylation to gene activation. *Cell* **84**: 843-851
- Choudhary C, Kumar C, Gnad F, Nielsen ML, Rehman M, Walther TC, Olsen JV, Mann M (2009) Lysine acetylation targets protein complexes and co-regulates major cellular functions. *Science* **325**: 834-840
- Choudhary C, Weinert BT, Nishida Y, Verdin E, Mann M (2014) The growing landscape of lysine acetylation links metabolism and cell signalling. *Nat Rev Mol Cell Biol* **15**: 536-550
- Evertts AG, Zee BM, Dimaggio PA, Gonzales-Cope M, Collier HA, Garcia BA (2013) Quantitative Dynamics of the Link Between Cellular Metabolism and Histone Acetylation. *J Biol Chem*
- Finzer P, Krueger A, Stohr M, Brenner D, Soto U, Kuntzen C, Krammer PH, Rosl F (2004) HDAC inhibitors trigger apoptosis in HPV-positive cells by inducing the E2F-p73 pathway. *Oncogene* **23**: 4807-4817
- Gu W, Roeder RG (1997) Activation of p53 sequence-specific DNA binding by acetylation of the p53 C-terminal domain. *Cell* **90**: 595-606
- Hanss J, Moore GE (1964) Studies of Culture Media for the Growth of Human Tumor Cells. *Exp Cell Res* **34**: 243-256
- Inoue S, MacFarlane M, Harper N, Wheat LM, Dyer MJ, Cohen GM (2004) Histone deacetylase inhibitors potentiate TNF-related apoptosis-inducing ligand (TRAIL)-induced apoptosis in lymphoid malignancies. *Cell Death Differ* **11 Suppl 2**: S193-206
- Kim D, Pertea G, Trapnell C, Pimentel H, Kelley R, Salzberg SL (2013) TopHat2: accurate alignment of transcriptomes in the presence of insertions, deletions and gene fusions. *Genome Biol* **14**: R36

- Li L, Fan B, Zhang LH, Xing XF, Cheng XJ, Wang XH, Guo T, Du H, Wen XZ, Ji JF (2016) Trichostatin A potentiates TRAIL-induced antitumor effects via inhibition of ERK/FOXO1 pathway in gastric cancer. *Tumour Biol*
- Mackmull MT, Iskar M, Parca L, Singer S, Bork P, Ori A, Beck M (2015) Histone Deacetylase Inhibitors (HDACi) Cause the Selective Depletion of Bromodomain Containing Proteins (BCPs). *Molecular & cellular proteomics : MCP* **14**: 1350-1360
- MacLean B, Tomazela DM, Shulman N, Chambers M, Finney GL, Frewen B, Kern R, Tabb DL, Liebler DC, MacCoss MJ (2010) Skyline: an open source document editor for creating and analyzing targeted proteomics experiments. *Bioinformatics* **26**: 966-968
- Manza LL, Stamer SL, Ham AJ, Codreanu SG, Liebler DC (2005) Sample preparation and digestion for proteomic analyses using spin filters. *Proteomics* **5**: 1742-1745
- Marks PA, Richon VM, Rifkind RA (2000) Histone deacetylase inhibitors: inducers of differentiation or apoptosis of transformed cells. *J Natl Cancer Inst* **92**: 1210-1216
- Minucci S, Pelicci PG (2006) Histone deacetylase inhibitors and the promise of epigenetic (and more) treatments for cancer. *Nat Rev Cancer* **6**: 38-51
- Morales JC, Ruiz-Magana MJ, Carranza D, Ortiz-Ferron G, Ruiz-Ruiz C (2010) HDAC inhibitors with different gene regulation activities depend on the mitochondrial pathway for the sensitization of leukemic T cells to TRAIL-induced apoptosis. *Cancer Lett* **297**: 91-100
- Olsen JV, de Godoy LM, Li G, Macek B, Mortensen P, Pesch R, Makarov A, Lange O, Horning S, Mann M (2005) Parts per million mass accuracy on an Orbitrap mass spectrometer via lock mass injection into a C-trap. *Mol Cell Proteomics* **4**: 2010-2021
- Ononye SN, van Heyst M, Falcone EM, Anderson AC, Wright DL (2012) Toward isozyme-selective inhibitors of histone deacetylase as therapeutic agents for the treatment of cancer. *Pharm Pat Anal* **1**: 207-221
- Pathan M, Keerthikumar S, Ang CS, Gangoda L, Quek CY, Williamson NA, Mouradov D, Sieber OM, Simpson RJ, Salim A, Bacic A, Hill AF, Stroud DA, Ryan MT, Agbinya JI, Mariadason JM, Burgess AW, Mathivanan S (2015) FunRich: An open access standalone functional enrichment and interaction network analysis tool. *Proteomics* **15**: 2597-2601
- Pertea M, Kim D, Pertea GM, Leek JT, Salzberg SL (2016) Transcript-level expression analysis of RNA-seq experiments with HISAT, StringTie and Ballgown. *Nat Protoc* **11**: 1650-1667

- Piperno G, LeDizet M, Chang XJ (1987) Microtubules containing acetylated alpha-tubulin in mammalian cells in culture. *J Cell Biol* **104**: 289-302
- Rosato RR, Almenara JA, Grant S (2003) The histone deacetylase inhibitor MS-275 promotes differentiation or apoptosis in human leukemia cells through a process regulated by generation of reactive oxygen species and induction of p21CIP1/WAF1 1. *Cancer Res* **63**: 3637-3645
- Schlosser A, Thomsen T, Moeller JB, Nielsen O, Tornøe I, Mollenhauer J, Moestrup SK, Holmskov U (2009) Characterization of FIBCD1 as an acetyl group-binding receptor that binds chitin. *J Immunol* **183**: 3800-3809
- Scholz C, Weinert BT, Wagner SA, Beli P, Miyake Y, Qi J, Jensen LJ, Streicher W, McCarthy AR, Westwood NJ, Lain S, Cox J, Matthias P, Mann M, Bradner JE, Choudhary C (2015) Acetylation site specificities of lysine deacetylase inhibitors in human cells. *Nat Biotech* **advance online publication**
- Shankar S, Singh TR, Fandy TE, Luetrakul T, Ross DD, Srivastava RK (2005) Interactive effects of histone deacetylase inhibitors and TRAIL on apoptosis in human leukemia cells: involvement of both death receptor and mitochondrial pathways. *Int J Mol Med* **16**: 1125-1138
- Shao Y, Gao Z, Marks PA, Jiang X (2004) Apoptotic and autophagic cell death induced by histone deacetylase inhibitors. *Proc Natl Acad Sci U S A* **101**: 18030-18035
- Simon RP, Robaa D, Alhalabi Z, Sippl W, Jung M (2016) KATching-Up on Small Molecule Modulators of Lysine Acetyltransferases. *J Med Chem* **59**: 1249-1270
- Subbannayya Y, Pinto SM, Gowda H, Prasad TS (2016) Proteogenomics for understanding oncology: recent advances and future prospects. *Expert review of proteomics*: 1-12
- Sung ES, Kim A, Park JS, Chung J, Kwon MH, Kim YS (2010) Histone deacetylase inhibitors synergistically potentiate death receptor 4-mediated apoptotic cell death of human T-cell acute lymphoblastic leukemia cells. *Apoptosis* **15**: 1256-1269
- Takahata S, Yu Y, Stillman DJ (2009) The E2F functional analogue SBF recruits the Rpd3(L) HDAC, via Whi5 and Stb1, and the FACT chromatin reorganizer, to yeast G1 cyclin promoters. *Embo J* **28**: 3378-3389
- Tao R, de Zoeten EF, Ozkaynak E, Chen C, Wang L, Porrett PM, Li B, Turka LA, Olson EN, Greene MI, Wells AD, Hancock WW (2007) Deacetylase inhibition promotes the generation and function of regulatory T cells. *Nat Med* **13**: 1299-1307

- Taunton J, Hassig CA, Schreiber SL (1996) A mammalian histone deacetylase related to the yeast transcriptional regulator Rpd3p. *Science* **272**: 408-411
- Telles E, Seto E (2012) Modulation of cell cycle regulators by HDACs. *Front Biosci (Schol Ed)* **4**: 831-839
- Trapnell C, Hendrickson DG, Sauvageau M, Goff L, Rinn JL, Pachter L (2013) Differential analysis of gene regulation at transcript resolution with RNA-seq. *Nat Biotechnol* **31**: 46-53
- Tu C, Sheng Q, Li J, Ma D, Shen X, Wang X, Shyr Y, Yi Z, Qu J (2015) Optimization of Search Engines and Postprocessing Approaches to Maximize Peptide and Protein Identification for High-Resolution Mass Data. *J Proteome Res* **14**: 4662-4673
- Vizcaino JA, Deutsch EW, Wang R, Csordas A, Reisinger F, Rios D, Dienes JA, Sun Z, Farrah T, Bandeira N, Binz PA, Xenarios I, Eisenacher M, Mayer G, Gatto L, Campos A, Chalkley RJ, Kraus HJ, Albar JP, Martinez-Bartolome S, Apweiler R, Omenn GS, Martens L, Jones AR, Hermjakob H (2014) ProteomeXchange provides globally coordinated proteomics data submission and dissemination. *Nat Biotechnol* **32**: 223-226
- Weinert BT, Wagner SA, Horn H, Henriksen P, Liu WR, Olsen JV, Jensen LJ, Choudhary C (2011a) Proteome-wide mapping of the Drosophila acetylome demonstrates a high degree of conservation of lysine acetylation. *Science signaling* **4**: ra48
- Weinert BT, Wagner SA, Horn H, Henriksen P, Liu WR, Olsen JV, Jensen LJ, Choudhary C (2011b) Proteome-wide mapping of the Drosophila acetylome demonstrates a high degree of conservation of lysine acetylation. *Sci Signal* **4**: ra48
- Wisniewski JR, Zougman A, Nagaraj N, Mann M (2009) Universal sample preparation method for proteome analysis. *Nat Methods* **6**: 359-362
- Woo YH, Li WH (2012) Evolutionary conservation of histone modifications in mammals. *Mol Biol Evol* **29**: 1757-1767
- Zhang J, Zhong Q (2014) Histone deacetylase inhibitors and cell death. *Cell Mol Life Sci*
- Zhang W, Ji W, Liu X, Ouyang G, Xiao W (2014) ELL inhibits E2F1 transcriptional activity by enhancing E2F1 deacetylation via recruitment of histone deacetylase 1. *Mol Cell Biol* **34**: 765-775

11. FIGURES

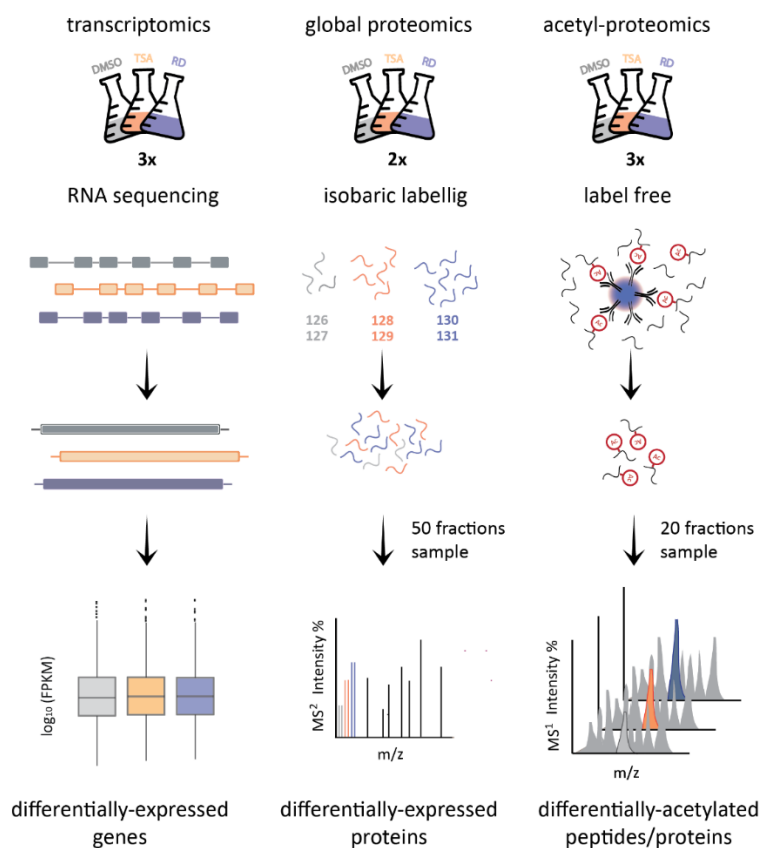
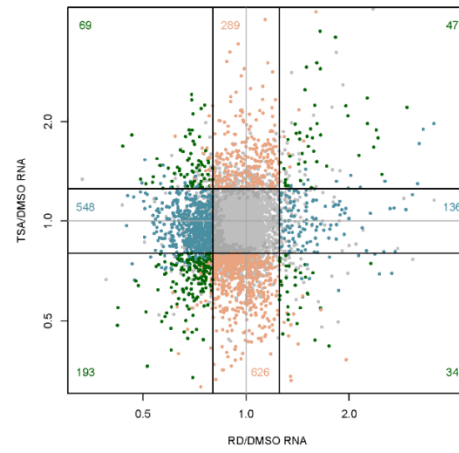
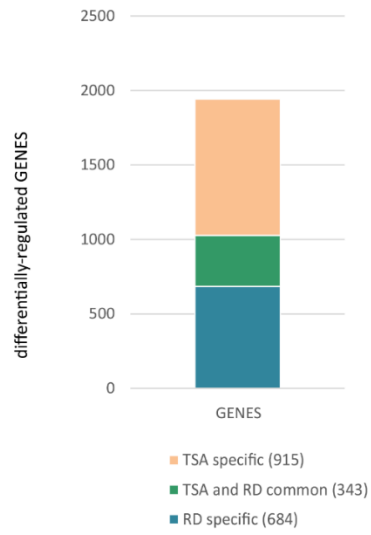
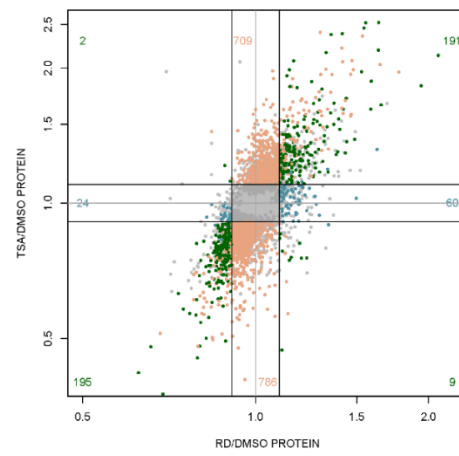
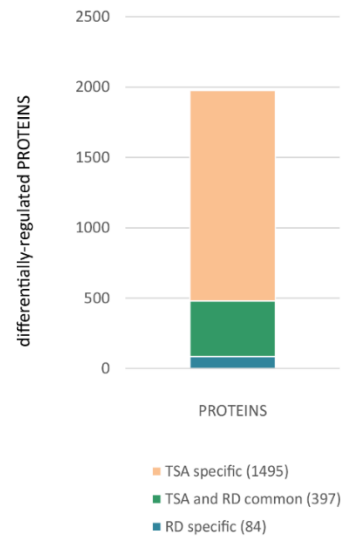


Figure 1. Systems Biology Workflow. Schematic representation of transcriptomic, proteomic and acetyl-proteomic experimental workflow comparing the number of replicates and crucial steps in the sample preparation procedure. In each approach, Jurkat T cells were treated with 0.1% DMSO (control), the pre-determined IC_{50} concentration of KDACi for 24 h. Transcriptomic and acetyl-proteomic data were collected from triplicates; whilst for the more reproducible global proteomic approach duplicates were sufficient. Changes in gene expression were assessed via RNA sequencing and quantitatively assigned to respective FPKM values. Differential protein expression was achieved by isobaric labelling of separately digested proteins (TMT) and MS^2 -based relative quantitation of reporter ions. Lastly, proteins that were altered in acetylation were digested, enriched by immunoprecipitation with anti-acetyl lysine antibody, and quantitated utilising a label-free MS^1 -based approach. Due to the amount and complexity of the sample mixture, both protein samples were pre-fractionated, and each fraction was subsequently analysed by LC-MSMS. DMSO, dimethylsulfoxide; FPKM, fragment per kilobase million; KDACi, lysine deacetylase inhibitor; RD, romidepsin; TSA, trichostatin A.

A**B**

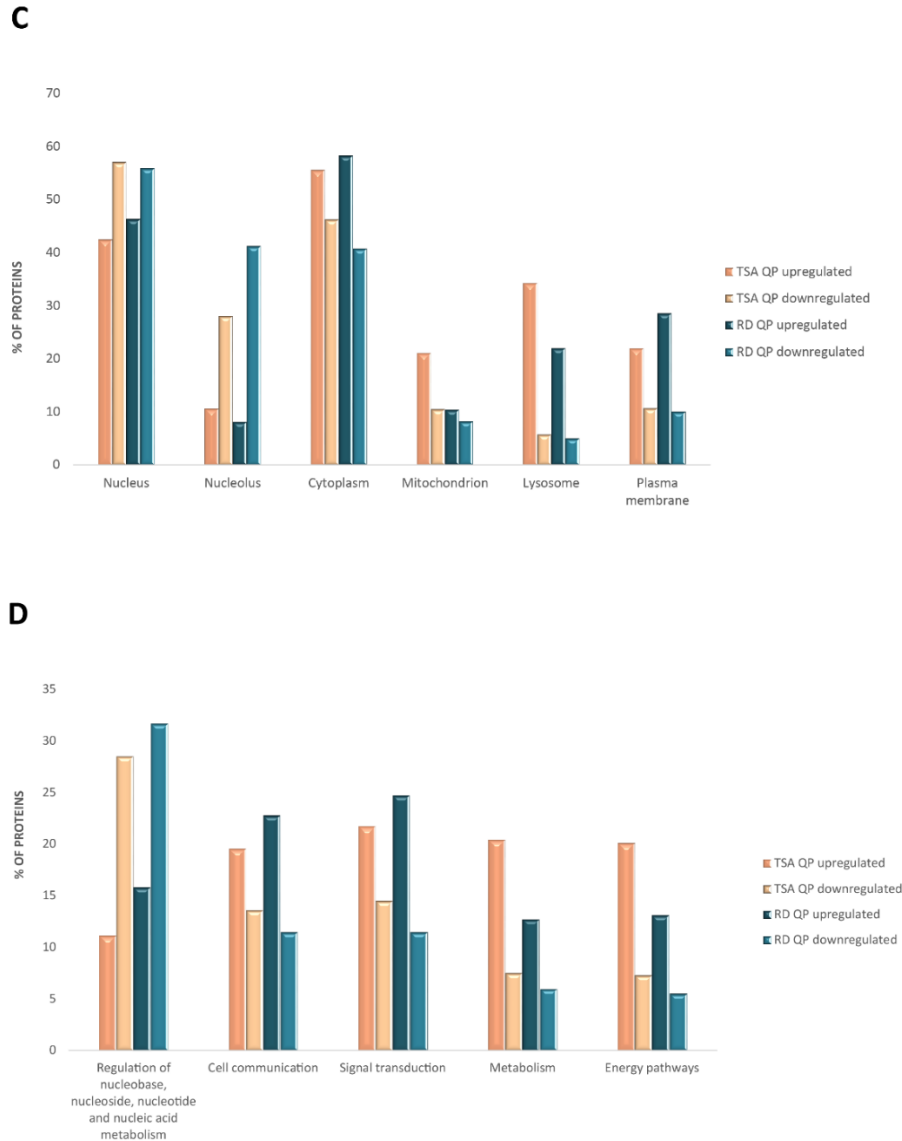


Figure 2. KDACi-induced Alterations in mRNA and Protein Abundance. TSA and RD treatment-induced alteration in (A) gene and (B) protein expression compared to the DMSO control. Left, the overall number of KDACi-specific and common differentially-regulated transcripts and proteins; right, correlation between the drug-treatments. Numbers in each corner represent significantly-altered genes ($q < 0.05$, relative FC ≥ 1.25 and $\leq 1/1.25$) and proteins ($q < 0.05$, relative FC ≥ 1.1 and $\leq 1/1.1$) colour-coded according to the corresponding bar graph (left). FunRich-based annotation of TSA- and RD-enriched proteins that are altered in expression according to (C) cellular localisation and (D) biological processes. DMSO, dimethylsulfoxide; KDACi, lysine deacetylase inhibitor; RD, romidepsin; TSA, trichostatin A.

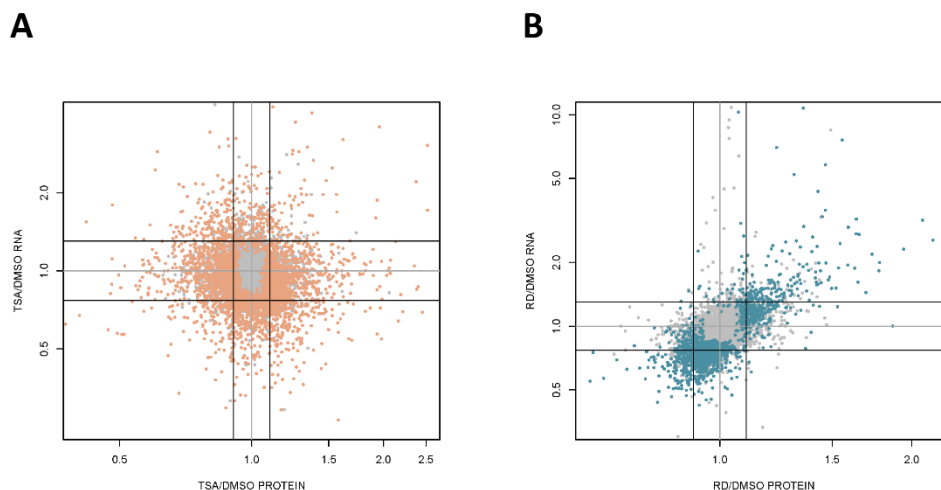


Figure 3. Correlation of the Transcriptomic and Proteomic Changes after KDACi Treatment.

Relative changes in protein and mRNA abundances were aligned for (A) TSA and (B) RD treatment. Changes at the transcriptional and (post)-translational level were plotted as a fold change (FC) compared to the DMSO-treated control. RD, KDACi that preferentially inhibits nuclear KDACs, regulated gene transcription that correlated with changes at the protein level ($R = 0.43$). This indicates that the alteration of the protein abundances is mostly due to respective changes of gene activation/repression. TSA treatment showed no correlation between altered proteins and transcripts ($R = 0.01$), suggesting a mechanistically different effect on protein abundance compared to RD. Cut-off for differentially-expressed proteins: $FC \geq 1.1$ and $\leq 1/1.1$, $q < 0.05$; transcriptional-relevant changes: $FC \geq 1.25$ and $\leq 1/1.1$, $q < 0.05$. DMSO, dimethylsulfoxide; KDACi, lysine deacetylase inhibitor; RD, romidepsin; TSA, trichostatin A.

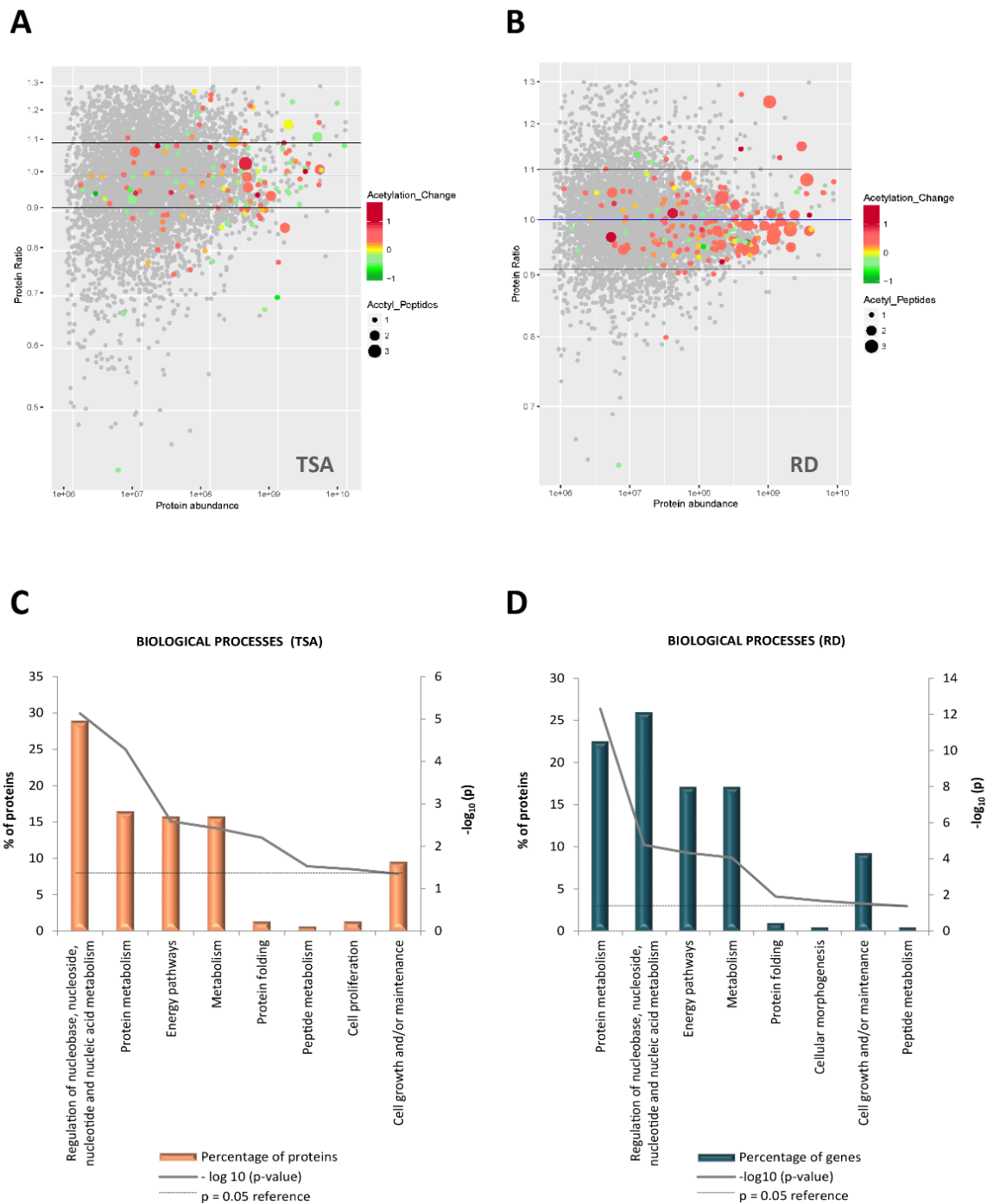


Figure 4. Mapping KDACi-mediated Acetylation Changes to Protein Absolute and Relative Expression. Protein changes in relative abundance after TSA (A) and RD (B) treatment were plotted against the absolute protein abundance. Coloured dots represent acetylated proteins after the respective drug treatment; increase (green) or decrease (red) in

acetylation relative to the DMSO control. Acetylated proteins that were identified but remained unaltered in acetylation regardless of the treatment (yellow). In addition, bubble size represents the number of acetylated peptides. Absolute protein abundance was assessed by the top3 quantitation method and a relative FC cut-off equal or greater than 1.1 for both the global and acetyl-proteomic experiments. Biological processes affected by acetylation changes upon (C) TSA and (D) RD treatment. Histone proteins were not considered for the functional analysis; whilst changes in non-histone acetylation were filtered according to the protein expression data. KDACi; lysine deacetylase inhibitor; RD, romidepsin; TSA, trichostatin A.

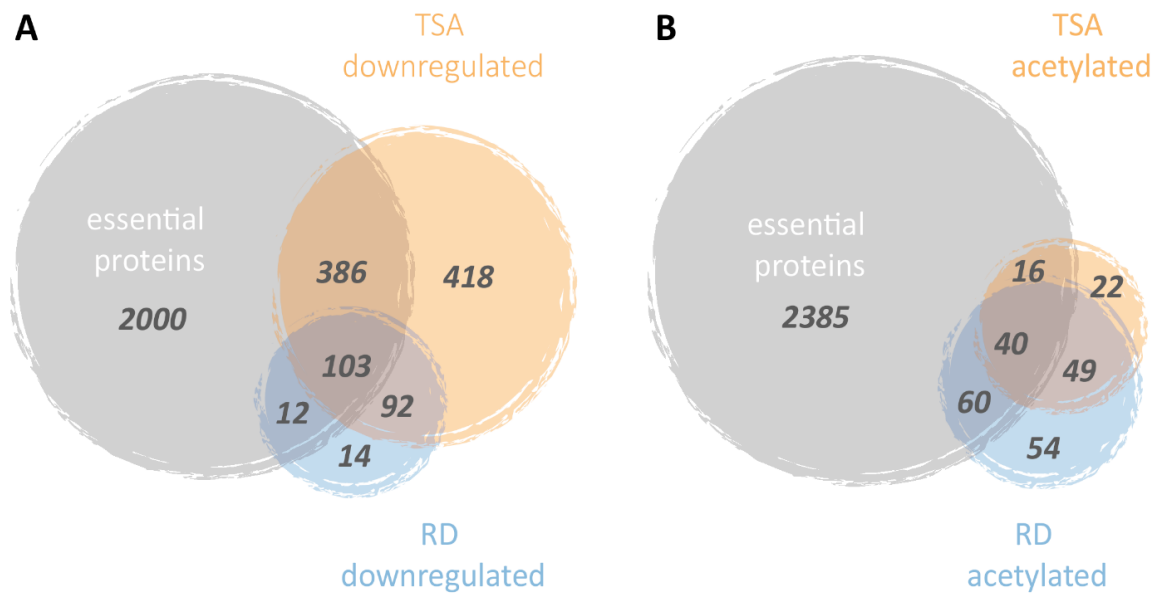


Figure 5. KDACi-mediated Changes in Abundance and Acetylation of the Proteins Essential for Cell Survival. (A) TSA- and RD-specific *essentiality* of downregulated proteins and (B) TSA- and RD-specific *essentiality* of differentially-acetylated proteins. (A) Proteins that were downregulated after TSA and RD treatment (compared to the DMSO control) were intersected with the pool of genes/proteins determined as essential for cell proliferation and survival. Both drugs downregulated 103 *essential* proteins; whilst additional 386 and 12 were specifically decreased in expression after TSA and RD treatment, respectively. For both drug treatments, only downregulated proteins with a $FC \leq 1/1.1$ relative to DMSO and a $q < 0.05$ were considered. (B) Intersection of the proteins altered in acetylation after the indicated drug treatments with the proteins essential for cell survival. In total, TSA- and RD mediated acetylation changes on 56 and 100 *essential* proteins, respectively. Forty *essential* proteins were differentially-acetylated by both treatments compared to the DMSO. DMSO, dimethylsulfoxide; FC, fold change; RD, romidepsin; TSA, trichostatin A.

A scatter plot showing the relationship between protein abundance (x-axis, log scale from 1e+06 to 1e+10) and protein ratio (y-axis, linear scale from 0.5 to 1.3). The plot is divided into three horizontal regions by two lines at y ≈ 0.92 and y ≈ 1.08. Proteins are represented by circles of varying sizes, where the size indicates the number of acetylated peptides (1, 2, or 3). The color of the circles represents the acetylation change, ranging from green (-1) to red (1). Numerous proteins are labeled, including MYC, NAA30, BRPF1, PHF20, BRD8, ANAPC7, SMNDC1, COX17, IKZF1, CNBP, GART, BCLAF1, RRP15, RBM10, EXOSC8, EIF2B3, CTGF, CTCT, CTCT2, CTCT3, CTCT4, CTCT5, CTCT6, CTCT7, CTCT8, CTCT9, CTCT10, CTCT11, CTCT12, CTCT13, CTCT14, CTCT15, CTCT16, CTCT17, CTCT18, CTCT19, CTCT20, CTCT21, CTCT22, CTCT23, CTCT24, CTCT25, CTCT26, CTCT27, CTCT28, CTCT29, CTCT30, CTCT31, CTCT32, CTCT33, CTCT34, CTCT35, CTCT36, CTCT37, CTCT38, CTCT39, CTCT40, CTCT41, CTCT42, CTCT43, CTCT44, CTCT45, CTCT46, CTCT47, CTCT48, CTCT49, CTCT50, CTCT51, CTCT52, CTCT53, CTCT54, CTCT55, CTCT56, CTCT57, CTCT58, CTCT59, CTCT60, CTCT61, CTCT62, CTCT63, CTCT64, CTCT65, CTCT66, CTCT67, CTCT68, CTCT69, CTCT70, CTCT71, CTCT72, CTCT73, CTCT74, CTCT75, CTCT76, CTCT77, CTCT78, CTCT79, CTCT80, CTCT81, CTCT82, CTCT83, CTCT84, CTCT85, CTCT86, CTCT87, CTCT88, CTCT89, CTCT90, CTCT91, CTCT92, CTCT93, CTCT94, CTCT95, CTCT96, CTCT97, CTCT98, CTCT99, CTCT100, CTCT101, CTCT102, CTCT103, CTCT104, CTCT105, CTCT106, CTCT107, CTCT108, CTCT109, CTCT110, CTCT111, CTCT112, CTCT113, CTCT114, CTCT115, CTCT116, CTCT117, CTCT118, CTCT119, CTCT120, CTCT121, CTCT122, CTCT123, CTCT124, CTCT125, CTCT126, CTCT127, CTCT128, CTCT129, CTCT130, CTCT131, CTCT132, CTCT133, CTCT134, CTCT135, CTCT136, CTCT137, CTCT138, CTCT139, CTCT140, CTCT141, CTCT142, CTCT143, CTCT144, CTCT145, CTCT146, CTCT147, CTCT148, CTCT149, CTCT150, CTCT151, CTCT152, CTCT153, CTCT154, CTCT155, CTCT156, CTCT157, CTCT158, CTCT159, CTCT160, CTCT161, CTCT162, CTCT163, CTCT164, CTCT165, CTCT166, CTCT167, CTCT168, CTCT169, CTCT170, CTCT171, CTCT172, CTCT173, CTCT174, CTCT175, CTCT176, CTCT177, CTCT178, CTCT179, CTCT180, CTCT181, CTCT182, CTCT183, CTCT184, CTCT185, CTCT186, CTCT187, CTCT188, CTCT189, CTCT190, CTCT191, CTCT192, CTCT193, CTCT194, CTCT195, CTCT196, CTCT197, CTCT198, CTCT199, CTCT200, CTCT201, CTCT202, CTCT203, CTCT204, CTCT205, CTCT206, CTCT207, CTCT208, CTCT209, CTCT210, CTCT211, CTCT212, CTCT213, CTCT214, CTCT215, CTCT216, CTCT217, CTCT218, CTCT219, CTCT220, CTCT221, CTCT222, CTCT223, CTCT224, CTCT225, CTCT226, CTCT227, CTCT228, CTCT229, CTCT230, CTCT231, CTCT232, CTCT233, CTCT234, CTCT235, CTCT236, CTCT237, CTCT238, CTCT239, CTCT240, CTCT241, CTCT242, CTCT243, CTCT244, CTCT245, CTCT246, CTCT247, CTCT248, CTCT249, CTCT250, CTCT251, CTCT252, CTCT253, CTCT254, CTCT255, CTCT256, CTCT257, CTCT258, CTCT259, CTCT260, CTCT261, CTCT262, CTCT263, CTCT264, CTCT265, CTCT266, CTCT267, CTCT268, CTCT269, CTCT270, CTCT271, CTCT272, CTCT273, CTCT274, CTCT275, CTCT276, CTCT277, CTCT278, CTCT279, CTCT280, CTCT281, CTCT282, CTCT283, CTCT284, CTCT285, CTCT286, CTCT287, CTCT288, CTCT289, CTCT290, CTCT291, CTCT292, CTCT293, CTCT294, CTCT295, CTCT296, CTCT297, CTCT298, CTCT299, CTCT300, CTCT301, CTCT302, CTCT303, CTCT304, CTCT305, CTCT306, CTCT307, CTCT308, CTCT309, CTCT310, CTCT311, CTCT312, CTCT313, CTCT314, CTCT315, CTCT316, CTCT317, CTCT318, CTCT319, CTCT320, CTCT321, CTCT322, CTCT323, CTCT324, CTCT325, CTCT326, CTCT327, CTCT328, CTCT329, CTCT330, CTCT331, CTCT332, CTCT333, CTCT334, CTCT335, CTCT336, CTCT337, CTCT338, CTCT339, CTCT340, CTCT341, CTCT342, CTCT343, CTCT344, CTCT345, CTCT346, CTCT347, CTCT348, CTCT349, CTCT350, CTCT351, CTCT352, CTCT353, CTCT354, CTCT355, CTCT356, CTCT357, CTCT358, CTCT359, CTCT360, CTCT361, CTCT362, CTCT363, CTCT364, CTCT365, CTCT366, CTCT367, CTCT368, CTCT369, CTCT370, CTCT371, CTCT372, CTCT373, CTCT374, CTCT375, CTCT376, CTCT377, CTCT378, CTCT379, CTCT380, CTCT381, CTCT382, CTCT383, CTCT384, CTCT385, CTCT386, CTCT387, CTCT388, CTCT389, CTCT390, CTCT391, CTCT392, CTCT393, CTCT394, CTCT395, CTCT396, CTCT397, CTCT398, CTCT399, CTCT400, CTCT401, CTCT402, CTCT403, CTCT404, CTCT405, CTCT406, CTCT407, CTCT408, CTCT409, CTCT410, CTCT411, CTCT412, CTCT413, CTCT414, CTCT415, CTCT416, CTCT417, CTCT418, CTCT419, CTCT420, CTCT421, CTCT422, CTCT423, CTCT424, CTCT425, CTCT426, CTCT427, CTCT428, CTCT429, CTCT430, CTCT431, CTCT432, CTCT433, CTCT434, CTCT435, CTCT436, CTCT437, CTCT438, CTCT439, CTCT440, CTCT441, CTCT442, CTCT443, CTCT444, CTCT445, CTCT446, CTCT447, CTCT448, CTCT449, CTCT450, CTCT451, CTCT452, CTCT453, CTCT454, CTCT455, CTCT456, CTCT457, CTCT458, CTCT459, CTCT460, CTCT461, CTCT462, CTCT463, CTCT464, CTCT465, CTCT466, CTCT467, CTCT468, CTCT469, CTCT470, CTCT471, CTCT472, CTCT473, CTCT474, CTCT475, CTCT476, CTCT477, CTCT478, CTCT479, CTCT480, CTCT481, CTCT482, CTCT483, CTCT484, CTCT485, CTCT486, CTCT487, CTCT488, CTCT489, CTCT490, CTCT491, CTCT492, CTCT493, CTCT494, CTCT495, CTCT496, CTCT497, CTCT498, CTCT499, CTCT500, CTCT501, CTCT502, CTCT503, CTCT504, CTCT505, CTCT506, CTCT507, CTCT508, CTCT509, CTCT510, CTCT511, CTCT512, CTCT513, CTCT514, CTCT515, CTCT516, CTCT517, CTCT518, CTCT519, CTCT520, CTCT521, CTCT522, CTCT523, CTCT524, CTCT525, CTCT526, CTCT527, CTCT528, CTCT529, CTCT530, CTCT531, CTCT532, CTCT533, CTCT534, CTCT535, CTCT536, CTCT537, CTCT538, CTCT539, CTCT540, CTCT541, CTCT542, CTCT543, CTCT544, CTCT545, CTCT546, CTCT547, CTCT548, CTCT549, CTCT550, CTCT551, CTCT552, CTCT553, CTCT554, CTCT555, CTCT556, CTCT557, CTCT558, CTCT559, CTCT560, CTCT561, CTCT562, CTCT563, CTCT564, CTCT565, CTCT566, CTCT567, CTCT568, CTCT569, CTCT570, CTCT571, CTCT572, CTCT573, CTCT574, CTCT575, CTCT576, CTCT577, CTCT578, CTCT579, CTCT580, CTCT581, CTCT582, CTCT583, CTCT584, CTCT585, CTCT586, CTCT587, CTCT588, CTCT589, CTCT590, CTCT591, CTCT592, CTCT593, CTCT594, CTCT595, CTCT596, CTCT597, CTCT598, CTCT599, CTCT600, CTCT601, CTCT602, CTCT603, CTCT604, CTCT605, CTCT606, CTCT607, CTCT608, CTCT609, CTCT610, CTCT611, CTCT612, CTCT613, CTCT614, CTCT615, CTCT616, CTCT617, CTCT618, CTCT619, CTCT620, CTCT621, CTCT622, CTCT623, CTCT624, CTCT625, CTCT626, CTCT627, CTCT628, CTCT629, CTCT630, CTCT631, CTCT632, CTCT633, CTCT634, CTCT635, CTCT636, CTCT637, CTCT638, CTCT639, CTCT640, CTCT641, CTCT642, CTCT643, CTCT644, CTCT645, CTCT646, CTCT647, CTCT648, CTCT649, CTCT650, CTCT651, CTCT652, CTCT653, CTCT654, CTCT655, CTCT656, CTCT657, CTCT658, CTCT659, CTCT660, CTCT661, CTCT662, CTCT66

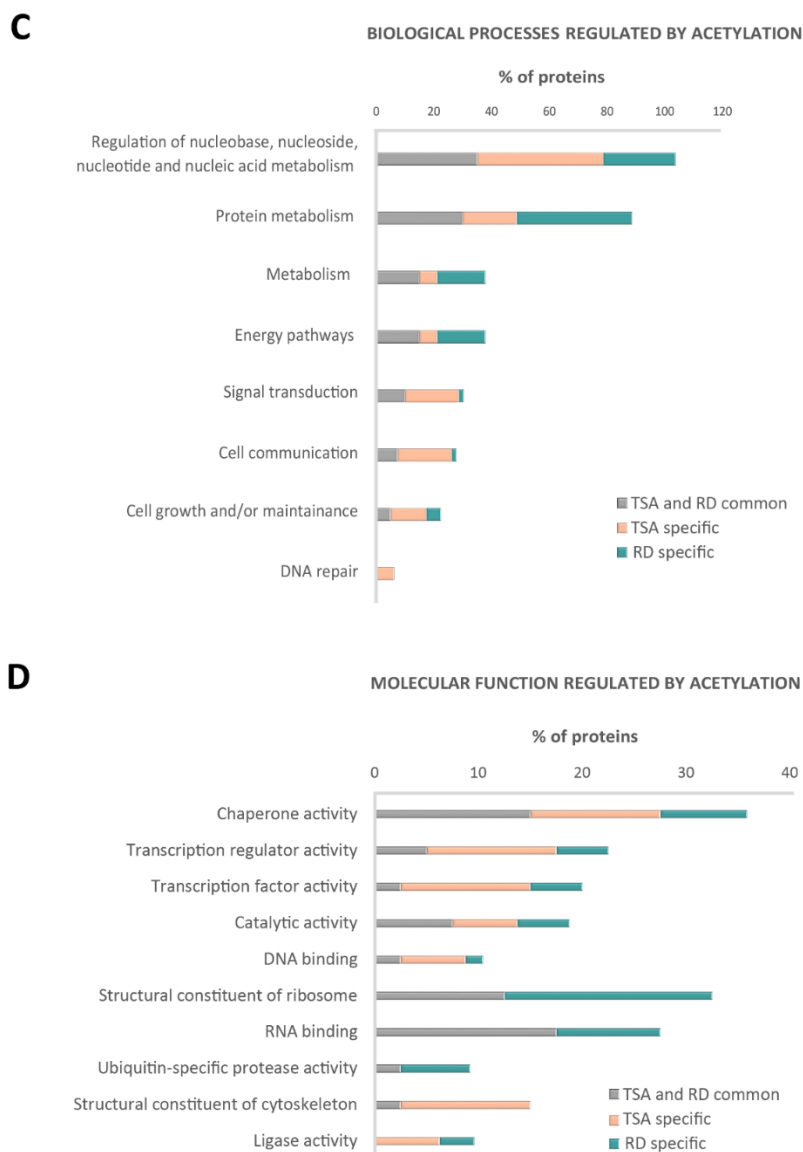
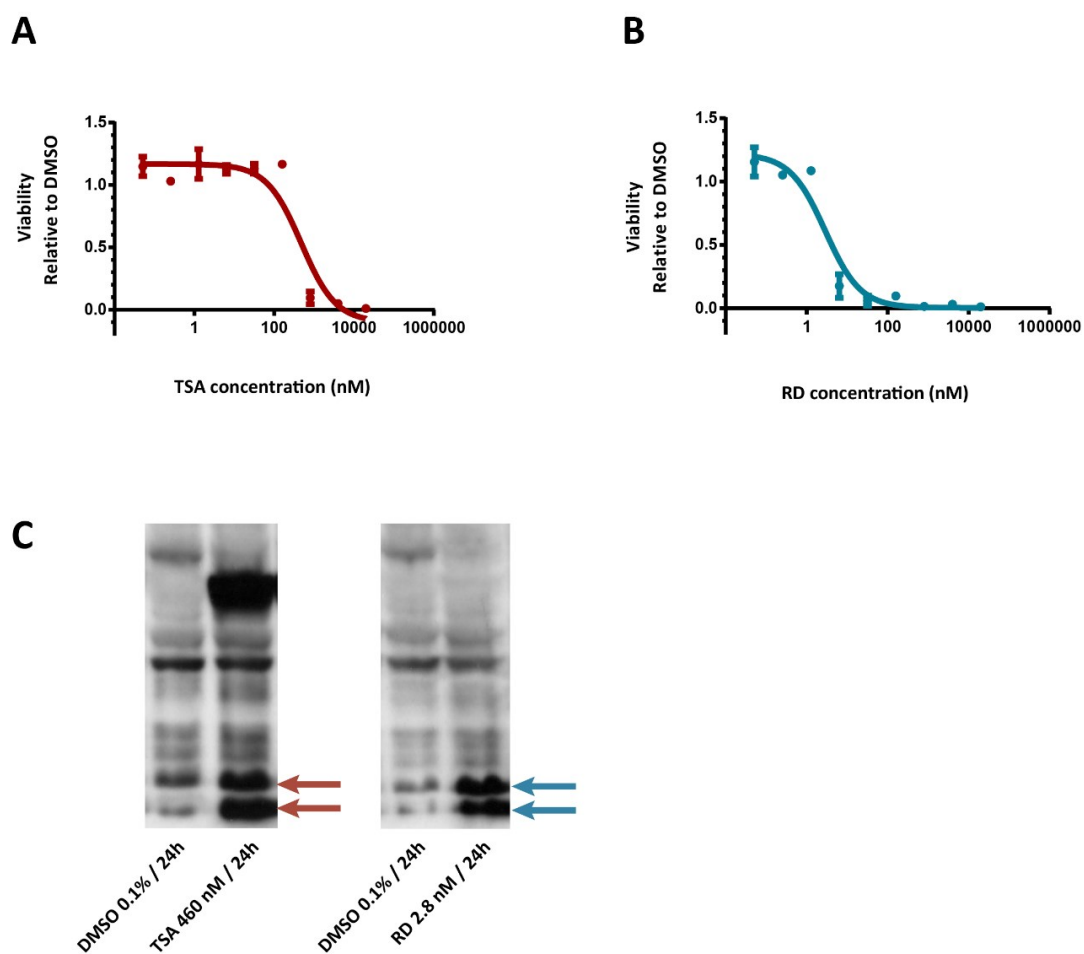


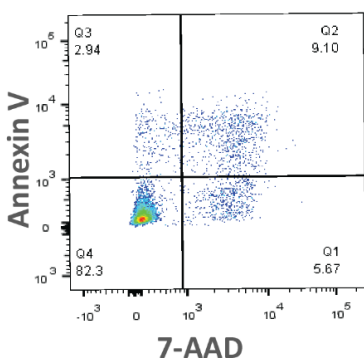
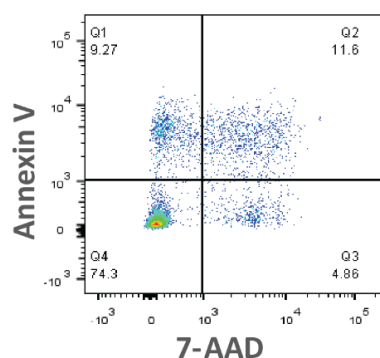
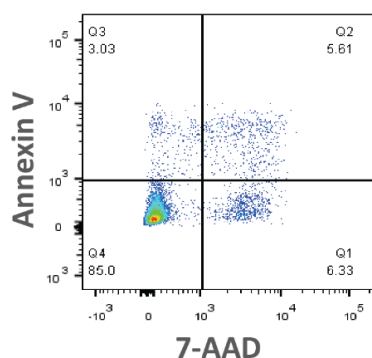
Figure 6. Differences in Specific Acetylation Changes in Proteins Essential for Survival after TSA and RD Treatment.

Essential proteins with altered acetylation after (A) TSA and (B) RD treatment. To distinguish KDACi-specific acetylation changes, proteins that are uniquely altered in acetylation by one of the drug are coloured in red or green, depending whether there is an increase or decrease in acetylation, respectively. *Essential* proteins altered in acetylation that were shared between the two drug treatments are depicted in black. (C) biological processes and (D) molecular function of the *essential* proteins uniquely-altered in acetylation after treatment with TSA (orange) and RD (blue), or both KDACis (grey). DMSO, dimethylsulfoxide; FC, fold change; RD, romidepsin; TSA, trichostatin A.

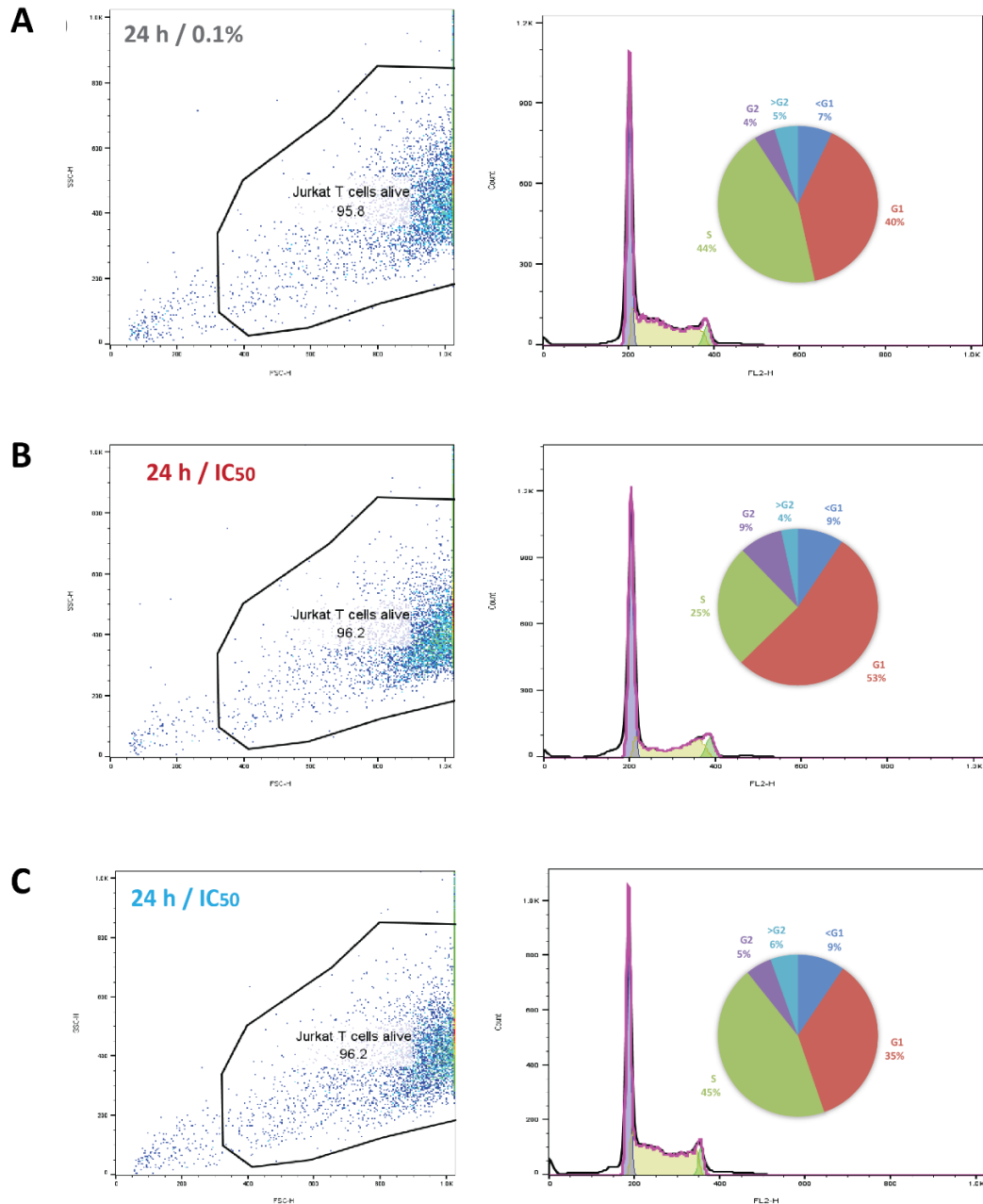
12. SUPPLEMENTARY FIGURES



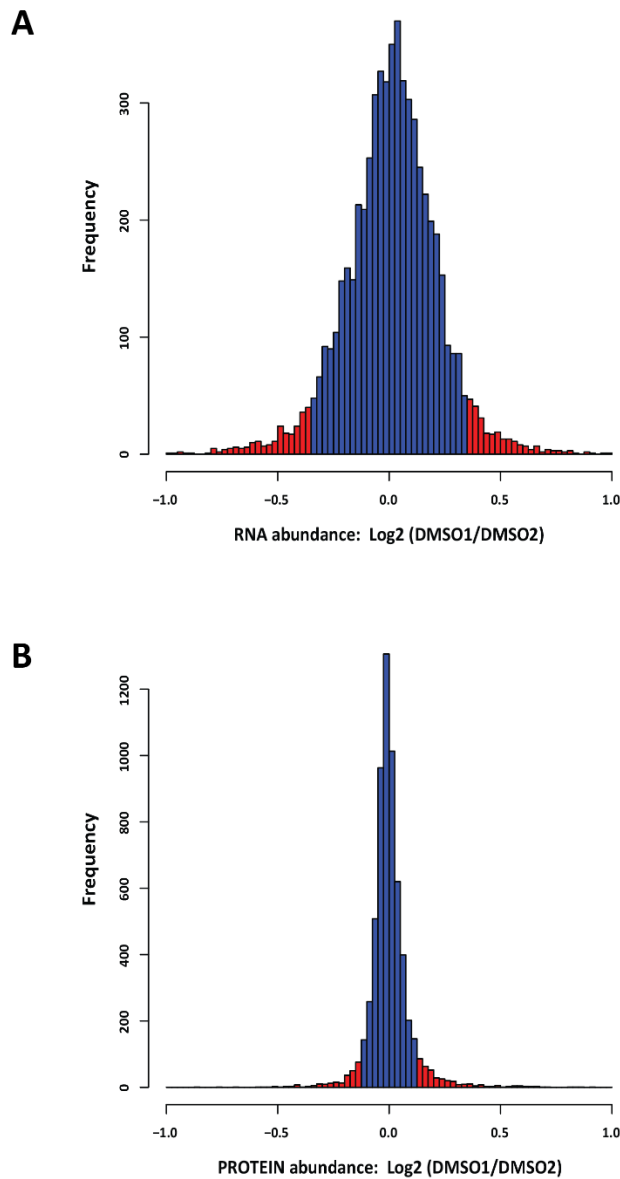
Supplementary Figure S1. Cell Viability Assay. Drug treatment effect on the Jurkat T cells was examined via a cell viability assay and determination of the IC_{50} concentration for: (A) TSA and (B) RD. The non-selective KDACi (TSA) reproducibly showed a higher IC_{50} (460 nM) than the class I specific KDACi (RD) with an IC_{50} in the nM range (2.8 nM). (C) immunoblot staining of acetylated proteins after DMSO, TSA and RD treatment of the Jurkat T cells. Arrows denote the regions of increased histone acetylation after KDACi treatment. DMSO, dimethyl sulfoxide; KDACi; lysine deacetylase inhibitor; IC_{50} , half-maximal inhibitory concentration; TSA, trichostatin A; RD, romidepsin.

A**B****C**

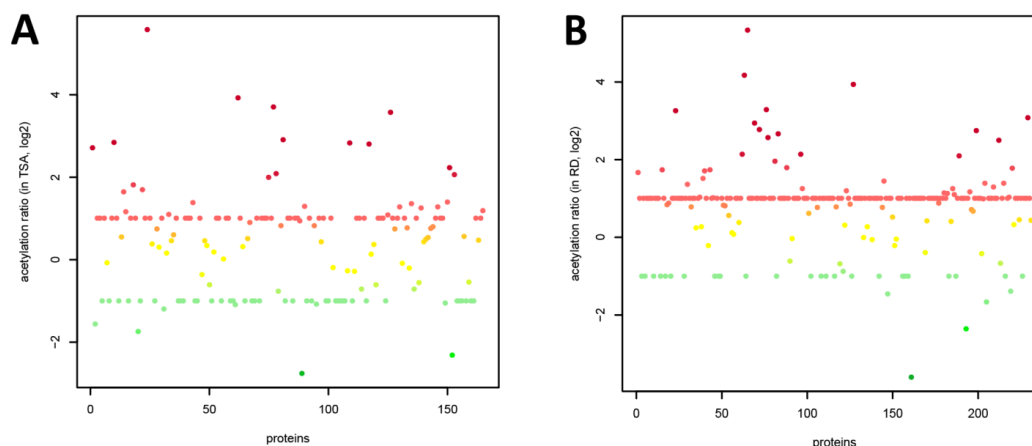
Supplementary Figure S2. Cell Apoptosis Assay. KDACi-induced apoptosis of the Jurkat T cells after: (A) DMSO, (B) TSA, and (C) RD treatment was assessed via cell surface staining for the early and late apoptotic markers annexin V and 7-AAD, respectively. Cells were treated at the IC_{50} concentration. No significant increase in the population of apoptotic cells was observed after 24 h drug treatment. DMSO, dimethyl sulfoxide; KDACi; lysine deacetylase inhibitor; IC_{50} , half-maximal inhibitory concentration; TSA, trichostatin A; RD, romidepsin.



Supplementary Figure S3. Cell Cycle Assay. The proportion of the cells in each phase of the cell cycle was determined for the Jurkat T cells treated with: (A) DMSO, (B) TSA, and (C) RD. After RD treatment, there were no apparent differences in the proportion of the cells in different stages of the cell cycle. After TSA treatment, cell cycle arrest in the G1/S transition was apparent. DMSO, dimethyl sulfoxide; KDACi, lysine deacetylase inhibitor; RD, romidepsin; TSA, trichostatin A.



Supplementary Figure S4. Reproducibility of the Transcriptomic and Proteomic Data Sets. Reproducibility of the experimental data was assessed between two DMSO-treated biological replicates and plotted as a histogram of (A) RNA or (B) protein identifications against the frequency of the quantitated transcripts and proteins, respectively. The frequency histogram showed a narrower distribution of quantitated proteins than transcripts. Blue bins within the histogram represent 90% of the observed ratios, whereas the red regions mark the most extreme 5%. DMSO, dimethyl sulfoxide.



Supplementary Figure S5. Colour-mapped Protein Acetylation Changes after KDACi Treatment. Abundance of each acetylated peptide was plotted against the FC (\log_2 scale) for (A) TSA- and (B) RD-treated Jurkat T cells relative to the DMSO control. In cases where there were more acetylated peptides quantitated per protein, the protein with the most extreme change in abundance was chosen as a representative. For the proteins that were identified and quantitated in all three drug treated replicates, but in neither of the control samples, or *vice versa*, were assigned arbitrary fold change of 2.0 or 0.5, respectively. Colour-coded range represents the distribution of acetylation changes from the most decreased in abundance (green) towards the most increased in abundance (red). FC, fold change; RD, romidepsin; TSA, trichostatin A.

13. SUPPLEMENTARY TABLES

Supplementary Table T1. Differentially-acetylated Proteins After KDACi Treatment. A list of differentially-acetylated proteins after TSA and RD treatment of the Jurkat T cells, compared to the DMSO control. Only non-histone proteins that were altered in acetylation, but remained unaltered in abundance are reported. Additionally, non-histone proteins that showed reversed changes in acetylation and abundance were included. The FC represents an average value from the replicate measurements. The acetylation FC of 2.0 and 0.5 was assigned to acetylated proteins that were present in the KDACi treated samples, but absent in the DMSO control, or *vice versa*, respectively. The n.a. indicates missing values for the proteins that were not quantitated. Cut-off for differentially-acetylated proteins: $FC \geq 1.1$ and $\leq 1/1.1$. DMSO, dimethyl sulfoxide; KDACi, lysine deacetylase inhibitor; n.a., not applicable; RD, romidepsin; TSA, trichostatin A.

TSA				RD			
PROTEIN	Acetylation FC	Abundance FC	Abundance q value	PROTEIN	Acetylation FC	Abundance FC	Abundance q value
CCDC40	47.6251	1.0895	0.3154026	NUCKS1	15.3357	0.9226	0.469958
HSP90AB4P	12.9644	1.0108	0.4912660	BRPF1	9.5487	0.9667	0.395482
RPL10A	11.9137	0.9432	0.0400289	ZNF512	8.4586	1.0126	0.489150
IDH2	7.4874	1.0349	0.2510305	SPTY2D1	6.7155	1.0312	0.376929
ARHGAP9	7.1850	0.9482	0.1771968	HN1	6.3349	0.9806	0.478473
PRKAG1	7.0039	0.9501	0.1279457	TMSB10	5.6462	1.1252	0.058243
ACADM	6.5680	1.0847	0.0013024	IDH2	4.3937	1.0286	0.423738
TMSB10	4.6735	0.7734	0.0021851	SHMT2	4.2610	1.0428	0.274823
HSPA1L	4.2549	n.a.	n.a.	HSP90AA1	3.4765	0.9782	0.468635
TUBA1A	4.1805	1.0347	0.4683096	VCP	3.4434	1.0010	0.639026
HSP90AA1	3.9880	1.0166	0.4086850	ATAD3A	3.3274	0.9193	0.211998
BRPF1	3.2440	1.0014	0.5607257	CREBBP	3.3200	0.9511	0.479468
BAZ1A	3.1262	0.8130	0.0012826	CNBP	3.2661	0.9036	0.005221
TCP1	2.6202	0.8811	0.0079258	ACADM	3.1859	1.0571	0.010624
EXOC4	2.6137	1.0897	0.0032221	CHRA1	2.8455	n.a.	n.a.
RRP15	2.5670	0.8026	0.0000028	PRKAR1A	2.7223	1.0475	0.150313
MAP3K9	2.4457	n.a.	n.a.	SUPT16H	2.6288	0.9772	0.465356
RPL31	2.4313	0.8875	0.0073745	TUBA1A	2.6162	1.1499	0.443846
ZNF770	2.2730	n.a.	n.a.	CCT3	2.5708	0.9584	0.309902
BAZ1B	2.2438	0.9384	0.0596748	THOC7	2.4584	0.9934	0.730686
CNBP	2.1413	0.7570	0.0000003	SARNP	2.3823	1.0041	0.499304

RHOB	2.1109	n.a.	n.a.	IFI16	2.3744	0.9714	0.423111
FEN1	2.0028	1.0145	0.4377198	NAA50	2.2990	0.9442	0.250298
ACTR3	2.0	1.0268	0.3531019	SMAD2	2.2448	1.0819	0.006731
RPS20	2.0	0.9784	0.3687267	RPS27A	2.2030	0.9927	0.499410
MCM4	2.0	0.9079	0.0633127	RPS5	2.1900	0.9638	0.368308
RPL30	2.0	0.9135	0.0236439	SDHA	2.1419	1.0479	0.183709
HNRNPU	2.0	0.9410	0.4658278	CHD3	2.0462	1.0113	0.490592
ARHGDIB	2.0	0.8564	0.0616900	UBE2O	2.0455	0.9577	0.328063
SEPT9	2.0	0.9440	0.2534936	CSNK2B	2.0322	0.9861	0.485804
RPL15	2.0	0.9043	0.0004578	GRWD1	2.0	0.9162	0.089942
ENO3	2.0	n.a.	n.a.	PUF60	2.0	0.9243	0.129370
AKAP5	2.0	0.9712	0.4691331	RPL28	2.0	0.9332	0.027765
JADE3	2.0	0.9194	0.0977204	CRNKL1	2.0	0.9400	0.084581
ING4	2.0	1.0709	0.0767418	RPL30	2.0	0.9416	0.023495
STK36	2.0	n.a.	n.a.	NUDT21	2.0	0.9456	0.171937
ZFP1	2.0	1.0373	0.4419769	HSPA8	2.0	0.9484	0.256087
ZNF512B	2.0	0.8807	0.0484664	SKP1	2.0	0.9539	0.393957
RAC3	2.0	1.0943	0.0087501	MEAF6	2.0	0.9556	0.421776
HSP90AB1	2.0	0.9718	0.3551999	SLTM	2.0	0.9683	0.370696
IKZF1	2.0	0.7471	0.0000148	HSPD1	2.0	0.9734	0.434333
SPTBN1	2.0	0.9560	0.2502866	PGK2	2.0	0.9753	0.493165
BRD1	2.0	0.9550	0.1621913	GLUD1	2.0	0.9773	0.465527
EIF2B3	2.0	1.0064	0.4921743	ENO1	2.0	0.9801	0.465356
RAN	2.0	0.9031	0.0018742	VDAC3	2.0	0.9825	0.476209
HNRNPA1L2	2.0	n.a.	n.a.	RPL8	2.0	0.9892	0.490671
CALM1	2.0	n.a.	n.a.	HP1BP3	2.0	1.0050	0.607157
PPP2CA	2.0	0.9990	0.7011548	PPIA	2.0	1.0091	0.496816
HNRNPM	2.0	0.9719	0.2918179	TPI1	2.0	1.0142	0.479468
ENO1	2.0	0.9886	0.4279047	ACP1	2.0	1.0335	0.464099
BEND6	2.0	n.a.	n.a.	CAPZA2	2.0	1.0335	0.373173
RUFY4	2.0	n.a.	n.a.	MYH9	2.0	1.0368	0.380500
CCT2	2.0	0.9149	0.0602499	MTPN	2.0	1.0411	0.438887
CTCF	2.0	0.8880	0.0248315	PARP1	2.0	1.0498	0.228757
CFL1	2.0	1.0669	0.1006554	RPS20	2.0	0.9861	0.479468
PKM	2.0	1.0749	0.1076381	CCDC86	2.0	0.7987	0.007856
NQO2	2.0	1.3923	0.1240534	RPL18A	2.0	0.9470	0.061705
PJA2	2.0	0.9627	0.3029085	SKIV2L2	2.0	0.9427	0.136376
HDAC2	2.0	0.9746	0.3195877	RPL3	2.0	0.9426	0.094464
RBBP4	2.0	0.9645	0.2823973	TKT	2.0	0.9588	0.327058
KAT7	2.0	0.8903	0.0010366	ZNF512B	2.0	0.9441	0.272936
LMNB1	1.9119	0.9947	0.4780489	MED28	2.0	0.9521	0.479468
HLTF	1.8652	0.8519	0.0004113	PSMA2	2.0	0.9392	0.173784
MTHFD1	1.7629	0.9281	0.0364954	GLRX	2.0	0.9703	0.498003

HSPD1	1.7615	1.0118	0.4344177	ZNF292	2.0	1.0524	0.482676
SMNDC1	1.7396	0.8711	0.0049215	ING4	2.0	1.0559	0.260165
RPS27A	1.7013	1.0410	0.4044093	RPL4	2.0	0.9513	0.294513
RPL18A	1.6794	0.9257	0.0096448	RAN	2.0	0.9499	0.086761
CCT8	1.6787	0.9016	0.0096187	PGAM1	2.0	0.9903	0.835373
CSNK2B	1.5225	1.0150	0.4230616	FAM192A	2.0	0.9553	0.290352
USP34	1.4755	0.9991	0.4989228	BRD1	2.0	0.9465	0.179599
ATAD3A	1.4665	0.9706	0.3529270	IMPDH2	2.0	0.9997	0.693231
SMAD2	1.4480	1.0703	0.0159863	MCM4	2.0	0.9751	0.465527
ZNF512	1.3850	0.9660	0.3699440	PRDX6	2.0	0.9922	0.557585
COX17	1.3753	0.7716	0.0181697	MARS	2.0	0.9702	0.363043
GART	1.3739	0.8002	0.0000034	PSMA6	2.0	0.9440	0.302189
SEPT7	1.3539	1.0055	0.5366634	IARS	2.0	0.9707	0.385418
NAA30	1.3430	0.9965	0.5122891	TBCB	2.0	0.9564	0.171937
CCT3	1.3025	0.9025	0.0243405	SH2D1A	2.0	0.9578	0.419354
PRR12	1.2874	n.a.	n.a.	AHCY	2.0	0.9774	0.429615
GNPAT	1.2662	1.0012	0.6289124	CBLL1	2.0	0.9521	0.490632
CENPV	1.2329	0.8872	0.0021812	HSPA9	2.0	0.9877	0.490632
CHD5	1.1104	n.a.	n.a.	RPL36	2.0	0.9771	0.411581
NUDT21	0.8756	0.9610	0.1551017	HNRNPA1	2.0	0.9959	0.554041
PGAM1	0.8297	1.0106	0.4382944	ARHGDIB	2.0	1.0076	0.495108
PHF20	0.8230	0.9321	0.4104387	ADH5	2.0	0.9791	0.445372
GAPDH	0.7753	1.0147	0.4001784	DCPS	2.0	0.9035	0.028190
VDAC1	0.6859	0.9785	0.3709680	TCP1	2.0	0.9453	0.195291
SARNP	0.6816	0.9828	0.4305992	RBM10	2.0	1.0022	0.679084
RSF1	0.6086	0.9321	0.1150592	MAPRE1	2.0	0.9964	0.607773
PPIA	0.6083	1.0212	0.3859167	NONO	2.0	0.9926	0.495702
HSPA8	0.5847	0.9176	0.0674812	RPS4X	2.0	0.9510	0.153199
INVS	0.5	n.a.	n.a.	CFL1	2.0	0.9838	0.467771
ANAPC7	0.5	0.8988	0.0622816	PRKDC	2.0	0.9955	0.734524
ARPC5L	0.5	1.0643	0.3859167	RPS2	2.0	0.9464	0.095901
CCT6A	0.5	0.9172	0.0555647	JADE3	2.0	1.0272	0.469321
HN1	0.5	1.0236	0.3951996	ATF2	2.0	1.0549	0.233735
EEF1D	0.5	1.1062	0.1035285	U2AF1	2.0	0.9008	0.000320
BROX	0.5	1.0864	0.0105208	RPL27A	2.0	0.9263	0.127765
VCP	0.5	1.0837	0.0402145	RPS13	2.0	0.9373	0.100459
MBTD1	0.5	0.9596	0.4438843	POLR3A	2.0	0.9449	0.192069
HNRNPD	0.5	0.9611	0.3565088	RPL14	2.0	0.9525	0.326180
PRDX1	0.5	1.2405	0.0000021	KAT7	2.0	0.9533	0.193659
NPM1	0.5	0.9642	0.2504483	ZC3H14	2.0	0.9612	0.317429
PEBP1	0.5	1.0133	0.4224829	XRCC6	2.0	0.9631	0.391054
YWHAH	0.5	0.9541	0.1697525	RPL10	2.0	0.9635	0.293264
NIF3L1	0.5	0.9967	0.7187668	ALDOA	2.0	0.9650	0.375922

DHX15	0.5	0.9260	0.0724466	PDHA1	2.0	0.9783	0.465527
HNRNPA1	0.5	0.9484	0.2097698	HSP90AB1	2.0	0.9795	0.483706
FANCD2OS	0.5	n.a.	n.a.	ARPC2	2.0	0.9810	0.465527
MKI67	0.5	1.2109	0.0000062	KIF5B	2.0	0.9857	0.485636
UBE2O	0.5	1.0045	0.4814827	CORO1A	2.0	0.9873	0.491669
YWHAQ	0.5	1.0382	0.2464522	PUM2	2.0	0.9982	0.542471
PGK2	0.5	1.0799	0.1795123	SRSF6	2.0	0.9999	0.688388
TUBB	0.5	0.9685	0.3759857	WAPAL	2.0	1.0070	0.580433
EXOSC8	0.5	1.0098	0.4320189	PGK1	2.0	1.0119	0.491715
PCMT1	0.5	1.1958	0.0008484	TLN1	2.0	1.0309	0.377237
UFC1	0.5	0.8946	0.0648578	CDCA7	2.0	1.0530	0.429615
PDS5B	0.5	1.1311	0.0056663	SKI	2.0	1.0601	0.495108
RBM10	0.5	0.9808	0.4102005	SPTBN1	2.0	1.0638	0.036323
DDAH2	0.5	1.4237	0.0000004	HINT1	2.0	1.0053	0.598487
PCNA	0.5	1.0222	0.3482683	CCT5	2.0	0.9547	0.331133
SUB1	0.4824	1.1131	0.0023172	ARID4B	2.0	1.0041	0.498742
CHD3	0.4375	0.9754	0.3755402	TBCA	2.0	0.9901	0.492311
ACTB	0.3398	1.0908	0.1057415	RPL15	2.0	0.9537	0.091213
BRD8	0.2976	0.9576	0.3286127	RPL6	2.0	0.9490	0.171769
TMSB4X	0.1999	0.6975	0.2207402	CAT	2.0	1.0701	0.103005
LONP2	0.1469	0.9472	0.4316849	BLVRA	2.0	1.0871	0.040560
				PCCA	2.0	1.1011	0.281362
				FUT8	2.0	1.1214	0.361123
				HNRNPU	2.0	1.2515	0.440749
				ACTG2	2.0	n.a.	n.a.
				C17orf80	2.0	n.a.	n.a.
				CDCA5	2.0	n.a.	n.a.
				HNRNPA1L2	2.0	n.a.	n.a.
				MAGI1	2.0	n.a.	n.a.
				MICU3	2.0	n.a.	n.a.
				PABPC1L	2.0	n.a.	n.a.
				POTEE	2.0	n.a.	n.a.
				RPL38	2.0	n.a.	n.a.
				STK36	2.0	n.a.	n.a.
				SUB1	1.9934	1.0625	0.221689
				RPS17L	1.8464	0.9454	0.215172
				BAZ1B	1.8406	0.9875	0.489150
				NPM1	1.7953	0.9865	0.490592
				BAZ1A	1.7820	0.9877	0.490592
				EXOC4	1.7709	1.0386	0.118327
				EXOSC8	1.7572	0.9595	0.292378
				CCT8	1.7162	0.9647	0.319351
				MTHFD1	1.7119	0.9716	0.396930

PRKAG1	1.7099	1.0308	0.330443
LMNB1	1.7079	0.9917	0.498742
SMC3	1.6376	1.0294	0.387263
SMNDC1	1.5979	0.9349	0.081112
INTS4	1.5289	0.9973	0.569447
FEN1	1.4711	1.0234	0.465527
PSMC6	1.4258	0.9658	0.333804
XPNPEP1	1.3632	1.0721	0.102731
ZNF770	1.3493	n.a.	n.a.
RPL35A	1.3388	0.9340	0.013883
RSF1	1.3259	1.0179	0.473777
GNPAT	1.3051	1.0265	0.408137
VDAC1	1.2481	0.9698	0.396930
NAA30	1.2445	1.0012	0.680113
PGAM5	1.2088	0.9507	0.183709
CHD5	1.2080	n.a.	n.a.
CENPV	1.1857	0.9330	0.122713
COX17	0.8606	1.0906	0.413365
PTGES3	0.8603	0.9589	0.188568
RPL31	0.7640	0.9532	0.199685
STRAP	0.7442	0.9790	0.459233
HSP90AB4P	0.6519	1.0537	0.495702
TMSB4X	0.6294	1.0138	0.499410
NAA10	0.5424	0.9618	0.280224
ACTG1	0.5	n.a.	n.a.
ADA	0.5	0.9570	0.310547
ARHGAP9	0.5	0.9745	0.466131
ARPC5L	0.5	0.9609	0.491556
ATP7A	0.5	n.a.	n.a.
BCLAF1	0.5	0.9476	0.475150
CCDC40	0.5	0.9983	0.499710
CYLC1	0.5	n.a.	n.a.
DDAH2	0.5	1.1160	0.000224
DHX15	0.5	0.9720	0.442329
HLTF	0.5	1.0175	0.457227
INVS	0.5	n.a.	n.a.
MAP3K9	0.5	n.a.	n.a.
MBTD1	0.5	0.9828	0.498742
MKI67	0.5	1.1227	0.000426
NRAP	0.5	n.a.	n.a.
PRDX1	0.5	1.0047	0.573610
RBBP4	0.5	0.9619	0.261278
RBBP7	0.5	0.9813	0.490632

	RHOB	0.5	n.a.	n.a.
	RRP15	0.5	0.9115	0.045447
	SEPT7	0.5	1.0203	0.464401
	TUBB	0.5	0.9981	0.499710
	YWHAH	0.5	0.9715	0.295492
	USP34	0.3797	0.9417	0.482676
	PRR12	0.3635	n.a.	n.a.
	TBC1D4	0.3157	1.1309	0.003433
	SLC9A3R1	0.1949	0.9494	0.371052
	RPL10A	0.0820	0.9579	0.227691

Supplementary Table T2. KDACi-mediated Downregulation of Proteins Essential for Cell Survival. List of the essential proteins that are downregulated by TSA and RD treatment in the Jurkat T cells. TSA specifically downregulated 386 essential proteins; whilst RD-specific downregulation was observed on 12 proteins essential for cell survival. Both drugs commonly downregulated 103 essential proteins. Cut-off for downregulated proteins: $FC \leq 1/1.1$, $q < 0.05$. Complete list of *essential* proteins was taken from Blomen *et al.* (Blomen et al, 2015). DMSO, dimethyl sulfoxide; KDACi; lysine deacetylase inhibitor; RD, romidepsin; TSA, trichostatin A.

KDACi-mediated downregulation of <i>essential</i> proteins									
TSA protein abundance ↓							RD protein abundance ↓	RD & TSA protein abundance ↓	
PSMD4	RPL19	MTA2	RAD51	NAA25	CDK5RAP2	ZCCHC9	AAMP	RANGAP1	DDX54
CWC22	NAE1	DDX18	AURKA	SMARCC1	ALYREF	PTMA	BCCIP	CDC123	TRAPPC5
NAA10	DKC1	NUDC	OXA1L	SMARCD2	PDAP1	KANSL1	DCPS	IWS1	RBM5
CDC23	RPS9	URB1	MSTO1	NOB1	TXLNG	YBX1	ELL	GNL3	RSL1D1
RPS19	EIF3H	RPL4	CHTOP	RNF168	NHP2	RPL7L1	MED27	NUP188	POLR1A
RPS15A	DHPS	NAA15	RPTOR	SMARCA4	MRPL3	FAM32A	NOL9	MPHOSPH10	ZMAT2
YARS2	RANBP1	RPS15	METAP2	UTP11L	CXorf56	ORC6	TIMM50	NUP88	TRMT6
PSMC3	GRWD1	TOP3A	EIF5	RNASEH1	MRPL20	RBBP8	TRMT61A	GTPBP4	KDM2A
NDUFA6	URB2	CUL1	CLPB	RPIA	NUFIP2	CCNL1	WIBG	UTP15	WDR75
TCERG1	NUP205	TCP1	DIDO1	ATXN10	BCLAF1	FAM204A	DDI2	EIF3D	RNMTL1
SNRPA1	MTOR	EIF3G	LENG1	CSDE1	ZNHIT6	PDSS1	TNPO1	NOL6	TSR1
MRPL9	ANAPC1	ANKHD1	HSPH1	C19orf43	GEMIN8	ZC3H3	AKAP8L	HEATR1	UTP20
YARS	RPS27	DNAJC17	CDK6	SDE2	SNRPF	ISG20L2		EBNA1BP2	RBM19
MRPS28	EP300	RHOA	SON	NOC3L	PAN3	CLSPN		CNBP	TFRC
NOL10	SCD	PFDN5	CAD	UTP6	COX17	COA4		ACACA	HCFC1
AASDHPPT	STAG2	RPS25	ZC3H15	CCDC174	DIEXF	NOL12		EIF4A1	ZBTB11
MRPL12	PA2G4	CCT7	EIF4G2	CYTH1	GNL2	ESCO2		POLR3B	WDR74
TTI1	ADSL	FAU	GABPB1	TACC3	DCAF13	WEE1		DDX20	C9orf78
POLA1	ELOVL5	MIS18A	BRIX1	BMS1	ADSS	GMNN		RBM22	HK2
MRPL19	RPL26	ATIC	METTL16	NOP2	CDK4	MCM10		C11orf57	GAR1
RPL6	BUB1B	SRCAP	PSAT1	DDX11	TFPT	USP1		DNAJC2	NOP14
AATF	LIG3	CNOT1	MAX	FAM120A	GLE1	LRRRC41		CIRH1A	NOP16
SERBP1	PUF60	CWF19L2	SPDL1	KRR1	RPF1	UBE2T		DDX52	WDR43
YEATS4	CNOT10	RPS24	TMA16	SCAF11	SNW1	TIMM8B		U2AF1	VPS72
RPL15	SKIV2L2	RPS16	ZWINT	ALDH18A1	CHEK1	RRM2		ELAC2	C9orf114
MRPS23	RCL1	SYMPK	NLE1	KIAA0020	TDP2	MYBL2		NOM1	DDX21
PINX1	PRPF40A	PRMT1	SMARCB1	NGDN	DTL			POLR1E	RSL24D1

HMGCS1	BPTF	EIF3E	CTPS1	STAT5B	TRIT1	GTF2I	CENPH
MRPL38	RPS28	EIF3A	PN01	KANSL3	SASS6	C21orf59	USP36
ACLY	RAF1	PDCL3	SPEN	RIOK1	GTF3A	CIR1	MYBBP1A
SMG9	SF3A3	ZC3H11A	U2SURP	SKP2	TRIAP1	SLC2A1	POLRMT
ZMYND8	RPS13	ZNF207	ELMO1	NCL	SYF2	CDK12	MTHFD1L
USP7	MCM7	CENPF	CKS1B	NOC4L	BLM	RTFDC1	KRI1
RAN	NUP35	PABPC1	MRPL1	WDR18	IKZF1	OGT	MCRS1
RIOK2	KAT7	BUD13	NAA50	IMP4	SMG7	WDR12	RRP1
RPL28	DDX27	EIF3B	ZNF148	GCN1L1	RRP36	TTC27	PPAN
ELP4	ABCE1	POLR3A	DNTTIP2	RBM28	EIF4B	NOL7	DNAJA1
SF3A1	CHMP4B	TPT1	TBRG4	NOL8	YEATS2	SURF6	CCDC94
TTK	PEX14	SMARCD1	DDX47	UXT	UBL5	NOLC1	RRP7A
CCT3	TPX2	GMPS	KDM3B	BTF3	CDC20	NOL11	GLTSCR2
RPS18	PSMB5	NAT10	DHX30	NDUFA8	LARP4	ANP32B	DHX33
CCT8	PUM1	SMNDC1	E2F3	MIS18BP1	RPS19BP1	DNAJC7	PES1
EXOSC2	PPIL2	SDAD1	RPF2	CCNA2	NUPL2	EIF3I	CWC25
ERAL1	CTCF	KPNB1	SYNCRIP	HAUS7	C1orf131	PCNT	UBTF
DRG1	RPL31	FTSJ3	PDCD11	RRP15	DDX56	UTP14A	DDX49
HAUS6	PNN	G3BP2	SETD2	NSA2	RIF1	POLR1C	GPATCH4
MRPL39	PCM1	EXOSC4	MPHOSPH6	UBAP2L	SHQ1	BOP1	CCDC86
SMARCA5	ACTR6	EIF3M	WDR46	GART	C12orf45	UTP18	OTUD5
POLD2	PHF5A	UPF1	SCAF8	DAXX	MYB	FNBP4	GNL3L
DLGAP5	SAE1	MDN1	LTV1	FPGS	CNOT2	RRP12	CBFA2T3
MRPS27	PFDN2	ZC3H8	PRCC	DDX3X	SLBP	MRT04	MYC
PSMB1	EEF1A1	C19orf53	TGS1	SRFBP1	RPS29	DDX10	
RPS3A	HAUS1	SART1	BYSL	KLF16	TYMS		
SZRD1	DDB1	MRPL17	TOE1	RPUSD3	YRDC		
ATAD5	MCM2	SMARCE1	TTF1	ESF1	NUP153		
MRPL11	SEH1L	FLI1	MAT2A	GATC	ADAT2		
KIFC1	GEMIN4	TUBGCP4	PFAS	POLR1B	RRM1		
CNOT3	HAUS4	ANKRD17	NUP50	MORF4L1	MLLT10		
MCM6	TRRAP	ERBB2IP	MRPL47	PPP1R11	CCP110		
CABIN1	PAICS	TTI2	TTF2	POLE3	POLR3D		

Supplementary Table T3. KDACi-regulated Acetylation of *Essential* Proteins. KDACi treatment altered acetylation of 116 proteins that are essential for cell survival. TSA and RD specifically altered acetylation of 16 and 60 *essential* proteins, respectively. Out of 40 *essential* proteins that were changed in acetylation by both KDACis, 15 proteins showed reverse acetylation changes depending on the drug treatment. Cut-off for differentially-acetylated proteins: $FC \geq 1.1$ and $\leq 1/1.1$. Complete list of *essential* proteins was taken from Blomen *et al.* (Blomen *et al.*, 2015). DMSO, dimethyl sulfoxide; KDACi; lysine deacetylase inhibitor; RD, romidepsin; TSA, trichostatin A.

KDACi-mediated acetylation of <i>essential</i> proteins								
<i>essentiality</i> TSA-specific		<i>essentiality</i> RD-specific		<i>essentiality</i> TSA and RD common				
Ac ↑	Ac ↓	Ac ↑	Ac ↓	TSA: Ac ↑ RD: Ac ↑	TSA: Ac ↓ RD: Ac ↓	TSA: Ac ↑ RD: Ac ↓	TSA: Ac ↓ RD: Ac ↑	
ACTR3	BRD8	AHCY	RPL6	BCLAF1	BRPF1	DHX15	RRP15	NUDT21
CCT2	CCT6A	ALDOA	RPS13	NAA10	TCP1	TUBB	RPL31	PGAM1
CTCF	GAPDH	ARPC2	RPS2	STRAP	EXOC4		RBBP4	SARNP
EIF2B3	PCNA	CCDC86	RPS4X	PTGES3	CNBP		RPL10A	HSPA8
GART	ANAPC7	CCT5	SDHA		FEN1		COX17	EXOSC8
HNRNPM	HNRNPD	CDCA5	SHMT2		ENO1			HNRNPA1
PPP2CA	ACTB	CREBBP	SKIV2L2		HNRNPU			NPM1
IKZF1	PHF20	CRNKL1	SKP1		HSP90AB1			RBM10
		DCPS	SMC3		KAT7			VCP
		GRWD1	SUPT16H		MCM4			SUB1
		HSPA9	TBCA		RAN			
		IARS	TBCB		RPL15			
		IMPDH2	THOC7		RPL30			
		INTS4	TKT		RPS20			
		MARS	TPI1		MTHFD1			
		MED28	U2AF1		HSPD1			
		NAA50	WAPAL		SMNDC1			
		NONO	XRCC6		RPS27A			
		PGK1	MEAF6		RPL18A			
		POLR3A	MYH9		CCT8			
		PSMA2	SKI		CSNK2B			
		PSMC6	SLTM		NAA30			
		RPL14	CBLL1		CCT3			
		RPL27A	PUF60					
		RPL28	PUM2					
		RPL3	RPL36					
		RPL38	RPL8					
		RPL4	SRSF6					

3.2. Functional Characterisation of KDACi-mediated Alteration in Protein Acetylation

Investigation of the effect of KDACis on the systems biology level enables discovery of cancer specific pathways that are regulated by acetylation. Nevertheless, to utilise this knowledge for development of the novel therapeutic strategies, it is necessary to characterise changes in protein function that are mediated by acetylation. This can be achieved by:

- Structural studies: *in silico* localisation of the acetylation site within the native conformation of the protein and prediction of conformational changes that can be mediated by acetylation, *i.e.*, protein-protein interaction, oligomerisation, ligand binding *etc.*
- Enzymatic studies: mass spectrometry-based metabolic profiling of the changes in substrate(s) and product(s) of certain enzymatic function. Changes in abundance thereof can be utilised to predict whether the altered acetylation triggers gain or loss of enzymatic function
- Interaction studies: co-immunoprecipitation of the protein of interest with the known interaction partner (protein, RNA, DNA) in order to investigate whether acetylation changes increases or decreases the affinity of the protein to bind to the interaction partner(s)

The focus of the study covered within Manuscript #1 is on the KDACi-mediated protein changes that are *essential* for cell survival. The majority of these proteins were involved in metabolic pathways. Particular interest is on investigating the changes that occur within cancer-specific pathways, that can foster the development of cancer-specific therapies with decreased side effects compared to the currently available treatments.

3.2.1. Structural Role of Lysine Acetylation in SHMT2 Oligomerisation

SHMT2 was identified in the Jurkat T cells with no change in expression after KDACi-treatment compared to the DMSO control. The mitochondrial isoform, but not the cytoplasmic counterpart, was increased in acetylation upon drug treatment. To our knowledge, acetylation of SHMT2 has not been investigated so far in the context of catalytic activity nor protein oligomerisation, a necessary requirement for enzymatic function. Therefore, structural relevance of the acetylated sites was assessed in order to investigate how the function of SHMT2 can be influenced by altered acetylation. Figure 10 shows *in silico* modelling and positioning of the lysine residues that were altered in acetylation after KDACi treatment. Lysine K245 and K474 are positioned on the outer surface of the SHMT2 dimer indicating a potential role as a docking site for SHMT2 interaction with another proteins. On the contrary, lysine K95 is localised at the dimer interface superimposed onto the acidic glutamic acid residue E77. When K95 is not acetylated, the positive charge on the lysine side chain can interact with the negatively-charged E77 residue and thus favouring dimer formation. On the other hand, acetylation of K95 neutralises the positive charge and prevent SHMT2 homodimer formation. As K95 is within the catalytic domain, it is of interest to further investigate whether this residue is directly exposed to the ligand binding (pocket) that could have a direct influence on the SHMT2 enzymatic function. To this end, targeting the lysine residue that might be responsible for oligomerisation and/or enzymatic function of the SHMT2, represents a powerful tool to further investigate novel therapeutic strategies to treat malignancies that are characterised by altered SHMT2 expression and/or activation.

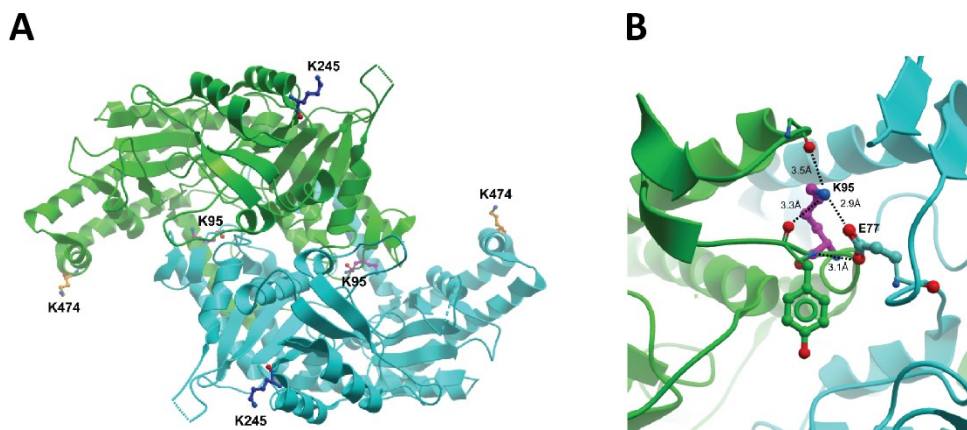


Figure 10. Influence of KDACi-mediated Acetylation Changes on the Structure of SHMT2.

(A) Crystal structure of the human SHMT2 dimer (green and cyan, PDB 4PVF) revealed that the two acetylated lysines K245 (blue) and K474 (orange) lie on the outer edge of the domain. Modification could affect putative protein-protein interactions. K95 (pink) lies at the dimerisation interface. (B) K95 (pink sticks) contributes to the SHMT2 dimerisation interface via contact with E77 (cyan) of the opposite protomer and the backbone of other loops (green sticks). Acetylation of this residue might prevent oligomerisation of SHMT2. Correct positioning of K95, which lies in the region supporting the active site, might be relevant for the catalytic activity of the protein. K95 likely plays a structural role which might be disrupted by acetylation.

3.2.2. The Role of Lysine Acetylation in MTHFD1 Function

Interestingly, similar alterations in acetylation were observed on another enzyme within the SOG pathway, MTHFD1, also known as C-1-tetrahydrofolate synthase (C1-THF synthase). MTHFD1 is a multifunctional enzyme that mediates the one-carbon cycle in the cytosol. Lysine K553 of the MTHFD1 was increased in acetylation by both KDAC inhibitor treatments; whilst mitochondria-localised enzymes that separately catalyse the same reactions (MTHFDL1, MTHFDL2 and MTHFD2) were not affected by acetylation.

Lysine residue K553 within the dimeric MTHFD1 structure was visualised in order to investigate the outcome that KDACi-mediated acetylation can have on the rearrangement of the protein structure and/or function. Available crystal structure of the mouse MTHFD1 was aligned with a homology model of the human MTHFD1 isoform (Figure 11.A). The interface between the monomers in the vicinity of lysine K553 was enlarged in order to inspect the spatially neighbouring residues that can interact with the K553 side chain (Figure 11.B). K553 from one of the protein monomers is positioned in close proximity to K542 and R543 from the opposing protein molecule. Unmodified, positively-charged K553 is not favourable for interaction with the positively-charged K542 and R543 residues. Nevertheless, acetylation of K553 might allow these interactions with an increased probability of MTHFD1 dimerisation. Moreover, K553 lies within the MTHFD1 catalytic domain formyltetrahydrofolate synthetase (amino acid residues 306-935). Therefore, a change in acetylation can also modulate enzymatic function. Additionally, the same loop region was projected from murine to bacteria to show that at the position of acetylated K553 there is an asparagine residue (Figure 11.C). Structural analysis showed that in this case, the asparagine residue (mimicking the charge of an unmodified lysine residue) is in the vicinity of the opposing arginine and asparagine residues with which a polar interaction is formed that is beneficial for protein oligomerisation. From this projection, it is possible to assume that changes in the charge that is mediated by K553 acetylation can mediate crucial interactions that are responsible for protein dimer formation.

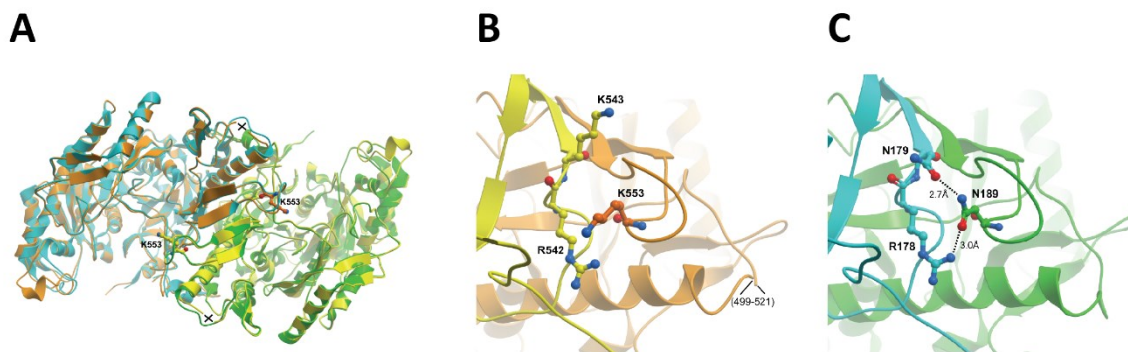


Figure 11. Influence of KDACi-mediated Acetylation Changes on the Structure of MTHFD1.

(A) Crystal structure of the dimeric formate-tetrahydrofolate ligase (FTHFS) domain of a bacterial Mthfd1 homolog (*Moorella thermoacetica* N10-Formyltetrahydrofolate Synthetase, green and cyan, PDB code 4JIM) aligned with a homology model of human MTHFD1 (orange and yellow). Residues with poor homology to the template (499-521) were omitted from the homology model (marked with "X"). (B) Magnified interface between protein monomers (orange and yellow) of human MTHFD1 in the vicinity of acetylated K553 (orange sticks). Neighbouring K542 and R543 side chains in the opposite monomer (yellow sticks) could potentially be repulsed by a non-acetylated lysine K553 and disrupt dimerisation. Acetylation might relieve charge repulsion and positively contribute to dimerisation. Since the FTHFS domain acts as an oligomer, the oligomerisation state is likely to affect catalytic activity. (C) The interface between protein monomers in the structures of *Moorella thermoacetica* homolog in the same loop region (green and cyan, PDB entry 4jim). The asparagine N189 homologous to the acetylated lysine (in green sticks) forms conserved polar interactions with arginine and asparagine side chains (cyan colored sticks). These interactions might support dimerisation, and tetramerisation of the FTHFS domain.

3.3. Manuscript #2: FASIL-MS: An Integrated Proteomic and Bioinformatic Workflow To Universally Quantitate In Vivo-Acetylated Positional Isomers

Dijana Vitko, Peter Májek, Erika Schirghuber, Stefan Kubicek, and Keiryn L. Bennett

The following article was published in the *Journal of Proteome Research*. It represents the development and validation of a novel experimental workflow to quantitate differentially-acetylated positional isomers of histone proteins. The focus was directed towards KDACi-mediated changes in histone acetylation that complements the systems-biology approach introduced earlier in this thesis.

N-acetoxy-D₃-succinimide (D₃-NAS) was utilised to modify free lysine residues after KDACi-treatment and DMSO control of the HeLa cell line. In this case, lysine residues that were acetylated during the treatment were modified by H₃-acetyl group (protonated, light); whilst the residual unmodified lysine residues were modified *in vitro* with D₃-acetylation (deuterated, heavy). The sample preparation was streamlined by utilising a filter-based approach to exchange the aqueous and organic solvents prior to protein digestion. Moreover, the mass spectrometric method was adapted to simultaneously isolate and co-fragment the clusters of H₃-/D₃-acetylated histone peptides. Finally, an informatic tool was developed to enable the MS²-based quantitation of differentially-acetylated histone peptides, with the additional function of specifically localising H₃-/D₃-acetylated lysine residues.

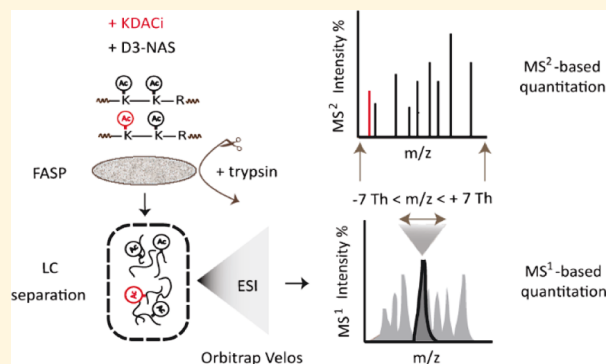
FASIL-MS: An Integrated Proteomic and Bioinformatic Workflow To Universally Quantitate In Vivo-Acetylated Positional Isomers

Dijana Vitko,[†] Peter Májek,[†] Erika Schirghuber,^{†,‡,§} Stefan Kubicek,^{†,‡} and Keiryn L. Bennett^{*,†}[†]CeMM Research Center for Molecular Medicine of the Austrian Academy of Sciences, A-1090 Vienna, Austria[‡]Christian Doppler Laboratory for Chemical Epigenetics and Antiinfectives, CeMM Research Center for Molecular Medicine of the Austrian Academy of Sciences, A-1090 Vienna, Austria

Supporting Information

ABSTRACT: Dynamic changes in histone post-translational modifications (PTMs) regulate gene transcription leading to fine-tuning of biological processes such as DNA replication and cell cycle progression. Moreover, specific histone modifications constitute docking sites for recruitment of DNA damage repair proteins and mediation of subsequent cell survival. Therefore, understanding and monitoring changes in histone PTMs that can alter cell proliferation and thus lead to disease progression are of considerable medical interest. In this study, stable isotope labeling with *N*-acetoxy-*D*₃-succinimide (*D*₃-NAS) was utilized to efficiently derivatize unmodified lysine residues at the protein level. The sample preparation method was streamlined to facilitate buffer exchange between the multiple steps of the protocol by coupling chemical derivatization to filter-aided sample preparation (FASP). Additionally, the mass spectrometry method was adapted to simultaneously coisolate and subsequently cofragment all differentially H₃/*D*₃-acetylated histone peptide clusters. Combination of these multiplexed MS² spectra with the implementation of a data analysis algorithm enabled the quantitation of each and every in vivo-acetylated DMSO- and SAHA-treated H4(4–17) and H3(18–26) peptide. We have termed our new approach FASIL-MS for filter-aided stable isotopic labeling coupled to mass spectrometry. FASIL-MS enables the universal and site-specific quantitation of peptides with multiple in vivo-acetylated lysine residues. Data are available via ProteomeXchange (PXD003611).

KEYWORDS: FASP, histone acetylation, lysine deacetylase inhibitor, mass spectrometry, MS²-based quantitation, *N*-acetoxy-*D*₃-succinimide, protein derivatization



INTRODUCTION

DNA modifications and alterations in histone post-translational modifications (PTMs) affect chromatin structure and thus influence the transcription of specific gene loci. Moreover, histone PTMs regulate fundamental cellular processes such as DNA replication¹ and DNA damage repair.^{2,3} Hence, altered histone modifications in oncogene and tumor suppressor gene promoters correlate with a range of diseases, including different types of cancer.^{4,5}

The N-termini of histones are rich in lysine and arginine residues. Side chains of these amino acids contain positively charged amino groups that are targeted by enzymes such as lysine acetyltransferases (KATs) and lysine methyltransferases (KMTs), resulting in post-translational modification of the histones. The activity of KATs and KMTs are in dynamic equilibrium with functionally opposing enzymes, i.e., lysine deacetylases and demethylases (KDACs and KDMs). KDAC inhibitors (KDACi) have found widespread use in studying the role of certain KDACs and monitoring the changes in acetylation that occur as a consequence of inhibition. In particular, suberoylanilide hydroxamic acid (SAHA) is a commonly utilized, nonselective KDACi that inhibits a subset

of the 11 classical, Zn²⁺-dependent KDACs,⁶ whereas NAD⁺-dependent sirtuins are unaffected. Moreover, SAHA has attracted broad interest in cancer-related research since receiving FDA approval in 2006 for clinical use in the treatment of cutaneous T-cell lymphoma.⁷

Due to both high frequency and heterogeneity of the modified amino acid residues, histone PTMs are notoriously difficult to analyze with conventional methods, e.g., immunoprecipitation and direct protein sequencing.^{8,9} These approaches face limitations in terms of availability of site-specific antibodies, cross-reactivity with multiple PTMs, and in some cases the large amount of material that is required.^{10–12} Additionally, the identification of novel modifications via available antibody-recognition approaches is not feasible. The occupancy of the same residues by different PTMs;^{1,13} or the simultaneous occurrence of multiple modifications in close proximity, exacerbates the challenge of investigating the function of a specific histone PTM. Mass spectrometry (MS) has thus emerged as a versatile technology to study histone

Received: February 12, 2016

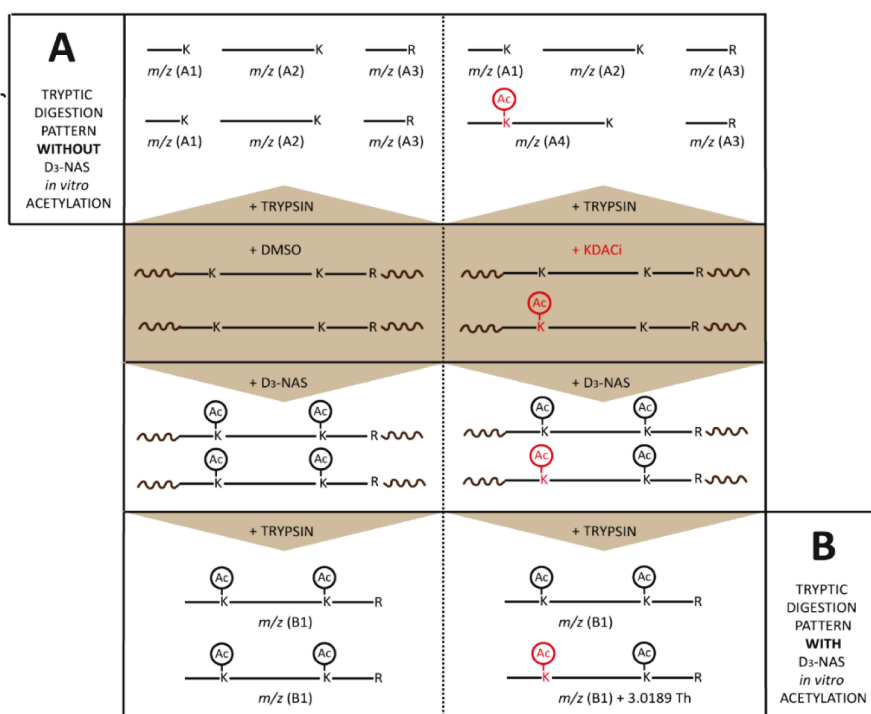


Figure 1. Effect of in vitro lysine residue acetylation with D₃-NAS on the tryptic digestion pattern of a protein. (A) Acetylated lysine residues are not hydrolyzed by trypsin, thus different digestion patterns for KDACI- compared to DMSO-treated HeLa cells occur. (B) Derivatization of nonacetylated lysine residues with D₃-NAS introduces an isotopically labeled acetyl group (COCD₃, D₃-acetylation). Tryptic digestion now occurs at arginine residues only. Regardless of the initial drug/vehicle treatment, peptides with same length, amino-acid sequence and charge state are generated.

PTMs by (i) identifying distinct and combinatorial PTMs; (ii) quantitating changes in histone PTMs across multiple samples and, most importantly; (iii) investigating novel PTMs.

Sophisticated mass spectrometric-based approaches to monitor global PTM changes on histone proteins has dramatically improved over the last two decades.¹⁴ Most of the caveats, however, are still due to the use of trypsin to digest proteins in “bottom-up” proteomic approaches. The active site of trypsin recognizes the positively charged lysine (K) and arginine (R) residue side chains and subsequently hydrolyses the peptide bond at the C-terminus. Given that N-termini of histone proteins contain multiple K and R residues, the tryptic peptides that are generated are highly hydrophilic and often not observed by MS. In addition, when the lysine side chain is modified, the peptide bond is usually not hydrolyzed by trypsin.

Exogenous perturbations with drugs that affect lysine residue modifications, e.g., KDAC inhibitors, therefore complicates the quantitation of certain peptide species as the cleavage sites in the controlled versus perturbed condition differ. As shown in Figure 1A, PTM-induced miscleavage sites of lysine residues generates longer peptides with higher *m/z* values. For some proteins, the size of these peptide species can exceed the mass range of common mass spectrometry methods and/or produce tandem mass spectra that have poor fragmentation patterns, resulting in reduced peptide-to-spectrum (PSM) matching. These caveats have been alleviated to some degree with the advent of electron-transfer dissociation (ETD)¹⁵ and middle-down approaches.¹⁶ The status quo of MS-based methodologies to investigate histone modifications has been recently reviewed by Önder et al.¹⁷

To partially overcome the problem of variable tryptic miscleavage sites between two conditions, propionylation and,

to a lesser extent, acetylation of unmodified histone lysine residues are utilized. Due to the in vitro introduction of a lysine modification, however, it is impossible to distinguish endogenous modifications from those that have been chemically introduced. Therefore, deuterated versions of propionic and acetic anhydride have been used to modify lysine residues with a D₁₀-propionyl¹⁸ or D₂/D₃-acetyl^{19–21} group(s), respectively.

For accurate quantitative MS analyses, it is crucial that the labeling prior to protein digestion is efficient and reproducible. To improve the effectiveness of in vitro modification, chemical derivatization of lysine residues via acetic anhydride can be performed twice: once at the protein level, and additionally, at the peptide level following tryptic digestion.²² This, however, does not entirely solve the issue of increased sample variability due to incomplete lysine derivatization prior to digestion. As an alternative, protein digestion with the Arg-C peptidase that cleaves C-terminally to arginine residues, followed by in vitro derivatization of the peptides has also been utilized.^{19,23} Nevertheless, Arg-C has a lower digestion efficiency and specificity compared to trypsin^{23–25} and is thus not generally the enzyme of choice in proteomic analyses.

An additional drawback with a two-step propionylation or acetylation protocol is that derivatization at the peptide level results in modification of both the ε-amino group on the lysine residue side chains and the α-amino group on peptide N-termini. Thus, the N-termini are no longer available for further labeling with different amino-reactive reagents, e.g., isobaric tags such as iTRAQ or TMT. Moreover, derivatization of the peptide N-termini is less favorable for MS analysis as the charge state is reduced. This often results in peptide species with only one positive charge at the C-terminal arginine residue.

Here we utilize the NHS-reactive reagent, *N*-acetoxy- D_3 -succinimide (D_3 -NAS). Compared to anhydride counterparts, *N*-hydroxysuccinimide esters are more efficient in derivatizing unmodified lysine residues.²³ When derivatization is performed at the protein level, full occupancy of all lysine residues by either endogenous H_3 -acetylation ($COCH_3$) or chemically introduced D_3 -acetylation ($COCD_3$) restricts tryptic digestion to the C-termini of arginine residues. As depicted in Figure 1B, regardless of the differential acetylation that occurs upon *in vivo* KDACi treatment, the peptides that are generated are now the same length, have the same charge state and amino acid composition. Therefore, these closely related peptide species essentially coelute during chromatographic separation²⁶ and, in theory, have comparable ionization and fragmentation efficiencies. Moreover, the constant mass shift of 3.0188 Da between endogenous and chemically introduced acetyl groups provides a means of predicting, observing and deconvoluting such peptide “cluster” patterns.

The improved and streamlined method described in this study combines the succinimide ester chemistry of D_3 -NAS with the filter-aided sample preparation (FASP) protocol.^{27,28} Furthermore, a targeted MS method similar to Smith et al.^{21,29} was used to simultaneously coisolate H_3 / D_3 -differentially acetylated peptide species. This was achieved by broadening the precursor-ion isolation window to concurrently fragment the differentially modified peptide “clusters”. Additionally, a data analysis algorithm based on the initial work of Smith et al.²⁹ was extended and implemented to deconvolute the complex MS^2 H_3 / D_3 -acetylated fragment ions; thus providing an unbiased relative quantitation of the differentially acetylated positional isomers based on MS^2 -ion intensity values. We have termed our approach FASIL-MS, for filter-aided stable isotope labeling coupled to mass spectrometry to profile and universally quantitate endogenous lysine acetylated positional isomers. To demonstrate the applicability of FASIL-MS, the streamlined workflow was applied to histone extracts from KDACi-treated compared to DMSO-treated cells.

■ EXPERIMENTAL SECTION

D_3 -Acetylation of Synthetic Peptides

N-Acetoxy- D_3 -succinimide (D_3 -NAS, SIGMA-Aldrich, St. Louis, MO) was incubated with the synthetic peptide AYAGKAGAR (CASLO Laboratory ApS, Lyngby, DK) in a 20- to 120-fold molar excess relative to primary amino groups. The reaction was performed for 2 h in 80% isopropanol (IPA) containing 100 mM TEAB buffer, pH 7.5–8, and quenched with 30% TFA to hydrolyze excess D_3 -NAS.

Histone H4 synthetic peptides were utilized for development and training of the data analysis algorithm. Unmodified H4, and 5 differentially acetylated H4 peptides were purchased from New England Peptide Inc. (Gardner, USA): histone H4(1–21) NTPEGBiot, H4(1–21)K5ac NTPEGBiot, H4(1–21)K8ac NTPEGBiot, H4(1–21)K12ac NTPEGBiot, H4(1–21)K16ac NTPEGBiot, H4(1–21)K5acK8acK12acK16ac NTPEGBiot. One nanomole (approximately 2.5 μ g) of each peptide was incubated separately with 100-fold molar excess of D_3 -NAS as described above. The reaction was quenched after 2 h with 5 μ L 5% hydroxylamine solution (SIGMA-Aldrich, Munich, DE). Organic solvent was removed via vacuum centrifugation, the samples were reconstituted in 30 μ L 50 mM TEAB buffer containing 25 ng trypsin (Promega Corporation, Madison, WI) and digested overnight at 37 °C. Half of the digested peptides

(500 pmol, 1.25 μ g) were acidified with 20 μ L 30% TFA, dried in vacuum concentrator and reconstituted in 50 μ L 50 mM TEAB buffer (10 pmol/ μ L). To assess purity, single peptides were diluted 200 \times in 5% FA and 8 μ L analyzed by LC–MS. The six single peptides were then mixed in a ratio of 1:0.25:0.25:0.25:0.25:1 in the same order as the peptides listed earlier in this section and analyzed by LC–MS as back-to-back technical quadruplicates.

Derivatization of Protein Lysine Residues with D_3 -NAS Coupled to Filter-Aided Sample Preparation

Filter-aided sample preparation was performed on 30 kDa molecular weight cutoff filters (VIVACON 500; Vivaproducts Inc., Littleton, MA) according to the procedure described by Manza et al.²⁷ and Wisniewski et al.²⁸ Briefly, 2 mg/mL bovine serum albumin (BSA, Roche Diagnostics Corporation, city, IN) was dissolved in 50 mM HEPES buffer pH 8.5 supplemented with 2% sodium dodecyl sulfate (SDS). Reduction of disulfide bonds was achieved by adding 100 mM dithiothreitol (DTT) and heating at 95 °C for 5 min. Volumes corresponding to 100 μ g BSA were transferred to 2 \times 5 filter units. Each sample was mixed with 200 μ L 8 M urea in 100 mM Tris-HCl (SIGMA-Aldrich, St. Louis, MO) pH 8.5 (UA) and centrifuged at 14 000g for 15 min at 20 °C to remove SDS. The remaining SDS was exchanged with urea by two additional 200 μ L UA washes. The proteins were alkylated on the filter by adding 100 μ L 50 mM iodoacetamide (IA) in 8 M urea buffer at room temperature in the dark for 30 min. The filter units were then centrifuged twice at 14 000g for 15 min with 1 \times 100 μ L UA wash step between each centrifugation. An additional 3 \times 100 μ L washes of 80% IPA in 100 mM TEAB buffer (SIGMA-Aldrich, St. Louis, MO) were performed to exchange the UA with the buffer required for the reaction with the D_3 -NAS. One hundred microliters 50 mM D_3 -NAS in 80% IPA/100 mM TEAB was added to the 5 filter units. Another set of 5 filters containing BSA and solvent only were used as controls. All the samples were incubated on a shaker at 20 °C for 2 h and the excess D_3 -NAS in 80% IPA/100 mM TEAB, or solvent alone (BSA controls), was removed by centrifugation at 14 000g for 15 min at 20 °C. All samples were washed three times with 100 μ L 50 mM TEAB buffer and centrifuged at 14 000g for 15 min at 20 °C. When the buffer was slow to permeate the filter (usually the first centrifugation step with 80% IPA in 100 mM TEAB), centrifugation was increased to 16 000g for 20 min. Five replicates of D_3 -acetylated and unmodified BSA controls were digested with trypsin overnight at 37 °C. Following incubation, digested peptides were recovered from the filter with 40 μ L 50 mM TEAB buffer and 50 μ L 0.5 M NaCl (SIGMA-Aldrich, St. Louis, MO). The peptides were acidified with 5 μ L 30% TFA, desalted using two C18 spin columns with 5–60 μ g peptide-binding capacity per sample (The Nest Group, Southborough, MA), concentrated and reconstituted with 5% formic acid (FA) to 0.02 μ g/ μ L prior to LC–MS analysis.

Cell Culture

Adherent HeLa (ATCC CCL-2; LGC Standards, Wesel, Germany) cells were cultured in 1 \times Dulbecco's modified eagle medium (DMEM) (Sigma-Aldrich, Steinheim, GE) supplemented with 10% fetal bovine serum (Life Technologies, Paisley, UK) and 1% penicillin/streptomycin (Sigma-Aldrich, Steinheim, GE) at 37 °C and 5% CO₂. Five million cells were seeded per 15 cm dish (Corning, Corning, NY) and treated the following day with 0.1% dimethyl sulfoxide (DMSO; Merck,

Darmstadt, GE) or 10 μ M suberoylanilide hydroxamic acid (SAHA; Santa Cruz Biotechnology, Dallas, TX) for 18 h in duplicate.

Acid Histone Extraction

Acid histone extraction was performed according to the protocol provided by Abcam (www.abcam.com). Cells were trypsinised with 0.25% trypsin-EDTA (Gibco, Life Technologies, Paisley, UK), harvested and washed twice in 1× phosphate-buffered saline (PBS; Sigma-Aldrich, Steinheim, GE) by centrifugation at 135g for 5 min at 20 °C. Ten million cells were resuspended in 1 mL triton extraction buffer (TEB) (PBS containing 0.5% Triton X-100 (v/v); Sigma-Aldrich, Steinheim, GE), supplemented with 2 mM phenylmethylsulfonylfluoride (PMSF; AppliChem, Darmstadt, GE), and 0.02% (w/v) sodium azide (NaN_3 ; Sigma-Aldrich, Steinheim, GE). After 10 min lysis on ice, cells were centrifuged at 376g for 10 min at 4 °C. The supernatant was discarded and the nuclei were resuspended in 500 μ L TEB. Following centrifugation at 376g for 10 min at 4 °C, the pellets were resuspended in 100–250 μ L 0.2 N hydrochloric acid (HCl, Sigma-Aldrich, Steinheim, GE). Histones were extracted overnight at 4 °C on a rotating wheel. Samples were centrifuged at 16 363g for 10 min at 4 °C, and the supernatants were transferred to new tubes. The acidic extracts were neutralized by the addition of 2/5 volume (v/v) 1 M disodium hydrogen phosphate (Na_2HPO_4 ; Sigma-Aldrich, Steinheim, GE) supplemented with 2.5 mM dithiothreitol (Sigma-Aldrich, Steinheim, GE), 3.5% (v/v) deacetylase inhibitors (Active Motif, La Hulpe, Belgium), 3.5% (v/v) protease inhibitors (Active Motif, La Hulpe, Belgium), and 3.5% (v/v) phosphatase inhibitors (Active Motif, La Hulpe, Belgium). The pH was assessed with pH-indicator strips (Merck, Darmstadt, GE). Samples were snap frozen in liquid nitrogen and stored at –80 °C.

Protein Assay

The protein abundance of the histone extracts was determined via the bicinchoninic acid (BCA) assay (ThermoScientific, Rockford, IL) using a BSA standard (ThermoScientific, Rockford, IL). Briefly, 50 μ L BCA reagent mix and 6.25 μ L BSA standard or sample per well of a 384 well plate (Corning, Corning, NY) were incubated for 30 min at 37 °C. Absorbance at 562 nm was determined on a plate reader using Softmax pro v6.3 (Molecular Devices, Sunnyvale, CA). Samples were adjusted to 1 mg/mL in 1× PBS supplemented with 1× protease inhibitors (Roche Diagnostics, Mannheim, GE), snap frozen in liquid nitrogen and stored at –80 °C.

Quantitative Immunoblot

Five micrograms of the acid-extracted histones were separated on a 16% SDS-PAGE gel, and proteins were transferred onto a 0.45 μ m pore size nitrocellulose transfer membrane (GE Healthcare Life Sciences, Vienna, AT). Unless otherwise indicated, all reactions steps were performed at room temperature (20–25 °C). Membranes were blocked in Odyssey blocking buffer (OBB) (Li-Cor Biosciences, Lincoln, NE) for 1 h, and incubated with the antibodies at 1:1000 dilutions in OBB containing 0.1% Tween 20 (v/v) (Sigma-Aldrich, Steinheim, GE) (OBBT) and 0.05% sodium azide (v/v) (Sigma-Aldrich, Steinheim, GE) on an end-overend tube rotator overnight at 4 °C. Primary antibodies used were Ac-K, H3, H3K14ac (Cell Signaling Technology, Beverly, MA); H3K18ac (Abcam, Cambridge, UK); H4K5acK8acK12acK18ac (Merck Millipore, Vienna, AT). After 3 washes for 5 min in 1× PBS containing

0.1% Tween 20 (v/v) (PBST), membranes were incubated with antisppecies fluorophore-conjugated antibodies at 1:15 000 dilutions in OBBT protected from light. Secondary antibodies used were: goat antirabbit IRDye 680RD and goat antimouse IRDye800CW (Li-Cor Biosciences, Lincoln, NE) for 1 h. After 3 washes for 5 min in PBST, blots were imaged at 700 and 800 nm on the Li-Cor Odyssey instrument (Li-Cor Biosciences, Lincoln, NE) using Image Studio v3.1 (Li-Cor Biosciences, Lincoln, NE). The intensities of the fluorescence signal corresponding to the abundance of modifications was measured, and normalized to global histone levels. Bar graphs were visualized using GraphPad Prism v6 (GraphPad Software, La Jolla, CA). Images were further processed using Adobe Photoshop CS5 v12.04 × 32 (Adobe Systems, San Jose, CA) and Adobe Illustrator CS5.1 v15.1.0 (Adobe Systems, San Jose, CA).

Propionylation of Histone Proteins with Propionic Anhydride

Propionylation was performed in solution on the histones extracted from the HeLa cells treated with SAHA or DMSO. Ten micrograms of acid-extracted histones were incubated with 20 μ L 50 mM NH_4HCO_3 (Sigma-Aldrich, Steinheim, GE) and 1 μ L propionic anhydride (Sigma-Aldrich, Steinheim, GE) for 30 min. Eighteen microliters saturated NH_4HCO_3 (pH > 8) and 1 μ L propionic anhydride were added and incubated for another 30 min. The reaction was quenched by adding 20 μ L saturated NH_4HCO_3 and 2 μ L ethanolamine (Sigma-Aldrich, Steinheim, GE) for 10 min. Samples were digested with 2 μ L trypsin gold (12.5 ng/ μ L; Promega, Mannheim, GE) in 50 mM NH_4CO_3 and 2 μ L 0.1 μ M CaCl_2 (Sigma-Aldrich, Steinheim, GE) and incubated for 1 h at 37 °C. An additional 2 μ L trypsin gold and 2 μ L 0.1 μ M CaCl_2 were added and incubated for 18 h at 37 °C. Reactions were quenched by adding 20 μ L 0.5% TFA (Sigma-Aldrich, Steinheim, GE). Samples were purified using UltraMicroSpin Column (Biozym Scientific, Hessisch Oldendorf, GE) activated with 200 μ L methanol (Sigma-Aldrich, Steinheim, GE). Prior to loading the sample, the columns were equilibrated with 200 μ L stage tip buffer (STB; 0.4% formic acid, 2% TFA). Thereafter, the column was washed once with 200 μ L STB, and peptides were eluted with 100 μ L elution buffer (0.4% formic acid, 90% acetonitrile). Peptides were lyophilized in a vacuum concentrator and reconstituted with 5% FA to approximately 0.05 μ g/ μ L. Eight microliters was injected and analyzed by LC–MS as technical replicates.

Filter-Aided Stable Isotopic Labeling (FASIL) of Histone Proteins

On-filter D_3 -acetylation was performed on the same histone extracts as the propionylation reaction described above. Two replicates each of 50 μ g histone extracts from DMSO- and SAHA-treated HeLa cells were transferred to VIVACON 500 filter units. D_3 -acetylation of unoccupied lysine residues was performed as described for BSA with minor modifications. Quenching of D_3 -NAS was achieved by adding excess of hydroxylamine solution followed by 3 × 100 μ L 50 mM TEAB buffer washes and centrifugation at 14 000g for 15 min at 20 °C. After on-filter protein digestion, peptides were recovered from the filter and desalted via C18 spin columns with 5–60 μ g peptide-binding capacity per sample (The Nest Group, Southborough, MA). Peptides were concentrated, reconstituted with 5% FA to approximately 0.05 μ g/ μ L and 8 μ L was injected and analyzed by LC–MS as technical replicates.

Liquid Chromatography Mass Spectrometry

Mass spectrometry analysis was performed on a hybrid linear trap quadrupole (LTQ) Orbitrap Velos mass spectrometer (ThermoFisher Scientific, Waltham, MA, USA) using the Xcalibur software (version 2.1.0). The instrument was coupled to an Agilent 1200 HPLC nanoflow system with a dual pump, one precolumn and one analytical column (Agilent Bio-technologies, Palo Alto, CA, USA) via a nanoelectrospray ion source with a liquid junction (Proxeon, Odense, Denmark). The peptide mixtures were automatically loaded from the thermostated autosampler (4 °C) onto a trap column (Zorbax 300SB-C18 5 μ m, 5 \times 0.3 mm, Agilent Biotechnologies, Palo Alto, CA, USA) with the binary pump solvent comprised of 0.1% trifluoroacetic acid (TFA) in water at a flow rate of 45 μ L/min. The peptides were eluted by back-flushing from the trap column onto a 16 cm fused silica analytical column with an inner diameter of 50 μ m packed with C18 reversed-phase material (ReproSil-Pur 120 C18-AQ, 3 μ m, Dr. Maisch GmbH, Ammerbuch-Entringen, DE). Solvents for peptide separation were composed of 0.4% FA in water (solvent A) and 0.4% FA in 20% isopropanol, 70% methanol (solvent B). A multistep linear gradient elution of the peptides was achieved by a 27 min gradient ranging from 3 to 30% solvent B, followed by a 25 min gradient from 30 to 70% solvent B and, finally, a 7 min gradient from 70 to 100% solvent B at a constant flow rate of 100 nL/min.

The global MS analyses were performed in a data-dependent acquisition mode. The top 10 or 15 most intense ions were selected for higher-energy collision-induced dissociation (HCD) and collision-induced dissociation (CID), respectively. In both cases, normalized collision energy was 30%. Dynamic exclusion of selected ions for MS² fragmentation was 60 s and a single lock mass at m/z 445.120024 for the siloxane Si(CH₃)₂O)₆³⁰ was used for internal mass calibration with a target loss mass abundance of 0%. Maximal ion accumulation time allowed for MS¹ was 500 ms in the C-trap, and for MS², ion accumulation times were 50 ms in the LTQ (CID) and 200 ms in the C-trap (HCD). Overfilling of the C-trap was prevented by automatic gain control (AGC) and set to 10⁶ ions for a full FTMS scan and 5 \times 10⁵ ions for MSⁿ mode. Intact peptides were detected in the Orbitrap mass analyzer at a resolution of 60 000 (CID) and 30 000 (HCD). Fragment ion resolution for HCD was 7500. Signal threshold for triggering MS² fragmentation was 5000 and 2000 ion counts for HCD and CID, respectively.

The MS acquisition method for the targeted approach was as described above with the following changes. An inclusion list was utilized to target the differentially H₃/D₃-acetylated H4(4–17) and H3(18–26) peptides for fragmentation. Dynamic exclusion was disabled to increase recurrent fragmentation of the targeted monoisotopic m/z values. The precursor ion masses that were monitored were recalculated from H₃/D₃-acetylated doubly charged peptide species that were distinguishable in the MS¹ spectrum. For the H4(4–17) and H3(18–26) histone proteins, 5 and 3 m/z values were chosen, respectively (H4(4–17): 719.910515, 721.41993, 722.929345, 724.43876, and 725.948175 m/z ; and H3(18–26): 535.820085, 537.3295, and 538.838915 m/z). Additionally, the precursor-ion isolation width was broadened to ± 7.0 Th to simultaneously isolate and subsequently fragment coeluted doubly charged peptide species in the H₃/D₃-acetylated histone H4 or H3 “cluster”.

MS¹-Based Peptide Quantitation of Global Mass Spectrometry Analyses

Raw MS files were analyzed with Proteome Discoverer version 1.4 (ThermoFisher Scientific, Waltham, MA, USA) using Mascot³¹ for peptide/protein identification. The precursor ion mass tolerance was ± 10 ppm, whereas the fragment ion mass tolerances were ± 0.6 and ± 0.02 Da for CID- and HCD-fragmented peptides, respectively. Data files were searched with trypsin as the defined protease with up to 4 miscleavage sites. BSA peptide identification was performed by searching the resultant peak list against the SwissProt bovine database version 2014–07 (6,515 sequences including isoforms obtained from varsplic.pl³² and appended known contaminants). Carbamidomethylation of cysteine residues was set as a static modification, whereas methionine oxidation and lysine D₃-acetylation were set as dynamic modifications.

Peak lists from the global histone MS analyses were searched against the human SwissProt database version 2014–07 (40 984 sequences including isoforms obtained from varsplic.pl³² and appended known contaminants). Carbamidomethylation of cysteine residues was again a static modification, whereas methionine oxidation and lysine H₃-acetylation were set as dynamic modifications. In addition, dynamic D₃-acetylation and propionylation of lysine residues was set in the search parameters for the D₃-NAS and PA modified histone extracts, respectively.

For the global and targeted MS analyses, the *Percolator* and *Target Decoy PSM Validator* nodes of Proteome Discoverer, respectively, were utilized to remove peptides with a false discovery rate (FDR) of $>1\%$. Calculation of the FDR was based on the q -value after the decoy database search. MS¹ peak area-under-the-curves were assigned to peptides via the *Precursor Ion Area Detection* node with a mass precision of ± 2 ppm. On the basis of manual inspection of the MS² spectra, peptides with a Mascot ion score <18 were poorly annotated and were thus removed from further data analysis. In addition, only peptides with a minimum length of 6 amino acid residues, high peptide confidence and ranked 1 were considered. Statistically significant changes between the results were calculated with GraphPad Prism version 6.00 for Windows (GraphPad Software, La Jolla California USA; www.graphpad.com), utilizing 2 sample t test for assignment of the p -values. Exact p -values were additionally calculated and verified utilizing a 2-sample t test in the R package.

An Extended MS²-Based Peptide Quantitation Algorithm

MS²-based quantitation of H₃/D₃-acetylated peptides was based on a set of linear equations initially introduced by Smith et al.²⁹ The analysis method presented here solves for relative abundance of all possible H₃/D₃-acetylation states of a peptide p consisting of L amino acid residues from which N are lysines located at positions x_1, \dots, x_N . Each of the N lysines can be either H₃- or D₃-acetylated, thus resulting in 2^N possible acetylation states of the peptide p , each of which is annotated by a unique number from the set $\{1, \dots, 2^N\}$. For example, the isoform with all H₃-acetylated lysines will be annotated as 1 while the isoform with all D₃-acetylated lysines will be 2^N . The exact order of numbers assigned to the different acetylation states is, however, not crucial for the analysis as long as each acetylation state is uniquely annotated.

Any b-ion of peptide's k^{th} fragment is further defined as b^k , with k in the range 1, ..., L . As previously noted, MS data were collected by targeting $N + 1$ possible doubly charged

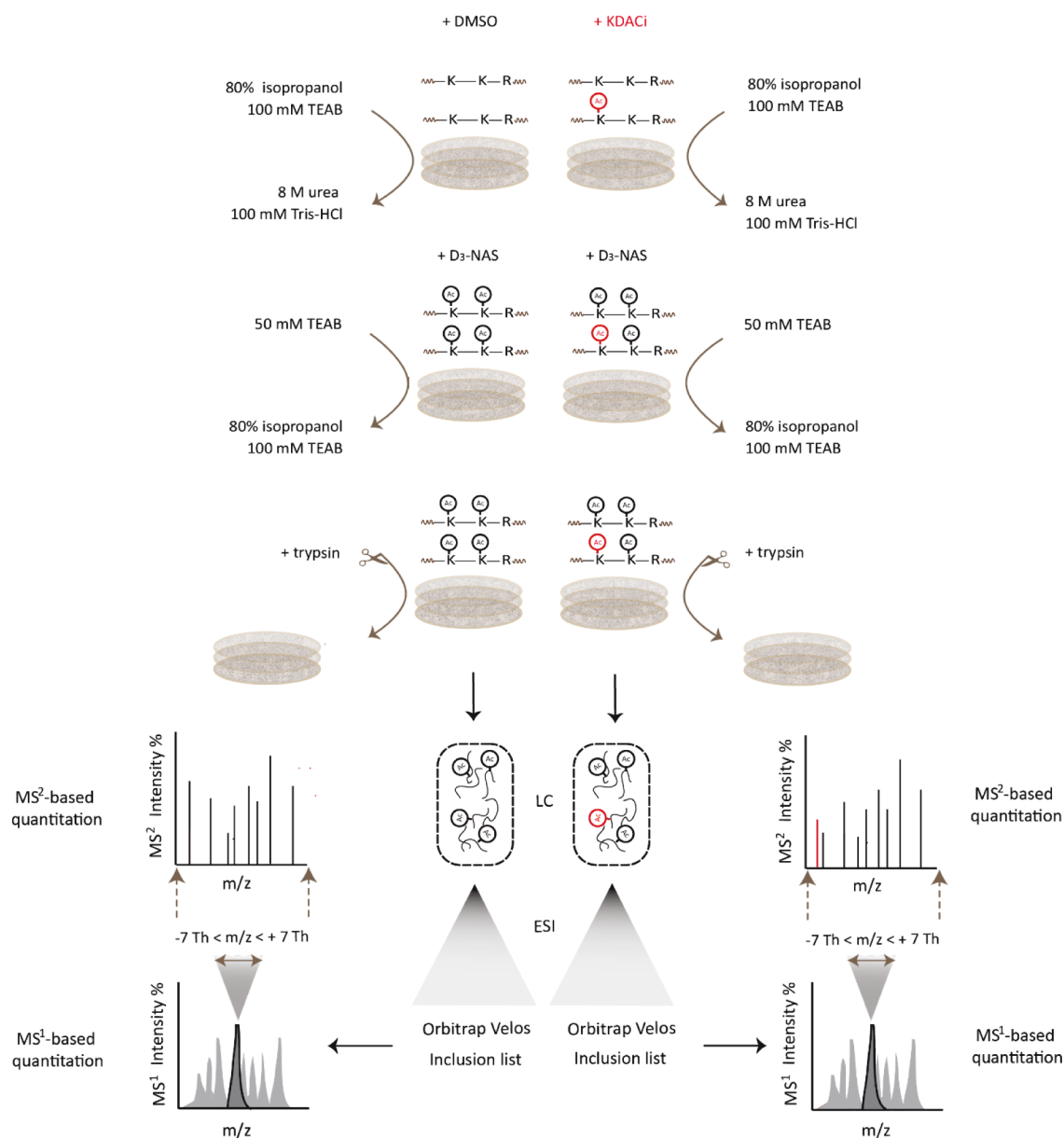


Figure 2. Schematic representation of the FASIL-MS workflow. A 30 kDa molecular-weight cutoff filter was utilized to exchange solvents between the various sample preparation steps. Fully lysine residue-acetylated proteins were digested with trypsin and analyzed by liquid chromatography tandem mass spectrometry. Label-free quantitation by area-under-the-curve peak integration of the differentially acetylated peptides was performed on the MS¹ trace. The precursor-ion isolation width for targeted peptide species was broadened to encompass the differentially H₃/D₃-acetylated peptide clusters and relative quantitation of the isobaric peptides species was determined from the intensities of b- and y-ions present in MS² spectra via an automated bioinformatic algorithm. In vivo-acetylated lysine residues (H₃-acetylated) are depicted in red; whereas the chemically introduced lysine modifications (D₃-acetylated) are marked in black.

monoisotopic precursor ion masses of the peptide p . The utilized MS method (i.e., with an inclusion list and a broadened precursor ion isolation window) can be extended to target different charge states of the histone peptides. The doubly charged ions, however, were the predominant species in the mass spectra and were thus used in the algorithm.

The relative abundance of a specific b-ion can be estimated from the measured MS² intensities. To account for variable abundances of the targeted peptides present in the sample, MS²-based intensities in each spectrum were initially normalized by the corresponding filling time and then integrated over the retention time (t_R) of the peptide p . The normalized and integrated abundances of different b^k ions can

be attributed to a mixture of different 2^N acetylation states via a set of linear equations similar to those used by Smith et al.²⁹ that can be equivalently described in the following matrix form:

$$t_{b_k} \mathbf{M}_{b_k} \mathbf{P} + \boldsymbol{\epsilon}_k = \mathbf{I}_{b_k} \quad (1)$$

where the scalar value t_{b_k} represents the total observed abundance of all possible b^k ions; \mathbf{P} is a vector of relative proportions of each acetylation state (p_1, \dots, p_{2^N}) such that $\sum p_i = 1$; \mathbf{I}_{b_k} is a vector ($I_{b_{k1}}, \dots, I_{b_{kN}}$) of integrated intensities of k^{th} b-ions for each individual acetylation isoform 1, ..., 2^N ; $\boldsymbol{\epsilon}_k$ is a noise vector, and \mathbf{M}_{b_k} is a design matrix describing which acetylation state can generate given b^k ions. The dimensionality

of the matrix \mathbf{M}_{b_k} and the noise vector $\boldsymbol{\varepsilon}_k$ are $2^N \times 2^N$ and 2^N , respectively. Due to the background noise of MS measurements, the noise vector $\boldsymbol{\varepsilon}_k$ that was not modeled in Smith et al.²⁹ is close to, but not necessarily equal to, $\mathbf{0}$. In cases when multiple acetylation isoforms have identical m/z values for the b^k ion, the corresponding elements of the \mathbf{I}_{b_k} vector will have identical values. The design matrix \mathbf{M}_{b_k} of eq 1 is thus defined as

$$\forall i, j \in \{1, \dots, 2^N\} \quad \mathbf{M}_{b_k}[i, j] = \begin{cases} 1 & \text{if } m/z \text{ of } b^k \text{ ion of acetylation isoforms } i \\ & \text{and } j \text{ are equal} \\ 0 & \text{otherwise} \end{cases}$$

Due to the above relation, the matrix \mathbf{M}_{b_k} does not have to be manually derived for each peptide but can be generated automatically by the algorithm. The meaning of eq 1 is that the total observed intensity of each given b^k ion, I_{b_k} , must proportionally correspond to the relative abundances of individual acetylation isoforms (up to the measurement noise $\boldsymbol{\varepsilon}_k$). The above definition of $\mathbf{M}_{b_k}[i, j]$ means that a measured intensity of k -th b-ion corresponding to the isoform i can be observed due to the presence of those, and only those isoforms j that can generate the k -th b-ion of the same m/z value as that of the isoform i .

The unknown vector \mathbf{P} of eq 1 is determined by minimizing the norm of the noise vector $\boldsymbol{\varepsilon}_k$. Eq 1 corresponding to a given b-ion does not necessarily have a unique solution for the vector \mathbf{P} . For example, b-ions not containing any lysine residue have identical m/z values in all H_3/D_3 -acetylated isoforms of peptide p , and thus do not provide any information about the vector \mathbf{P} . Indeed, given that the N lysine residues of the peptide p are on positions x_1, \dots, x_N , then the design matrices $\mathbf{M}_{b_1}, \dots, \mathbf{M}_{b_{(x_1-1)}}$ have all elements equal to 1. Likewise, for each $n \in \{1, N\}$ all b-ions in the range $b^{x_n}, \dots, b^{(x_{n+1}-1)}$ have an identical design pattern and the corresponding matrices \mathbf{M}_{b_i} are identical. Thus, instead of considering a separate eq 1 for each of the L b-ions, the following equation can be equivalently written for each $n \in \{1, \dots, N\}$:

$$\left(\sum_{i=x_n}^{x_{n+1}-1} t_{b_i} \mathbf{M}_{b_i} \right) \mathbf{P} + \sum_{i=x_n}^{x_{n+1}-1} \boldsymbol{\varepsilon}_i = \sum_{i=x_n}^{x_{n+1}-1} \mathbf{I}_{b_i} \quad (2)$$

An important advantage of the set of N eq 2 is that the set of these equations is not singular as opposed to the original set of L equations of type (1).

As previously suggested by Smith et al.,²⁹ the above reasoning for b-ions can be equally applied to y-ions. Therefore, the following equations for each $n \in \{1, \dots, N\}$ were obtained:

$$\left(\sum_{i=x_{n-1}+1}^{x_n} t_{y_i} \mathbf{M}_{y_i} \right) \mathbf{P} + \sum_{i=x_{n-1}+1}^{x_n} \boldsymbol{\varepsilon}'_i = \sum_{i=x_{n-1}+1}^{x_n} \mathbf{I}_{y_i} \quad (3)$$

The terms \mathbf{M}_{y_i} , \mathbf{I}_{y_i} , and $\boldsymbol{\varepsilon}'_i$ in eq 3 are defined the same way as the b-ion related equivalents, while the unknown vector of relative proportions \mathbf{P} is shared with eq 2. To solve for the relative proportions \mathbf{P} , the sum $\sum |\boldsymbol{\varepsilon}_i|^2 + |\boldsymbol{\varepsilon}'_i|^2$ from all $2N$ eqs 2 and 3 was minimized with a constrain of $p_j \geq 0$ for all $j \in \{1, \dots, 2^N\}$. Minimizing the above sum of the noise norms squared is equivalent to determining the maximum likelihood solution of eq 2 and 3 under the assumption of independent Gaussian

distribution of each noise element with mean zero and same standard deviation. Under our experimental conditions the noise is $<1\%$ (see Figure 6D).

The described algorithm is fully automated as a set of scripts employing a penalised constrained least-squares fitting method from the mgcv package in R and is available for download from Zenodo at <https://zenodo.org/record/51189> and GitHub at <https://github.com/petomajci/FASIL-MS>.

RESULTS AND DISCUSSION

Filter-Aided Stable Isotopic Labeling of Lysine Residues at the Protein Level with D_3 -NAS is Reproducible

The labeling of primary amines with D_3 -NAS was demonstrated on an intact protein to show the reproducibility of lysine residue derivatization by D_3 -acetylation prior to enzymatic digestion. Due to a high proportion of lysine residues ($\sim 10\%$ of the protein amino-acid sequence), BSA was chosen as a model protein. Optimisation of the experimental conditions was first performed on a synthetic peptide AYAGKAGAR (data not shown), and then applied to BSA. In the latter case, the in vitro derivatization of lysine residues was simultaneously coupled to FASP. Combining the stable isotopic labeling of the lysine residues with D_3 -NAS with on-filter protein digestion, reduced sample preparation time compared to previously reported methods utilizing NHS-reactive reagents.^{20,33,34} In particular, lysine residues were labeled in a single derivatization step after 2 h and the exchange of the various buffers that are required for reduction, alkylation, D_3 -NAS derivatization and digestion was simplified. As shown schematically in Figure 2, solvents were exchanged from an aqueous system for reduction and alkylation of the proteins, to 80% isopropanol for D_3 -NAS labeling of the lysine side chains and back to an aqueous buffer for tryptic digestion of the acetylated proteins. All the steps were performed on the filter and each buffer was removed via centrifugation, thus providing yet another advantage compared to previously reported methods where acetone precipitation, lyophilization and/or concentration in a vacuum concentrator were utilized.^{19,22,23,33}

The reproducibility of the D_3 -acetylated BSA tryptic digest was assessed on $5 \times 100 \mu\text{g}$ BSA and compared to $5 \times 100 \mu\text{g}$ unlabeled BSA controls. Following lysine acetylation with D_3 -NAS, the sequence coverage of the tryptically digested BSA decreased from 80 ± 1 to $20 \pm 1\%$. This result was expected, simply due to the fact that the amino acid sequence of BSA contains more lysine in comparison to arginine residues. Ideally, no peptides with C-terminal lysine residues should be observed after D_3 -acetylation of BSA. Nevertheless, a single, triply charged peptide GLVLIAFSQYLQQCPFDEHVK at m/z 831.4269 was apparent in 4 of the 5 samples. The abundance of this peptide, however, was 3 orders of magnitude lower than all other peptides culminating in a C-terminal arginine residue (Figure 3).

The reproducibility of the on-filter BSA derivatization and tryptic digestion thereof was assessed by comparing the variability in the MS^1 area-under-the-curve quantitation of underivatized and D_3 -NAS derivatized BSA. Only peptides with a C-terminal arginine residue were considered. Quintuplicate measurements for the underivatized and D_3 -acetylated BSA resulted in mean values of the cumulative peptide areas equal to 8.6×10^8 and 7.8×10^8 , respectively (Supplementary Table S1). The corresponding coefficient of variation (CV) was $<10\%$ higher for D_3 -acetylated BSA compared to the unlabeled

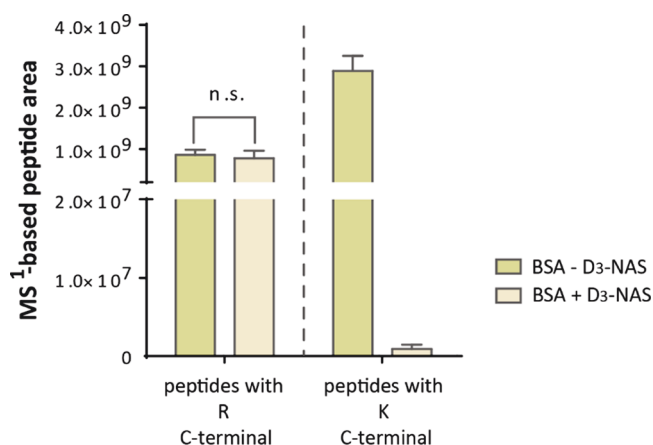


Figure 3. Comparison of the tryptic digestion pattern of unlabeled and D₃-acetylated BSA to assess the reproducibility of D₃-NAS derivatization at the protein level. Unmodified BSA was digested with trypsin to generate peptides with both C-terminal arginine and lysine residues. D₃-acetylation of the BSA lysine residues resulted in tryptic peptides with C-terminal arginine residues only. The coefficient of variation (CV) of the cumulative MS¹ areas of the peptides with a C-terminal arginine residue was utilized to assess the reproducibility of D₃-NAS-modified compared to unmodified BSA. Peptides were fragmented in the linear trap and the generated data analyzed with Proteome Discoverer.

samples. In particular, the CV of the total MS¹ area of the BSA peptides culminating in an arginine residue was 15% and 23.5% for unlabeled and D₃-NAS derivatized BSA, respectively (Supplementary Table S1). Overall, the reproducibility of D₃-acetylation of the protein and subsequent tryptic digestion was reliable and comparable to the unlabeled protein.

SAHA-Treatment of HeLa Cells Increases In Vivo Acetylation of Histone Proteins

Dynamic changes in protein acetylation were monitored in HeLa cells treated with 0.1% DMSO (control) and 10 μ M SAHA for 18 h. KDAC inhibition was verified by SDS-PAGE of histones extracted by acid and quantitative immunoblotting against global, histone H3(C-terminal), H3K14ac and H3K18ac, and global H4(C-terminal) H4K5acK9acK12acK14ac marks. Compared to the DMSO-treated samples, an approximate 10-fold increase in global histone acetylation patterns was observed following SAHA treatment. These data confirmed that the drug concentration utilized in this study was efficient in inhibiting nuclear KDACs (Figure S1A). In particular, acetylation of the H4(4–17) and H3(18–26) peptides GKGKGLGKGGAKR and KQLATKAAR was increased by 5- and 3-fold, respectively (Figure S1B and C). Once alterations in histone acetylation were confirmed by these immunoblot experiments, the samples were used throughout the study as described in the following sections.

Derivatization Efficiency of Lysine Residues with D₃-NAS at the Protein Level is Increased Compared to Propionylation

D₃-NAS was assessed for lysine residue derivatization efficiency and compared to one of the existing standard methods used in the analysis of histone PTMs. Histone extracts from DMSO- and SAHA-treated HeLa cells were separately modified with D₃-NAS and propionic anhydride (PA), digested with trypsin and analyzed by LC–MS. Similar to D₃-NAS, PA is a reagent that modifies lysine residues which have not been acetylated in vivo. Derivatization of histone proteins via PA is a

straightforward procedure and can be performed in an aqueous solution without any additional steps such as solvent exchange. The labeling of lysine residues at the protein level with PA, however, is not often complete.²³ Therefore, the labeling efficiency is usually boosted by two derivatization steps.²² Each round of modification is followed by incubation prior to a final quenching of the reaction with ethanolamine.

The two methods of lysine residue labeling at the protein level were compared to assess the efficiency of lysine derivatization. Different labeling techniques and the modification(s) introduced were evaluated on the histone H4(4–17) peptide GKGKGLGKGGAKR by monitoring efficiently and inefficiently modified lysine residues. In both cases, lysine derivatization efficiency was evaluated via the relative abundance of the peptide that was either fully modified (4 lysine modifications present) or partially modified (<4 modified lysine residues). Peptides that were not fully derivatized can be further cleaved by trypsin, generating shorter peptide fragments than the peptides with all four lysine residues occupied. Therefore, H4(4–17) peptides that were only partially modified and/or shorter in length are indicative of inefficient D₃-NAS or PA derivatization at the protein level. In order to obtain a relative abundance of efficiently and inefficiently derivatized H4(4–17) peptide species, the MS¹ area-under-the-curve was obtained for every differentially modified peptide species that was identified. In each sample, derivatization efficiency was assessed by determining the relative abundance of efficiently versus inefficiently derivatized H4(4–17) peptides. D₃-NAS showed a higher efficiency in lysine derivatization via succinimide ester chemistry compared to the conventional PA method (Figure 4, Supplementary Table S2). The relative abundance of the efficiently derivatized H4(4–17) peptide was approximately 15% and 5% higher in DMSO- and SAHA-treated samples, respectively. The observed difference in labeling efficiency of D₃-NAS and PA between the two conditions was not entirely unexpected. SAHA-induced in vivo H₃-acetylation naturally results in a higher occupancy of

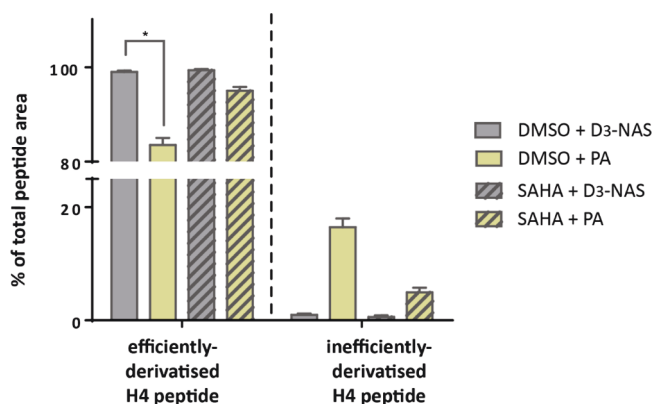


Figure 4. Comparison of D₃-NAS and PA labeling efficiency on histone lysine residues at the protein level. All 4 lysine residues were modified (in vivo or in vitro) in the fully derivatized H4(4–17) peptide. If derivatization is incomplete, free lysine residues are cleaved by trypsin. The abundance of these shorter peptides and the full-length peptides with <4 modifications can be utilized to assess the abundance of inefficiently derivatized H4 peptides. Compared to propionic anhydride (PA), D₃-acetylation of histone lysine residues resulted in an up to 15% increase in derivatization efficiency. Peptides were fragmented in the HCD cell and the generated data analyzed with Proteome Discoverer.

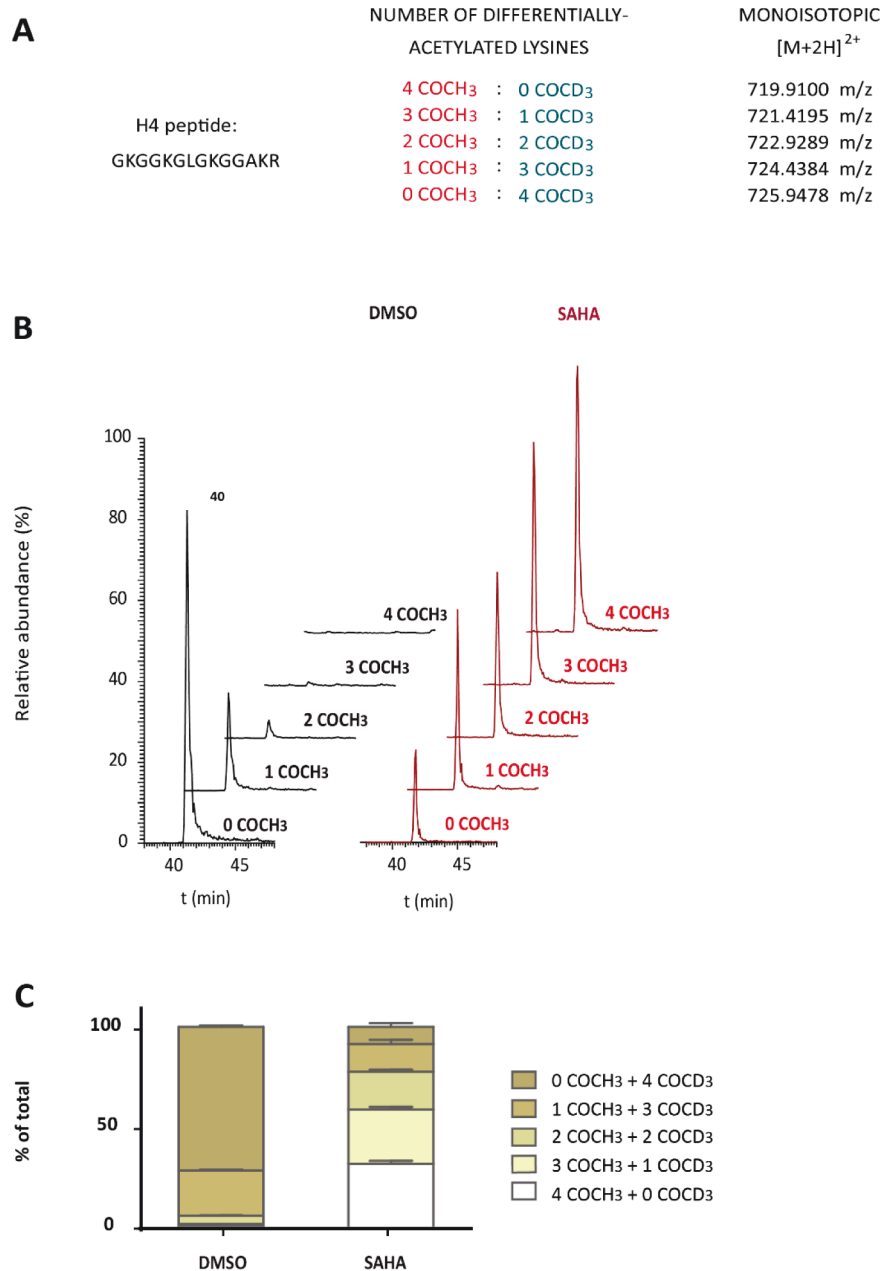


Figure 5. MS¹ quantitation of the differentially H₃/D₃-acetylated peptides from the N-terminal tail of histone H4. (A) List of expected monoisotopic *m/z* values corresponding to the differentially H₃/D₃-acetylated doubly charged H4(4–17) histone peptides. (B) Representative extracted ion chromatograms for the *m/z* values corresponding to the differentially H₃/D₃-acetylated doubly charged GKGGKGLGKGGAKR peptide after DMSO and SAHA treatment. Data is normalized to the most intense peak. (C) Area-under-the-curve determined from the MS¹ trace via peak integration for each doubly charged peptide species represented as percentage of the total area. The values are the mean of biological and technical replicates for both DMSO and SAHA treatments. For simplicity, D₃-acetylation has been omitted and only the number of H₃-acetylated lysines are indicated on the chromatograms. MS² data acquisition was performed in the HCD cell.

the lysine residues. Subsequently, the number of unmodified lysine residues available for *in vitro* derivatization by either D₃-NAS or PA is reduced with an apparent improvement in labeling efficiency by PA in the SAHA-treated samples.

Taken together, D₃-NAS resulted in a significantly higher (*p* = 0.0131) relative abundance of fully derivatized H4 peptides with fewer and less abundant inefficiently labeled peptide species. This advantage over the methods commonly utilized in the field of histone proteomics leads to reduced MS¹ spectral heterogeneity and potentially increases the accuracy of histone PTM quantitation. Moreover, the improvement in the labeling

efficiency is promising for the quantitative LC–MS analysis of endogenous acetylation levels of more complex biological samples.

In Vitro D₃-Acetylation of Histone Extracts Coupled to FASP Enables Global Monitoring of SAHA-Induced Endogenous Acetylation Changes in HeLa Cells

Lysine residues that were not endogenously acetylated *in vivo* in the DMSO- and SAHA-treated samples were blocked *in vitro* with D₃-NAS. Following tryptic digestion, peptides containing H₃-acetyl groups were the result of endogenous acetylation; whereas lysine residues not acetylated *in vivo* were marked via

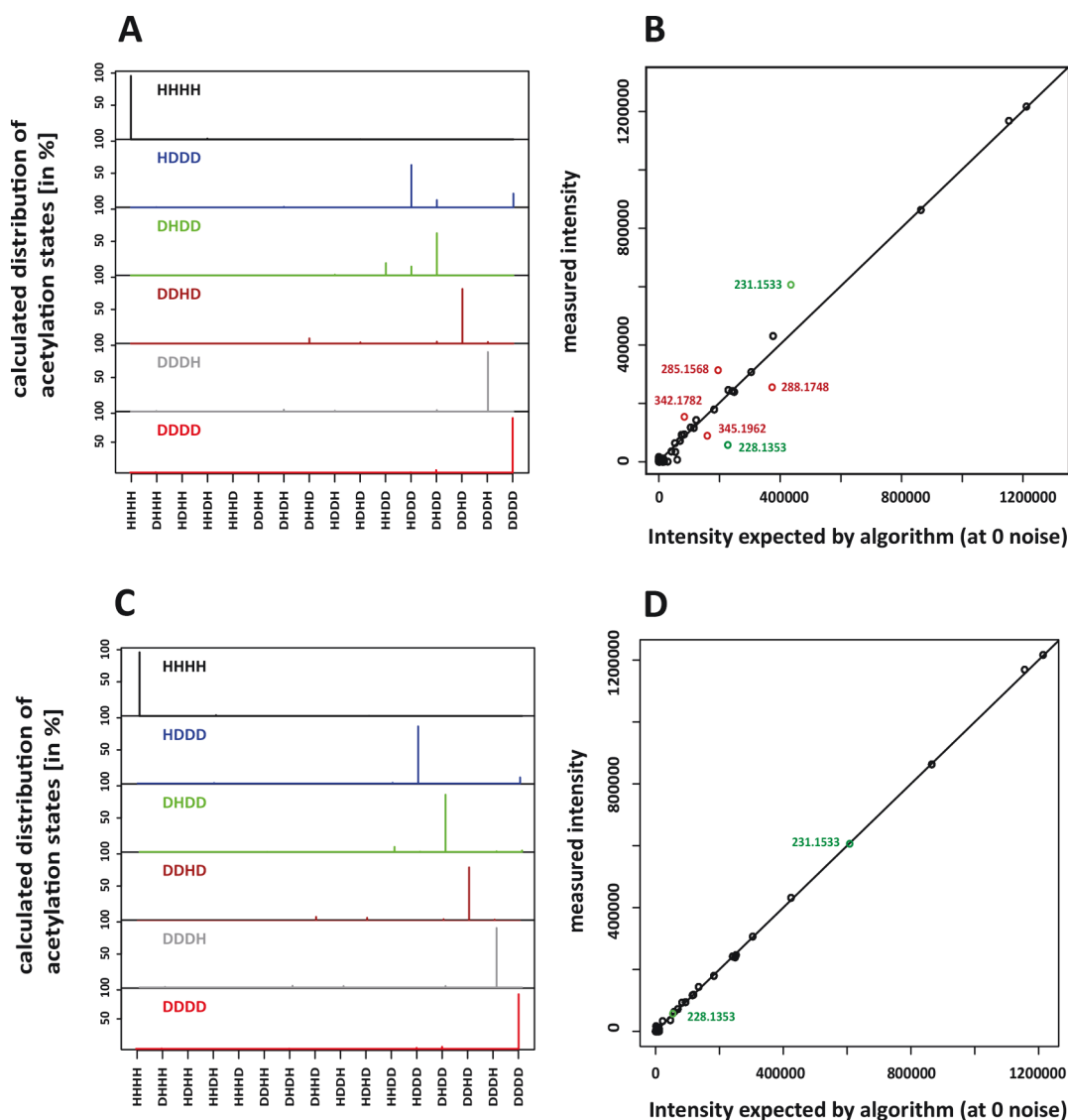


Figure 6. Adaptation of the MS²-based quantitation algorithm via purity-profiling of differentially H₃/D₃-acetylated histone H4(4–17) peptides. (A) Purity of the six H4(4–17) synthetic peptides as assessed via separate LC–MS analyses: (i) 4 D₃-acetylated lysine residues (DDDD); (ii) 4 positional isomers containing 3 D₃- and 1 H₃-acetylated lysine residues (HDDD, DHDD, DDHD and DDDH); and (iii) 4 H₃-acetylated lysine residues (HHHH). (B) The correlation plot of observed and expected intensities of each b- and y-ion for the H4K8ac synthetic peptide (i.e., DHDD) with initial fitting of the expected and measured values of all MS² fragment ions. (C, D) Corrected purity profile and correlation of the expected and measured MS² ion intensities for H4K8ac after removal of the interfering b3- and b4-ions. b3- and b4-ions that were removed are marked in red, while the b2-ions are colored in green. For simplicity, H₃- and D₃-acetylation are labeled as H and D, respectively. The sequence order correlates with the position of the lysine residues in the peptide. MS² data acquisition was performed in the HCD cell.

the chemical introduction of a deuterated D₃-acetyl group. The MS¹ spectra of differentially H₃/D₃-acetylated histone peptides were initially manually screened to identify clusters indicative of acetylation. For doubly charged ions there is only 1.5059 Th between the different acetylated peptide species (Figure 5A). Extracted ion chromatograms (XICs) of *m/z* values corresponding to differentially acetylated peptide species of histone H4(4–17) were obtained as represented in Figure 5B. The peak areas were integrated over the HPLC retention time (*t_R*) and the relative abundance of each H₃/D₃-acetylated peptide species is represented as a percentage of the total cumulative area of the peptide with the same amino-acid sequence (Figure 5C, Supplementary Table S3). In this way, global changes in the number of in vivo-acetylated lysine residues can be evaluated between the DMSO- and SAHA-treated samples. Compared to the DMSO control, the histone H4(4–17)

peptide GKGGKGLGKGGAKR showed an increase in the in vivo H₃-acetylated lysine residues following treatment with SAHA. After DMSO treatment, the predominant differentially acetylated species was the peptide with no in vivo acetylation. Approximately 70% and 25% of the peptides contained no and one H₃-acetylation, respectively; followed by ~4% of the peptides with two in vivo-acetylated lysine residues, and <1% with three- and four H₃-acetyl groups. After 10 μM SAHA treatment for 18 h, however, peptides containing no or one H₃-acetyl group were under-represented (9% and 14%, respectively), while the predominant peptide species contained three or all four H₃-acetylated lysine residues (approximately 30% each). These data thus confirmed previous reports where treatment of SAHA resulted in an increase in apoptotic cells and pro-caspase 3 expression, accompanied by a time-

dependent increase in either total or single histone H4 lysine acetylation.³⁵

Similarly, an increase in SAHA-mediated in vivo H₃-acetylation was observed on the histone H3(18–26) peptide KQLATKAAR. Conversely to histone H4(4–17), the H3(18–26) lysine H₃-acetylation increased to a lesser degree with approximately 20–25% of the lysine residues unaffected by the drug treatment. [Supplementary Table S3](#) contains the absolute values of the manually integrated MS¹ peak areas. In addition, the relative abundances normalized to the total cumulative areas for each H₃/D₃-acetylated peptide species and standard deviation (SD) of two biological and technical replicates are included. The maximal SD's for the calculations of the H4 and H3 peptide peak areas were 2.0% and 0.6%, respectively.

Application of an MS²-Based Data Analysis Algorithm Enabled Quantitation of Differentially H₃/D₃-Acetylated Positional Isomers

Monitoring the MS¹ spectra of the differentially H₃/D₃-acetylated peptides revealed global increases in in vivo (H₃) lysine acetylation upon KDACi treatment. The integrated MS¹ areas could not, however, be utilized to assign an increase in a particular positional H₃-acetylated lysine residue. Thus, an MS²-based quantitative approach was developed in order to quantitate relative changes in H₃/D₃-acetylation on each and every lysine residue.

To achieve this aim, differentially H₃/D₃-acetylated histone H4(4–17) synthetic peptides were utilized to train an improved and extended MS²-based algorithm for quantitation of positional isomers. This is based on the original work of Smith et al.^{21,29} Single histone H4(1–21) NTPEG-biotinylated peptides containing a different number and/or localization of H₃-acetylated lysine residues were modified in vitro with D₃-NAS. Prior to in vitro modification, the peptides were comprised of the following lysine residue modifications: (i) all four H₃-acetylated lysine residues; (ii) one H₃-acetylation at K5, K8, K12 and K16; and (iii) no acetylation at any of the four lysine residues. Following D₃-NAS labeling, the peptides subsequently contained: (i) four H₃-acetylated lysine residues; (ii) three D₃- plus one H₃-acetylation; and (iii) four D₃-acetylated lysine residues, respectively. The D₃-NAS-labeled NTPEG-biotinylated peptides were digested with trypsin to generate histone H4(1–21) peptides that would normally be observed in a biological setting. The individual samples were analyzed by LC–MS to verify the presence of the predicted acetylated peptide species. An inclusion list with all the theoretical monoisotopic *m/z* values corresponding to doubly charged H4(4–17) precursor ions (i.e., *m/z* 719.9105, 721.4199, 722.9293, 724.4388, and 725.9482) were targeted for fragmentation with dynamic exclusion disabled. This resulted in recurrent fragmentation of the targeted monoisotopic precursor ion(s) across the entire elution profile. In addition, a broad precursor-ion isolation window of ± 7.0 Th was used to coisolate and subsequently cofragment any other H₃/D₃-acetylated peptide species that may be present as a contaminant in the individual synthetic peptide samples. The MS²-based quantitative algorithm confirmed that four of the six peptides contained H₃/D₃-acetyl groups at the correct positions ([Figure 6A](#)). The peptides with a H₃-acetylation at position H4K5 and H4K8, however, did not return the expected results. Manual inspection of multiple MS² spectra for H₃-acetylated H4K8 revealed that there were unexpected peaks corresponding to b₃- and b₄-ions of the H4K8-D₃-acetylated form of the

peptide (data not shown). These two ions deviated by 3.018 Th from the calculated monoisotopic *m/z* values of 285.1564 and 342.1778 ([Figure 6B](#)). The most plausible explanation for such observations and the subsequent skewing of the MS²-based quantitation is due to the generation of internal fragment ions that have similar monoisotopic *m/z* values as the b-ions that were used to assess H4K8 H₃/D₃-acetylation. Thus, for H4K5 and H4K8 H₃-acetylation, this internal fragmentation resulted in additional “contaminating” ions that originated from GK, GKG, and GKGG each with a D₃-acetyl moiety. Coincidentally, these internal fragments with a D₃-acetylated lysine residue have an identical monoisotopic *m/z* value to D₃-acetylated (+3.0188 Th) b₂-, b₃- and b₄-ions. For the b₂-ion, a contaminating peak that deviated by +3.018 Th was also apparent. The intensity of this ion, however, was approximately 90% lower than the correct b₂-ion. Thus, the b₂-ion was included in assessing the relative quantitation of H₃/D₃-acetylation at the H4K5 lysine residue, and only the b₃- and b₄-ions were removed from the algorithm for the MS²-based quantitation. Implementation of the above changes resulted in accurate relative quantitation of the H4(4–17) positional isomers ([Figure 6C and 6D](#)).

These observations were a key and important point in the experimental design outlined in this study. Therefore, in silico prediction of potential interfering ions that could potentially influence MS²-based quantitation was implemented into the algorithm. These theoretical fragment ions, however, are not always observed under all MS experimental settings. Thus, it is advisable to individually assess the synthetic version(s) of the peptide of interest to manually exclude ions that can distort the MS²-quantitation.

As specified by the manufacturer, the D₃-NAS-derivatized synthetic peptides were confirmed by LC–MS as >90% pure ([Figure 6C](#)). The H4K12ac peptide, however, had a slightly lower purity than the other peptides (83%). Overall, the observed contamination from other H4(4–17) H₃/D₃-acetylated species was minor, and thus considered negligible.

The MS²-based quantitative algorithm was then assessed on the six synthetic peptide mix that contained differentially H₃/D₃-acetylated lysine residues to mimic the peptide “cluster” that would occur after D₃-NAS derivatization of a biological sample. The sample was analyzed using our targeted MS method with dynamic exclusion disabled and a precursor-ion isolation window of ± 7.0 Th. The fully H₃- and fully D₃-acetylated H4(4–17) were mixed in an equimolar ratio. The isobaric peptide species containing one H₃- and three D₃-acetylated lysine residues, however, had altered ratios and thus MS²-based quantitation was required to delineate the data. In particular, peptides with one H₃-acetyl group located at different lysine residues, i.e., H4K5, H4K8, H4K12, and H4K16 (724.4388 *m/z*) were first mixed in an equimolar ratio and then supplemented with the equivalent amount of H4(4–17) peptide with 4 H₃- or 4 D₃-acetyl groups (719.9105 and 725.9482 *m/z*, respectively).

Application of the MS²-based method enabled relative quantitation of the differentially acetylated peptides in the mixture. The ratios calculated by the MS²-based method were in agreement with the input mixing ratios ([Supplementary Figure S2](#)). Modest discrepancies between the theoretical and experimentally observed ratios, however, were evident for two of the H₃-acetylated (DDHD, DDDH) and the fully D₃-acetylated (DDDD) H4(4–17) peptide. This observation can be partially explained by the impurities present in the original

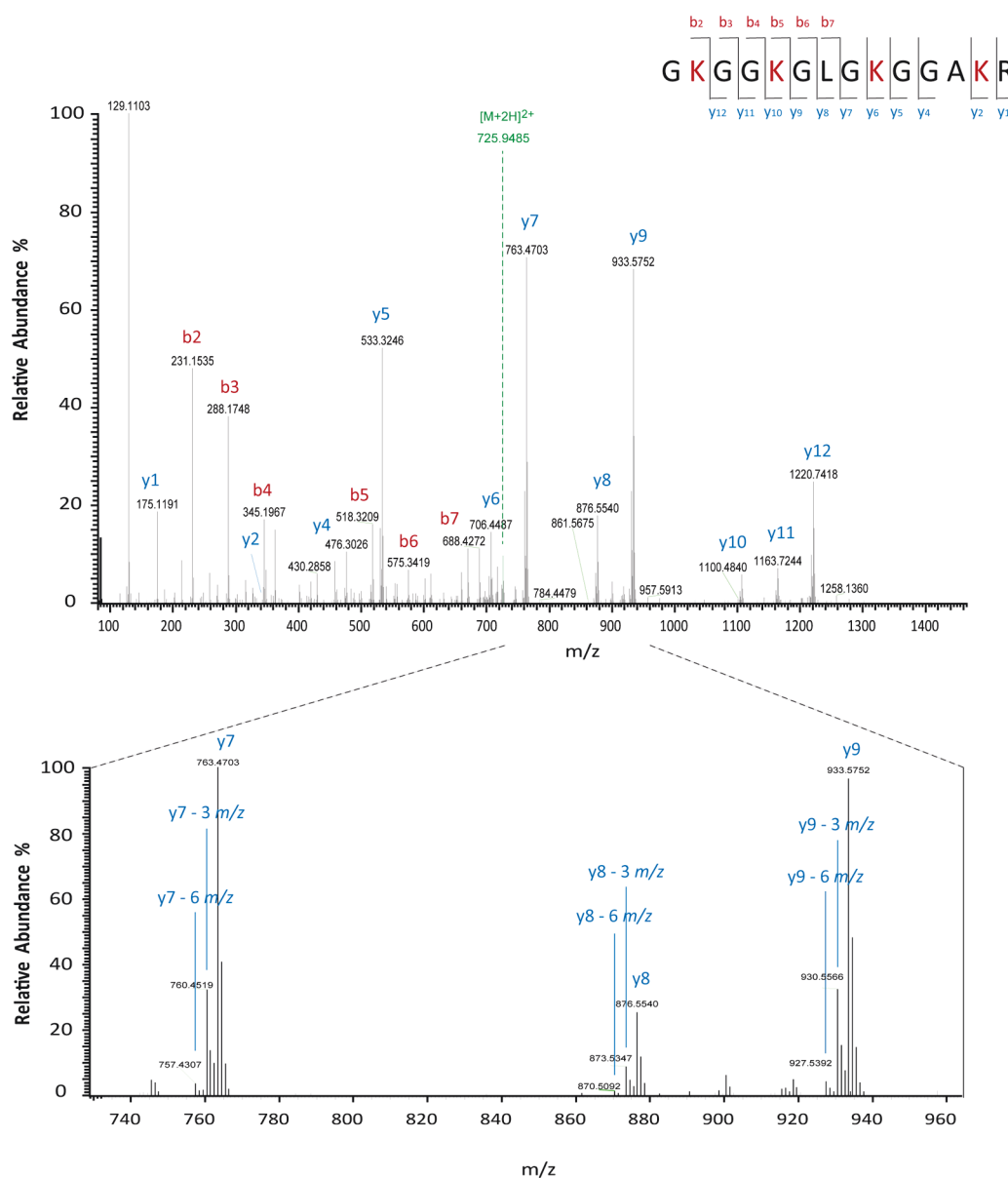


Figure 7. Annotation of an MS² spectrum of the H4 peptide (GKGGKGLGKGGAKR) obtained from MS¹ and using a precursor-ion isolation window of 14.0 Th. A broad precursor-ion isolation width enabled simultaneous isolation and cofragmentation of all 5 differentially acetylated H4(4–17) peptide species. As shown in the zoomed region, clusters of y-ions differing in mass corresponding to 3 Th are indicative of both H₃- and D₃-acetylated fragment ions. The intensities of these fragment ions were extracted and utilized for relative quantitation of differentially acetylated positional isomers present in the sample. MS² data acquisition was performed in the HCD cell.

synthetic-peptide sample. Nevertheless, underestimation of the abundance of the DDDD peptide was most likely due to the ± 7 Th isolation window that was utilized. When such an isolation window is centered at the targeted monoisotopic m/z of the fully H₃-acetylated peptide (HHHH), not all the isotopes from the DDDD peptide are selected for MS² fragmentation. This could be overcome by opening the isolation window. The trade-off, however, is that interference from unrelated coeluting peptide species can occur. Therefore, the isolation width should be adjusted (narrowed or broadened) according to the number of differentially H₃/D₃-acetylated peptide species observed in the MS¹ spectra, and the absence/presence of unrelated peptides. Overall, these results demonstrate the applicability of our data analysis algorithm for a complex peptide mixture that requires MS²-based quantitation of coeluting and isobaric peptide species.

FASIL-MS Accurately Quantitates Acetylated Positional Isomers Following Treatment of HeLa Cells with the KDAC Inhibitor SAHA

The HeLa cells treated with DMSO (vehicle control) or SAHA (KDACi) were analyzed with our FASIL-MS workflow. The broad isolation window around the targeted monoisotopic precursor-ion m/z values plus a disabled dynamic exclusion; resulted in the acquisition of sufficient recurrent fragmentation spectra of all the multiple versions of the H₃/D₃-acetylated peptide species. This concept is akin to the previous work by Smith et al.,^{21,29} where a means to solve relative acetylation of each of the four lysine residues in the H4(4–17) peptide was first proposed. Smith et al.^{21,29} used deuterated acetic anhydride to D₃-acetylate the recombinant histone H4 protein. A standard data-dependent LC–MS method was applied, and the average mass (m/z 723.3) of the peptide cluster was targeted for

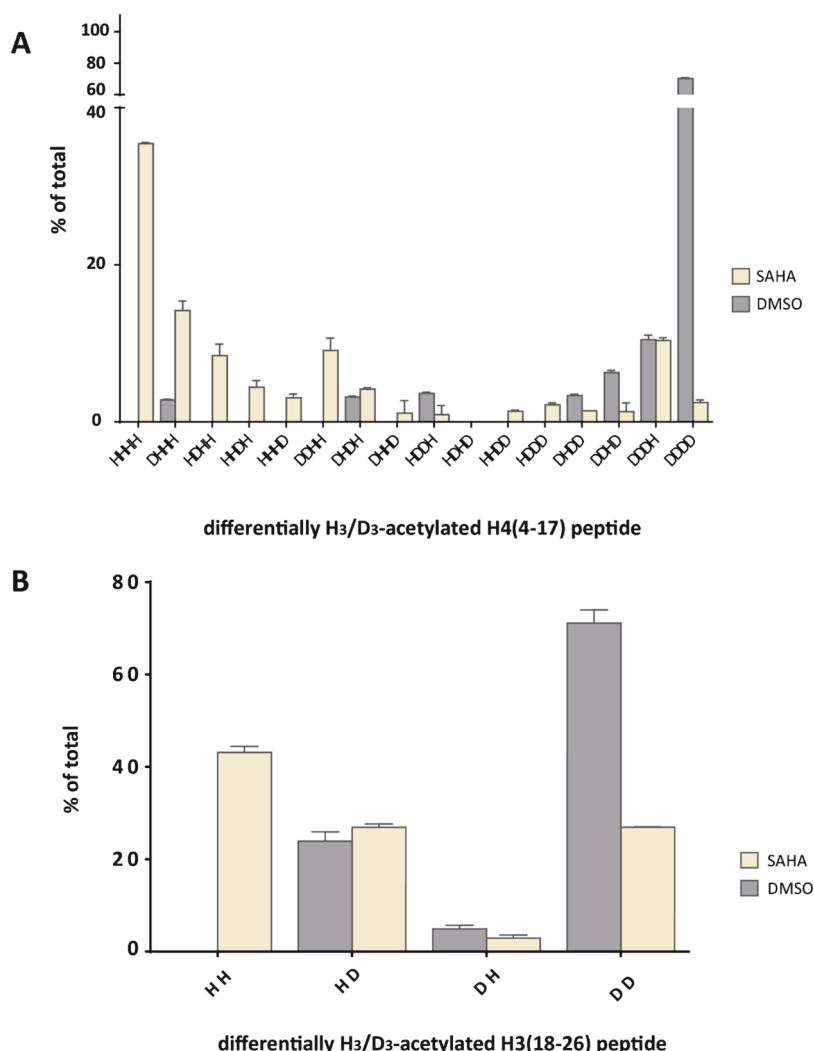


Figure 8. FASIL-MS to quantitate H4(4–17) and H3(18–26) multiply acetylated positional isomers. MS² intensity-based quantitation of H₃/D₃-acetylated histone (A) H4(4–17) and (B) H3(18–26) peptides. Intensities of corresponding b-/y- ions for each 16 (A) and 4 (B) differentially acetylated isomers were summarized and normalized to 100% within a single replicate measurement. The plotted abundances represent averaged values across two technical replicates and mean thereof for two biological replicates. For simplicity, H₃- and D₃-acetylation are labeled as H and D, respectively. The sequence of the letters correspond to the position of the lysine residue in the peptide sequence. Data acquisition was performed with MS² fragmentation in the HCD cell.

fragmentation. A precursor-ion isolation width of 8 Da was used to select and concurrently fragment all the doubly charged differentially acetylated peptide species, followed by manual calculation of a relatively complex set of linear equations to assign the positional isomers.

In our study, the generated data were analyzed using our automated algorithm that deconvolutes chimeric patterns of H₃/D₃-acetylated fragment ions. By coisolating and cofragmenting differentially acetylated peptide clusters (shown schematically in [Supplementary Figure S3](#)) rather than individual species, the intensities of the fragment ions can be utilized to provide occupancy information on all possible positional isomers. The major improvements provided by our algorithm compared to those developed to date; are in the unbiased assessment of the relative ratios of in vivo acetylation for each lysine residue together with the relative abundances of the peptides containing multiple acetylated lysine residues. Shown in [Figure 7](#) is an example of an MS² spectrum from the histone extract treated with DMSO. The spectrum is comprised of b- and y-ions originating from all targeted peptides present in

the cluster. In this way, the single MS² spectrum contains clusters of b- and y-ions that contain sufficient information for relative quantitation of H₃/D₃-acetylated positional isomers utilizing our extended and improved algorithm. Such information was not feasible with the MS¹-based approach nor, to our knowledge, with any MS²-based algorithms available to date.

For the H4(4–17) peptide, the data confirmed that the predominant species in the DMSO- and SAHA-treated samples were those without any H₃-acetylation, and full occupancy of all four lysine residues with an H₃-acetyl modification, respectively ([Figure 8A](#)). Interestingly, DMSO-treated cells were preferentially acetylated on the lysine residue distal to the protein N-terminus, i.e., H4K16ac > H4K12ac > H4K8ac (DDDH > DDHD > DHDD). In addition, no singly acetylated peptide at H4K5 (HDDD) was observed. Following drug treatment, doubly and triply H₃-acetylated H4(4–17) peptides showed the same in vivo acetylation preference (H4K16ac > H4K12ac > H4K8ac > H4K5ac). The observed decrease in abundance of the singly acetylated peptides upon SAHA treatment is most

probably due to additional *in vivo* lysine acetylation, and could be thus explained by the corresponding increase in the doubly and triply H₃-acetylated H4(4–17) peptide species (i.e., DHDH and DHHD; HHHD, HDDH, HDHH, and DHHH). H4K16ac (DDDHH, ~11%) did not show a significant alteration in abundance upon HDACi-treatment. DHDD, DHDH, HDDH and DHHH were equally represented in the DMSO-treated sample (~4%), however, showed diverse changes in abundance upon SAHA treatment. DHHH increased 3-fold, HDDH and DHDD decreased 2-fold, while DHDH and DDDH remained basically unaltered. Interestingly, H4K5acK12ac (HDDH) was not observed in either condition, suggesting absence from both the control and SAHA-treated HeLa cells. This effect was present after 18 h of 10 μ M SAHA treatment, and thus could be potentially altered depending on drug exposure time and concentration.

Similarly, our FASIL-MS approach revealed SAHA-dependent acetylation of the H3(18–26) peptide (Figure 8B). In this case, the overall abundance of the *in vivo* singly acetylated H3 peptide was not significantly altered (HD and DH). Nevertheless, the partial conversion in abundance of unmodified (DD) to fully *in vivo* acetylated (HH) peptide was observed (approximately 45%). For both of the monitored peptides, 70% of the lysine residues were unmodified in the unperturbed control cells, i.e., upon DMSO-vehicle treatment. SAHA-mediated lysine acetylation, however, preferentially affected the histone H4(4–17) peptide. The H3(18–26) peptide was affected to a lesser degree, where up to 25% of the peptides remained unmodified following drug-treatment.

Compared to the study of Smith et al.,^{21,29} several improvements were made in FASIL-MS. First, a more efficient *in vitro* derivatization of lysine residues at the protein level was achieved with D₃-NAS compared to the commonly used acetic anhydride. Second, adaptation of the FASP protocol enabled on-filter D₃-NAS derivatization and subsequent streamlining of the sample preparation prior to protein digestion. Third, the calculated monoisotopic *m/z* values for all possible differentially H₃/D₃-acetylated H4(4–17) and H3(18–26) peptide species were added to an inclusion list rather than using the average *m/z* of the entire peptide cluster. Finally, data analysis was markedly improved via an extended algorithm that utilizes b- and y-ions in an unbiased fashion to assign relative abundances of all *in vivo*-acetylated positional isomers.

CONCLUSION

FASIL-MS was developed as a simple, mass spectrometry-based workflow to profile endogenous acetylation. The benefits of FASIL-MS over existing approaches were demonstrated by profiling the acetylation changes that occur on the histones peptides H4(4–17) and H3(18–26) following SAHA-treatment of HeLa cells compared to the DMSO-treated control. With current peak-selection algorithms and a standard mass window of ± 0.6 Th, the shift introduced by D₃-NAS is too minor for selection and fragmentation of all the individual peptide species within the differentially H₃/D₃-acetylated peptide clusters. Broadening the mass window to simultaneously fragment the entire population of coeluting acetylated peptides combined with an extended and improved data analysis algorithm that deconvolutes these complex multi-overlaid MS² spectra, enabled quantitation of all the positional isomers of the differentially modified peptides. FASIL-MS is a streamlined and simplistic approach for analyzing histone acetylation that combines: (i) highly efficient derivatization to

modify lysine residues at the protein level; (ii) on-filter stable isotopic labeling to simplify and minimize sample preparation prior to MS analysis; and (iii) adaptation of a targeted MS method accompanied by a data analysis package for quantitation of all existing variations of singly and multiply acetylated histone peptide species. The unbiased nature of FASIL-MS approach is essential in the context of determining the abundance of acetylated-lysine positional isomers upon perturbation where the final outcome cannot be predicted, i.e., abundance and the presence of certain H₃/D₃-acetylated peptide species. Further applications of this method are in studying the function of particular site-specific acetylation patterns. Assuming that the peptide of interest falls within the mass range of a standard mass spectrometry method, FASIL-MS can be used to relatively quantitate any combination of H₃/D₃-acetylation on any peptide containing one or more lysine residues. Utilizing the appropriate reagent containing deuterated version of PTM of interest, FASIL-MS has the potential to be extended to other histone PTMs.

ASSOCIATED CONTENT

Supporting Information

The Supporting Information is available free of charge on the ACS Publications website at DOI: 10.1021/acs.jproteome.6b00130.

Supporting tables and figures (PDF)

AUTHOR INFORMATION

Corresponding Author

*E-mail: kbennett@cemm.oeaw.ac.at. Tel: +43-1-40160-70010. Fax: +43-1-40160-970000.

Present Address

§(E.S.): Roche Diagnostics GmbH, A-1210 Vienna, Austria

Notes

The authors declare no competing financial interest.

ACKNOWLEDGMENTS

The authors would like to thank all members of the Bennett laboratory for support and advice. Thanks are also extended to Viktoria Dorfer from the University of Applied Sciences Upper Austria, Hagenberg for input and discussion on the data analysis. Research in our laboratories is supported by the Austrian Academy of Sciences. Research in the Kubicek laboratory is supported by the Austrian Federal Ministry of Science, Research and Economy, and the National Foundation for Research, Technology, and Development. In addition, the research leading to these results has received funding from the European Union Seventh Framework Programme (FP7/2007-2013) under grant agreement no. 293921. The mass spectrometry proteomic data have been deposited into the ProteomeXchange Consortium³⁶ via the PRIDE partner repository with the dataset identifier PXD003611. The algorithm for MS²-based quantitation of differentially H₃/D₃-acetylated positional isomers can be downloaded from Zenodo (<https://zenodo.org/record/51189>) or GitHub (<https://github.com/petomajci/FASIL-MS>).

ABBREVIATIONS

BCA, bicinchoninic acid; FA, formic acid; FASP, filter-aided sample preparation; LC–MS/MS, liquid chromatography

tandem mass spectrometry; KAT, lysine acetyltransferases; KDAC, lysine deacetylase; KDACi, lysine deacetylase inhibitor; KDM, lysine demethylase; KMT, lysine methyltransferase; PTM, post-translational modification; SAHA, suberoylanilide hydroxamic acid; SDS, sodium dodecyl sulfate; TEAB, triethylammonium bicarbonate; t_R , retention time

REFERENCES

- (1) Beltrao, P.; Bork, P.; Krogan, N. J.; van Noort, V. Evolution and functional cross-talk of protein post-translational modifications. *Mol. Syst. Biol.* **2013**, *9*, 714.
- (2) Ajiro, K.; Scoltock, A. B.; Smith, L. K.; Ashasima, M.; Cidlowski, J. A. Reciprocal epigenetic modification of histone H2B occurs in chromatin during apoptosis in vitro and in vivo. *Cell Death Differ.* **2010**, *17* (6), 984–993.
- (3) Masumoto, H.; Hawke, D.; Kobayashi, R.; Verreault, A. A role for cell-cycle-regulated histone H3 lysine 56 acetylation in the DNA damage response. *Nature* **2005**, *436* (7048), 294–98.
- (4) Zhang, L.; Freitas, M. A.; Wickham, J.; Parthun, M. R.; Klisovic, M. I.; Marcucci, G.; Byrd, J. C. Differential expression of histone post-translational modifications in acute myeloid and chronic lymphocytic leukemia determined by high-pressure liquid chromatography and mass spectrometry. *J. Am. Soc. Mass Spectrom.* **2004**, *15* (1), 77–86.
- (5) Bartke, T.; Borgel, J.; DiMaggio, P. A. Proteomics in epigenetics: new perspectives for cancer research. *Briefings Funct. Genomics* **2013**, *12* (3), 205–18.
- (6) Bradner, J. E.; West, N.; Grachan, M. L.; Greenberg, E. F.; Haggarty, S. J.; Warnow, T.; Mazitschek, R. Chemical phylogenetics of histone deacetylases. *Nat. Chem. Biol.* **2010**, *6* (3), 238–43.
- (7) Mann, B. S.; Johnson, J. R.; Cohen, M. H.; Justice, R.; Pazdur, R. FDA approval summary: vorinostat for treatment of advanced primary cutaneous T-cell lymphoma. *Oncologist* **2007**, *12* (10), 1247–52.
- (8) Beck, H. C.; Nielsen, E. C.; Matthiesen, R.; Jensen, L. H.; Sehested, M.; Finn, P.; Grauslund, M.; Hansen, A. M.; Jensen, O. N. Quantitative proteomic analysis of post-translational modifications of human histones. *Mol. Cell. Proteomics* **2006**, *5* (7), 1314–25.
- (9) Benson, L. J.; Gu, Y.; Yakovleva, T.; Tong, K.; Barrows, C.; Strack, C. L.; Cook, R. G.; Mizzen, C. A.; Annunzio, A. T. Modifications of H3 and H4 during chromatin replication, nucleosome assembly, and histone exchange. *J. Biol. Chem.* **2006**, *281* (14), 9287–96.
- (10) Fuchs, S. M.; Strahl, B. D. Antibody recognition of histone post-translational modifications: emerging issues and future prospects. *Epigenomics* **2011**, *3* (3), 247–49.
- (11) Bock, I.; Dhayalan, A.; Kudithipudi, S.; Brandt, O.; Rathert, P.; Jeltsch, A. Detailed specificity analysis of antibodies binding to modified histone tails with peptide arrays. *Epigenetics* **2011**, *6* (2), 256–63.
- (12) Egelhofer, T. A.; Minoda, A.; Klugman, S.; Lee, K.; Kolasinska-Zwierz, P.; Alekseyenko, A. A.; Cheung, M. S.; Day, D. S.; Gadel, S.; Gorchakov, A. A.; Gu, T.; Kharchenko, P. V.; Kuan, S.; Latorre, I.; Linder-Basso, D.; Luu, Y.; Ngo, Q.; Perry, M.; Rechtsteiner, A.; Riddle, N. C.; Schwartz, Y. B.; Shanower, G. A.; Vielle, A.; Ahringer, J.; Elgin, S. C.; Kuroda, M. I.; Pirrotta, V.; Ren, B.; Strome, S.; Park, P. J.; Karpen, G. H.; Hawkins, R. D.; Lieb, J. D. An assessment of histone-modification antibody quality. *Nat. Struct. Mol. Biol.* **2011**, *18* (1), 91–93.
- (13) Guan, X.; Rastogi, N.; Parthun, M. R.; Freitas, M. A. Discovery of histone modification crosstalk networks by stable isotope labeling of amino acids in cell culture mass spectrometry (SILAC MS). *Mol. Cell. Proteomics* **2013**, *12* (8), 2048–59.
- (14) Su, X.; Ren, C.; Freitas, M. A. Mass spectrometry-based strategies for characterization of histones and their post-translational modifications. *Expert Rev. Proteomics* **2007**, *4* (2), 211–25.
- (15) Young, N. L.; DiMaggio, P. A.; Plazas-Mayorca, M. D.; Baliban, R. C.; Floudas, C. A.; Garcia, B. A. High throughput characterization of combinatorial histone codes. *Mol. Cell. Proteomics* **2009**, *8* (10), 2266–84.
- (16) Moradian, A.; Kalli, A.; Sweredoski, M. J.; Hess, S. The top-down, middle-down, and bottom-up mass spectrometry approaches for characterization of histone variants and their post-translational modifications. *Proteomics* **2014**, *14* (4–5), 489–97.
- (17) Onder, O.; Sidoli, S.; Carroll, M.; Garcia, B. A. Progress in epigenetic histone modification analysis by mass spectrometry for clinical investigations. *Expert Rev. Proteomics* **2015**, *12* (5), 499–517.
- (18) Plazas-Mayorca, M. D.; Zee, B. M.; Young, N. L.; Fingerma, I. M.; LeRoy, G.; Briggs, S. D.; Garcia, B. A. One-pot shotgun quantitative mass spectrometry characterization of histones. *J. Proteome Res.* **2009**, *8* (11), 5367–74.
- (19) Nakayasu, E. S.; Wu, S.; Sydor, M. A.; Shukla, A. K.; Weitz, K. K.; Moore, R. J.; Hixson, K. K.; Kim, J. S.; Petyuk, V. A.; Monroe, M. E.; Pasa-Tolic, L.; Qian, W. J.; Smith, R. D.; Adkins, J. N.; Ansong, C. A method to determine lysine acetylation stoichiometries. *Int. J. Proteomics* **2014**, *2014*, 730725.
- (20) Noga, M. J.; Asperger, A.; Silberring, J. N-terminal H3/D3-acetylation for improved high-throughput peptide sequencing by matrix-assisted laser desorption/ionization mass spectrometry with a time-of-flight/time-of-flight analyzer. *Rapid Commun. Mass Spectrom.* **2006**, *20* (12), 1823–27.
- (21) Smith, C. M. Quantification of acetylation at proximal lysine residues using isotopic labeling and tandem mass spectrometry. *Methods* **2005**, *36* (4), 395–403.
- (22) Maile, T. M.; Izrael-Tomasevic, A.; Cheung, T.; Guler, G. D.; Tindell, C.; Masselot, A.; Liang, J.; Zhao, F.; Trojer, P.; Classon, M.; Arnott, D. Mass spectrometric quantification of histone post-translational modifications by a hybrid chemical labeling method. *Mol. Cell. Proteomics* **2015**, *14* (4), 1148–58.
- (23) Liao, R.; Wu, H.; Deng, H.; Yu, Y.; Hu, M.; Zhai, H.; Yang, P.; Zhou, S.; Yi, W. Specific and efficient N-propionylation of histones with propionic acid N-hydroxysuccinimide ester for histone marks characterization by LC–MS. *Anal. Chem.* **2013**, *85* (4), 2253–59.
- (24) Olsen, J. V.; Ong, S. E.; Mann, M. Trypsin cleaves exclusively C-terminal to arginine and lysine residues. *Mol. Cell. Proteomics* **2004**, *3* (6), 608–14.
- (25) Krueger, R. J.; Hobbs, T. R.; Mihal, K. A.; Tehrani, J.; Zeece, M. G. Analysis of endoproteinase Arg C action on adrenocorticotrophic hormone by capillary electrophoresis and reversed-phase high-performance liquid chromatography. *J. Chromatogr.* **1991**, *543* (2), 451–61.
- (26) Zhang, R.; Sioma, C. S.; Wang, S.; Regnier, F. E. Fractionation of isotopically labeled peptides in quantitative proteomics. *Anal. Chem.* **2001**, *73* (21), 5142–49.
- (27) Manza, L. L.; Stamer, S. L.; Ham, A. J.; Codreanu, S. G.; Liebler, D. C. Sample preparation and digestion for proteomic analyses using spin filters. *Proteomics* **2005**, *5* (7), 1742–45.
- (28) Wisniewski, J. R.; Zougman, A.; Nagaraj, N.; Mann, M. Universal sample preparation method for proteome analysis. *Nat. Methods* **2009**, *6* (5), 359–62.
- (29) Smith, C. M.; Gafken, P. R.; Zhang, Z.; Gottschling, D. E.; Smith, J. B.; Smith, D. L. Mass spectrometric quantification of acetylation at specific lysines within the amino-terminal tail of histone H4. *Anal. Biochem.* **2003**, *316* (1), 23–33.
- (30) Olsen, J. V.; de Godoy, L. M.; Li, G.; Macek, B.; Mortensen, P.; Pesch, R.; Makarov, A.; Lange, O.; Horning, S.; Mann, M. Parts per million mass accuracy on an Orbitrap mass spectrometer via lock mass injection into a C-trap. *Mol. Cell. Proteomics* **2005**, *4* (12), 2010–21.
- (31) Perkins, D. N.; Pappin, D. J.; Creasy, D. M.; Cottrell, J. S. Probability-based protein identification by searching sequence databases using mass spectrometry data. *Electrophoresis* **1999**, *20* (18), 3551–67.
- (32) Kersey, P.; Hermjakob, H.; Apweiler, R. VARSPIC: alternatively-spliced protein sequences derived from SWISS-PROT and TrEMBL. *Bioinformatics* **2000**, *16* (11), 1048–49.
- (33) Chakraborty, A.; Regnier, F. E. Global internal standard technology for comparative proteomics. *J. Chromatogr. A* **2002**, *949* (1–2), 173–84.

- (34) Yu, Y.; Chen, J.; Gao, Y.; Gao, J.; Liao, R.; Wang, Y.; Oyang, C.; Li, E.; Zeng, C.; Zhou, S.; Yang, P.; Jin, H.; Yi, W. Quantitative Profiling of Combinational K27/K36 Modifications on Histone H3 Variants in Mouse Organs. *J. Proteome Res.* **2016**, *15* (3), 1070–79.
- (35) Barbetti, V.; Gozzini, A.; Cheloni, G.; Marzi, I.; Fabiani, E.; Santini, V.; Dello Sbarba, P.; Rovida, E. Time- and residue-specific differences in histone acetylation induced by VPA and SAHA in AML1/ETO-positive leukemia cells. *Epigenetics* **2013**, *8* (2), 210–19.
- (36) Vizcaino, J. A.; Deutsch, E. W.; Wang, R.; Csordas, A.; Reisinger, F.; Rios, D.; Dianes, J. A.; Sun, Z.; Farrah, T.; Bandeira, N.; Binz, P. A.; Xenarios, I.; Eisenacher, M.; Mayer, G.; Gatto, L.; Campos, A.; Chalkley, R. J.; Kraus, H. J.; Albar, J. P.; Martinez-Bartolome, S.; Apweiler, R.; Omenn, G. S.; Martens, L.; Jones, A. R.; Hermjakob, H. ProteomeXchange provides globally coordinated proteomics data submission and dissemination. *Nat. Biotechnol.* **2014**, *32* (3), 223–6.

SUPPORTING INFORMATION

FASIL-MS: An Integrated Proteomic and Bioinformatic Workflow to Universally Quantitate *in vivo*-acetylated Positional Isomers

Dijana Vitko,¹ Peter Májek,¹ Erika Schirghuber,^{1,2#} Stefan Kubicek,^{1,2} Keiryn L. Bennett^{1*}

¹CeMM Research Center for Molecular Medicine of the Austrian Academy of Sciences, A-1090 Vienna, Austria

²Christian Doppler Laboratory for Chemical Epigenetics and Antiinfectives, CeMM

Current address: Roche Diagnostics GmbH, A-1210 Vienna, Austria

* To whom correspondence should be addressed: Keiryn L. Bennett, CeMM Research Center for Molecular Medicine of the Austrian Academy of Sciences, Lazarettgasse 14, AKH Building BT 25.3, A-1090 Vienna, Austria, E-mail: kbennett@cemm.oeaw.ac.at, Tel: [+43-1-40160-70010](tel:+43-1-40160-70010), Fax: +43-1-40160-970000

Supplementary Figure S1. Immunoblot of the histone acetylation marks altered by SAHA treatment.

Supplementary Figure S2. Validation of the MS²-based quantitation algorithm on a mixture of six differentially H₃/D₃-acetylated H4(4-17) peptides.

Supplementary Figure S3. Mass spectrum of the H₃/D₃-acetylated H4 histone peptide GKGGKGLGKGGAKR.

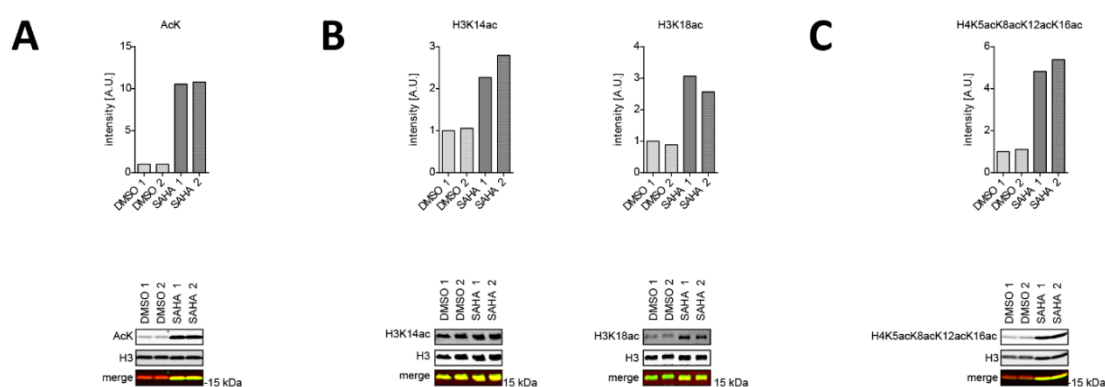
Supplementary Table S1. MS¹-based quantitation of the unlabeled and D₃-derivatised BSA peptides containing either K or R on the C-termini after trypsin digestion.

Supplementary Table S2. Area-under-the-curve for efficiently- and inefficiently-derivatised HeLa histone peptide H4(4-17) in DMSO- and SAHA-treated samples.

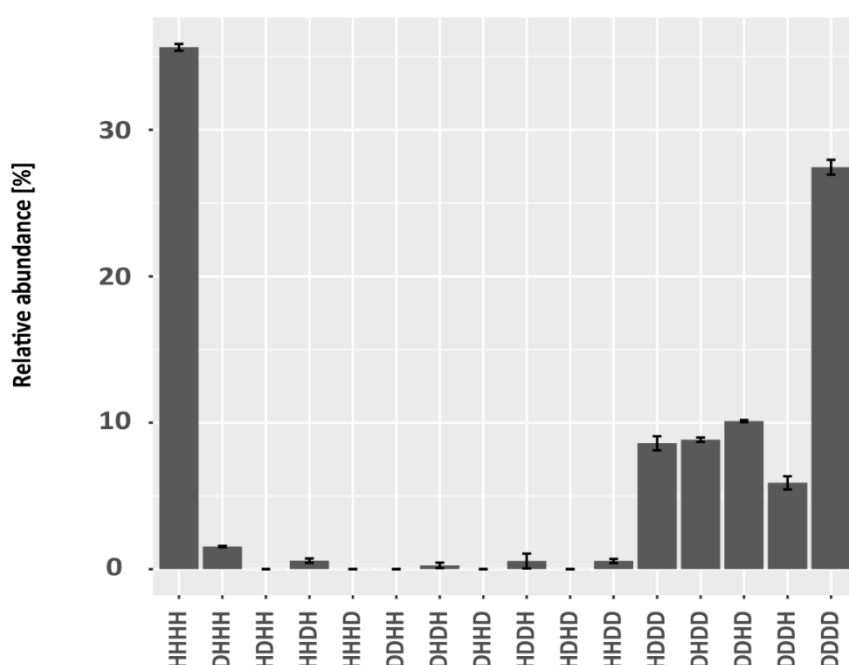
Supplementary Table S3. MS¹-based absolute and relative quantitation of H4(4-17) and H3(18-23) differentially H₃/D₃-acetylated peptide species via manual integration of peptide peak areas.

Supplementary Figure S1. Immunoblot of the histone acetylation marks altered by SAHA treatment.

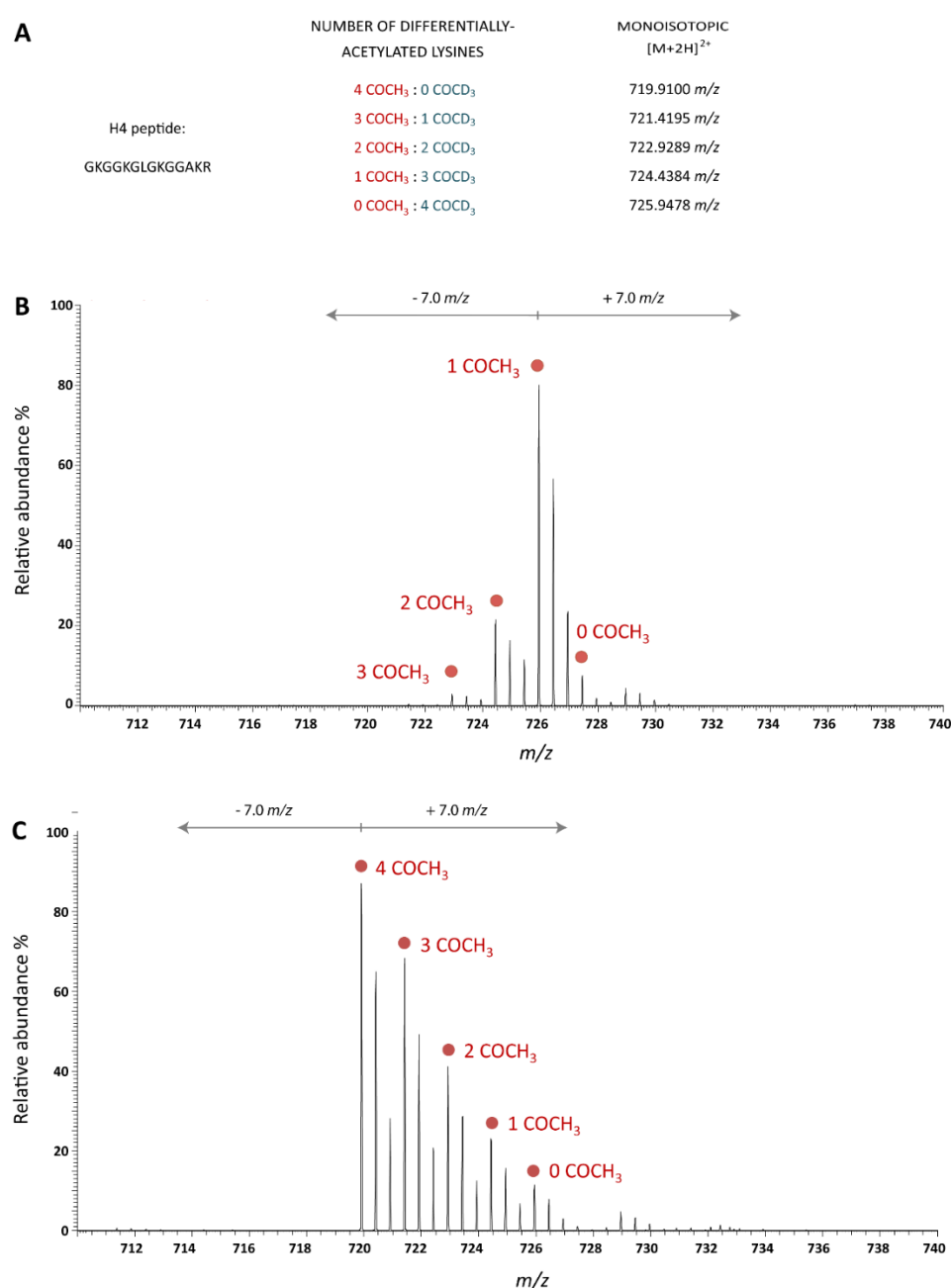
Increase in acetylation on H3 and H4 histone N-terminal peptides was assessed via immunoblotting. The global acetylation of the histone proteins was increased (A). Specific acetylation marks on H3K14ac and H3K18ac (B) and H4K4acK8acK12acK16ac (C) were verified by site-specific acetylation antibody recognition. An antibody against the histone H3 protein was utilized as a gel loading control. The signal was recorded via the Li-Cor Odyssey instrument and the relative changes in the signal intensity were normalized to the control.



Supplementary Figure S2. Validation of the MS²-based quantitation algorithm on a mixture of six differentially H₃/D₃-acetylated H4(4-17) peptides. MS²-based quantitation of peptide mixture containing four peptides with one H₃-acetyl group located at different lysine residues, *i.e.*, H4K5, H4K8, H4K12, and H4K16 (*m/z* 724.4388) in equimolar ratios and the equivalent amount (based on MS¹ area) of peptide H4(4-17) peptide with 4 H₃- and 4 D₃-acetyl groups (*m/z* 719.9105 and 725.9482, respectively). For simplicity, H₃- and D₃-acetylation are marked as H and D, respectively; in the sequential order as the lysine residues affected by the modification. MS² data acquisition was performed in the HCD cell.



Supplementary Figure S3. Mass spectrum of the H₃/D₃-acetylated H4 histone peptide GKGGKGLGKGGAKR. (A) List of expected m/z values corresponding to differentially H₃/D₃-acetylated H4 histone peptide. Isotopic clusters of the five differentially-acetylated GKGGKGLGKGGAKR peptides in the (B) DMSO- and (C) SAHA-treated samples. The mass shift between the doubly-charged peptide species differing in one H₃/D₃-acetyl group is 1.5095 Th. For simplicity, D₃-acetylation was omitted in the representative mass spectra; and only the number of H₃-acetylated lysines are indicated. MS² data acquisition was performed in the HCD cell.



Supplementary Table S1. MS¹-based quantitation of the unlabeled and D₃-derivatised BSA peptides containing either K or R on the C-termini after trypsin digestion. (A) Cumulative MS¹-based peptide areas of unmodified and D₃-NAS labelled BSA. Peptide areas were separated according to the amino-acid residue on the C-terminus. (B) Reproducibility assessment of unmodified and D₃-NAS labelled BSA. Experiments were performed as quintuplicates, and only peptides with arginine on C-termini were considered. Statistical values were calculated with GraphPad Prism software V6.0. D₃-NAS, D₃-N-acetoxysuccinimide.

A.

	Peptide area BSA - NAS					Peptide area BSA + NAS				
R termini	864000000	890000000	737000000	1060000000	755000000	815000000	527000000	1040000000	792000000	734000000
K termini	2840000000	3270000000	2530000000	3280000000	2550000000	1474000	1216000	910300	896600	0

B.

	BSA – NAS Areas of peptides with R C-terminal	BSA + NAS Areas of peptides with R C-terminal
Number of values	5	5
Minimum	7.370e+008	5.270e+008
Median	8.640e+008	7.920e+008
Maximum	1.060e+009	1.040e+009
Mean	8.612e+008	7.816e+008
Std. Deviation	1.295e+008	1.838e+008
Std. Error of Mean	5.791e+007	8.218e+007
Coefficient of variation	15.04%	23.51%
Sum	4.306e+009	3.908e+009

Supplementary Table S2. Area-under-the-curve for efficiently- and inefficiently-derivatised HeLa histone peptide H4(4-17) in DMSO-and SAHA-treated samples. (A) HeLa histone extracts treated with DMSO and derivatised with D₃-NAS. (B) HeLa histone extracts treated with SAHA and derivatised with D₃-NAS. (C) HeLa histone extracts treated with DMSO and derivatised with PA. (D) HeLa histone extracts treated with SAHA and derivatised with PA. D₃-NAS, D₃-N-acetoxysuccinimide; PA, propionic anhydride.

A. HeLa histone extracts treated with DMSO + D₃-NAS derivatization

Accession	Description	ΣCoverage	Σ# Proteins	Σ# Unique Peptides	Σ# Peptides	Σ# PSMs	A5: Area	B5: Area	C5: Area	D5: Area	Score A2
P62805	Histone H4 OS=Homo sapiens GN=HIST1H4A - [H4_HUMAN]	77.67	1	14	14	656	1.430E10	1.380E10	6.668E9	6.434E9	3904.60
Sequence	# PSMs	# Proteins	# Protein Groups	Protein Group Accessions	Modifications	MH+ [Da]	A5: Area	B5: Area	C5: Area	D5: Area	
GGKGLGKGGAKR	4	1	1	P62805	K3(Acetyl:2H(3)); K7(Acetyl:2H(3)); K11(Acetyl:2H(3))	1220.74101	4.860E7	4.437E7	2.675E7	2.545E7	
GKGGKGLGK	2	1	1	P62805	K2(Acetyl:2H(3)); K5(Acetyl:2H(3)); K9(Acetyl:2H(3))	936.58245	1.555E7	0.000E0	0.000E0	1.026E7	
GKGGKGLGKGGAKR	9	1	1	P62805	K2(Acetyl:2H(3)); K5(Acetyl:2H(3)); K9(Acetyl:2H(3))	1405.85918	3.153E7	2.804E7	1.635E7	1.616E7	
GKGGKGLGKGGAKR	7	1	1	P62805	K2(Acetyl); K5(Acetyl:2H(3)); K9(Acetyl:2H(3)); K13(Acetyl:2H(3))	1447.86882	1.221E7	9.633E6	0.000E0	0.000E0	
GKGGKGLGKGGAKR	123	1	1	P62805	K2(Acetyl:2H(3)); K5(Acetyl:2H(3)); K9(Acetyl:2H(3)); K13(Acetyl:2H(3))	1450.88689	1.156E10	1.081E10	5.122E9	5.053E9	
GLGKGGAKR	2	1	1	P62805	K4(Acetyl:2H(3)); K8(Acetyl:2H(3))	933.57506	0.000E0	0.000E0	1.215E7	1.271E7	
SUM							1.167E10	1.089E10	5.178E9	5.118E9	
fully derivatized (%)							99.18%	99.34%	98.93%	98.74%	
partially derivatized (%)							0.82%	0.66%	1.07%	1.26%	

B. HeLa histone extracts treated with SAHA + D₃-NAS derivatization

Accession	Description	ΣCover age	Σ# Proteins	Σ# Unique Peptides	Σ# Peptides	Σ# PSMs	A5: Area	B5: Area	C5: Area	D5: Area	Score A2
P62805	Histone H4 OS=Homo sapiens GN=HIST1H4A - [H4_HUMAN]	76.7	1	12	12	509	10289314781	9386041932	4499630557	4482543107	3313.808138
Sequence	# PSMs	# Proteins	# Protein Groups	Protein Group Accessions	Modifications	MH+ [Da]	A5: Area	B5: Area	C5: Area	D5: Area	
GGKGLGKGGAKR	4	1	1	P62805	K3(Acetyl); K7(Acetyl); K11(Acetyl)	1211.684008	0	18500098.88	10473138.19	6767036.156	
GGKGLGKGGAKR	1	1	1	P62805	K3(Acetyl:2H(3)); K7(Acetyl); K11(Acetyl)	1214.702928	0	15053449	0	0	
GKGGKGLGKGGAKR	2	1	1	P62805	K2(Acetyl); K9(Acetyl); K13(Acetyl)	1396.799608	7182611.625	6182523.875	0	0	
GKGGKGLGKGGAKR	73	1	1	P62805	K2(Acetyl); K5(Acetyl); K9(Acetyl); K13(Acetyl)	1438.810961	4915118336	4422434560	2004885728	1949818048	
GKGGKGLGKGGAKR	3	1	1	P62805	K2(Acetyl:2H(3)); K5(Acetyl); K9(Acetyl); K13(Acetyl)	1441.830248	0	0	0	0	
GKGGKGLGKGGAKR	4	1	1	P62805	K2(Acetyl:2H(3)); K5(Acetyl:2H(3)); K9(Acetyl); K13(Acetyl)	1444.849047	0	17667147.75	0	0	
GKGGKGLGKGGAKR	6	1	1	P62805	K2(Acetyl:2H(3)); K5(Acetyl:2H(3)); K9(Acetyl:2H(3)); K13(Acetyl:2H(3))	1450.886888	1034559091	947979292.4	478606828.7	469955326.4	
GLGKGGAKR	4	1	1	P62805	K4(Acetyl); K8(Acetyl)	927.5378284	13332541.63	12757372.06	4837599.938	5092407.188	
SUM							5.970E9	5.441E9	2.499E9	2.432E9	
fully derivatized (%)							99.66%	99.04%	99.39%	99.51%	
partially derivatized (%)							0.34%	0.96%	0.61%	0.49%	

C. HeLa histone extracts treated with DMSO + PA derivatization

Accession	Description	ΣCover age	Σ# Proteins	Σ# Unique Peptides	Σ# Peptides	Σ# PSMs	A5: Area	B5: Area	C5: Area	D5: Area	Score A2
P62805	Histone H4 OS=Homo sapiens GN=HIST1H4A - [H4_HUMAN]	78.64	1	18	18	614	1389408380	1318029780	1608859543	1547481473	3757.880215
Sequence	# PSMs	# Proteins	# Protein Groups	Protein Group Accessions	Modifications	MH+ [Da]	A5: Area	B5: Area	C5: Area	D5: Area	
GGKGLGKGGAK	4	1	1	P62805	K3(Propionyl); K7(Propionyl)	1041.605516	1362295.844	1737641.469	5368530.688	5085236.719	
GGKGLGKGGAKR	10	1	1	P62805	K7(Propionyl); K11(Propionyl)	1197.705295	2799585.172	2948311.375	2053650.594	1816038.156	
GGKGLGKGGAKR	8	1	1	P62805	K3(Propionyl); K7(Acetyl); K11(Propionyl)	1239.716234	22741812.19	22467051.5	26379724.31	26403190.44	
GGKGLGKGGAKR	12	1	1	P62805	K3(Propionyl); K7(Propionyl); K11(Propionyl)	1253.732225	74789469.03	74626304.16	86022498.28	84246133	
GGKGLGKGGAKR	2	1	1	P62805	K7(Propionyl); K11(Acetyl)	1183.689379	0	1461054.125	702250.3594	0	
GKGGKGLGK	4	1	1	P62805	K2(Propionyl)	857.5202502	3816017.094	3304454.719	3350799.031	3333336.313	
GKGGKGLGK	3	1	1	P62805	K2(Propionyl); K5(Propionyl)	913.5452746	122511685.8	115333545.7	158282713.3	0	
GKGGKGLGK	4	1	1	P62805	K2(Propionyl); K5(Propionyl); K9(Propionyl)	969.5728015	8255103.406	8185308.383	10019167.63	10481197.75	
GKGGKGLGKGGAK	11	1	1	P62805	K5(Propionyl); K9(Propionyl)	1226.721483	3893429.297	3558343.375	10409066.69	10074202.28	
GKGGKGLGKGGAK	5	1	1	P62805	K2(Propionyl); K5(Propionyl); K9(Acetyl)	1268.731005	0	2673411.844	9359996.75	9460901.75	
GKGGKGLGKGGAK	6	1	1	P62805	K2(Propionyl); K5(Propionyl); K9(Propionyl)	1282.747118	39499126.5	38457939	115087818.5	112379760.4	
GKGGKGLGKGGAK	1	1	1	P62805	K2(Propionyl); K5(Propionyl); K9(Propionyl); K13(Propionyl)	1338.777025	0	4882528.547	0	0	
GKGGKGLGKGGAKR	1	1	1	P62805		1270.771335	81475.34766	0	0	0	
GKGGKGLGKGGAKR	14	1	1	P62805	K5(Propionyl); K9(Propionyl)	1382.822313	11330450.65	16002186.54	4699919.211	4171978.172	
GKGGKGLGKGGAKR	8	1	1	P62805	K5(Propionyl); K9(Acetyl); K13(Acetyl)	1410.819017	2694094.844	2786168.262	2990992.938	2744335.5	
GKGGKGLGKGGAKR	13	1	1	P62805	K2(Propionyl); K5(Propionyl); K13(Acetyl)	1424.833055	22039584.38	45085402.22	21859591.35	20988149.69	
GKGGKGLGKGGAKR	42	1	1	P62805	K2(Propionyl); K5(Propionyl); K13(Propionyl)	1438.848436	208005286.6	196143181.7	170514331.9	169211623.6	
GKGGKGLGKGGAKR	7	1	1	P62805	K2(Propionyl); K5(Acetyl); K9(Acetyl); K13(Acetyl)	1452.827318	44745520.91	42752425.47	51620394.91	53204080.63	
GKGGKGLGKGGAKR	20	1	1	P62805	K2(Propionyl); K5(Acetyl); K9(Propionyl); K13(Acetyl)	1466.843798	179451250.8	174939541.2	218048159.9	212802514.1	
GKGGKGLGKGGAKR	58	1	1	P62805	K2(Propionyl); K5(Propionyl); K9(Acetyl); K13(Propionyl)	1480.859056	894750936.1	859167748.6	1033246780	1036400422	
GKGGKGLGKGGAKR	158	1	1	P62805	K2(Propionyl); K5(Propionyl); K9(Propionyl); K13(Propionyl)	1494.874315	2287125587	2178572763	2712372922	2611948172	
GKGGKGLGKGGAKR	1	1	1	P62805	K5(Propionyl); K13(Acetyl)	1368.806932	0	482659.875	0	0	

GKGGKGLGKGGAKR	2	1	1	P62805	K2(Acetyl); K5(Acetyl); K9(Acetyl); K13(Acetyl)	1438.806932	0	0	5628126.137	4555101.563
GLGKGGAKR	2	1	1	P62805		843.5150012	114328.8809	110684.4541	0	0
GLGKGGAKR	4	1	1	P62805	K4(Propionyl); K8(Acetyl)	941.5525378	30329331.65	29592473.52	39571650.97	37250631.73
GLGKGGAKR	7	1	1	P62805	K4(Propionyl); K8(Propionyl)	955.5683459	122762624.3	116117976.6	159579454.4	147990147.6
GLGKGGAKR	4	1	1	P62805	K8(Propionyl)	899.5419787	0	6927863.25	6703414.5	7363575.813
GVLVFLENVIR	2	1	1	P62805	K4(Propionyl)	1442.871385	2146184.734	0	26064456	0
SUM						4.085E9	3.948E9	4.880E9	4.572E9	
fully derivatized (%)						83.38%	82.57%	82.40%	85.72%	
partially derivatized (%)						16.62%	17.43%	17.60%	14.28%	

D. HeLa histone extracts treated with SAHA + PA derivatization

Accession	Description	ΣCoverage	Σ# Proteins	Σ# Unique Peptides	Σ# Peptides	Σ# PSMs	A5: Area	B5: Area	C5: Area	D5: Area	Score A2
P62805	Histone H4 OS=Homo sapiens GN=HIST1H4A - [H4_HUMAN]	78.64	1	17	17	559	1760720584	1654329698	825042786.4	815953517.2	3537.182092
Sequence	# PSMs	# Proteins	# Protein Groups	Protein Group Accessions	Modifications	MH+ [Da]	A5: Area	B5: Area	C5: Area	D5: Area	
GGKGLGKGGAKR	13	1	1	P62805	K3(Acetyl); K7(Acetyl); K11(Acetyl)	1211.68535	28976187.67	25492654.39	15306417.54	15804585.8	
GGKGLGKGGAKR	5	1	1	P62805	K3(Propionyl); K7(Acetyl); K11(Propionyl)	1239.716722	20015751.78	19027415.69	9649625.594	9722041.313	
GGKGLGKGGAKR	4	1	1	P62805	K3(Propionyl); K7(Propionyl); K11(Propionyl)	1253.732469	11464745.05	9573767.195	5367748.25	6328081.375	
GKGGKGLGK	2	1	1	P62805	K2(Acetyl); K5(Acetyl)	885.5151843	8315007.02	8027642	0	0	
GKGGKGLGK	2	1	1	P62805	K2(Propionyl); K5(Propionyl)	913.5449695	34057712.25	30041622.81	0	0	
GKGGKGLGKGGAK	1	1	1	P62805	K5(Propionyl); K9(Propionyl)	1226.721971	1293781.586	0	0	0	
GKGGKGLGKGGAK	2	1	1	P62805	K2(Acetyl); K5(Acetyl); K9(Acetyl)	1240.700121	4364471.844	4312522.188	0	0	
GKGGKGLGKGGAK	2	1	1	P62805	K2(Propionyl); K5(Acetyl); K9(Acetyl)	1254.714891	6715187.313	5541624	0	0	
GKGGKGLGKGGAK	3	1	1	P62805	K2(Propionyl); K5(Propionyl); K9(Acetyl)	1268.731371	10320607	9143321.313	0	1141063.594	
GKGGKGLGKGGAK	4	1	1	P62805	K2(Propionyl); K5(Propionyl); K9(Propionyl)	1282.747362	19795537.13	18276295.63	2881603	2833702.344	
GKGGKGLGKGGAKR	16	1	1	P62805	K2(Acetyl); K5(Acetyl); K13(Acetyl)	1396.799242	37000116.88	31255620.73	23376728.31	22158915.39	

GKGGKGLGKGGAKR	14	1	1	P62805	K2(Propionyl); K9(Acetyl); K13(Acetyl)	1410.81743	42677156.88	36505903.13	13782979.06	11810195.16
GKGGKGLGKGGAKR	17	1	1	P62805	K2(Propionyl); K5(Propionyl); K13(Acetyl)	1424.833788	36192414.62	32224808.05	21136483.36	21093237.39
GKGGKGLGKGGAKR	128	1	1	P62805	K2(Acetyl); K5(Acetyl); K9(Acetyl); K13(Acetyl)	1438.813036	2158440932	1948001763	1179893568	1157179333
GKGGKGLGKGGAKR	85	1	1	P62805	K2(Propionyl); K5(Acetyl); K9(Acetyl); K13(Acetyl)	1452.824877	1721918047	1556892093	872092223	889310364.6
GKGGKGLGKGGAKR	49	1	1	P62805	K2(Propionyl); K5(Propionyl); K9(Acetyl); K13(Acetyl)	1466.84392	1208295958	1058025796	595995156.5	604825764.5
GKGGKGLGKGGAKR	36	1	1	P62805	K2(Propionyl); K5(Propionyl); K9(Acetyl); K13(Propionyl)	1480.85869	837899086.8	790944262	390966318.6	391264139.2
GKGGKGLGKGGAKR	14	1	1	P62805	K2(Propionyl); K5(Propionyl); K9(Propionyl); K13(Propionyl)	1494.876268	421090547	386646757	201656448.6	202893102.5
GKGGKGLGKGGAKR	4	1	1	P62805	K2(Propionyl); K5(Propionyl); K13(Propionyl)	1438.850634	0	0	4328892.563	4494475.25
GKGGKGLGKGGAKR	1	1	1	P62805	K9(Acetyl); K13(Acetyl)	1354.793033	0	0	0	1563997.313
GKGGKGLGKGGAKR	1	1	1	P62805	K9(Propionyl); K13(Propionyl)	1382.821995	0	0	0	1068679.461
GLGKGGAKR	4	1	1	P62805	K4(Acetyl); K8(Acetyl)	927.5361194	67527139.69	56071341.91	24485690.09	25519967.75
GLGKGGAKR	4	1	1	P62805	K4(Propionyl); K8(Acetyl)	941.5522326	34190494.06	33278871.84	14059500.72	13727160.75
GLGKGGAKR	4	1	1	P62805	K4(Propionyl); K8(Propionyl)	955.5692615	23984626.47	20239798.78	8629866.156	8268154.563
SUM						6.735E9	6.080E9	3.384E9	3.391E9	
fully derivatized (%)						94.26%	94.42%	95.77%	95.71%	
partially derivatized (%)						5.74%	5.58%	4.23%	4.29%	

Supplementary Table S3. MS¹-based absolute and relative quantitation of H4(4-17) and H3(18-23) differentially H₃/D₃-acetylated peptide species through manual integration of peptide peak areas.

A. H4(4-17) PEPTIDE (GKGGKGLGKGAKR)

H4(4-17) H ₃ /D ₃ -ACETYLATED PEPTIDES - absolute values						
	4 H + 0 D	3 H + 1 D	2 H + 2 D	1 H + 3 D	0 H + 4 D	SUM
DMSO 1.1	1609704	3912830	16264330	84817360	270846900	377451124
DMSO 1.2	887807	3942122	19529820	102680700	331301200	458341649
DMSO 2.1	927004	3564601	15682310	84647790	278623700	383445405
DMSO 2.2	795211	3865753	17855230	93649040	289177300	405342534
SAHA 1.1	201222900	172213900	116816400	116816400	77413940	684483540
SAHA 1.2	263721800	227420700	156456700	105806500	62483420	815889120
SAHA 2.1	263721800	227420700	156456700	105806500	62483420	815889120
SAHA 2.2	263585200	227410200	162852500	107483400	65039180	826370480
H4(4-17) H ₃ / D ₃ -ACETYLATED PEPTIDES - normalized to the total area (%)						
	4 H + 0 D	3 H + 1 D	2 H + 2 D	1 H + 3 D	0 H + 4 D	
DMSO 1.1	0.426466872	1.036645476	4.308989685	22.47108423	71.75681374	
DMSO 1.2	0.193699831	0.860083741	4.260974328	22.40265536	72.28258674	
DMSO 2.1	0.24175645	0.929624127	4.089841682	22.07557814	72.6631996	
DMSO 2.2	0.196182471	0.953700309	4.404973202	23.10367952	71.3414645	
SAHA 1.1	29.39777047	25.15968463	17.06635634	17.06635634	11.30983223	
SAHA 1.2	32.3232402	27.8739714	19.17622091	12.968245	7.658322494	
SAHA 2.1	32.3232402	27.8739714	19.17622091	12.968245	7.658322494	
SAHA 2.2	31.89673474	27.51915824	19.70696001	13.00668436	7.870462653	
AVERAGE DMSO	0.26	0.95	4.27	22.51	72.01	
STDEV DMSO	0.1	0.1	0.1	0.4	0.6	
AVERAGE SAHA	31.49	27.11	18.78	14.00	8.62	
STDEV SAHA	1.4	1.3	1.2	2.0	1.8	

B. H3(18-26) PEPTIDE (KQLATKAAR)

H3(18-26) H ₃ /D ₃ -ACETYLATED PEPTIDES - absolute values				
	2 H + 0 D	1 H + 1 D	0 H + 2 D	SUM
DMSO 1.1	6499257	133309200	403873600	543682057
DMSO 1.2	6235721	132608600	399612100	538456421
DMSO 2.1	5402409	124478600	363445500	493326509
DMSO 2.2	572094	133451700	403503400	537527194
SAHA 1.1	214020100	292141200	130218000	636379300
SAHA 1.2	222409700	296299800	132651000	651360500
SAHA 2.1	300832700	401043500	176320900	878197100
SAHA 2.2	313589200	416787600	181649400	912026200
H3(18-26) H ₃ /D ₃ -ACETYLATED PEPTIDES - normalized to the total area (%)				
	2 H + 0 D	1 H + 1 D	0 H + 2 D	
DMSO 1.1	1.195415025	24.51969828	74.28488669	
DMSO 1.2	1.158073478	24.62754549	74.21438104	
DMSO 2.1	1.095098054	25.23249769	73.67240425	
DMSO 2.2	0.106430708	24.82696717	75.06660212	
SAHA 1.1	33.6309022	45.90677289	20.46232491	
SAHA 1.2	34.14540796	45.48937186	20.36522018	
SAHA 2.1	34.25571549	45.66668462	20.07759989	
SAHA 2.2	34.38379292	45.69908189	19.91712519	
AVERAGE DMSO	0.89	24.80	74.31	
STDEV DMSO	0.5	0.3	0.6	
AVERAGE SAHA	34.10	45.69	20.21	
STDEV SAHA	0.3	0.2	0.3	

4. DISCUSSION

4.1. General Discussion

Lysine deacetylases are evolutionary-conserved enzymes that regulate mechanisms crucial for cell proliferation. These include DNA replication, DNA damage repair and gene transcription. Aberrant expression of different KDAC isoforms is observed in certain types of cancer and often, increased expression of KDACs correlates with a poor prognosis for patient survival (Glozak & Seto, 2007; Nakagawa et al, 2007; Regna et al, 2015; Yang et al, 2014). Consequently, inhibition of KDAC activity has shown promise in clinical trials as a means to arrest cell cycle and trigger apoptosis of rapidly-proliferating cancerous cells (Manal et al, 2016; Qiu et al, 2017; Sweet et al, 2012; Wanczyk et al, 2011; West & Johnstone, 2014; Zhang & Zhong, 2014). Transformed cells proliferate at a higher rate compared to normal cells in the human body. Therefore, a greater effect of KDAC inhibition can be observed with malignant cell types compared to normal cells.

Prolonged exposure to KDACis affects different cellular compartments, and eventually leads to cell death or apoptosis (Zhang & Zhong, 2014). Various triggers of apoptosis have been investigated in the past. This includes an increase in DNA damage (Robert et al, 2011), oxidative stress, and altered tumour suppressor (Monte et al, 2006) or oncogene expression (Jiang et al, 2011). Moreover, KDACi-mediated cell death via both extrinsic and intrinsic apoptotic pathways was observed depending on the cell type investigated, class of KDACi and concentration thereof utilised in the study (Inoue et al, 2006). Commonly, a harsh treatment is applied to trigger cell death. This thesis, however, focuses mainly on the initial response to KDACis. Therefore, a mild KDACi treatment was employed in order to investigate the onset of early changes in affected cellular pathways. These might be masked in a later drug-treatment stage when a plethora of secondary apoptotic events occurs. The work performed in this thesis is comprised of a systems-biology approach to characterise the cellular processes affected by lysine deacetylase inhibitors, and how this information could be employed in the context of cancer treatment.

4.1.1. KDACi-mediated Isoform-specific Alteration in Histone Acetylation

Histone proteins are small, ~20 kDa nuclear proteins that interact with DNA and various multi-protein complexes in order to regulate DNA replication and gene transcription. Various histone

PTMs have been identified to aid and fine tune these processes. Acetylation is one of the most common histone modifications. Due to the close proximity of multiple lysine residues that can be cleaved by trypsin, digested histone peptides are often: (i) too small to be retained on the chromatography reverse-phase separation column; and/or (ii) fall outside the mass range mass spectrometer. Moreover, when modified, lysine residues are not recognised nor cleaved by trypsin. In this case it is impossible to determine the relative abundance of the modified peptide compared to the unmodified counterpart. Chemical derivatisation of unmodified lysine residues is thus utilised to restrict histone digestion to the arginine residues in the protein sequence. Our combination of a simplified sample preparation method combined with adjustment of the MS method and bioinformatic analysis provided an improved approach to quantitate site-specific alteration in histone acetylation.

This methodology can be further extended to other histone modifications, and/or be utilised to monitor the dynamics of histone PTMs within a specific time course. Finally, single or multiple modified residues can be further utilised to design a chromatin precipitation experiments (ChIP). This approach will aid our understanding on how a particular histone PTM influences the gene expression in the context of disease progression and/or a particular drug treatment.

4.1.2. KDACi-driven Changes at the Systems Biology Level

The predominant mechanism of KDACi-induced gene alteration is explained by inhibition of deacetylase function that leads to increased acetylation of histone proteins and subsequent transcriptional activation of the targeted gene loci (Allfrey et al, 1964; Rajagopal et al, 2014; Smith et al, 2003). KDACi-treatment conditions examined here, however, significantly up- and downregulated gene transcription. This indicates the existence of a considerably more complex mechanism behind KDACi-mediated regulation of gene transcription that extends beyond the oversimplified dogma of histone acetylation.

Improvements in analytical methods together with an increase in the sensitivity of mass spectrometry instrumentation has thus enabled a more detailed investigation of the molecular mechanisms that drive malignant cell transformation. Significant advancements in sensitivity have been achieved in the fields of gene and protein expression analysis. Moreover, developed bioinformatic tools have enabled the successful integration of multi-omic studies. This is beneficial in distinguishing changes that occur at the transcriptional and (post)translational level in a disease state or after drug-driven perturbation compared to the control condition. The integrative approach

in this thesis distinguished changes that occurred in protein expression, that did not necessarily correlate with changes observed at the gene expression level.

Integration of the transcriptomic and proteomic data revealed differential responses following TSA and RD treatment of Jurkat T cells. Upon RD treatment, but not TSA, a correlation between altered gene and protein expression was evident. To some extent, this observation indicated that gene expression can be utilised to predict protein expression changes after inhibition of nuclear KDACs. Nevertheless, the same reasoning cannot be applied to the inhibition of KDACs that are localised in the cytoplasm, or those that shuttle between the cytoplasm and nucleus, *i.e.*, class II and IV KDACs. Besides, not all altered transcripts could be mapped to identified proteins. This is predominantly due to the alteration of protein non-coding RNAs, or the transcripts of proteins that are difficult to purify and/or observe by mass spectrometry. The latter primarily refers to highly hydrophobic membrane-bound proteins, *i.e.*, receptors and transporters. As mentioned in the previous section, highly basic proteins such as histones, generate tryptic peptides that are too short to be retained on the chromatographic column and/or outside the mass detection range of most mass spectrometry methods. Therefore, transcriptomic analysis offers additional information about significant alterations within the cell when proteomic analysis *per se* is not sufficient. Moreover, histone and non-histone acetylation has a distinct effect on cell physiology, and thus is an important addition to transcriptomic and proteomic expression data.

The experimental conditions for KDACi treatment that were defined earlier, suggested that the major changes that occur after sub-apoptotic TSA and RD treatment of Jurkat T cells occur in metabolic pathways. To this end, further discussion is focused towards the current knowledge in cancer-specific metabolic pathways, and how these are related to the KDACi effects observed. Moreover, the data presented in the included manuscripts was extended to potential applications in a clinical context.

4.1.3. Energy Metabolism of Normal and Cancer Cells

Within living organisms or as single-cell entities, the metabolism of cells can be divided into catabolic and anabolic pathways. Catabolism is comprised of metabolic reactions where nutrients or macromolecules are degraded, with a subsequent release of energy. On the contrary, anabolism refers to utilisation of available energy in the cell to generate complex molecular structures from smaller precursors. In general, these pathways coordinate three crucial functions for cell survival and replication: (i) energy production from nutrients; (ii) synthesis of

macromolecules that are constitutively form cell integrity; and (iii) mediate synthesis/degradation of molecules with a specific (enzymatic) function. It is not surprising that the coordination between these processes must be well-structured and orchestrated in order to accommodate current, yet unstable, cellular demands.

Metabolic pathways and the activity of the enzymes involved, are largely dependent on available nutrients and the level of oxygen. Normally, glucose is absorbed by cells via glucose transporters localised within the plasma membrane. Glucose catabolism begins with glycolysis in the cytosol. The glycolytic pathway generates two molecules of pyruvate from one glucose and two molecules of adenosine triphosphate (ATP) are released. Nevertheless, how the cell processes glucose depends on the cell type, the availability of the oxygen, metabolic and transformation state. For instance, if oxygen is restricted, pyruvate is converted to lactate via the activity of lactate dehydrogenase. Alternatively, when oxygen is sufficient, pyruvate enters the mitochondria, is reduced by pyruvate dehydrogenase to acetyl-CoA, and enters the tricarboxylic acid (TCA) cycle, also known as Krebs or citric acid cycle (Figure 12.) (Abbona et al, 1956; Domagk & Zech, 1967). Combined with oxidative phosphorylation in the mitochondria, the TCA cycle generates energy in the form of ATP. This indicates that glycolysis *per se* is not preferentially utilised by the cell to generate a high level of energy required for cellular function. The enzymes that regulate cellular energy metabolism are connected to the *side* pathways that utilise glycolytic and/or TCA-cycle intermediates as precursors for protein, nucleic acid and/or lipid synthesis. Acetyl-CoA can be directed towards synthesis of fatty acids and further to triacylglycerides and phospholipids. Moreover, various intermediates of glycolysis and TCA function as further catabolites of proteins by providing different amino acids precursors. Equally important are the pathways that lead to the synthesis of the nucleic acids, precursors for replication of the genetic information (deoxyribonucleic acids, DNA), and the various mediators of the multiple steps in proteins biogenesis (ribonucleic acids, RNA). Taken together, glucose catabolism allows cells to either: (i) generate energy in the form of ATP; or (ii) utilise intermediates of the glycolytic and TCA pathways for the synthesis of precursors required for nucleotide, protein and lipid synthesis. Both outcomes are important for cell survival.

Cells that do not rapidly proliferate but maintain a steady metabolism to sustain certain cellular function, require more energy than constitutive molecular precursors for replication (Tarrado-Castellarnau et al, 2016). This is true for most of the cells in the human body. Nevertheless, exceptions to this are: (i) immune cells that need to rapidly proliferate to provide an adequate and

rapid response to protect against foreign antigens; and (ii) cancer-related, transformed cells that bear mutation or epigenetic alterations that drive uncontrolled cell proliferation.

To this end, for cancer cells it is more important to activate the pathways that are required for the synthesis of macromolecular precursors than solely generating energy in the form of ATP. This can be further utilised to investigate the pathways that are crucial for the former in order to specifically target highly-proliferative malignant cells whilst sparing healthy, resting differentiated cells.

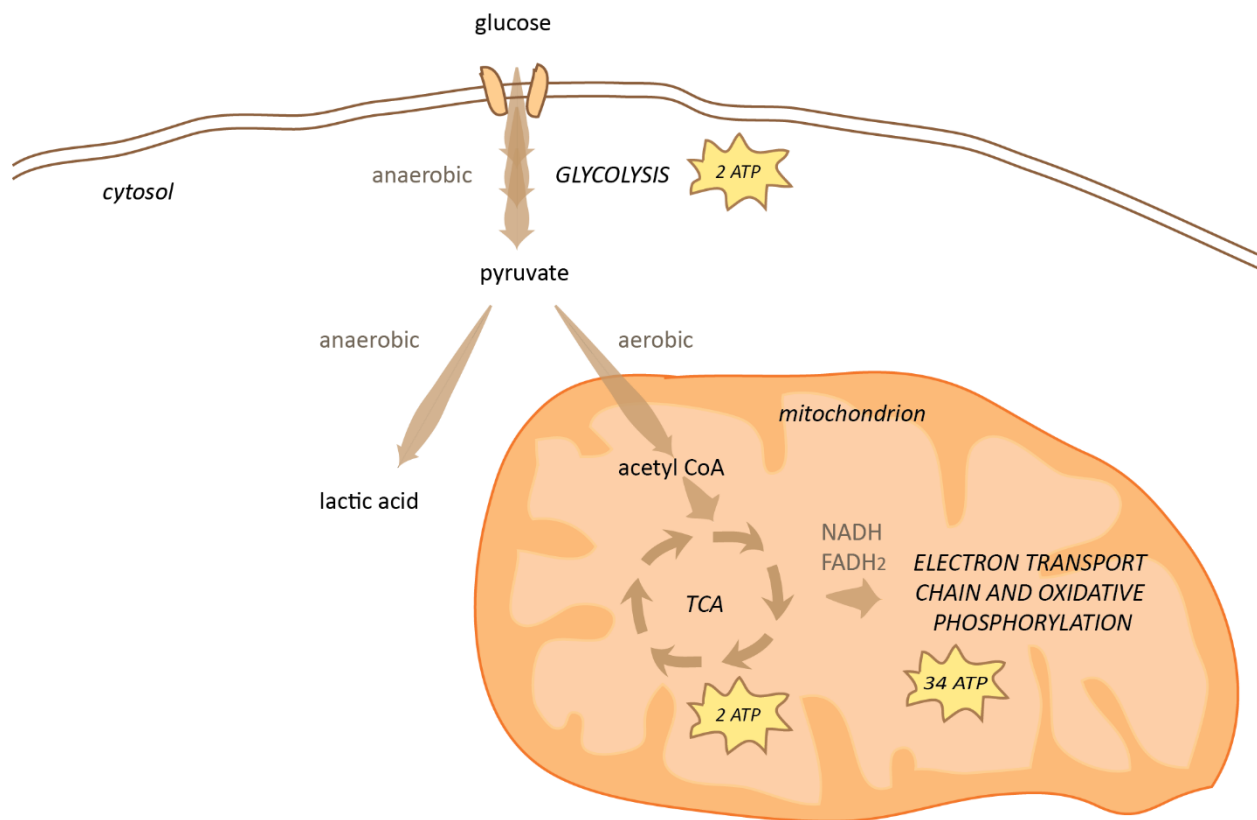


Figure 12. Glucose Metabolism.

Under anaerobic conditions, glucose is transported through the cell membrane via glucose transporters and catabolised to pyruvate in the cytosol. Under conditions where anaerobic conditions persist, pyruvate is converted to lactic acid. Nevertheless, in human cells that have the capacity to utilise oxygen, pyruvate is converted to acetyl-CoA in the mitochondria and enters the TCA cycle. Multiple oxidative steps of the TCA cycle utilise the cofactors NAD^+ and FAD . These cofactors are reduced to NADH and FADH_2 , and are further utilised in oxidative phosphorylation to generate energy in the form of ATP. FAD , flavin adenine dinucleotide; NAD , nicotinamide adenine dinucleotide; TCA, tricarboxylic acid (cycle).

4.1.4. Acetylation-mediated Impact on Tumour Metabolism

The development of new enrichment strategies combined with improvements in existing analytical methods, has resulted in the investigation of protein PTMs gaining more interest compared to the previously-dominated gene/protein expression studies. Additionally, the increased sensitivity of mass spectrometers enables an unprecedented deeper analysis of low-abundance PTMs. The importance thereof, however, is only appreciated when combined with protein abundance data. Without the latter, it is not possible to determine whether the observed change occurs on the PTM or at the protein abundance level. PTM alterations that do not reflect changes in protein abundance are of particular interest to further relate the specific PTM to protein function.

In general, protein modifications are a favourable means to rapidly modulate specific biological processes/pathway(s) via altering protein function; whilst protein synthesis/degradation does not necessarily need to occur. To this end, acetylation has been functionally related to integration of metabolic flux (Baeza et al, 2016; Cluntun et al, 2015; Menzies et al, 2016; Stefely et al, 2016; Zhao et al, 2014) and energy production (Baeza et al, 2016; Menzies et al, 2016), regulation of cell cycle (Chuang et al, 2010; Rajendran et al, 2013; Thiel et al, 2012) and DNA damage repair (Bennetzen et al, 2013; Bharti & Brosh, 2016; Bouwman & Jonkers, 2012; Robert & Rassool, 2012; Sulli et al, 2012). To date, KDACs have been investigated in the context of regulating the metabolic state of cells in health and disease (Lin et al, 2014; Zhao et al, 2014). Metabolism and energy pathways are tightly bound to the mitochondria that direct metabolism-related questions towards mitochondrion-localised sirtuins rather than the classical, zinc-dependent KDACs (Baeza et al, 2016; Stefely et al, 2016). Mitochondria, however, are not the only important organelle that controls cell proliferation of metabolically-reprogrammed cancer cells. In the context of tumour metabolism, the Warburg effect is one example of where the consequences of protein acetylation should be investigated beyond mitochondrial function.

4.1.5. Cancer Cell Metabolism is Characterised by the Warburg Effect

Otto Warburg was the first to observe differences in the metabolism and energy production between normal and cancer cells. In 1924, he observed that cancer cell have a distinct way of metabolising glucose as the main source of the energy (Warburg et al, 1927). Cancerous cells proliferate at a higher rate compared to normal cells, and thus it was not surprising that the uptake of glucose was increased accordingly. The unexpected observation, however, was that these cells metabolise glucose to pyruvate, and then to lactate that normally occurs under anaerobic

conditions. Warburg later observed that it was not the hypoxic condition that caused the effect as the cancer cells produced lactic acid even under normal oxygen levels (Warburg, 1956).

The cancer cells, therefore, preferred the *aerobic glycolysis* over the usual oxidative phosphorylation (Figure 13). This metabolic switch from normal, oxidative phosphorylation to the *aerobic glycolytic* pathway was contradictory to the belief that highly proliferative cells required more energy to support growth. On the contrary, *aerobic glycolysis* generates negligible amounts of ATP molecules compared to the full oxidative catabolism of glucose. This was an important realisation that redirected research on energy-related pathways of tumour cells from ATP-dependency (energy) towards dependency of the tumour growth on metabolic intermediates that are important for the cellular integrity of the dividing cells.

Rapid growth and a high influx of required nutrients suggests that transformed cells might adopt a reprogrammed metabolism to adjust replicative requirements. Nevertheless, a switch from the regular TCA cycle and oxidative phosphorylation that yields a high energy level towards an energy-inefficient *aerobic glycolysis* was surprising. Reasons to explain this phenomenon were postulated and include: (i) cytoplasm-restricted glucose catabolism due to dysfunctional mitochondria; and (ii) potential benefits of cancer-cell adaptation to acidic conditions (lactic acid production and secretion) compared to the surrounding cells that do not tolerate a low pH. Further studies, however, revealed that in these cells: (i) mitochondria are still active; and (ii) the benefit of lactic acid production could not be rationalised (Vander Heiden et al, 2009).

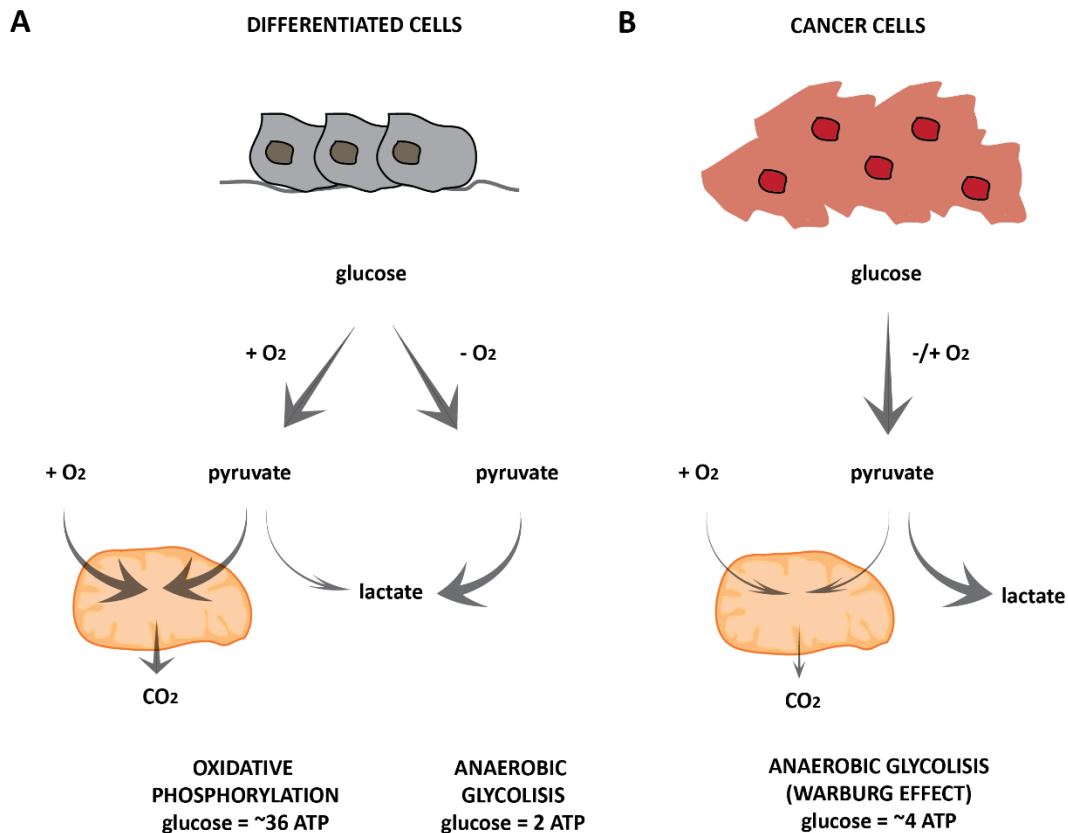


Figure 13. Differences in the Glucose Metabolism of Differentiated and Proliferative Cells.

(A) Cells that are fully-differentiated typically catabolise glucose under aerobic (+O₂) conditions. In this case, the major energy release occurs in mitochondria via oxidative phosphorylation. When oxygen is not available, *i.e.*, under anaerobic (-O₂) conditions, the final product of glucose metabolism is lactate. (B) Cells that proliferate at a high rate, *e.g.*, immune cells and transformed (tumour) cells, preferentially produce lactate even under aerobic conditions. This effect is commonly known as *aerobic glycolysis* (Warburg effect). The figure was adapted from Vander Heiden *et al.* (Vander Heiden *et al.*, 2009).

4.1.6. Active Serine Synthesis, One-carbon (Folate) Metabolism and Glycine Cleavage System (SOG Pathway) is Required for Biosynthesis of Macromolecular Precursors in Proliferating Cells

Vazquez and colleagues confirmed that highly-proliferative cells do not have higher demands for energy consumption compared to resting cells (Vazquez et al, 2010). Thus, the scientific focus was on the alternative mechanisms behind the metabolic switch towards *anaerobic glycolysis* that give cancer cells a proliferative advantage. Surprisingly, it was found that to be metabolically 'maintained', highly-proliferating cells consume less energy compared to normal, quiescent cells. On the contrary, the requirement for intermediates of the glycolytic pathway that are utilised to generate precursors for cellular biomass was essential.

Recently, the enzymes controlling SOG pathways were shown to be increased in tumour tissue (Jain et al, 2012). In particular, the availability and the uptake of glycine, folate and serine contributed to the requirements of highly-proliferative cells (Tedeschi et al, 2013). Moreover, the variability in expression and activity of enzymes that constitute the SOG pathway directly influences the availability of metabolites that are required to feed the one-carbon metabolic pathway and regulate nucleotide and protein synthesis (Figure 14). On the other hand, little is known about the function of particular acetylation site on the proteins within SOG pathway and the consequence that altered acetylation can have on cell survival/proliferation.

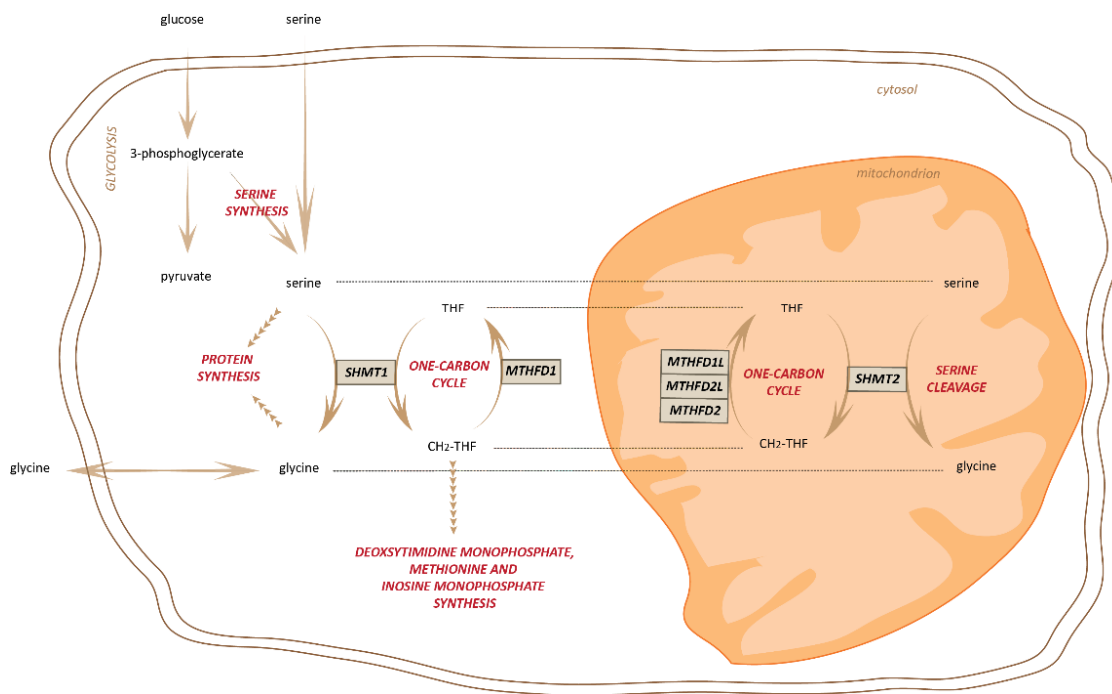


Figure 14. SOG Pathway.

Glucose, serine and glycine are transported into the cell from the extracellular matrix. Serine can be additionally acquired within the cell via the serine synthesis pathway from the intermediate of glucose catabolism, *i.e.*, 3-phosphoglycerate. Glycine, on the other hand, can be produced in the cell from serine conversion via SHMT that transfers a β -carbon unit from serine to THF, generating a glycine and CH₂-THF. Serine to glycine conversion in the cytosol is catalysed by SHMT1; whilst the same reaction in the mitochondria is performed by SHMT2. The reverse reaction that closes the one carbon cycle and regenerates THF is catalysed by the trifunctional enzyme in the cytosol, MTHFD1. In the mitochondria, however, these reactions are coordinated through three different enzymes, namely MTHFD1L, MTHFD2L and MTHFD2. Intermediates of these reactions are critical for protein and nucleotide synthesis pathways required for replication of highly-proliferating cells. 5,10-methylene-tetrahydrofolate, 5,10-CH₂-THF (CH₂-THF); MTHFD1, methylenetetrahydrofolate dehydrogenase 1; MTHFD1L, formyltetrahydrofolate synthetase (mitochondrial); MTHFD2 methylenetetrahydrofolate dehydrogenase/cyclohydrolase (mitochondrial); MTHFD2L putative methylenetetrahydrofolate dehydrogenase/cyclohydrolase 2 (mitochondrial); SHMT, serine hydroxymethyltransferase (SHMT1 and SHMT2 cytoplasmic and mitochondrial, respectively); THF, tetrahydrofolate.

4.1.7. Functional Assessment of the KDACi-mediated Acetylation of Enzymes Within the SOG Pathway

Altered expression of the enzymes that constitute the SOG pathway has previously been related to certain types of cancer. For instance, a clinical study that involved biopsies from 76 breast cancer patient showed positive histochemical staining for the presence of SHMT2 (Yin, 2015). SHMT2 regulates mitochondrion-specific interconversion between glycine and serine and contributes to the *de novo* mitochondrial thymidylate biosynthesis pathway. SHMT2 was identified in the tumour tissue and the expression level was positively-correlated with the stage of cancer progression. In the matching normal tissue, however, SHMT2 was not observed (Yin, 2015). This indicated that the SHMT2 is tumour specific and, potentially, can be utilised as a predictive marker for patient survival. The presence of SHMT2 in tumour tissues and the lack thereof in healthy cells has been suggested as an attractive target for the future cancer treatment. Although mitochondrial SHMT2 has a distinct cellular role compared to the cytoplasmic isoform SHMT1, these two enzymes have a similar protein sequence and catalytic activity. Therefore, development of isoform-specific inhibitors represents the greatest challenge for this type of treatment (Giardina et al, 2015).

Emphasis of this thesis was on proteins that were essential for cell survival and increased in acetylation under investigated, non-apoptotic KDACi treatment conditions (*i.e.*, IC₅₀ concentration for 24 h). As promising candidates, two proteins involved in SOG pathway were investigated. MTHFD1 and SHMT2 were increased in acetylation after KDACi treatment; but remained unaltered at the protein expression level. These are involved in the cytoplasmic and mitochondrial branch of the SOG pathway that is required for tumour survival. Interestingly, alterations in acetylation on the isoforms expressed in the cytosol and mitochondrion, respectively, were not identified.

In silico investigation of the structural role of a particular acetylation site that was altered after KDACis treatment was performed. This was to aid the hypothesis on how certain acetylation changes mediated by KDACi treatment influence protein structure and/or function. Two lysine residues of SHMT2 that were altered in acetylation after KDACi treatment were localised on the surface of the SHMT2 dimer. That indicates potential role of acetylation in protein-protein interaction. Another lysine residue that was increased in acetylation localises at the interface of SHMT2 dimer and, in particular, within the catalytic domain. The latter indicates potential role of acetylation in modulating enzymatic function. Similarly, KDACi-mediated acetylation of MTHFD1 can alter protein oligomerisation or directly influence enzymatic function.

These two examples indicate that the effect of KDACis extends to both cytosolic and mitochondrial metabolic pathways. The recent work of Ducker *et al.* (Ducker et al, 2016) revealed that the cytosolic SOG pathway can compensate for the loss of mitochondrial purine synthesis requirements for tumour growth. Utilising a genetic knock-out (KO) approach in mice, these researchers observed that SHMT1 compensates for the loss of MTHFD2. In the case of the double KO of SHMT1 and MTHFD2, however, reduced tumour growth was observed. Further investigation is required to determine whether the same is true for the combination of reduced expression of SHMT2 and MTHFD1. Contrary to our results, these data focused only on reduced expression of these enzymes. It will be interesting to determine whether observed increase in acetylation impairs function of these enzymes, without altering protein abundance. In theory, this would have comparable 'synthetic lethality' effect on cancer proliferation as observed by Ducker *et al.* (Ducker et al, 2016; Ducker & Rabinowitz, 2017) and open alternative strategies for diagnosis and targeted cancer therapies, *i.e.*, treatment of patients with SHMT2-positive malignancies.

Taken together, overexpression of a particular enzymes required for tumour cell growth can be utilised as a disease diagnostic or prognostic biomarker. Ongoing studies of tumour-related protein acetylation as potential biomarkers will aid diagnostics when protein expression data show no differences between a healthy and diseased condition. Moreover, gained knowledge will lead to development of novel treatment options that might be targeted to the tumour-specific isoform of the enzyme that is crucial for cell survival.

4.2. Conclusion and Future Prospects

This thesis is comprised of two manuscripts that focus on distinct aspects of acetylation changes that occur after inhibition of KDACs. These key enzymes are responsible for the removal of acetyl groups from histone and non-histone protein substrates. In one of the manuscripts, a simplified mass-spectrometry workflow, termed FASIL-MS, was developed to quantitate isoform-specific changes in histone acetylation upon KDAC inhibition. In the second manuscript, however, the focus was centred on the versatile role of KDACs at a systems-biology level. Here, alteration in gene and protein expression, together with changes in non-histone protein acetylation after KDAC inhibition was investigated. Our results showed that the data provide valuable and unique insights into characterising the changes that KDACis evoke in malignant cells. Contrary to the previous studies, we focused on the early response to KDACis. This was performed in order to identify alterations in protein abundance and acetylation that is not a consequence of the various apoptotic pathways triggered by prolonged, severe KDACi treatment. Moreover, KDACi-mediated alteration of the proteins involved in cancer-specific metabolic pathways were identified. Many of these changes were observed on metabolic enzymes that are *essential* for tumour survival. Therefore, this data represents a rationale to further investigate acetylation changes in the context of disease biomarkers. Moreover, assessment of the functional consequence that altered lysine acetylation has on protein function will undoubtedly aid in developing alternative strategies for targeted cancer treatments.

5. MATERIALS AND METHODS

Materials and methods that were utilised are covered within the two included manuscripts. Additional methods that were not described are included below.

5.1. Cell Proliferation Assay

Violet proliferation dye 450 (VPD450, BD Horizon™, Heidelberg, DE) was utilised to stain the cells as previously described (Lyons, 2000; Lyons & Doherty, 2004a; Lyons & Doherty, 2004b). Briefly, commercial VPD450 was diluted in 100% DMSO to give a 1 mM stock solution and single-use aliquots were frozen at -80°C for further cell staining. Jurkat T cells were washed twice with 1× PBS in polypropylene tubes to remove residual serum proteins with a centrifugation step in between. Cells were resuspended in 1× PBS at a concentration of 1 million cells per mL and the VPD450 stock solution was added to the cell suspension at a final concentration of 1 µM. The dye was incubated with the cells for 10 min at 37°C. The cell suspension was diluted 1:10 with 1× PBS and centrifuged to remove excess dye that remained in the supernatant. After an additional wash step with 100 mL complete RPMI-1640 medium (described above), cells were seeded at 1×10^6 cells per mL in the 6-well plates and treated with 0.1% DMSO, 460 nM TSA or 2.8 nM RD, and left to proliferate for 72 h at 37°C and 5% CO₂. Aliquots containing approximately 0.5×10^6 cells were removed immediately after drug treatment (0 h), 24 h, 48 h, and 72 h post treatment for FACS analysis with the flow cytometry analyser BD LSR Fortessa™ (BD Biosciences, San Jose, CA). The violet excitation laser was set to 405 nm to activate the fluorochrome VPD450 in order to detect the emission spectra at 450 nm.

5.2. Assessment of KDACi-mediated Changes in Cell Morphology

Cell morphology was visually assessed after TSA and RD treatment of the Jurkat T cells at the determined IC₅₀ concentrations. To obtain an appropriate number of suspension cells to clearly visualise morphology, cells were seeded at a concentration of 1×10^6 /mL in a 6-well plate. In all the other experiments, cells were seeded at 1.5×10^6 /mL. Images were taken soon after seeding the cells (untreated), and after 24 h treatment with 0.1% DMSO, or IC₅₀ concentration of KDACis, 460 nM and 2.8 nM for TSA and RD, respectively.

5.3. *In Silico* Structural Analysis of Acetylation Sites of MTHFD1 and SHMT2

Experimental crystal structures of proteins were obtained from the Protein Data Bank database (PDB entry codes 4pvf, 4jim). The homology model of human MTHFD1 (residues 315-935, covering the FTHFS domain) was obtained from SWISS-MODEL (Biasini et al, 2014) using *Moorella thermoacetica* N10-Formyltetrahydrofolate Synthetase structure (PDB entry 4jim) as a template (with 54% sequence identity). Structural models were visualized with ICM-Browser (Molsoft L.L.C.).

6. REFERENCES

- Abbona C, Bellotti R, Ravera M (1956) [In vivo research on the activity of various manganese salts on the intermediate metabolism of carbohydrates]. *Arch Maragliano Patol Clin* **12**: 683-690
- Abraham RT, Weiss A (2004) Jurkat T cells and development of the T-cell receptor signalling paradigm. *Nat Rev Immunol* **4**: 301-308
- Ahringer J (2000) NuRD and SIN3 histone deacetylase complexes in development. *Trends Genet* **16**: 351-356
- Agudelo Garcia PA, Hoover ME, Zhang P, Nagarajan P, Freitas MA, Parthun MR (2017) Identification of multiple roles for histone acetyltransferase 1 in replication-coupled chromatin assembly. *Nucleic Acids Res*
- Allfrey VG, Faulkner R, Mirsky AE (1964) Acetylation and Methylation of Histones and Their Possible Role in the Regulation of Rna Synthesis. *Proc Natl Acad Sci U S A* **51**: 786-794
- Arrowsmith CH, Bountra C, Fish PV, Lee K, Schapira M (2012) Epigenetic protein families: a new frontier for drug discovery. *Nat Rev Drug Discov* **11**: 384-400
- Atadja P (2009) Development of the pan-DAC inhibitor panobinostat (LBH589): successes and challenges. *Cancer Lett* **280**: 233-241
- Baeza J, Smallegan MJ, Denu JM (2016) Mechanisms and Dynamics of Protein Acetylation in Mitochondria. *Trends Biochem Sci* **41**: 231-244
- Bantscheff M, Hopf C, Savitski MM, Dittmann A, Grandi P, Michon AM, Schlegl J, Abraham Y, Becher I, Bergamini G, Boesche M, Delling M, Dumpelfeld B, Eberhard D, Huthmacher C, Mathieson T, Poeckel D, Reader V, Strunk K, Sweetman G, Kruse U, Neubauer G, Ramsden NG, Drewes G (2011) Chemoproteomics profiling of HDAC inhibitors reveals selective targeting of HDAC complexes. *Nat Biotechnol* **29**: 255-265
- Becher I, Dittmann A, Savitski MM, Hopf C, Drewes G, Bantscheff M (2014) Chemoproteomics reveals time-dependent binding of histone deacetylase inhibitors to endogenous repressor complexes. *ACS chemical biology* **9**: 1736-1746

- Bennetzen MV, Larsen DH, Dinant C, Watanabe S, Bartek J, Lukas J, Andersen JS (2013) Acetylation dynamics of human nuclear proteins during the ionizing radiation-induced DNA damage response. *Cell Cycle* **12**: 1688-1695
- Bharti SK, Brosh RM, Jr. (2016) Fine-Tuning DNA Repair by Protein Acetylation. *Cell Cycle*: 0
- Biasini M, Bienert S, Waterhouse A, Arnold K, Studer G, Schmidt T, Kiefer F, Gallo Cassarino T, Bertoni M, Bordoli L, Schwede T (2014) SWISS-MODEL: modelling protein tertiary and quaternary structure using evolutionary information. *Nucleic Acids Res* **42**: W252-258
- Bieliauskas AV, Pflum MK (2008) Isoform-selective histone deacetylase inhibitors. *Chem Soc Rev* **37**: 1402-1413
- Blanco-Garcia N, Asensio-Juan E, de la Cruz X, Martinez-Balbas MA (2009) Autoacetylation regulates P/CAF nuclear localization. *J Biol Chem* **284**: 1343-1352
- Bodiford A, Bodge M, Talbott MS, Reddy NM (2014) Profile of belinostat for the treatment of relapsed or refractory peripheral T-cell lymphoma. *Onco Targets Ther* **7**: 1971-1977
- Bouwman P, Jonkers J (2012) The effects of deregulated DNA damage signalling on cancer chemotherapy response and resistance. *Nat Rev Cancer* **12**: 587-598
- Bradner JE, West N, Grachan ML, Greenberg EF, Haggarty SJ, Warnow T, Mazitschek R (2010) Chemical phylogenetics of histone deacetylases. *Nat Chem Biol* **6**: 238-243
- Bressi JC, Jennings AJ, Skene R, Wu Y, Melkus R, De Jong R, O'Connell S, Grimshaw CE, Navre M, Gangloff AR (2010) Exploration of the HDAC2 foot pocket: Synthesis and SAR of substituted N-(2-aminophenyl)benzamides. *Bioorg Med Chem Lett* **20**: 3142-3145
- Brunmeir R, Lagger S, Seiser C (2009) Histone deacetylase HDAC1/HDAC2-controlled embryonic development and cell differentiation. *The International Journal of Developmental Biology* **53**: 275-289
- Butler R, Bates GP (2006) Histone deacetylase inhibitors as therapeutics for polyglutamine disorders. *Nat Rev Neurosci* **7**: 784-796
- Celeste LR, Chai G, Bielak M, Minor W, Lovelace LL, Lebioda L (2012) Mechanism of N10-formyltetrahydrofolate synthetase derived from complexes with intermediates and inhibitors. *Protein Sci* **21**: 219-228

- Choi JH, Kwon HJ, Yoon BI, Kim JH, Han SU, Joo HJ, Kim DY (2001) Expression profile of histone deacetylase 1 in gastric cancer tissues. *Jpn J Cancer Res* **92**: 1300-1304
- Choudhary C, Kumar C, Gnad F, Nielsen ML, Rehman M, Walther TC, Olsen JV, Mann M (2009) Lysine acetylation targets protein complexes and co-regulates major cellular functions. *Science* **325**: 834-840
- Chuang C, Lin SH, Huang F, Pan J, Josic D, Yu-Lee LY (2010) Acetylation of RNA processing proteins and cell cycle proteins in mitosis. *J Proteome Res* **9**: 4554-4564
- Cluntun AA, Huang H, Dai L, Liu X, Zhao Y, Locasale JW (2015) The rate of glycolysis quantitatively mediates specific histone acetylation sites. *Cancer Metab* **3**: 10
- Daigle D, Megyola C, El-Guindy A, Gradoville L, Tuck D, Miller G, Bhaduri-McIntosh S (2010) Upregulation of STAT3 marks Burkitt lymphoma cells refractory to Epstein-Barr virus lytic cycle induction by HDAC inhibitors. *J Virol* **84**: 993-1004
- Dawson MA, Kouzarides T, Huntly BJ (2012) Targeting epigenetic readers in cancer. *N Engl J Med* **367**: 647-657
- de Ruijter AJ, van Gennip AH, Caron HN, Kemp S, van Kuilenburg AB (2003) Histone deacetylases (HDACs): characterization of the classical HDAC family. *Biochem J* **370**: 737-749
- Desai R, Peretz A, Idelson H, Lazarovici P, Attali B (2000) Ca²⁺-activated K⁺ channels in human leukemic Jurkat T cells. Molecular cloning, biochemical and functional characterization. *J Biol Chem* **275**: 39954-39963
- Domagk GF, Zech R (1967) [Intermediate metabolism of carbohydrates. New knowledge and its medical significance]. *Hippokrates* **38**: 333-343
- Ducker GS, Chen L, Morscher RJ, Ghergurovich JM, Esposito M, Teng X, Kang Y, Rabinowitz JD (2016) Reversal of Cytosolic One-Carbon Flux Compensates for Loss of the Mitochondrial Folate Pathway. *Cell Metab* **23**: 1140-1153
- Ducker GS, Rabinowitz JD (2017) One-Carbon Metabolism in Health and Disease. *Cell Metab* **25**: 27-42
- Dunn J, Rao S (2017) Epigenetics and immunotherapy: The current state of play. *Molecular immunology* **87**: 227-239

- Falkenberg KJ, Johnstone RW (2014) Histone deacetylases and their inhibitors in cancer, neurological diseases and immune disorders. *Nat Rev Drug Discov* **13**: 673-691
- Filippakopoulos P, Picaud S, Mangos M, Keates T, Lambert JP, Barsyte-Lovejoy D, Felletar I, Volkmer R, Muller S, Pawson T, Gingras AC, Arrowsmith CH, Knapp S (2012) Histone recognition and large-scale structural analysis of the human bromodomain family. *Cell* **149**: 214-231
- Friend C, Scher W, Holland JG, Sato T (1971) Hemoglobin synthesis in murine virus-induced leukemic cells in vitro: stimulation of erythroid differentiation by dimethyl sulfoxide. *Proc Natl Acad Sci U S A* **68**: 378-382
- Friend C, Scher W (1975) Stimulation by dimethyl sulfoxide of erythroid differentiation and hemoglobin synthesis in murine virus-induced leukemic cells. *Ann N Y Acad Sci* **243**: 155-163
- Ge Z, Nair D, Guan X, Rastogi N, Freitas MA, Parthun MR (2013) Sites of acetylation on newly synthesized histone h4 are required for chromatin assembly and DNA damage response signaling. *Mol Cell Biol* **33**: 3286-3298
- Gershey EL, Vidali G, Allfrey VG (1968) Chemical studies of histone acetylation. The occurrence of epsilon-N-acetyllysine in the f2a1 histone. *J Biol Chem* **243**: 5018-5022
- Giardina G, Brunotti P, Fiascarelli A, Cicalini A, Costa MG, Buckle AM, di Salvo ML, Giorgi A, Marani M, Paone A, Rinaldo S, Paiardini A, Contestabile R, Cutruzzola F (2015) How pyridoxal 5'-phosphate differentially regulates human cytosolic and mitochondrial serine hydroxymethyltransferase oligomeric state. *Febs J* **282**: 1225-1241
- Gil J, Ramirez-Torres A, Encarnacion-Guevara S (2017) Lysine acetylation and cancer: A proteomics perspective. *J Proteomics* **150**: 297-309
- Hancock WW, Akimova T, Beier UH, Liu Y, Wang L (2012) HDAC inhibitor therapy in autoimmunity and transplantation. *Annals of the rheumatic diseases* **71 Suppl 2**: i46-54
- Glozak MA, Seto E (2007) Histone deacetylases and cancer. *Oncogene* **26**: 5420-5432
- Halkidou K, Gaughan L, Cook S, Leung HY, Neal DE, Robson CN (2004) Upregulation and nuclear recruitment of HDAC1 in hormone refractory prostate cancer. *Prostate* **59**: 177-189
- Hass MR, Yankner BA (2005) A γ -secretase-independent mechanism of signal transduction by the amyloid precursor protein. *J Biol Chem* **280**: 36895-36904

- Hsu KC, Liu CY, Lin TE, Hsieh JH, Sung TY, Tseng HJ, Yang JM, Huang WJ (2017) Novel Class IIa-Selective Histone Deacetylase Inhibitors Discovered Using an in Silico Virtual Screening Approach. *Sci Rep* **7**: 3228
- Huang H, Sabari BR, Garcia BA, Allis CD, Zhao Y (2014) SnapShot: histone modifications. *Cell* **159**: 458-458 e451
- Inoue S, MacFarlane M, Harper N, Wheat LM, Dyer MJ, Cohen GM (2004) Histone deacetylase inhibitors potentiate TNF-related apoptosis-inducing ligand (TRAIL)-induced apoptosis in lymphoid malignancies. *Cell Death Differ* **11 Suppl 2**: S193-206
- Inoue S, Mai A, Dyer MJ, Cohen GM (2006) Inhibition of histone deacetylase class I but not class II is critical for the sensitization of leukemic cells to tumor necrosis factor-related apoptosis-inducing ligand-induced apoptosis. *Cancer Res* **66**: 6785-6792
- Itoh Y, Suzuki T, Miyata N (2008) Isoform-selective histone deacetylase inhibitors. *Curr Pharm Des* **14**: 529-544
- Jain M, Nilsson R, Sharma S, Madhusudhan N, Kitami T, Souza AL, Kafri R, Kirschner MW, Clish CB, Mootha VK (2012) Metabolite profiling identifies a key role for glycine in rapid cancer cell proliferation. *Science* **336**: 1040-1044
- Jakopovic M, Thomas A, Balasubramaniam S, Schrump D, Giaccone G, Bates SE (2013) Targeting the epigenome in lung cancer: expanding approaches to epigenetic therapy. *Front Oncol* **3**: 261
- Jiang Z, Kamath R, Jin S, Balasubramani M, Pandita TK, Rajasekaran B (2011) Tip60-mediated acetylation activates transcription independent apoptotic activity of Abl. *Mol Cancer* **10**: 88
- Joshi P, Greco TM, Guise AJ, Luo Y, Yu F, Nesvizhskii AI, Cristea IM (2013) The functional interactome landscape of the human histone deacetylase family. *Mol Syst Biol* **9**: 672
- Katika MR, Hendriksen PJ, Shao J, van Loveren H, Peijnenburg A (2012) Transcriptome analysis of the human T lymphocyte cell line Jurkat and human peripheral blood mononuclear cells exposed to deoxynivalenol (DON): New mechanistic insights. *Toxicol Appl Pharmacol* **264**: 51-64
- Khochbin S, Kao HY (2001) Histone deacetylase complexes: functional entities or molecular reservoirs. *FEBS Lett* **494**: 141-144

- Kim B, Hong J (2015) An overview of naturally occurring histone deacetylase inhibitors. *Curr Top Med Chem* **14**: 2759-2782
- Kim JE, White FM (2006) Quantitative analysis of phosphotyrosine signaling networks triggered by CD3 and CD28 costimulation in Jurkat cells. *J Immunol* **176**: 2833-2843
- Klimek VM, Fircanis S, Maslak P, Guernah I, Baum M, Wu N, Panageas K, Wright JJ, Pandolfi PP, Nimer SD (2008) Tolerability, pharmacodynamics, and pharmacokinetics studies of depsipeptide (romidepsin) in patients with acute myelogenous leukemia or advanced myelodysplastic syndromes. *Clin Cancer Res* **14**: 826-832
- Kuzmichev A, Reinberg D (2001) Role of histone deacetylase complexes in the regulation of chromatin metabolism. *Curr Top Microbiol Immunol* **254**: 35-58
- Lee HZ, Kwitkowski VE, Del Valle PL, Ricci MS, Saber H, Habtemariam BA, Bullock J, Bloomquist E, Li Shen Y, Chen XH, Brown J, Mehrotra N, Dorff S, Charlab R, Kane RC, Kaminskas E, Justice R, Farrell AT, Pazdur R (2015) FDA Approval: Belinostat for the Treatment of Patients with Relapsed or Refractory Peripheral T-cell Lymphoma. *Clinical cancer research: an official journal of the American Association for Cancer Research* **21**: 2666-2670
- Lee JS, Smith E, Shilatifard A (2010) The language of histone crosstalk. *Cell* **142**: 682-685
- Lin R, Zhou X, Huang W, Zhao D, Lv L, Xiong Y, Guan KL, Lei QY (2014) Acetylation control of cancer cell metabolism. *Curr Pharm Des* **20**: 2627-2633
- Liu N, Zhuang S (2015) Treatment of chronic kidney diseases with histone deacetylase inhibitors. *Front Physiol* **6**: 121
- Lombardi PM, Cole KE, Dowling DP, Christianson DW (2011) Structure, mechanism, and inhibition of histone deacetylases and related metalloenzymes. *Curr Opin Struct Biol* **21**: 735-743
- Luo J, Su F, Chen D, Shiloh A, Gu W (2000) Deacetylation of p53 modulates its effect on cell growth and apoptosis. *Nature* **408**: 377-381
- Lyons AB (2000) Analysing cell division in vivo and in vitro using flow cytometric measurement of CFSE dye dilution. *J Immunol Methods* **243**: 147-154
- Lyons AB, Doherty KV (2004a) Flow cytometric analysis of cell division by dye dilution. *Curr Protoc Cytom* **Chapter 9**: Unit 9 11

- Lyons AB, Doherty KV (2004b) Flow cytometric analysis of cell division by dye dilution. *Curr Protoc Cytom* **Chapter 9**: Unit 9 11
- Ma N, Luo Y, Wang Y, Liao C, Ye WC, Jiang S (2016) Selective Histone Deacetylase Inhibitors with Anticancer Activity. *Curr Top Med Chem* **16**: 415-426
- Manal M, Chandrasekar MJ, Gomathi Priya J, Nanjan MJ (2016) Inhibitors of histone deacetylase as antitumor agents: A critical review. *Bioorganic chemistry* **67**: 18-42
- Marmorstein R, Roth SY (2001) Histone acetyltransferases: function, structure, and catalysis. *Curr Opin Genet Dev* **11**: 155-161
- Marks PA, Breslow R (2007) Dimethyl sulfoxide to vorinostat: development of this histone deacetylase inhibitor as an anticancer drug. *Nat Biotechnol* **25**: 84-90
- Mayya V, Lundgren DH, Hwang SI, Rezaul K, Wu L, Eng JK, Rodionov V, Han DK (2009) Quantitative phosphoproteomic analysis of T cell receptor signaling reveals system-wide modulation of protein-protein interactions. *Science signaling* **2**: ra46
- Menzies KJ, Zhang H, Katsyuba E, Auwerx J (2016) Protein acetylation in metabolism - metabolites and cofactors. *Nat Rev Endocrinol* **12**: 43-60
- Monte M, Simonatto M, Peche LY, Bublik DR, Gobessi S, Pierotti MA, Rodolfo M, Schneider C (2006) MAGE-A tumor antigens target p53 transactivation function through histone deacetylase recruitment and confer resistance to chemotherapeutic agents. *Proc Natl Acad Sci U S A* **103**: 11160-11165
- Morales JC, Ruiz-Magana MJ, Carranza D, Ortiz-Ferron G, Ruiz-Ruiz C (2010) HDAC inhibitors with different gene regulation activities depend on the mitochondrial pathway for the sensitization of leukemic T cells to TRAIL-induced apoptosis. *Cancer Lett* **297**: 91-100
- Mottamal M, Zheng S, Huang TL, Wang G (2015) Histone deacetylase inhibitors in clinical studies as templates for new anticancer agents. *Molecules* **20**: 3898-3941
- Muller BM, Jana L, Kasajima A, Lehmann A, Prinzler J, Budczies J, Winzer KJ, Dietel M, Weichert W, Denkert C (2013) Differential expression of histone deacetylases HDAC1, 2 and 3 in human breast cancer--overexpression of HDAC2 and HDAC3 is associated with clinicopathological indicators of disease progression. *BMC Cancer* **13**: 215

- Nakagawa M, Oda Y, Eguchi T, Aishima S, Yao T, Hosoi F, Basaki Y, Ono M, Kuwano M, Tanaka M, Tsuneyoshi M (2007) Expression profile of class I histone deacetylases in human cancer tissues. *Oncol Rep* **18**: 769-774
- Phillips DM (1963) The presence of acetyl groups of histones. *Biochem J* **87**: 258-263
- Qiu X, Xiao X, Li N, Li Y (2017) Histone deacetylases inhibitors (HDACis) as novel therapeutic application in various clinical diseases. *Prog Neuropsychopharmacol Biol Psychiatry* **72**: 60-72
- Rajagopal N, Ernst J, Ray P, Wu J, Zhang M, Kellis M, Ren B (2014) Distinct and predictive histone lysine acetylation patterns at promoters, enhancers, and gene bodies. *G3 (Bethesda)* **4**: 2051-2063
- Rajendran P, Kidane AI, Yu TW, Dashwood WM, Bisson WH, Lohr CV, Ho E, Williams DE, Dashwood RH (2013) HDAC turnover, CtIP acetylation and dysregulated DNA damage signaling in colon cancer cells treated with sulforaphane and related dietary isothiocyanates. *Epigenetics* **8**: 612-623
- Regna NL, Vieson MD, Gojmerac AM, Luo XM, Caudell DL, Reilly CM (2015) HDAC expression and activity is upregulated in diseased lupus-prone mice. *Int Immunopharmacol* **29**: 494-503
- Robert C, Rassool FV (2012) HDAC inhibitors: roles of DNA damage and repair. *Adv Cancer Res* **116**: 87-129
- Robert T, Vanoli F, Chiolo I, Shubassi G, Bernstein KA, Rothstein R, Botrugno OA, Parazzoli D, Oldani A, Minucci S, Foiani M (2011) HDACs link the DNA damage response, processing of double-strand breaks and autophagy. *Nature* **471**: 74-79
- Rosato RR, Almenara JA, Grant S (2003) The histone deacetylase inhibitor MS-275 promotes differentiation or apoptosis in human leukemia cells through a process regulated by generation of reactive oxygen species and induction of p21CIP1/WAF1 1. *Cancer Res* **63**: 3637-3645
- Roth SY, Denu JM, Allis CD (2001) Histone acetyltransferases. *Annu Rev Biochem* **70**: 81-120
- Saji S, Kawakami M, Hayashi S, Yoshida N, Hirose M, Horiguchi S, Itoh A, Funata N, Schreiber SL, Yoshida M, Toi M (2005) Significance of HDAC6 regulation via estrogen signaling for

- cell motility and prognosis in estrogen receptor-positive breast cancer. *Oncogene* **24**: 4531-4539
- Sanchez R, Zhou MM (2009) The role of human bromodomains in chromatin biology and gene transcription. *Curr Opin Drug Discov Devel* **12**: 659-665
- Schafer S, Saunders L, Schlimme S, Valkov V, Wagner JM, Kratz F, Sippl W, Verdin E, Jung M (2009) Pyridylalanine-containing hydroxamic acids as selective HDAC6 inhibitors. *ChemMedChem* **4**: 283-290
- Scholz C, Weinert BT, Wagner SA, Beli P, Miyake Y, Qi J, Jensen LJ, Streicher W, McCarthy AR, Westwood NJ, Lain S, Cox J, Matthias P, Mann M, Bradner JE, Choudhary C (2015) Acetylation site specificities of lysine deacetylase inhibitors in human cells. *Nat Biotech* advance online publication
- Schwammle V, Sidoli S, Ruminowicz C, Wu X, Lee CF, Helin K, Jensen ON (2016) Systems Level Analysis of Histone H3 Post-translational Modifications (PTMs) Reveals Features of PTM Crosstalk in Chromatin Regulation. *Molecular & cellular proteomics : MCP* **15**: 2715-2729
- Shao Y, Gao Z, Marks PA, Jiang X (2004) Apoptotic and autophagic cell death induced by histone deacetylase inhibitors. *Proceedings of the National Academy of Sciences of the United States of America* **101**: 18030-18035
- Siegel RL, Miller KD, Jemal A. Cancer statistics, 2015. *CA Cancer J. Clin.* 65(1), 5–29
- Sivaraj D, Green MM, Gasparetto C (2017) Panobinostat for the management of multiple myeloma. *Future Oncol* **13**: 477-488
- Smil DV, Manku S, Chantigny YA, Leit S, Wahhab A, Yan TP, Fournel M, Maroun C, Li Z, Lemieux AM, Nicolescu A, Rahil J, Lefebvre S, Panetta A, Besterman JM, Deziel R (2009) Novel HDAC6 isoform selective chiral small molecule histone deacetylase inhibitors. *Bioorg Med Chem Lett* **19**: 688-692
- Smith CM, Gafken PR, Zhang Z, Gottschling DE, Smith JB, Smith DL (2003) Mass spectrometric quantification of acetylation at specific lysines within the amino-terminal tail of histone H4. *Anal Biochem* **316**: 23-33
- Stahnke K, Fulda S, Friesen C, Strauss G, Debatin KM (2001) Activation of apoptosis pathways in peripheral blood lymphocytes by in vivo chemotherapy. *Blood* **98**: 3066-3073

- Stefely JA, Kwiecien NW, Freiburger EC, Richards AL, Jochem A, Rush MJ, Ulbrich A, Robinson KP, Hutchins PD, Veling MT, Guo X, Kemmerer ZA, Connors KJ, Trujillo EA, Sokol J, Marx H, Westphall MS, Hebert AS, Pagliarini DJ, Coon JJ (2016) Mitochondrial protein functions elucidated by multi-omic mass spectrometry profiling. *Nat Biotechnol* **34**: 1191-1197
- Su H, Altucci L, You Q (2008) Competitive or noncompetitive, that's the question: research toward histone deacetylase inhibitors. *Molecular cancer therapeutics* **7**: 1007-1012
- Sulli G, Di Micco R, d'Adda di Fagagna F (2012) Crosstalk between chromatin state and DNA damage response in cellular senescence and cancer. *Nat Rev Cancer* **12**: 709-720
- Sun XJ, Man N, Tan Y, Nimer SD, Wang L (2015) The Role of Histone Acetyltransferases in Normal and Malignant Hematopoiesis. *Front Oncol* **5**: 108
- Sweet MJ, Shakespear MR, Kamal NA, Fairlie DP (2012) HDAC inhibitors: modulating leukocyte differentiation, survival, proliferation and inflammation. *Immunol Cell Biol* **90**: 14-22
- Tang J, Yan H, Zhuang S (2013) Histone deacetylases as targets for treatment of multiple diseases. *Clin Sci (Lond)* **124**: 651-662
- Tarrado-Castellarnau M, de Atauri P, Cascante M (2016) Oncogenic regulation of tumor metabolic reprogramming. *Oncotarget* **7**: 62726-62753
- Tedeschi PM, Markert EK, Gounder M, Lin H, Dvorzhinski D, Dolfi SC, Chan LL, Qiu J, DiPaola RS, Hirshfield KM, Boros LG, Bertino JR, Oltvai ZN, Vazquez A (2013) Contribution of serine, folate and glycine metabolism to the ATP, NADPH and purine requirements of cancer cells. *Cell Death Dis* **4**: e877
- Thiel CS, Paulsen K, Bradacs G, Lust K, Tauber S, Dumrese C, Hilliger A, Schoppmann K, Biskup J, Golz N, Sang C, Ziegler U, Grote KH, Zipp F, Zhuang F, Engelmann F, Hemmersbach R, Cogoli A, Ullrich O (2012) Rapid alterations of cell cycle control proteins in human T lymphocytes in microgravity. *Cell Commun Signal* **10**: 1
- Tong JK, Hassig CA, Schnitzler GR, Kingston RE, Schreiber SL (1998) Chromatin deacetylation by an ATP-dependent nucleosome remodelling complex. *Nature* **395**: 917-921
- Van Damme M, Crompton E, Meuleman N, Mineur P, Bron D, Lagneaux L, Stamatopoulos B (2012) HDAC isoenzyme expression is deregulated in chronic lymphocytic leukemia B-cells and has a complex prognostic significance. *Epigenetics* **7**

- Vander Heiden MG, Cantley LC, Thompson CB (2009) Understanding the Warburg effect: the metabolic requirements of cell proliferation. *Science* **324**: 1029-1033
- Varghese S, Senanayake T, Murray-Stewart T, Doering K, Fraser A, Casero RA, Jr., Woster PM (2008) Polyaminohydroxamic acids and polyaminobenzamides as isoform selective histone deacetylase inhibitors. *J Med Chem* **51**: 2447-2456
- Vazquez A, Liu J, Zhou Y, Oltvai ZN (2010) Catabolic efficiency of aerobic glycolysis: the Warburg effect revisited. *BMC Syst Biol* **4**: 58
- Vempati RK, Jayani RS, Notani D, Sengupta A, Galande S, Haldar D (2010) p300-mediated acetylation of histone H3 lysine 56 functions in DNA damage response in mammals. *J Biol Chem* **285**: 28553-28564
- Wanczyk M, Roszczenko K, Marcinkiewicz K, Bojarczuk K, Kowara M, Winiarska M (2011) HDACi--going through the mechanisms. *Front Biosci (Schol Ed)* **16**: 340-359
- Warburg O (1956) On the origin of cancer cells. *Science* **123**: 309-314
- Warburg O, Wind F, Negelein E (1927) The Metabolism of Tumors in the Body. *J Gen Physiol* **8**: 519-530
- West AC, Johnstone RW (2014) New and emerging HDAC inhibitors for cancer treatment. *J Clin Invest* **124**: 30-39
- Weinert BT, Iesmantavicius V, Moustafa T, Scholz C, Wagner SA, Magnes C, Zechner R, Choudhary C (2014) Acetylation dynamics and stoichiometry in *Saccharomyces cerevisiae*. *Mol Syst Biol* **10**: 716
- Wong K, Zhang J, Awasthi S, Sharma A, Rogers L, Matlock EF, Van Lint C, Karpova T, McNally J, Harrod R (2004) Nerve growth factor receptor signaling induces histone acetyltransferase domain-dependent nuclear translocation of p300/CREB-binding protein-associated factor and hGCN5 acetyltransferases. *J Biol Chem* **279**: 55667-55674
- Xu Y (2003) Regulation of p53 responses by post-translational modifications. *Cell Death Differ* **10**: 400-403
- Yang H, Salz T, Zajac-Kaye M, Liao D, Huang S, Qiu Y (2014) Overexpression of histone deacetylases in cancer cells is controlled by interplay of transcription factors and epigenetic modulators. *Faseb J* **28**: 4265-4279

- Yang XJ, Gregoire S (2007) Metabolism, cytoskeleton and cellular signalling in the grip of protein Nepsilon - and O-acetylation. *EMBO Rep* **8**: 556-562
- Yin K (2015) Positive correlation between expression level of mitochondrial serine hydroxymethyltransferase and breast cancer grade. *Onco Targets Ther* **8**: 1069-1074
- Yoon S, Eom GH (2016) HDAC and HDAC Inhibitor: From Cancer to Cardiovascular Diseases. *Chonnam medical journal* **52**: 1-11
- Yoshida M, Kudo N, Kosono S, Ito A (2017) Chemical and structural biology of protein lysine deacetylases. *Proc Jpn Acad Ser B Phys Biol Sci* **93**: 297-321
- Zhang J, Zhong Q (2014) Histone deacetylase inhibitors and cell death. *Cellular and molecular life sciences : CMLS*
- Zhang L, Li M, Xu W (2013) Discovering the binding modes of natural products with histone deacetylase 1. *Med Chem* **9**: 126-132
- Zhang Z, Yamashita H, Toyama T, Sugiura H, Ando Y, Mita K, Hamaguchi M, Hara Y, Kobayashi S, Iwase H (2005) Quantitation of HDAC1 mRNA expression in invasive carcinoma of the breast*. *Breast Cancer Res Treat* **94**: 11-16
- Zhang Z, Yamashita H, Toyama T, Sugiura H, Omoto Y, Ando Y, Mita K, Hamaguchi M, Hayashi S, Iwase H (2004) HDAC6 expression is correlated with better survival in breast cancer. *Clinical cancer research : an official journal of the American Association for Cancer Research* **10**: 6962-6968
- Zhao D, Li FL, Cheng ZL, Lei QY (2014) Impact of acetylation on tumor metabolism. *Mol Cell Oncol* **1**: e963452
- Zhao Y, Tan J, Zhuang L, Jiang X, Liu ET, Yu Q (2005) Inhibitors of histone deacetylases target the Rb-E2F1 pathway for apoptosis induction through activation of proapoptotic protein Bim. *Proceedings of the National Academy of Sciences of the United States of America* **102**: 16090-16095
- Zhu P, Martin E, Mengwasser J, Schlag P, Janssen KP, Gottlicher M (2004) Induction of HDAC2 expression upon loss of APC in colorectal tumorigenesis. *Cancer Cell* **5**: 455-463

7. CURRICULUM VITAE

DIJANA VITKO

Date and place of birth: 4th May 1987, Zagreb, Croatia

Current address: Donaueschingenstraße 5a/8/15, 1200 Vienna, Austria

Mobile: +43(0)699/10424646

✉ dijanavitko@gmail.com

EDUCATION

09/2011 – current	Ph.D. in Immunology Medical University of Vienna (MUV), Austria
10/2009 – 07/2010	M.Sc. in Bio-industrial Techniques Faculty of Science, University of Orléans, France
09/2008 – 07/2010	M.Eng. in Molecular Biotechnology Faculty of Food Technology and Biotechnology, University of Zagreb, Croatia
09/2005 – 09/2008	B.Eng. in Biotechnology Faculty of Food Technology and Biotechnology, University of Zagreb, Croatia

PROFESSIONAL EXPERIENCE

09/2011– 12/2016	Ph.D. Student: Mass Spectrometry and Proteomics CeMM Research Center for Molecular Medicine of the Austrian Academy of Sciences (Austria)
01/2011 – 09/2011	Research Analyst at Teva Pharmaceutical Industries Ltd. - Pliva Croatia Ltd. (Croatia)
01/2010 – 06/2010	Student Trainee at Technologie Servier (France)

GRANTS & AWARDS

AuPA Best Poster Presentation Award at 14th Austrian Proteomic Research Symposium, Austria, September 2016

MUV Congress Travel Grant to attend HuPO 15th Annual World Congress, Taiwan, September 2016

AuPA travel grant to attend the 11th and 12th Austrian Proteomic Research Symposia, Austria, September 2013/14

AuPA student scholarship to attend the 6th EuPA Summer School, Austria, August 2012
EuPA Summer School in Proteomic Basis: FEBS Advanced Lecture Course - High Performance Proteomics

Erasmus scholarship, France, January 2010 - June 2010

Dean`s award, Croatia, April 2008

Undergraduate Study of Biotechnology, Faculty of Food Technology and Biotechnology

Croatian national scholarship, Croatia, January 2007 - September 2010

Ministry of Science, Education and Sports of the Republic of Croatia

SELECTED SYMPOSIUMS & WORKSHOPS

15th Human Proteome Organisation (HuPO) World Congress, Taipei, Taiwan; September 2016 (poster)

14th Austrian Proteomic Research Symposium, Vienna, Austria; September 2016 (poster)

APRS Symposium and Late Summer Meeting, Klosterneuburg, Austria; August 2015 (oral)

EMBO Practical Course: The characterization of PTMs, Odense, Denmark; April 2015 (poster)

12th Austrian Proteomic Research Symposium, Salzburg, Austria; September 2014 (poster)

2nd Copenhagen Bioscience Conference on PTMs in Cell Signalling, Hillerød, Denmark; September 2014 (poster)

62nd ASMS Conference on Mass Spectrometry and Allied Topics 2014, Baltimore, USA; June 2014 (poster)

11th Austrian Proteomic Research Symposium, Innsbruck, Austria; September 2013 (oral)

10th Austrian Proteomic Research Symposium, Graz, Austria; September 2012 (oral)

6th European Proteomic Association (EuPA) Summer School in Proteomic Basics: FEBS Advanced Lecture Course - High Performance Proteomics; Brixen, Italy, August 2012 (poster)

LANGUAGES & OTHER COMPETENCIES

Languages: Croatian (native), English (fluent), French (good), German and Spanish (basic)

Software: Microsoft Office tools, Adobe Illustrator, ChemStation, Proteome Discoverer

ASSOCIATIONS & MEMBERSHIPS

Human Proteome Organisation (HuPO); 2016-present

Austrian Proteomic Association (AuPA); 2010-2016

American Society for Mass Spectrometry (ASMS); 2014-2015

Austrian Society for Allergology and Immunology (ÖGAI); 2013-2014

8. PUBLICATION LIST

Vitko D, Majek P, Schirghuber E, Kubicek S, Bennett KL (2016) FASIL-MS: An Integrated Proteomic and Bioinformatic Workflow To Universally Quantitate In Vivo-Acetylated Positional Isomers. *Journal of proteome research* **15**: 2579-2594

Vitko D, Sialana FJ, Parapatics K, Koperek O, Pötzi C, Li S, Bennett KL (2016) Proteomic and Clinical Analysis of a Fine-Needle Aspirate Biopsy from a Single Cold Thyroid Nodule: A Case Study. *J Clin Case Rep* **6**: 4

Boucheron N, Tschismarov R, Goeschl L, Moser MA, Lagger S, Sakaguchi S, Winter M, Lenz F, **Vitko D**, Breitwieser FP, Muller L, Hassan H, Bennett KL, Colinge J, Schreiner W, Egawa T, Taniuchi I, Matthias P, Seiser C, Ellmeier W (2014) CD4(+) T cell lineage integrity is controlled by the histone deacetylases HDAC1 and HDAC2. *Nature immunology* **15**: 439-448